2015

Synthesis and biological evaluation of phenothiazinium-efflux pump inhibitor hybrids as new agents for use in antimicrobial photodynamic therapy

Ardeshir Rineh

University of Wollongong

Synthesis and Biological Evaluation of Phenothiazinium-Efflux Pump Inhibitor Hybrids as New Agents for use in Antimicrobial Photodynamic Therapy

A thesis submitted in fulfillment of the requirements for the award of the degree

DOCTOR OF PHILOSOPHY

Ardeshir Rineh

M.Sc. Organic Chemistry, B.Sc. Applied Chemistry

School of Chemistry

University of Wollongong

2015

Declaration

I, Ardeshir Rineh, declare that this thesis, submitted in fulfillment of the requirements for the award of Doctor of Philosophy, in the School of Chemistry, University of Wollongong, is wholly my own work unless otherwise referenced or acknowledged. The work has not been submitted for qualification at any other academic institution.

Ardeshir rineh

25th March 2015

Acknowledgements

Firstly, I would like to express my special appreciation and thanks to my supervisor Michael Kelso for his constant support and excellent mentorship. I appreciate the advice, freedom and friendship I have received along my PhD journey. A huge thanks to my collaborators, Michael Hamblin (Harvard Medical School) and George Tegos (University of New Mexico) for their advice and for making me feel a welcome member of their research group.

My special thanks to the many Chemistry members at the University of Wollongong, Stephen Ralph, Stephen Wilson, Nick Dixon, Stephen Pyne, Paul Keller, Danielle Skropeta, Jenny Beck, Glennys O'Brien and John Bremner for their valuable advice and assistance in research and teaching. I would also like to thank the Wellman Center for Photomedicine members and their team at the Massachusetts General Hospital, Conor Evans, Rox Anderson, Tayyaba Hasan, Tianhong Dai and Fatma Vatansever who spent valuable time teaching me about Photodynamic Therapy.

Thanks to all the tech staff and facility managers that contributed to my project, in particular; Wilford Lie, Celine Kelso, Steve Cooper, Roza Dimeska, Karin Maxwell, Ellen Manning, Louisa Willdin, Roger Kanitz, Hairuddin Idris, Joe Daunt and Peter Sara for their willingness to offer a hand and help explain something instrumental, laboratory or software related.

Thanks also to the members of Kelso, Hamblin and Kim Lewis groups: Bharat, Rao, Ghazala, Hayden, Nick, Alex, Louise, Naveen, Yingying, Masayoshi, Pinar, Daniela, Brijesh and Chao Chen for their companionship and encouragement.

Finally, I would like to thank my great wife, Mahsa, parents; Muhammad Ali and Talaat Rineh and my brother, Esfandyar for instilling an interest in science and discovery.

Abstract

Antimicrobial photodynamic therapy (aPDT) uses photosensitiser (PS) molecules in combination with visible light to generate reactive oxygen species (ROS; e.g. $^1O_2$ and •OH) that kill bacteria. The approach is highly suited to skin and other body surface infections, where photosensitisers and light can easily be applied directly to infection sites. As examples, the phenothiazinium PS methylene blue (MB) has been used in aPDT for the sterilisation of blood products, and aPDT with a related compound toluidine blue O (TBO) has been used for oral disinfection of dental cavities and for treating periodontitis.

It has been shown that membrane efflux pumps can limit bacterial cell killing during aPDT with MB, probably by lowering the levels of intracellular ROS produced. This observation suggests that combination approaches, where MB is used alongside small molecule efflux pump inhibitors (EPIs), might potentiate the aPDT effects of MB, allowing its use to be extended to multi-drug resistant (MDR) skin and soft-tissue infections, such as those mediated by methicillin-resistant *Staphylococcus aureus* (MRSA). Studies have confirmed that combinations of EPIs with MB do indeed show increased aPDT potency relative to MB.

This thesis explored a novel approach where MB was covalently linked to EPIs to create MB-EPI hybrid molecules. The rationale for the approach (Chapter 1) was based on prior studies showing that conjugation of the weak antibacterial berberine to the MDR inhibitor INF55 produced berberine-INF55 hybrids that show increased potency over berberine alone and berberine/INF55 combinations. The similarities

between berberine and MB (both planar, aromatic, hydrophobic cations) suggested a similar MB-EPI approach might be successfully adapted for use in aPDT. To explore this hypothesis, a 16 member MB-EPI hybrid library was conceived (compounds **47**-**62**), where members incorporated one of four known inhibitors of the NorA efflux pump in *S. aureus*; reserpine (**47**-**50**), pterostilbene (**51**-**54**), INF55 (**55**-**58**) or INF271 (**59**-**62**). The library contained four examples of each MB-EPI type that carried variations in the linker group between the EPI and MB. Two principal linker groups were employed; piperazine and *N*,*N*'-dimethylethylenediamine, and these were linked directly to the C7 position of MB and to EPIs through either *N*-alkyl (2 compounds) or *N*-acyl (2 compounds) linkages. It was rationalised that production of a library of this type, which scanned photophysical, EPI, physicochemical and other properties of hybrids, would maximise the chances of identifying one or more effective compounds.

Synthesis of the hybrids (Chapter 2) employed a convergent strategy that made use of a phenothiazinium salt common intermediate **63**, which had previously been used for the synthesis of asymmetric MB derivatives. The approach required that advanced secondary amine intermediates containing pre-assembled EPI and linker portions be synthesised first, before submitting these individually to reactions with common intermediate **63**, giving the target hybrids in the final step. The approach was used successfully to produce all 16 hybrids in pure form and in quantities suitable for the study.

In Chapter 3, the hybrids were first studied using UV/Vis spectroscopy for the effects of attaching the EPI-linker groups to MB on the absorption properties of their constituent MB chromophores. The wavelength maxima and extinction coefficients of

the MB absorption bands in all hybrids were found to change very little from those in MB, indicating that the structural changes introduced had not significantly impacted the chromophore. Chapter 3 also explored production of ROS $^1O_2$ and •OH from the hybrids upon illumination with 652 nm red light. All hybrids were observed to produce $^1O_2$ and •OH, albeit at lower levels than MB. Levels of $^1O_2$ were in general higher than •OH. As a class, the INF55-containing hybrids showed the strongest production of $^1O_2$.

All hybrids were next screened for aPDT activity using the test organism MRSA USA300 (Chapter 3). Pterostilbene-containing compounds **51**-**54** were found to be devoid of activity and only one reserpine-containing compound, **50**, showed slight activity at the highest concentration tested (20 μM). Three of the four INF271-containing hybrids **59**, **60** and **62**, on the other hand, showed enhanced aPDT activity relative to MB, as did two of the INF55-containing hybrids (**56** and **58**). Compound **58** was the most potent compound identified, producing an impressive 6-log reduction in MRSA USA300 cells at 20 μM (fluence = 6 J/cm^2) in this assay.

Based on the preliminary screening results, four hybrids (**56** and **58** from the INF55-containing compounds and **59** and **60** from the INF271 series) were advanced to further *in vitro* studies. The four leads were next studied for their aPDT effects against *S. aureus* strains expressing reduced (NorA-), basal (wild-type, WT) and high (NorA++) levels of the NorA efflux pump (Chapter 3). MB (20 μM) showed aPDT activity against these cells in the following order: NorA- > WT > NorA++, consistent with it being a substrate for the NorA pump, where pump activity removes the compound from cells resulting in lower intracellular ROS upon illumination. Hybrids **56**, **58**, **59** and **60** at 20 μM all showed enhanced aPDT effects against the WT and

NorA++ strains relative to MB, whilst showing similar effects to MB against the NorA- strain. This was consistent with the compounds functioning as designed; i.e. with their attached EPIs serving to reduce NorA-mediated efflux of the appended MB moiety, leading to increased intracellular ROS upon illumination and greater cell killing. Subsequent dose-response aPDT experiments with three of these hybrids (**56**, **58** and **60**, Chapter 3) revealed very high potency for the INF55-containing compounds **56** and **58**, which produced total eradication of NorA- and NorA++ cells at 40-80 μM.

Uptake of **56**, **58** and **60** into NorA-, WT and NorA++ *S. aureus* cells (Chapter 3) was found to be virtually unchanged across the three compounds and strains, consistent with these hybrids being poor substrates for NorA, and possibly acting to block the pumps. In comparison, MB showed high uptake into NorA- cells, which reduced in WT cells and was very low in NorA++ cells, consistent with it being a NorA substrate.

The question of whether active hybrids were (a) blocking the NorA pump in *S. aureus* cells or (b) simply evading its action, was addressed in two experiments. In the first of these, a series of synthetic intermediates containing INF55 or INF271 attached to the various linker types used in hybrids, while lacking the terminal MB moiety, were examined for their abilities to potentiate aPDT effects of co-administered MB in NorA++ cells. In all cases, the intermediates produced similar potentiation effects to the parent EPIs INF55 and INF271, suggesting that the structural changes introduced through attachment of linkers did not abrogate their pump-blocking activities. In the second type of experiments, the antibacterial activity of ciprofloxacin, a known substrate for NorA, was examined in the dark against a bioluminescent *S. aureus* strain,

both alone and in the presence of hybrids **56**, **58** and **60**. Each hybrid was found to potentiate the activity of ciprofloxacin, consistent with the hybrids inhibiting its efflux by blocking NorA activity.

The final part of the thesis (Chapter 4) explored the aPDT activity of lead hybrid **58** in a murine MRSA wound infection model. The primary goal of this study was to demonstrate superior efficacy of **58** over MB. Infections were established by inoculating bioluminescent MRSA into 1 cm^2 scratch wounds on the shaved dorsal surfaces of BALB/c female mice and monitored using real time bioluminescence imaging. Infections were studied in the presence/absence of MB and **58**, both with and without application of 652 nm light. aPDT treatment with **58** produced dramatically enhanced effects relative to MB. At very low fluence (12 J/cm^2), **58** reduced the bacterial load by ~ 98%, whereas a much higher fluence (~ 96 J/cm^2) was required to effect similar reductions with MB. Furthermore, a rebound in bacterial load was observed 1 day after treatment in the MB/aPDT group that was not observed in the group treated with **58**. Moreover, total clearance of the infection took only 4 days with **58** (7 days for MB) and the wounds healed faster (~ 4 days for **58**; ~ 7 days for MB).

Abbreviations

µL	Microliter
µM	Micromolar
•OH	Hydroxyl Radical
$^1O_2$	Singlet Oxygen
5'-MHC	5-Methoxy-Hydnocarpin
ABC	ATP-Binding Cassettes
ABI-PP	*tert*-Butyl Thiazolyl Aminocarboxyl Pyridopyrimidine
AcOH	Acetic Acid
aPDT	Antimicrobial Photodynamic Therapy
APF	3′-*p*-(Aminophenyl) Fluorescein
aq	Aqueous
AR	Analytical Reagent
Ar	Argon
ATP	Adenosine Triphosphate
AZA	Azure A
AZB	Azure B
BHI	Brain Heart Infusion
Boc	*tert*-Butyloxycarbonyl
Boc_2O	*tert*-Butyloxy Carbonyl Anhydride
br s	Board Singlet

C	Carbon
CA-MRSA	Community-Acquired MRSA
CDAD	*Clostridium difficile*-Associated Diarrhoea
CDC	Centres for Disease Control and Prevention (USA)
CFU	Colony-Forming Unit
CrEL	Cremophor EL
D	Doublet
DC	Dark Control
DCM	Dichloromethane
dd	Doublet of Doublet
DIPEA	Diisopropylethylamine
DMF	*N*,*N*-Dimethylformamide
DMMB	Dimethyl Methylene Blue
DMSO	Dimethyl Sulfoxide
DNA	Deoxyribose Nucleic Acid
dt	Doublet of Triplet
EGCG	Epigallocatechin Gallate
EMRSA	Epidemic MRSA
EP	Endoperoxide
EPEC	Enteropathogenic *E. coli*
EPIs	Efflux Pump Inhibitors
Et_2O	Diethyl Ether

ETEC	Enterotoxigenic *E. coli*
EtOAc	Ethyl Acetate
FDG	Fluorescein-di-β-D-Galactopyranoside
HA-MRSA	Hospital-Acquired MRSA
HATU	2-(7-Aza-1H-benzotriazole-1-yl)-1,1,3,3-Tetramethyluronium
HPD	Hematoporphyrin Derivative
HPF	3'-*p*-(Hydroxyphenyl) Fluorescein
HRESI-MS	High Resolution Electrospray Ionization Mass Spectroscopy
HRMS	High resolution mass spectrometry
Hz	Hertz
IC_{50}	Inhibitory concentration 50%
ICCD	Intensified Charge-Coupled-Device
INF55	5-Nitro-2-Phenyl Indole
IR	Infrared
i.p.	Intraperitoneal Injection
J	Coupling constant
LDL	Low-Density Protein
log ε	Extinction Coefficient
m	Multiplet
m/z	Mass-to-Charge Ratio
MATE	Multi-Antimicrobial Extrusion Protein
MB	Methylene Blue

MBC	Minimum Bactericidal Concentrations
MCE	Mixed-Cellulose-Ester
MDR	Multidrug Resistance
MeOH	Methanol
MET	Multidrug Endosomal Transporters
MFS	Major Facilitators
mg	Milligram
MGH	Massachusetts General Hospital
MHB	Mueller-Hinton Broth
MHz	Megahertz
MICs	Minimum Inhibitory Concentrations
mJ	Millijoule
mL	Millilitre
mM	Millimolar
MO	Methylene Orange
Mp	Melting Points
MRSA	Methicillin Resistant *Staphylococcus aureus*
MSSA	Methicillin-Susceptible *S. aureus*
mtr	Multiple Transferable Resistance
mW	Milliwatt
NADH	Nicotinamide Adenine Dinucleotide
NIH	Institutes of Health

NMB	New Methylene Blue
NMR	Nuclear Magnetic Resonance
NorA-	*S. aureus* NorA knockout
NorA++	*S. aureus* NorA-overexpressing
^{o}C	Degrees Celsius
OD600	Optical Density at 600 nm
OM	Outer Membrane
PaβN	Phenylalanine Arginyl β-naphthylamide
PBPs	Penicillin-Binding Proteins
PBS	Phosphate Buffered Saline
PDT	Photodynamic Therapy
PEI-	Polyethylenimine-
PET	Photoinduced Electron Transfer
Pet. Spirit	Petroleum Spirit
PL-F127	Triblock Copolymers F127
POL388	Poloxamer 388
PPh_3	Triphenyl Phosphine
ppm	Parts per Million
PS	Photosensitizer
Py-HCl	Pyridinium Chloride
R_f	Retention Factor
RLP068/Cl	Tetracationic Zn(II) Phthalocyanine Chloride

RNDs	Resistance-Nodulation Cell Division
ROS	Reactive Oxygen Species
rt	Room Temperature
SAR	Structure-Activity-Relationships
SDS	Sodium Dodecyl Sulphate
SEM	Standard Error of the Mean
SMR	Small Multidrug-Resistance Family
SOSG	Singlet Oxygen Sensor Green Reagent
T	Triplet
T60	Tween 60
TBO	Toluidine Blue O
TEA	Triethylamine
TFA	Trifluoroacetic Acid
THF	Tetrahydrofuran
TICT	Twisted Intramolecular Charge Transfer
TLC	Thin Layer Chromatography
UV/Vis	Ultraviolet–Visible Spectroscopy
VRE	Vancomycin Resistant *Enterococci*
VRSA	Vancomycin-Resistant *S. aureus*
WT	Wild-Type
λ_{max}	Lambda Maxima
$\Phi\Delta$	Quantum Yield

Contents

List of Figures

List of Tables

List of Schemes

Chapter 1

Introduction

1.1 Bacterial Resistance - A Global Health Threat

In today's world, no nation's health is secure due to the increasing threat posed by drug-resistant pathogens. Antimicrobial resistance arises when pathogens, including bacteria, fungi, viruses and parasites, no longer respond to drugs to which they were formerly sensitive.[1] For example, the Gram-positive bacteria *Staphylococcus aureus* and Gram-negatives like *Staphylococcus epidermis* and *Staphylococcus hemolyticus* have demonstrated an ability to develop resistance to each new generation of antibiotics. Methicillin-resistant *S. aureus* (MRSA) and vancomycin-resistant *Enterococcus faecium* (VRE) are two examples that are causing great clinical concern.[2] In some settings, as many as 90% of *S. aureus* infections are reported to arise from MRSA leading to ineffective treatments with standard antibiotics. This hospital-derived (nosocomial) 'superbug' has been estimated to increase the likelihood of patient death by 64%.[3] Of over two million people who contract antibiotic-resistant infections annually, at least 23,000 die directly from the infection and another 100,000 die from related complications.[3] According to the U.S. Centers for Diseases Control and Prevention (CDC), antibiotic-resistant pathogens cost the U.S. health care system between $21-34 billion each year.[4]

The glycopeptide antibiotic vancomycin is considered the last line of defense antibiotic against Gram-positives resistant to all β-lactams. These days, however, vancomycin-resistant *S. aureus* (VRSA) is recognised as a "concerning threat" by the CDC.[5] Many countries are also reporting high rates of resistance to third-generation cephalosporins, carbapenems and fluoroquinolones in *Escherichia coli* and *Klebsiella pneumoniae*, which are responsible for pneumonia and bloodstream infections.[3] Social

factors contributing to the problem include unnecessary prescribing of antibiotics, addition of antibiotics to feedstuffs, transmission of infections via international travellers and the rise in poverty in some countries. These factors in combination with cellular bacteria resistance mechanisms have created the worrying scenario we face today.[6]

A great concern is that we will enter a post-antibiotic era where standard antibiotic treatments no longer work and infections become more and more difficult or impossible to control. To counter this threat there is a continuing and urgent need to discover new antibiotics and antimicrobial strategies, preferably acting via novel mechanisms.

1.2 Bacterial Resistance Mechanisms

Existence on earth for more than three billion years[7] has allowed bacteria to evolve multiple mechanisms for surviving in diverse and challenging environments. They have learned how to detoxify harmful substances, like naturally occurring toxins and, in more recent times, antibiotics developed by humans. When we create new antibiotics, mankind encourages resistance development and expands the survival mechanisms available to bacteria.[8] Thus, while effective new antimicrobials are clearly needed it is imperative that they be developed in parallel with new tactics that address the problem of resistance.[9]

Three of the major cellular mechanisms that bacteria use to resist antimicrobials are summarized in Figure 1.1. Firstly, enzymatic inactivation of antibiotics can occur when bacteria express enzymes to detoxify compounds before they reach their

target(s).[10] β-lactamases, for examples, serve to deactivate β-lactam antibiotics by hydrolysing their essential β-lactam ring.[10-11] Both Gram-positive (e.g. *S. aureus* and *Bacillus cereus*) and Gram-negative (e.g. *Pseudomonas sp* and *Acinetobacter sp*) species produce β-lactamases.[12]

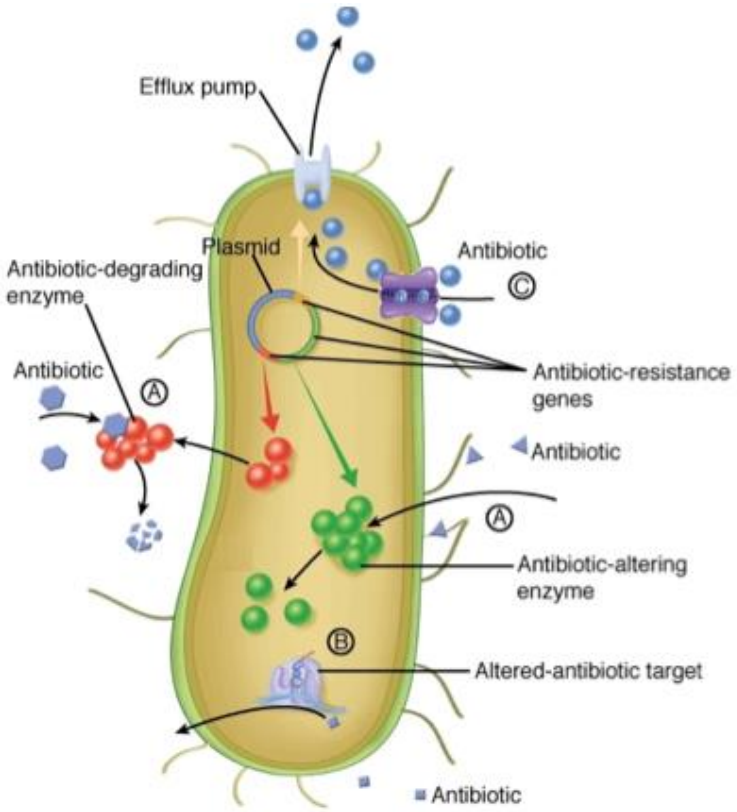

Figure 1.1 Three major bacterial antibiotic resistance mechanisms: (A) enzymatic inactivation, (B) drug target alteration and (C) expression of efflux pumps. Figure modified from Nordmann *et al*.[13]

A second mechanism that bacteria use to resist antimicrobials is to alter their drug targets through mutation. By modifying their targets, bacteria render antibiotics ineffective by reducing their target affinity, which nullifies their ability to inhibit microbial cell functions. As an example, when the peptidoglycan precursors used by

enterococci for cell wall synthesis are mutated from D-Ala-D-Ala to D-Ala-D-Lac, the binding of vancomycin is impaired.[14]

Expression of efflux pumps is a third major resistance mechanism and the focus of this PhD project. The role of efflux pumps in preventing molecules, including those produced by the host organism (e.g. bile) from accumulating in bacterial cells, was first described in 1980.[15] It is now accepted that efflux pumps are responsible for importing essential nutrients into cells and exporting a wide variety of toxic agents, such as dyes, drugs, cationic agents and metabolites.[16] Efflux pumps essentially serve as gatekeepers that shuttle molecules between the cell cytoplasm and the extracellular environment.[17]

1.3 Efflux Pumps - General

Membrane-bound efflux transporter proteins (pumps) are found in both prokaryotic and eukaryotic organisms.[16] The term Multi-Drug Resistance (MDR) pumps is used to differentiate pumps that are capable of transporting a wide variety of structurally diverse compounds from those that selectively extrude specific molecules. Based on sequence similarity and structural homology, efflux systems have been classified into six super-families. These include the ATP-binding cassettes (ABC), major facilitators (MFS), resistance-nodulation cell division (RND), small multidrug-resistance family (SMR), multi-antimicrobial extrusion protein family (MATE) and multidrug endosomal transporters (MET). The first five families are found in microorganisms, while the MET family appears to be restricted to higher eukaryotes. Representatives of all families are found in mammalian cells.[18]

1.4 Bacterial Efflux Pumps

Evidence that MDR pumps contribute to antibiotic resistance in bacteria comes from experiments showing that there is an increase in the minimum inhibitory concentration (MIC) of multiple antibiotics against a particular bacterium, compared to the MICs of the same antibiotics against non-MDR expressing parent strains.[19] It is well accepted that the 'intrinsic resistance' of Gram-negative bacteria to certain antibiotics is a result of efflux systems.[20]

A summary of bacterial efflux systems that illustrates their biological complexity, overlapping specificity and evolutionary adaptability to antimicrobials, is provided in Figure 1.2.

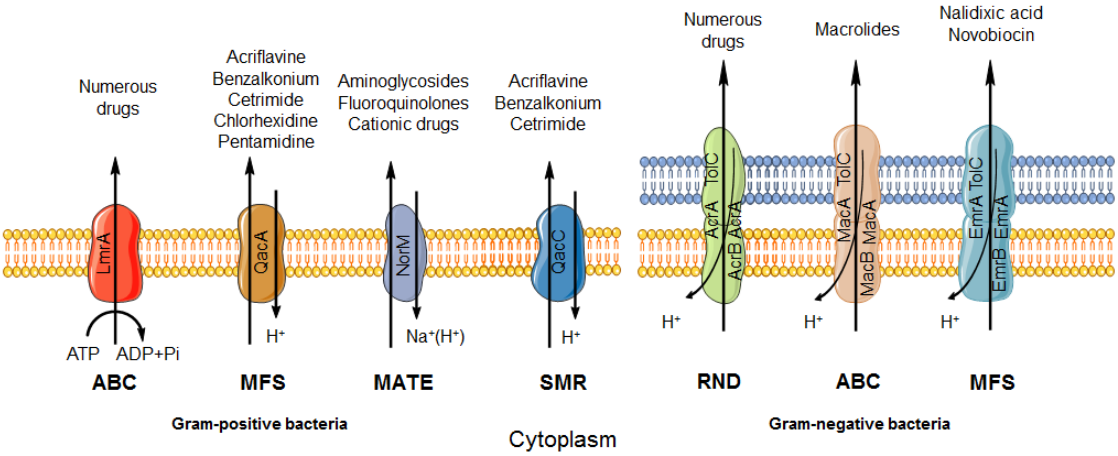

Figure 1.2 Summary of efflux systems found in Gram-positive and Gram-negative bacteria. Examples of individual proteins that comprise each class are shown, along with their typical substrates. MDRs expressed by Gram-negatives contain several components, with the outer membrane protein normally being TolC. Figure modified from Piddock *et al.*[21]

Both Gram-positive and Gram-negative bacteria can produce a variety of efflux systems that contribute to multidrug resistance, virulence and pathogenesis.[22]

Mechanisms that induce upregulation of efflux pumps include: (1) mutations in promoter regions or insertion elements located upstream from efflux pump genes, (2) mutations in local repressor genes and (3) mutations in global regulatory genes.

Substrates for individual efflux pumps vary depending on the pump and the bacteria. A typical substrate profile of an MDR pump might include chloramphenicol, quinolones (e.g. nalidixic acid, ciprofloxacin and norfloxacin), polycyclic dyes (e.g. acriflavine and ethidium bromide), some detergents (e.g. sodium dodecyl sulfate and Triton X-100) and biocides (e.g. cetrimide and triclosan).[23]

1.4.1 Efflux Pumps in Clinically Important Gram-Positive Bacteria

The major efflux systems implicated in Gram-positive bacterial drug resistance are comprised of six chromosomally encoded transporters, including MFS members NorA, NorB, NorC and MdeA, the MATE multidrug export protein mepRAB[24] and the SMR member SepA.[25] Three plasmid encoded pumps QacA, QacB,[26] and Tet(K) are also important.[27] These systems have broad and overlapping substrate specificities, extruding quinolones, tetracyclines, monovalent and divalent antimicrobial cations (i.e. intercalating dyes, quaternary ammonium compounds, diamidines, biguanidines) and plant secondary metabolites.[28]

Pumps belonging to the MFS superfamily in *S. aureus* are NorA, NorB, NorC, SdrM and Tet38. One study showed that 50% of 232 blood-borne *S. aureus* isolates were able to efflux more than two substrates. Overexpressed genes identified were *mepA* 4%, *mdeA* 11%, *norA* 23%, *norB* 25% and *norC* 17%. Another 20% of strains over-expressed two or more efflux genes.[29] Other genes, such as *mepA* (belonging to the

MATE family) and *sepA* (belonging to the SMR family), are also present in the *S. aureus* genome. Sav1866 is an ATP-binding cassette protein from the pathogen *S. aureus* which is frequently used to homology model human and microbial ABC multidrug transporters. The structure of the Sav1866 ABC pump from *S. aureus* is shown in Figure 1.3.

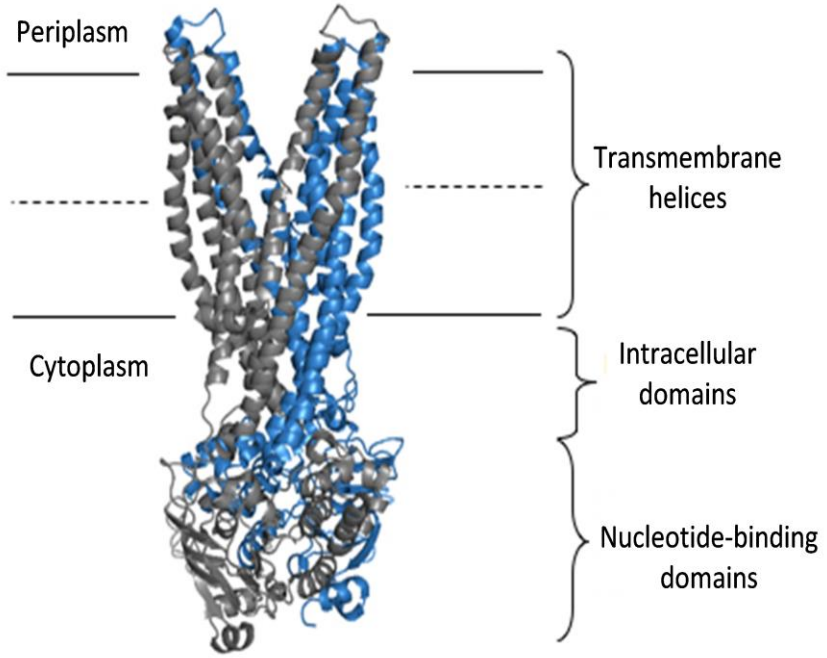

Figure 1.**3** Ribbon representation of the Sav1866 ABC pump in *S. aureus*. Two of six transmembrane helical domains and two intracellular nucleotide-binding domains are shown. Figure modified from Dawson and Locher.[30]

The clinical relevance of efflux pumps in *S. aureus* is best understood for NorA. The NorA pump confers resistance to fluoroquinolone antibiotics, as well as dyes and biocides.[31] While nafcillin, ciprofloxacin, vancomycin and linezolid are typically used for treatment of methicillin-susceptible *S. aureus* (MSSA) and MRSA infections, the MICs of these agents are generally not affected by NorA, except for ciprofloxacin.

Enterococcus faecium is a commensal (innocuous, coexisting) organism in the human intestine that can cause diseases such as neonatal meningitis. Analysis of food-borne infections revealed that Tet(L), Tet(M) and Tet(K) pumps are present in *E. faecium*. MsrC pumps (belonging to the ABC transporters) have been shown to confer resistance to macrolides and quinupristin in *E. faecium*, while EfmA pumps (MFS family) have been shown to confer intrinsic resistance to many fluoroquinolones and tetraphenylphosphonium ions. EmeA (a NorA homologue) has also been identified in *E. faecalis*.[32]

S. pneumonia infections can lead to fatal pneumonia, bronchitis and meningitis, particularly in the young and elderly. The MFS pumps in *S. pneumonia* MefA, MefE and PmrA, have been implicated in macrolide and fluoroquinolone resistance.[33] The PmrA (MFS family) pump in *S. pneumonia* shares 42% identity with NorA and 43% with Bmr pumps. It can export ciprofloxacin and norfloxacin, as well as the dyes acriflavine and ethidium bromide.[29,34] Overexpression of *pmrA* is not exclusively associated with norfloxacin-resistant *S. pneumonia* as it is also found in norfloxacin-susceptible isolates.[35]

The *mef* (MFS pump Mef) and *mel* (ABC pump Mel) genes, which are located on a conjugative transposon-related element in the genome of *S. pneumonia*, confer resistance to macrolides and are responsible for increasing resistance problems worldwide.[36]

1.4.2 Efflux Pumps in Clinically Important Gram-Negative Bacteria

The most clinically significant efflux systems in Gram-negative bacteria are the RND tripartite transporters, which show exceptionally broad substrate recognition profiles. These proton-driven pumps are highly conserved across representative proteobacteria and a representative example, AcrAB-TolC from *E. coli*, is shown in Figure 1.4. Several members of the RND superfamily encoded in the human genome are homologues of bacterial RND pumps (16% identity).[37]

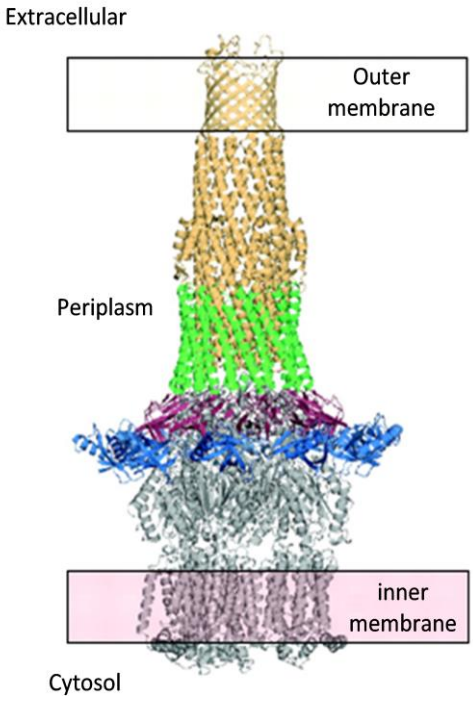

Figure 1.4 Model of the TolC-MexA-AcrB pump in *E. coli*. The pump comprises the α-helical domain of a nonameric MexA complex that accommodates the periplasmic end of the TolC efflux channel (pale orange), α/β barrel domain (blue), a "lipoyl" domain (red), an extended α-helical domain (green) and the AcrB pump (grey). Figure modified from Cuthbertson *et al.*[38]

Pseudomonas aeruginosa, *E. coli*, *Salmonella enterica*, *Campylobacter jejuni* and *Neisseria gonorrhoeae* are clinically relevant Gram-negative bacteria known to express MDR pumps. *P. aeruginosa* can cause pneumonia and other opportunistic infections (e.g. skin and soft-tissue infections in burns patients). Several antibiotics, including chloramphenicol, fluoroquinolones and tetracycline, as well as other substances like acriflavine, ethidium bromide and even some organic solvents, are exported by *P. aeruginosa* pumps. The clinically relevant pumps in *P. aeruginosa* are MexAB-OprM, MexCD-OprJ, MexEF-OprN and MexXY-OprM. These are expressed at basal levels in wild-type cells and can confer intrinsic resistance to many antimicrobials.[39] Expression of MexCD-OprJ and MexEF-OprN has only been observed in multi-drug resistant strains and is induced by pump substrates.[40] *P. aeruginosa* carries twelve related Mex efflux systems but only the above four have been shown to be clinically significant for resistance.[41]

Overexpression of pumps can occur as a result of mutations in operons within transcriptional regulatory regions.[42] For example, overexpression of mexAB-OprM in nalB strains due to mutations in the *mexR* gene confers multi-drug resistance in *P. aeruginosa*.[43] Other genes involved in the overexpression of MexAB-OprM include *nalC* and *nalD*. Hyperexpression of MexCD-OprJ in nfxB mutants of *P. aeruginosa* contributes resistance to fluoroquinolones and fourth generation cephems (e.g. cefpriome and cefozopran).[44]

Decisions on which antibiotics to use when treating *P. aeruginosa* infections depends on whether the compounds are Mex pump substrates.[45] For instance, the MexXY-OprM system exports aminoglycosides, the MexAB-OprM system certain β-

lactams and the MexCD-OprJ system novobiocin and cefsulodin. Another RND transporter, MexGHI-OpM, has been shown to facilitate quorum sensing and antibiotic susceptibility in *P. aeruginosa*, and to promote virulence and contribute to persistence.[45]

Although *E. coli* is a commensal organism found in the human gut it is often responsible for urinary-tract infections. Enteropathogenic *E. coli* (EPEC) and enterotoxigenic *E. coli* (ETEC) can cause severe diarrhoea.[21] Pumps in *E. coli* include EmrB, MdfA, TetA and Acr. Acr (i.e. AcrB) functions as a multi-subunit complex in association with the outer membrane channel TolC and the membrane fusion protein AcrA.[21] Figure 1.5 shows the structure of the AcrAB-TolC pump in *E. coli*.

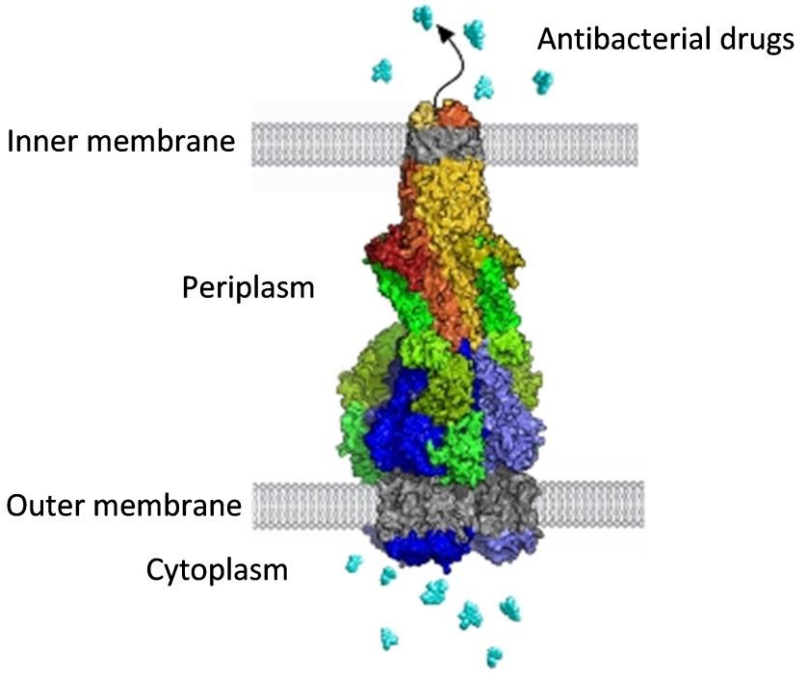

Figure 1.5 Example of an MDR efflux pump in *E. coli*. The pump is an AcrAB-TolC complex. The TolC trimer (orange, red, and yellow subunits with grey equatorial domains and membrane regions) was docked onto the AcrA (green) and AcrB trimer (blue/light blue subunits with grey membrane regions). Figure modified from Symmons *et al*.[46]

AcrAB-TolC from the RND family is remarkably polyspecific[47] and can be overexpressed in some clinical isolates.[48] Overexpression of AcrAB-TolC does not generally confer clinical resistance on its own. As with RND pumps in *P. aeruginosa*, AcrAB-TolC in *E. coli* is a tripartite complex formed between the RND pump AcrB, the membrane fusion protein AcrA and the low permeability outer membrane protein TolC.[37a] While a crystal structure has been reported and a model of the pump assembled[46] the exact role of each component during efflux remains largely unknown.

The AcrAB-TolC complex is capable of extruding a very broad range of substances that differ in both structure and charge. Examples include antibiotics like chloramphenicol, lipophillic β-lactams, tetracycline, rifamipicin, novabicin, fusidic acid and nalidixic acid.[47] Non-antibiotic substrates include disinfectants and detergents, bile salts, cationic dyes, ethidium bromide and some solvents.[49]

Treatment of *E. coli* infections usually involves administration of co-trimoxazole (trimethoprim-sulfamethoxazole), a nitrofurantoin or a fluoroquinolone. Ceftriaxone, a third-generation cephalosporin, is used for invasive or life-threatening *E. coli* infections.[50]

Salmonella enterica serovar Typhimurium and *Salmonella enterica* serovar Enteritidis can cause gastroenteritis, with invasive salmonellosis occurring in 1-4% of human infections.[51] When treatment is required the antibiotics most commonly used are fluoroquinolones (e.g. ciprofloxacin) or the cephalosporin ceftriaxone. The AcrAB-TolC system of *S.* Typhimurium is similar to that of *E. coli*. It has been shown that overexpression of AcrB in human and veterinary isolates and laboratory mutants of *S.* Typhimurium are associated with MDR.[52]

C. jejuni contains RND-family members and is the most common cause of bacterial gastroenteritis in developed countries. Overexpression of CmeB confers resistance to ciprofloxacin, erythromycin, ampicillin, chloramphenicol and tetracycline and decreases susceptibility to bile salts, SDS, Triton X-100 and triclosan.[53] Both human and veterinary isolates of *C. jejuni* have been found to overexpress *cmeB*.[54]

Resistance of *N. gonorrhoeae* to some antibiotics (i.e. erythromycin, penicillin and tetracycline) due to multiple transferable resistance (mtr) was first identified in the 1970s.[55] The mtr property is due to the action of the MtrC-MtrD-MtrE pump, which expels structurally diverse hydrophobic antimicrobial agents by an energy-dependent process.[56] Recently, overexpression of MtrC-MtrD-MtrE pumps due to an mtrR mutation was shown to confer chromosomally mediated penicillin resistance in *N. gonorrhoeae*.[57] *N. gonorrhoeae* is responsible for the sexually transmitted infection gonorrhoea but can also cause conjunctivitis, pharyngitis, prostatitis and orchitis.[58]

1.5 Strategies for Inhibiting Microbial Efflux Pumps

Strategies that have been investigated to date for overcoming efflux-mediated bacterial resistance are of three types: (1) biological inhibition of efflux pumps using neutralizing antibodies or antisense approaches. For example, use of small interfering RNAs (siRNAs) have been used for inhibition of the AcrAB efflux pump in *E. coli*;[59] (2) evasion of efflux systems, where the structure of antimicrobials is modified such that they are no longer substrates for pumps. For instance, newer antibiotics like sparfloxacin and trovafloxacin were purposely engineered to be less susceptible to efflux than their parent compounds, nalidixic acid and norfloxacin;[60] (3)

pharmacological inhibition of pumps, where small molecule inhibitors are used to selectively block pumps and restore potency of co-administered antibacterials.

1.6 Small Molecule Efflux Pump Inhibitors

Many of the small molecule inhibitors identified to date have been natural products, and it has been proposed that these compounds may have evolved to protect plants from infections by acting synergistically with other plant antibacterial compounds.[61] A potential clinical strategy that mimics this approach from nature is to use small molecule MDR pump inhibitors in combination with antibacterial agents. Whilst an attractive strategy, only a small numbers of lead chemotypes have been advanced to preclinical and clinical studies to date. Lack of broad activity and selective action against bacterial pumps over mammalian pumps appear to be key challenges for adopting the approach in the clinic.

Phenotypic assays with efflux systems have been used extensively in microbial efflux pump inhibitor (EPI) discovery. These functional assays typically employ a fluorescent dye pump substrate to report on efflux activity and have been successfully established in low- and mid-throughput formats.[62] Fluorescence microscopy and high-resolution multi-parametric flow cytometry are gradually superseding fluorimeters and plate readers in these assays because of their capacity for increased throughput and sensitivity.[62b]

1.6.1 EPIs against Gram-Negative Bacteria

The number of EPI chemotypes targeting Gram-negatives identified to date is much smaller than the number against Gram-positives. Phenyl-arginine-beta-naphthylamide (PaβN), also called MC-207 110 **1** (Figure 1.6), was the first EPI identified against Gram-negatives.[63] It was discovered by testing an array of synthetic and natural compounds against *P. aeruginosa* strains over-expressing the three intrinsic efflux systems (i.e. MexAB-OprM, MexCD-OprJ, MexEF-OprN) in the presence of levofloxacin.[64] Results of various microbiological assays suggested that MC-207 110 promoted a competition-like process during the recognition/transport of antibiotic molecules.[65] A derivative of PaβN, MC-04 124 **2**, showed improved EPI activity, pharmacokinetic properties and increased stability.[66] Both inhibitors were studied in preclinical work by Mpex Pharmaceuticals.[67] Recent investigations suggested the compounds show toxicity due to effects on membrane function.[68] PaβN/MC-207 110 remains as a valuable probe for exploring bacterial efflux systems.

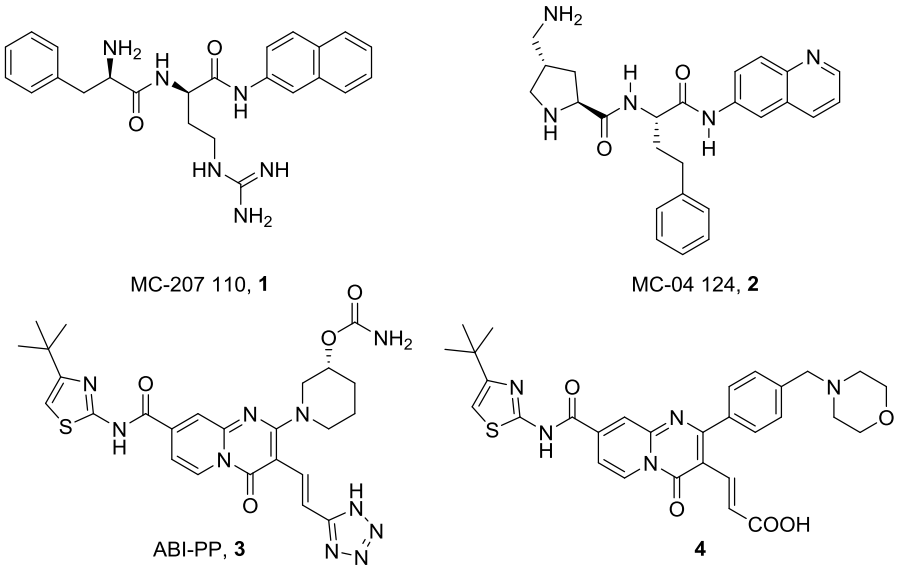

Figure 1.6 Examples of EPIs against Gram-negative bacteria.

EPI activity against RND pumps can be assessed using a microfluidic channel device and fluorescence microscope.[69] In these assays, fluorescein-di-β-D-galactopyranoside (FDG) is hydrolyzed by β-galactosidase in the cytoplasm of *E. coli* to produce the fluorescent dye fluorescein. Both FDG and fluorescein are effluxed in *E. coli*, allowing the effects of EPIs to be measured. This assay was used to validate the activity of MexB-specific *tert*-butyl thiazolyl aminocarboxyl pyridopyrimidine (ABI-PP) **3** and PaβN **1**.[70] Pyridopyrimidine-based EPIs carrying acrylic acid (e.g. **4**) were shown to be more soluble than **3** and showed acceptable safety profiles but they displayed only moderate activity *in vivo*.[71] Recently, co-crystallization of the MexB pump with PaβN and ABI-PP revealed tighter binding for the latter, leading the authors to propose a set of physicochemical parameters for development of EPIs.[72]

1.6.2 Natural Product EPIs

Numerous phytochemicals have been shown to act as EPIs in combination with antimicrobials against Gram-positive bacteria.[73] A selection of phenolic natural product EPIs is shown in Figure 1.7.

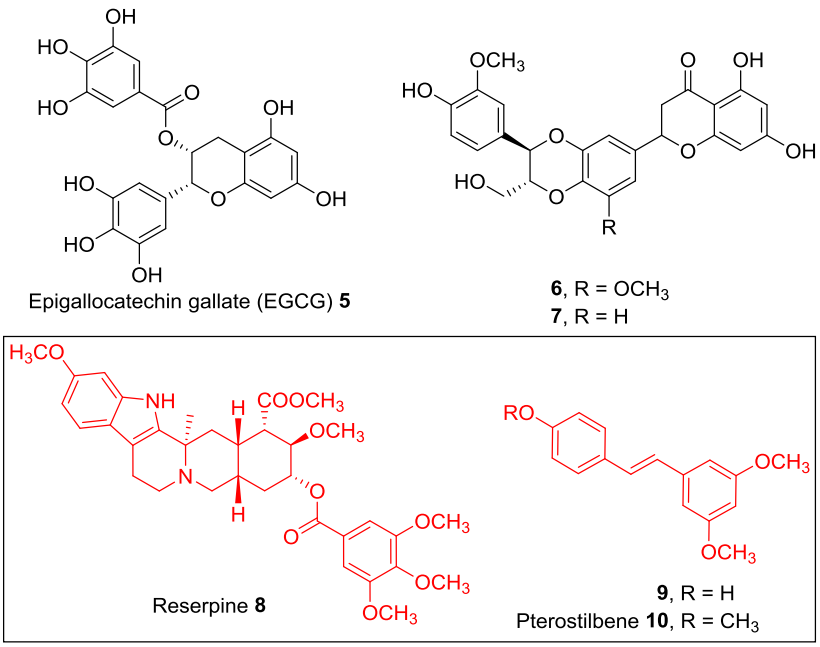

Figure 1.7 Examples of phenolic EPIs discovered from natural sources. Reserpine **8** and pterostilbene **10** were important compounds in this PhD project.

Epigallocatechin gallate (EGCG) **5**, a major polyphenol extracted from green tea,[74] shows resistance-modifying activities when used with norfloxacin and tetracycline at low concentrations.[75] At less than half its MIC (100 µg/mL) EGCG was able to reverse tetracycline resistance in staphylococcal isolates.[75] EGCG was also identified as a resistance-modifying agent in *Campylobacter* spp.[76]

The flavonolignan 5'-methoxyhydnocarpin (5'-MHC **6**) and its 5-desmethoxy analogue **7** (Figure 1.7) were isolated from *Hydnocarpus wightiana*.[77] Both compounds were shown to be MDR inhibitors without showing antibacterial activity on their own.[78] The compounds were evaluated against 20 clinical isolates of MRSA in combination with ampicillin or oxacillin, where they reduced MICs more than 4-fold.[79] Subinhibitory concentrations of the weak antibacterial alkaloid berberine with 1.2 µg/mL of **6** completely inhibited growth of *S. aureus* growth.[78a]

1.6.2.1 Reserpine

Reserpine **8** (Figure 1.7) is an anti-hypertensive alkaloid that was first extracted from the roots of *Rauwolfia vomitoria* in 1954.[80] The compound was originally shown to be a potent inhibitor of mammalian P-glycoprotein[81] but later investigations revealed its MDR inhibitory properties in the Gram-positive bacterium *Bacillus subtilis*,[82] where it was shown to inhibit tetracycline efflux by the Bmr pump. The study revealed that reserpine interacts directly with the Bmr protein at a hydrophobic site formed around Phe143, Val286 and Phe306.[82]

Reserpine reversal of NorA-mediated efflux in *S. aureu*s was shown to enhance the potency of fluoroquinolones,[83] where it lowered MICs by up to 4-fold when present at 20 μg/mL.[84] In a study by Schmitz *et al.* MICs and LC_{50} values were measured against 102 clonally non-related *S. aureus* strains from eight different countries for ciprofloxacin, sparfloxacin and moxifloxacin in the presence and absence of reserpine.[84] The potentiation effect of reserpine on the hydrophilic variants (e.g. ciprofloxacin) was greater than for the hydrophobic compounds (e.g. moxifloxacin and sparfloxacin).

Fluoroquinolone resistance mediated by the PmrA pump in *S. pneumoniae* (43% amino acid similarity to NorA) was shown to decrease in the presence of reserpine.[85] In an investigation by Markham *et al*, a single-step mutant of *S. pneumoniae* resistant to 3-4 fold MICs of ciprofloxacin was studied *in vitro* in the presence and absence of reserpine.[85b] A pronounced inhibition of selection of *S. pneumoniae* ATCC 49619 mutants resistant to ciprofloxacin was noted when reserpine (20 μg/mL) was present. In the absence of reserpine, 135 colonies of *S. pneumoniae* showed 3 x baseline MIC and 19 colonies showed 4 x baseline MIC. In the presence of reserpine only 3 colonies were

resistant to 3 x MIC (45-fold reduction) and no colonies were resistant to 4 x MIC (complete suppression). In these experiments reserpine affected neither the colony size nor the colony-forming ability of *S. pneumoniae* when plated in the absence of ciprofloxacin.[85b]

A significant problem with many natural product EPIs is their toxicity, which hinders their potential for clinical applications.[67,86] Reserpine is neurotoxic at the concentrations required to inhibit MDR pumps (20 µg/mL) and is thus not suitable as an antibacterial adjuvant in humans.[67] It remains, however, a widely used tool for evaluating bacterial efflux mechanisms.[87]

1.6.2.2 Pterostilbene 10

Organic extracts of *Dalea versicolor* in the presence of berberine showed strong potentiation effects against *S. aureus*.[88] Two pterostilbene derivatives **9** and **10** (Figure 1.7) were contained in the extract fractions and co-extracted with berberine. It was hypothesized that the MDR inhibitory properties of these molecules was being exploited by the plant to potentiate the antibacterial effects of berberine; that is, the compound combination was acting as the plant's antibacterial defence mechanism.[88-89] Both **9** and **10** showed only weak activity alone (MICs 250 and 500 µg/mL, respectively)[90] but **10** caused complete growth inhibition at low concentrations (~ 3.3 µg/mL) in combination with berberine. Compound **10** was also tested alone and in combination with berberine against the opportunistic pathogen *Bacillus cereus* and was shown to increase the activity of berberine 16-fold.[90]

1.6.3 Synthetic EPIs

An investigation aimed at exploring the effects of NorA inhibition in *S. aureus* studied the activities of fluoroquinolones (i.e. levofloxacin, ciprofloxacin and norfloxacin) in the presence and absence of various synthetic NorA inhibitors.[91] The H^+/K^+ ATPase pump inhibitor omeprazole **11** (Figure 1.8) was found to have moderate activity (less than reserpine) but significantly greater activity than verapamil. The compound decreased the frequency of ciprofloxacin resistance almost 100-fold.[92]

When the mammalian MDR inhibitor timcodar (VX-853) **12** was evaluated for EPI activity in a variety of bacteria,[93] it was found to potentiate the activity of ethidium bromide against *S. aureus*[94] and to decrease the MIC of fluoroquinolones. Against a NorA-overproducing strain (SA-1199B), VX-853 **12** reduced the MIC of norfloxacin 32-fold and 8-fold for ciprofloxacin.[93a]

A new generation of MDR modulators that included tariquidar **13** and elacridar **14** (Figure 1.8) was identified during screening for inhibitors of mammalian ABC-type transporters and breast cancer resistance proteins (BCRP, ABCG2).[95] Elacridar **14** had previously shown equipotent activity with reserpine in ciprofloxacin/norfloxacin combinations against *S. aureus* strains *in vitro*.[96] The potency of tariquidar **13** was also investigated in combination with ciprofloxacin and showed potent inhibitory effects against some efflux pumps.[97] The compound produced 10-fold reductions in the ciprofloxacin MIC against *S. aureus* while no effect was observed with *P. aeruginosa*.

An investigation by Influx Inc. aimed at discovering inhibitors of the NorA pump in *S. aureus* saw the screening of over 9,600 structurally distinct synthetic

compounds in the late 1990s.[98] The compounds were screened at 20 µg/mL and those that reversed NorA-mediated efflux of ethidium bromide whilst being nontoxic to bacteria on their own were considered hits. Initial efforts identified 399 compounds showing activity above threshold. Twenty-eight of the hits were at least as potent as reserpine, with eleven showing higher potency (effective at 5 µg/mL or less). Thirty of the compounds contained an indole moiety, while a significant number contained the toxic trichloromethylaminal group. However, seven compounds were relatively non-toxic nitroindoles. Out of 32 bisaryl ureas in the library eleven compounds were found to be active. Two of the most active EPIs from the investigation were the 5-nitroindole derivative INF55 **15** and bis-aryl urea INF271 **16** (Figure 1.8). Both compounds have since been studied further for their EPI effects in Gram-positive bacteria.[99]

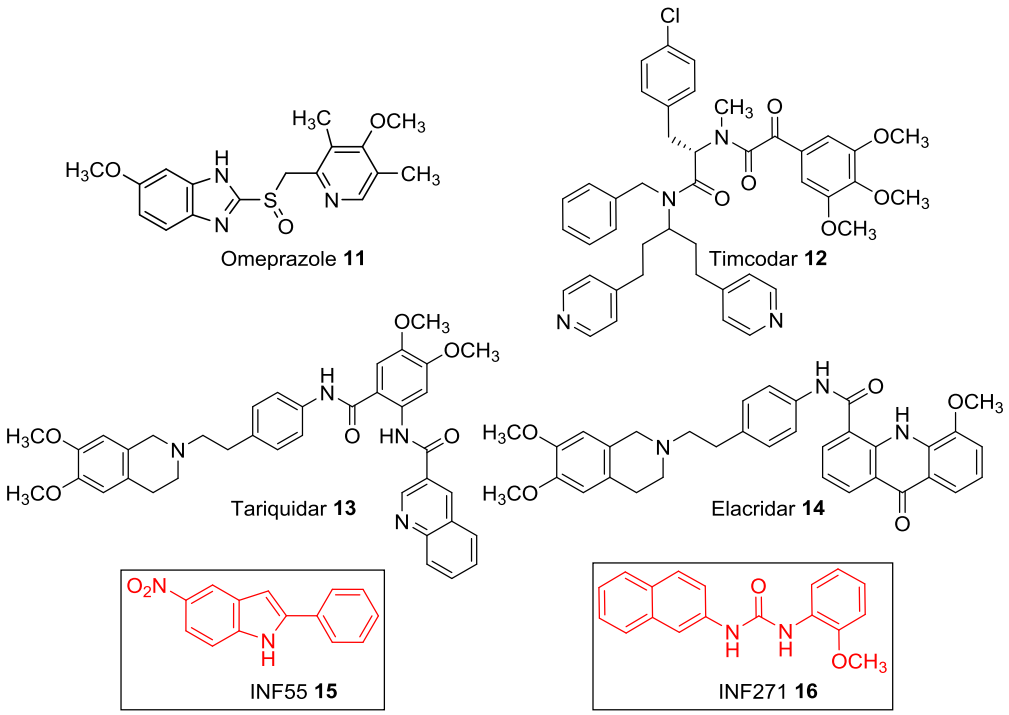

Figure 1.8 Representative synthetic EPIs identified to date. INF55 **15** and INF271 **16** were important compounds in this PhD project.

1.6.3.1 5-Nitro-2-phenylindole (INF55) 15

Markham *et al* described several indole-based inhibitors of multidrug transport proteins that showed potential for use in combination with existing antibacterial or antifungal agents.[100] The compounds were identified as inhibitors in bacteria expressing the NorA pump and fungi expressing another multidrug transport protein. A theoretical structure-activity study using COMFA (3D-QSAR) analysis suggested that replacement of the indole 5-nitro group of INF55 **15** with other electron-withdrawing substituents should be favourable for EPI inhibitory activity.[99b] A separate study identified a series of 2-arylbenzo[*b*]thiophenes related to INF55 as NorA inhibitors, suggesting that the indole NH group is not essential for activity.[101] Most of the compounds exhibited no antibiotic activity alone and several were shown to be inhibitors of the NorA pump in *S. aureus*.

An SAR study by Samosorn *et al* showed that various substituents around the 2-aryl ring of INF55 can affect NorA inhibitory potency.[102] For example, the INF55 analogue 5'-benzyloxy-2'-hydroxymethyl-5-nitroindole **17** (Figure 1.9) potentiated the activity of berberine (a known substrate of NorA) more than 15-fold against the NorA overexpressing *S. aureus* strain K2361 at a concentration of 0.8 μg/mL.[102] In later work the same group reported more SAR explorations around the 2-aryl ring of INF55 as well as the effects of substituting the indole 5-nitro group.[103] The study identified three new potent indole-based NorA EPIs, **18**, **19**, and **20** (Figure 1.9), along with a new indole derivative **21** that showed direct antibacterial activity against *S. aureus*.

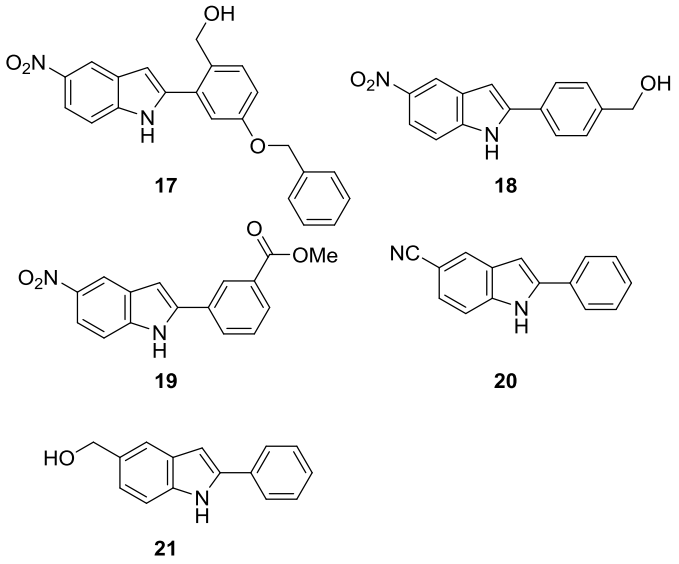

Figure 1.9 2-Arylindole-based inhibitors of the NorA pump in *S. aureus* related to INF55 **15**.

1.6.2.2 INF271

The bis-aryl urea INF271 **16** (Figure 1.8) inhibits the NorA pump in *S. aureus* at concentrations less than 1.5 µg/mL. It was shown to potentiate the action of ciprofloxacin,[98] where it decreased the IC_{50} 2.5-fold at an 8-fold lower concentration than reserpine. A decrease in cell viability recorded during these experiments using OD600 measurements showed that viability in the presence of 0.13 µg/mL ciprofloxacin alone was 3 x 10^7 CFU/mL. In the presence of reserpine (20 µg/mL) the number was reduced to 5 x 10^4 CFU/mL and to 1.2 x 10^5 CFU/mL with INF 271 (2.5 µg/mL) present.

Isoflavones **22-28** (Figure 1.10) isolated from *Lupinus argenteus* potentiate the activity of berberine and norfloxacin.[104] In one report INF271 **16** was studied alongside isoflavones to compare their EPI activities and berberine potentiation effects.[105] Accumulation of berberine in *S. aureus* cells alone and in the presence of the

isoflavones and INF271 **16** showed that INF271 was more potent. The results also suggested that there may be MDR pumps in *S. aureus* other than NorA that are inhibited by INF271.[105]

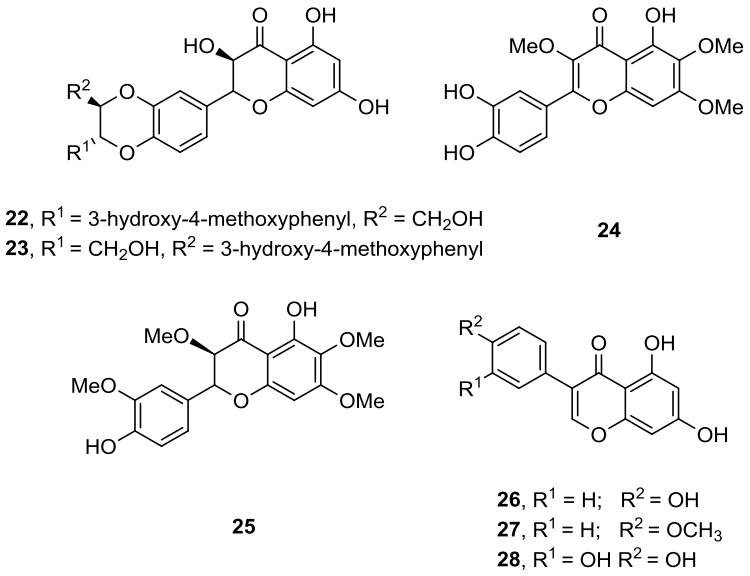

Figure 1.10 Examples of isoflavone-based EPIs.[105]

Studies have shown that INF271 and some plant-based EPIs strongly increase the penetration rate and accumulation of berberine in *S. aureus* cells.[98,106] This synergy has also been observed in some Gram-negative bacteria.[107] A study by Lewis *et al* examined the effects of INF271 **16** and MC-207 110 **1** on berberine accumulation in *S. enterica, S. typhimurium, Pseudomonas syringae, Xanthomonas campestris, E. carotovora* and *Sinorhizobium meliloti*.[107] Strongly elevated rates of accumulation of berberine were observed with MC-207 110, INF271 and both compounds together, and similar results were observed with other weak antibacterial compounds. For instance, coumestrol alone showed very little antibacterial activity against *Agrobacterium*

tumefaciens (MIC 500 µg/mL) but in the presence of INF271 and MC-207 110 its MIC decreased to 125 µg/mL. Greater increases in coumestrol activity were observed with other bacteria. For example, *p. aeruginosa* strains (MIC 500 µg/mL) expressing the MexAB pump showed 300-fold increases in sensitivity when INF271 and MC-207 110 were present.[107]

German *et al* have described hybrid compounds containing fluoroquinolone antibacterials covalently linked to various EPIs, including INF271-based hybrids **29** and **30**, as well as dipeptide-based hybrids **31** and **32** (Figure 1.11).[108] One of the conjugates significantly inhibited MexAB-mediated ethidium bromide efflux in *P. aeruginosa* and dipeptide-based conjugates **31** and **32** showed no inhibition of ethidium efflux in either NorA or MepA expressing *S. aureus* and *P. aeruginosa* strains. In contrast, the ofloxacin-based conjugate **29** was a potent inhibitor of NorA and MepA-mediated efflux in *S. aureus*. One conclusion from this study was that inhibition of NorA by conjugates **29** and **30** was not simply due to the attached INF271, but was probably a consequence of the entire structure of the molecules.

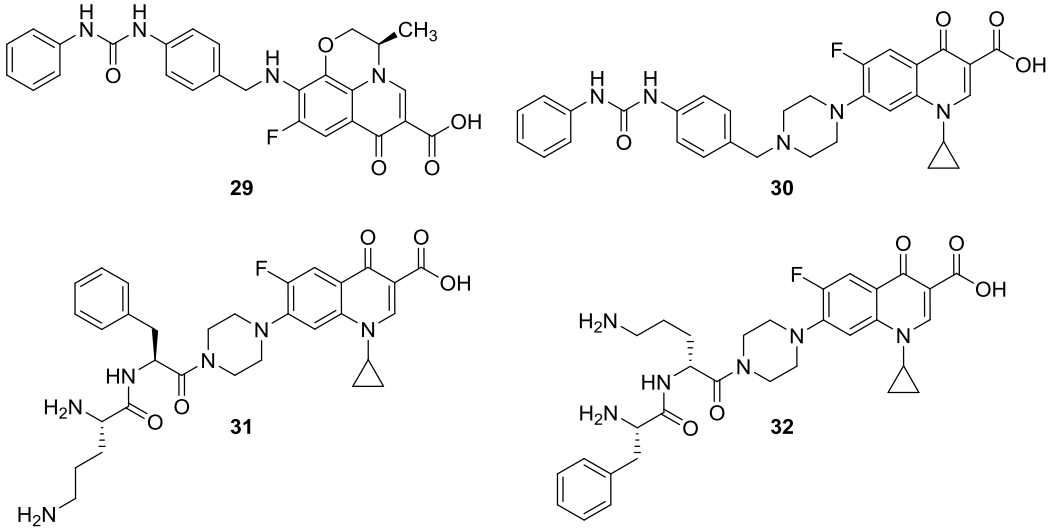

Figure 1.11 Fluoroquinolone-EPI hybrids reported by German *et al*.[108]

1.7 Photodynamic Therapy

Photodynamic therapy (PDT) uses the combined action of visible light of specific wavelengths and a dye or photosensitizer (PS) to generate cytotoxic reactive oxygen species (ROS), including singlet oxygen ($^1O_2$) and free radicals, to kill cells. In this approach, the administered photosensitizing compound is allowed to accumulate in and around target cells and visible light is applied[109] (Figure 1.12). The majority of PDT investigations to date have focused on its use in treating of solid tumours.

The mechanisms involved in obtaining selectivity against tumour cells during PDT are not well understood. Some characteristics of tumour cells that may play a role include high expression of low-density protein (LDL) receptors, involvement of macrophages, greater cellular proliferative rates and leaky vasculature.[110] Low *p*H and a high level of newly synthesized collagen in tumours have also been implicated.[111]

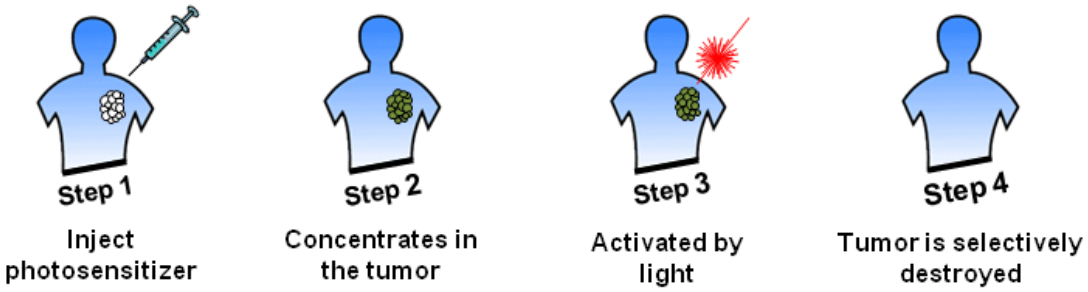

Figure 1.12 In PDT for cancer a photosensitizing compound is applied locally to lesions or injected intravenously. Healthy cells shed the drug allowing the agent to concentrate in and around cancer cells. The tumour is illuminated with an appropriate wavelength of visible light and the resulting ROS destroy tumour cells.

Lipson and Schwartz originally developed PDT at the Mayo Clinic (USA) in the 1960's to treat tumours during surgery.[112] When using a fluorescent tumour localizing

hematoporphyrin derivative they found that injecting crude preparations of the compound led to fluorescence of neoplasms upon illumination. Schwartz later treated the hematoporphyrin preparations with acetic acid and sulphuric acid to create a porphyrin mixture with improved tumour-localizing properties.[113] The mixture, termed hematoporphyrin derivative (HPD), was less active,[114] however, as it contained porphyrin monomers, dimers and oligomers. Partial purification to remove the less active porphyrins led to Photofrin®,[115] which remains the most widely used 1st-generation PS for clinical PDT.

One shortcoming of Photofrin® is that it causes long-lasting skin phototoxicity.[116] Another issue is that it absorbs light only up to about 640 nm, which cannot penetrate well through tissues. Second generation PSs were thus created to absorb light of longer wavelengths (650-850 nm). Examples include porphyrin derivatives and other compounds made after the late 1980's.[114] Third generation agents for anti-tumour PDT are showing increasing complexity, where PSs have been conjugated to tumour targeting monoclonal antibodies and other biologicals.[117]

The therapeutic uses of PDT continue to expand into various non-oncological indications, which include macular degeneration, autoimmune disorders and dermal pathologies.[118] A more recent area of research is antimicrobial photodynamic therapy (aPDT), where PDT is used to treat localized bacterial, fungal, viral and yeast infections.[119] A key driver of efforts to create effective aPDT treatments as alternative to antibiotics has been the global emergence of antibiotic resistance.[120]

1.8 Antimicrobial Photodynamic Therapy (aPDT)

The concept of aPDT was first described in 1900 by Oskar Raab in Munich.[121] Very little further work was done in the early 20th century, however, due to the discovery of antibiotics, starting with penicillin in 1929.[122] The Golden Age of antibiotics followed when over half of today's commonly used drugs were discovered. Concerns about antibiotic resistance have catalysed research into novel approaches for managing bacterial infections leading to a resurgence in interest in PDT.[123]

A major advantage of aPDT is that antibiotic-resistant bacteria are as susceptible to aPDT as their non-resistant counterparts.[124] The non-specific nature of cell killing through ROS-mediated photooxidative damage means there is little possibility for resistant strains to survive during aPDT.[125]

Other advantages of aPDT that have been identified include: (1) efficacy independent of antibiotic resistance patterns, (2) extensive pathogen reduction with limited damage to host tissues, (3) removal of photoresistant strains after multiple treatments, (4) absence of microorganism recovery following treatment, (5) direct application of PSs to infected areas, (6) low cost light sources and (7) more rapid inactivation of bacterial cells compared to traditional antimicrobials.[124c,126]

While aPDT shows promise as an alternative to antibiotics for treating localized infections, key issues still need to be addressed. These are: (1) ensuring that the treatment destroys sufficient numbers of disease-causing pathogens, (2) selectivity of PSs for bacterial cells over mammalian cells and (3) preventing recurrence of infections due to regrowth of small numbers of cells that survive treatment.[127]

In aPDT for localized infections, the PSs can be directly applied to the infected area via topical application, instillation, interstitial injection or through use of aerosols.[127] For a PS to be effective it should selectively accumulate around (or even better inside) target cells. Selective localization is facilitated by the net charge on PSs and the surface charges present on targeted cells. Gram-positive bacteria have a thick cell wall composed largely of peptidoglycan (~ 90%, c.f. 20% for Gram-negatives), along with teichoic acids, polysaccharides and peptidoglycolipids. The net negative charge of bacterial cell walls thus enables favourable electrostatic interactions with cationic PSs.[118] Indeed cationic PSs have been shown to be more effective at lower concentrations than neutral or anionic compounds in aPDT.[118,128]

Ideally, aPDT produces selective killing of pathogens whilst leaving host cells unharmed. Techniques for achieving selective killing include short incubation times, low PS concentrations and soft irradiation.[118] The external structures of bacteria targeted by ROS lead to cell death, so the PSs don't actually need to penetrate into bacteria. However, if the compounds could be concentrated inside bacterial cells it is predicted that the aPDT would become more effective due to increased potency and selectivity.[129]

1.9 Mechanisms of aPDT

The basic premise of aPDT is to use photoactive dyes that upon irradiation with visible light are able to generate toxic ROS to kill bacterial cells. When the dye absorbs light it is excited from the ground state to an excited singlet state that subsequently loses energy via three pathways: (1) non-radiative processes, where the excited state species release excess energy as heat through vibrational relaxation, internal conversion and intersystem crossing; (2) radiative processes, where excess energy is lost through

fluorescence and/or phosphorescence and (3) other processes, where the excited molecules undergo photochemical or photophysical reactions (i.e. photosensitization). When molecular oxygen is involved in the photosensitisation event such processes are called photodynamic action. Two different mechanisms of photodynamic action are possible and are termed Type I and Type II processes (Figure 1.13).

In Type I processes, the PS in its singlet or triplet excited state reacts with a substrate through electron transfer or via a hydrogen abstraction to yield unstable and reactive radicals (i.e. hydroxyl radicals and superoxide), which can further react with molecular O_2 to form peroxyl radicals. In Type II processes, the PS in its triplet excited state transfers energy to ground-state molecular oxygen and produces highly reactive singlet oxygen ($^1O_2$).

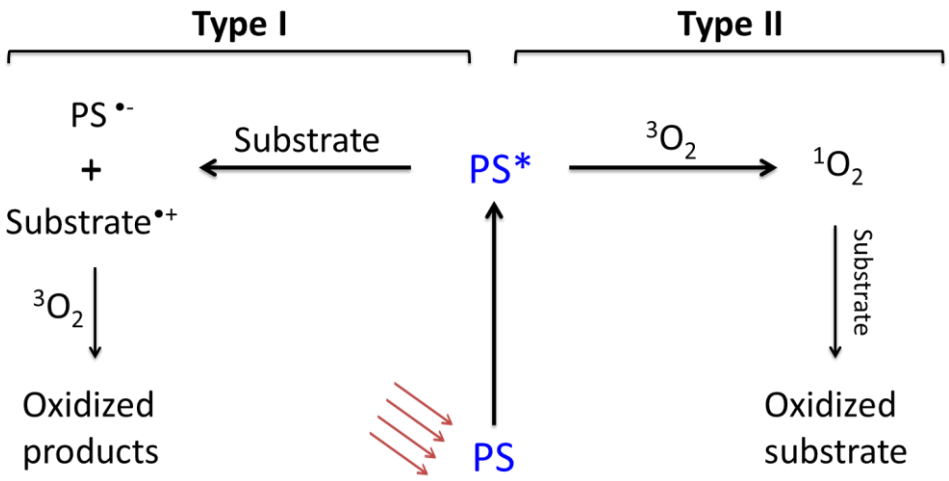

Figure 1.13 Type I and Type II processes in aPDT. PS = photosensitizer.

In bacterial cells both mechanisms lead to photooxidation of amino acids, nucleobases and lipids, leading to damaged proteins, DNA and membranes. Reactions based on Type I mechanisms have been shown to effect membrane permeability through

lipid peroxidation, causing loss of fluidity and increased ion permeability.[130] It has been suggested that Type I processes could potentially be employed in aPDT against anaerobic gut pathogens (e.g. *Clostridium difficile*) where O_2 is absent.[131] In Type II reactions, the resulting $^1O_2$ targets cell wall and membrane components (i.e. lipids, sterols and peptides). The individual reaction products from the two mechanisms can vary considerably. For instance, during Type I reactions, cholesterol is converted to cholesterol-7α and 7β-hydroperoxide but is converted to the 5α-isomer by $^1O_2$ in Type II reactions.[132]

Nucleic acids are targeted by both Type I and Type II processes. Hydroxyl radicals formed in Type I mechanisms can attack the sugar moiety of nucleic acids, while $^1O_2$ from Type II reactions targets guanine bases. These genotoxic events can cause base substitutions, strand cleavage, mutations and inhibition of replication.[130,133]

The types of mechanisms at play during aPDT depend on the PS used. Most photosensitizers are highly conjugated aromatic molecules capable of forming long-lived triplet states. The amount of energy required for production of ROS depends on the individual structures.[124a]

1.10 Photosensitizers in aPDT

Photosensitizers are defined as molecules that when activated by radiation or light cause nearby molecules to undergo chemical reactions.[119a] PSs for use in aPDT ideally display the following properties:[118,134]

(1) Efficacy against several classes of microorganisms at relatively low concentrations and low light fluence.

(2) Low toxicity in the absence of light (i.e. low dark toxicity).

(3) Selectivity for microbial cells over human cells.

(4) Hydrophilic character and net positive charges to allow better interactions with microbial cell walls.

(5) High extinction coefficients that allow efficient absorption of blue or red light.

(6) High superoxide and/or singlet oxygen quantum yields.

Over 400 compounds are known to exhibit photosensitizing properties, including dyes, drugs, cosmetics and many natural substances. The majority of PSs can be divided into three structural classes; the tricyclic dyes, tetrapyrroles and furocoumarins.[119a] The class relevant to this PhD project was the tricyclic phenothiazinium dyes.

1.10.1 Phenothiazinium Dyes as Photosensitizers

Phenothiazinium dyes have been reported as effective photosensitisers that inactivate a wide range of microorganisms upon illumination with red light. An important property of aPDT with these dyes is that bacteria that show resistance to frontline antibiotics like methicillin and vancomycin are easily inactivated.[135] Importantly, members of the class are also known to be relatively nontoxic to humans[136] and are currently used for aPDT disinfection of blood products.[137]

Phenothiazinium dyes are hydrophobic cationic salts that show limited permeability across cell membranes. They exhibit strong reactivity towards proteins, lipoproteins and nucleic acids upon illumination. Methylene blue (MB) **33** (Figure 1.14) is the parent member of the class. Various substituents around the phenothiazinium core

can have a pronounced effect on photochemical properties, e.g. maximum absorption wavelength and lipophilicity.[138] Variations in these properties can affect the type and cellular location of photodamage. Cellular uptake is also affected by a combination of charge type/distribution and lipophilicity, which vary with substituents patterns.[139]

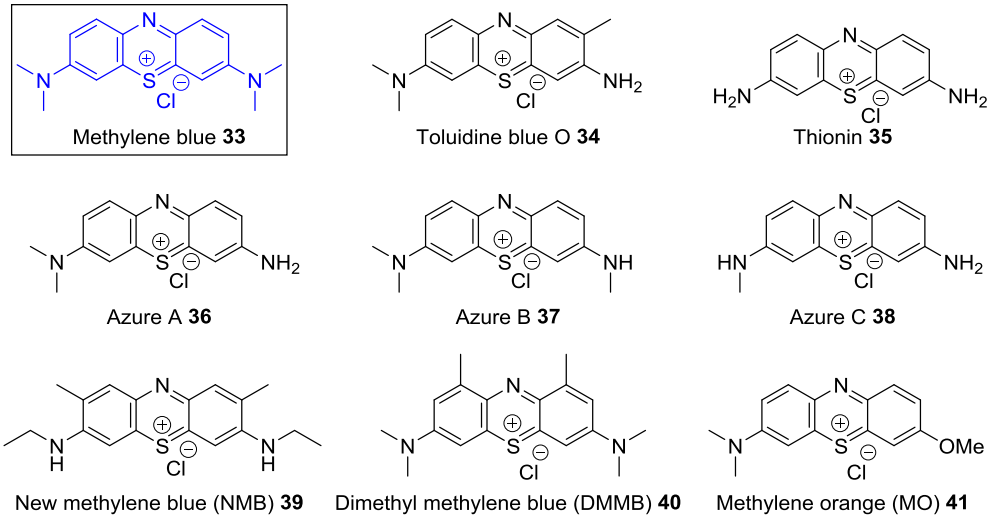

Figure 1.14 Methylene blue (MB) and related phenothiazinium photosensitizers.

Phenothiazinium PSs related to MB include toluidine blue O (TBO) **34**, thionin **35**, azure A **36**, azure B **37**, azure C **38**, new methylene blue (NMB) **39**, dimethyl methylene blue (DMMB) **40** and methylene orange (MO) **41** (Figure 1.14). The compounds are all planar, tricyclic, aromatic molecules with an intrinsic positive charge and they all show an intense absorption band between 600 - 680 nm. MB and TBO are used clinically in aPDT.[137a]

1.10.1.1 aPDT with Methylene Blue (MB)

aPDT with MB is used to sterilize blood products, where it serves to inactivate HIV, hepatitis B and C and other viruses.[137e] MB has also been used to treat

methemoglobinemia in humans and has been investigated clinically as a PDT photosensitizer in the treatment of bladder cancers, adenocarcinomas, inoperable esophageal tumours and psoriasis.[140] TBO is predominantly used in aPDT as an oral disinfectant for sterilizing dental cavities and root canals and for treating periodontitis[141]

aPDT with intravenously administrated MB has been examined against various Gram-positive and Gram-negative bacteria.[142] Wainwright *et al* have demonstrated the photobactericidal activity of MB during aPDT against VRE and MRSA.[143] The hydrophilicity of MB along with its low molecular weight and positive charge are thought to facilitate its passage across porin channels in the outer membrane of Gram-negative bacteria. Studies have demonstrated the promising photodynamic action of MB on *E. coli*.[144]

Inactivation of bacteria by MB during aPDT can occur via both Type I and/or Type II processes, depending on the cell type being studied and the experimental conditions. For example, Type I processes occur when the photodynamic action of MB is coupled to reduction of the photoexcited dye by nicotinamide adenine dinucleotide (NADH).[145]

The photochemical properties of MB (and its analogues) make it highly suitable for aPDT. It exhibits $^1O_2$ quantum yield upwards of 0.5, it has a low reduction potential and shows an intense absorption maximum around 664 nm in water.[146]

The absorption spectrum of MB is concentration-dependent due to dimerisation, with the equilibrium constant for dimerization in water being 3.8×10^3 M^{-1}.[146c] MB monomers and dimers show different absorbtion spectra, with monomers showing a

maximum at 664 nm that shifts to 590 nm for dimers. Monomers and dimers can be involved in different kinds of photochemical reactions and can affect the mechanisms and efficiency of cell killing.[146c,147] Use of MB to treat a patient with an arm tumour revealed that in 20 μM aqueous solutions only MB monomers were present, while after local injections of a 2% MB solution the absorption maximum shifted to 580 nm, indicating the presence of dimers.[146c]

Singlet oxygen is produced in Type II processes from MB where its triplet state energy is transferred to oxygen. Singlet oxygen is also formed from MB in Type I processes when reducing agents donate an electron to triplet MB to form semi-reduced radicals.[146c] Different concentrations of MB can influence which mechanisms predominate. At high MB concentrations, where the compound exists mostly as dimers, Type I reactions are limited.[146c] In homogeneous monomer solutions MB produces a high quantum yield of singlet oxygen.[148] The *p*H of solutions can also influence whether MB undergoes Type I or Type II processes. MB has been shown to be less active at lower *p*Hs due to lower $^1O_2$ quantum yields.[149]

MB can distribute into subcellular compartments like lysosomes and mitochondria. As a cation, MB is attracted to the negative electrochemical environment of the mitochondrial matrix.[150] Once localized in mitochondria, the optical density of MB at the excitation wavelength changes, as does its $^1O_2$ quantum yield.[151] It is thought that decreases in $^1O_2$ as MB accumulates in and around mitochondria is due to formation of MB dimers. MB is sometimes referred to as a mitochondrial sensitizer as it is the only PS that can selectively oxidize mitochondrial NAD(P)H.[152]

Upon irradiation with visible light MB has been shown to liberate lysosomal enzymes from human fibroblast cells. One interesting study showed that MB localized in lysosomes can actually migrate to the nucleus, but only after light activation. The cell nucleus is also a known site of localization of MB[153] and it has been suggested that when the compound enters cells it increases the effectiveness of aPDT.[154]

1.12 Microbial Resistance in aPDT

In section 1.6 it was discussed how plants appear to use synergistic combinations of weak antibacterials and EPIs as a defence against bacterial pathogens.[155] A study by Lewis *et al* showed that the alkaloid berberine **42** (Figure 1.15), widely found in Barberry (*Berberis*) plants, co-extracts with 5-methoxy-hydnocarpin (5'-MHC). Berberine is a hydrophobic cation that exhibits weak antibacterial effects by increasing membrane permeability and via interactions with DNA.[156] Due to its positive charge it could conceivably accumulate in bacterial cells due to the electrochemical gradient across the membrane. However, hydrophobic cations are the preferred substrates of many classes of MDR pumps,[157] which is probably why its antibacterial activity is weak. Lewis & Stermitz showed that 5'-MHC, which has no antimicrobial activity on its own, strongly potentiates the antibacterial activity of berberine against *S. aureus* through inhibition of efflux,[158] indicating that it is the berberine/5'-MHC combination that provides plants with antibacterial defence (Figure 1.15).

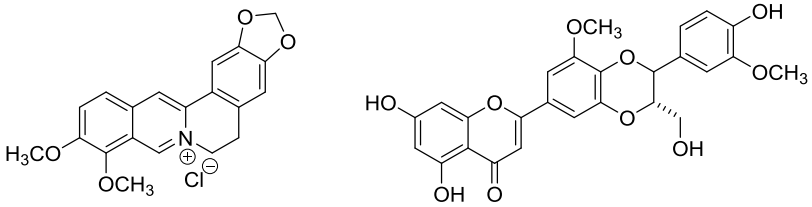

Figure 1.15 Structures of berberine (antibacterial) and 5'-MHC (EPI).

Like berberine, MB **33** is a planar, aromatic hydrophobic cation, which suggests it too might be a preferred substrate for microbial efflux systems. A comprehensive study by Tegos *et al* revealed that the three cationic phenothiazinium photosensitizers MB **33**, TBO **34**, and DMMB **40** are indeed all susceptible to efflux, whereas the neutral PS Rose Bengal is not.[154] The study demonstrated that MB **33** shows different uptake levels in three *S. aureus* strains varying in expression of the NorA MDR pump: i.e. NorA knockout, wild-type and NorA-overexpressing. The NorA knockout strain took up $1.22 \pm 0.22 \times 10^9$ molecules/cell of MB, compared to $0.06 \pm 0.01 \times 10^9$ for the wild type and $0.021 \pm 0.003 \times 10^9$ for the NorA-overexpressing strain.[154] Other non-phenothiazinium PSs showed equivalent uptake across all three NorA phenotypes, demonstrating that these non-phenothiaziniums are not NorA substrates. It was suggested that efflux of phenothiazinium PSs from cells by MDRs reduces their phototoxicity upon illumination.[154]

1.13 Combination aPDT with MB and EPIs

The discovery that bacterial MDRs contribute to aPDT resistance through efflux of MB, combined with studies showing that plants use the hydrophobic cation berberine in combination with 5'-MHC to provide antibacterial defence, suggested that combinations of MB with an MDR inhibitor might increase aPDT activity.

Tegos *et al* demonstrated that the effectiveness of photodynamic inactivation mediated by MB in *S. aureus* was inversely proportional to the level of NorA expression using three *S. aureus* strains; wild-type 8325-4, NorA knockout K1758 and NorA overexpresser K2378.[154] The same strains were then used to test whether the NorA inhibitors INF271 **16**, reserpine **8** and INF55 **15** potentiate the aPDT activity of MB.

Wild-type cells incubated with MB in the presence of INF271 and illuminated at 635 nm showed light-dependent cell killing increases 2-5 log units above levels observed when INF271 was absent. No significant killing in the presence of INF271 alone was observed in the light or dark. Reserpine showed slightly better activity while similar results were obtained with INF55.[154]

Tegos *et al* showed that Gram-positive bacteria tend to show better potentiation effects in aPDT than Gram-negatives when using combinations of phenothiazinium salts and EPIs.[99a] An interesting observation was that pre-incubation of strains with EPIs produced a stronger aPDT effect than when EPIs and PSs are added together.[99a] It was suggested that this may be because of competition between EPIs and PSs for pump binding sites.

The simplest application of a combination therapy aPDT approach would be in localized dermal infections, where both the PS and light could easily be delivered to the infection site. Although some work has been done towards discovering and optimizing EPI structures for use in combination with PSs, no clinical studies have been reported. This may be because some EPIs show unacceptable toxicity when tested in rodent infection models, possibly due to the multitude of normal physiological roles of related

pumps in eukaryotic cells (e.g. p-glycoprotein).[159] Clinical development of drug combinations also presents higher regulatory barriers due to the need to prove efficacy and safety in not one, but two active agents.

1.14 MB-EPI Hybrids for use in aPDT

One strategy being explored to address the clinical challenges associated with co-administering antibacterials with EPIs is to covalently link the EPI and antibacterial components together into a single (non-cleavable) hybrid molecule.[160] Such hybrids carry the potential advantage of delivering equimolar quantities of the two agents to infection sites whilst avoiding some of the complications arising through multi-agent co-dosing.[161]

Bremner *et al* described the first such hybrid, termed SS14-O **43** in 2006 (Figure 1.16), consisting of berberine substituted at its 13-position via a methylene linkage to INF55 **15**.[162] In designing the hybrid it was reasoned that the berberine portion could show enhanced antibacterial effects due to higher intracellular concentrations arising through inhibition of NorA-mediated efflux by the appended INF55 **15** component. The hybrid was shown to accumulate in wild-type, norA-knockout and NorA overexpressing strains of *S. aureus* and showed higher antibacterial potency than berberine alone or in combination with INF55.

A follow-up study investigated the effects of varying the relative orientations of the berberine and INF55 components by comparing the activities of isomers SS14-O **43**, SS14-M **44** and SS14-P **45** (Figure 1.16).[99e] The isomers showed surprisingly similar MICs given their structural differences, which remained almost unchanged across wild-

type, norA-knockout, and NorA overexpressing *S. aureus* cells. A important conclusion from these studies was that berberine-INF55 hybrids are not substrates for NorA, although ethidium bromide uptake experiments suggested that they might also block the NorA pump.[99e] In another study, an SS14 analogue bearing an extended methylene ether linkage (**46**, Figure 1.16) was shown to have similar antibacterial properties to the other hybrids against the *S. aureus* panel.[99d]

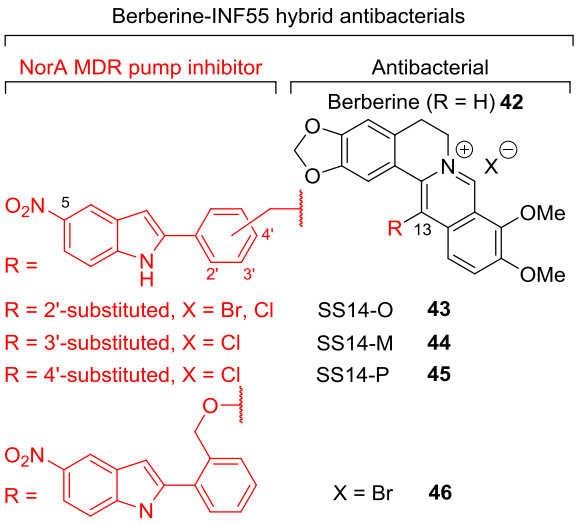

Figure 1.16 Berberine-INF55 hybrid antibacterials **43-46**.[99d,e,160a]

As mentioned previously, berberine **42** and methylene blue **33** are both amphipatic cations and thus share similar physicochemical properties. Evidence has revealed that both are also substrates for NorA efflux pumps in *S. aureus*, hinting that an MB-EPI hybrid strategy analogues to the berberine-INF55 approach might be successfully adapted in aPDT.[99a] Hybrids formed by linking MB to EPIs may decrease efflux of the PS, leading to increased intracellular concentrations and therefore increased microbial cell killing upon illumination. This idea is summarized in Figure 1.17.

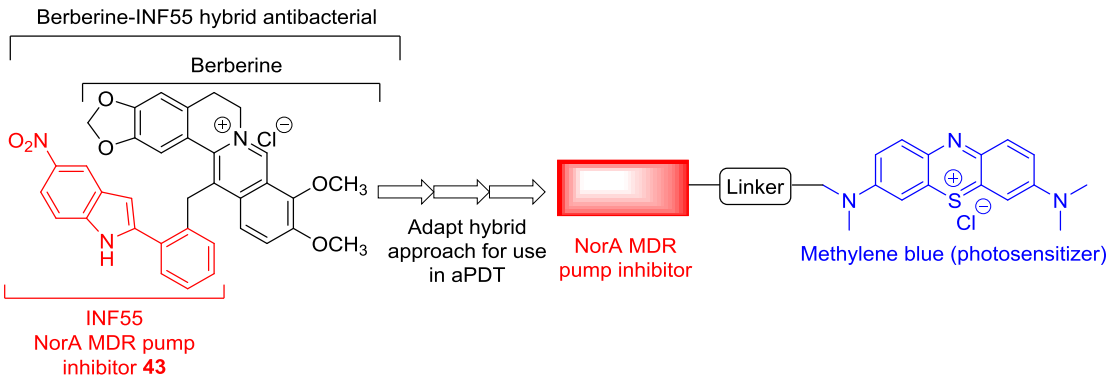

Figure 1.17 Adapting the berberine-INF55 hybrid antibacterial concept to MB-EPI hybrids for use in aPDT.

1.15 Thesis Aims

This PhD project aimed to synthesise a 16 compound library of MB-EPI hybrids and explore their potential as agents for use in aPDT. Methylene blue **33** was chosen as the PS for inclusion in the hybrids, along with the NorA pump inhibitors reserpine **8** (Section 1.6.2.1), pterostilbene **10** (Section 1.6.2.2), INF55 **15** (Section 1.6.3.1) and INF271 **16** (Section 1.6.3.2). Four different linkages between the MB and EPI portions were also incorporated into the target structures, which are shown in Figure 1.18.

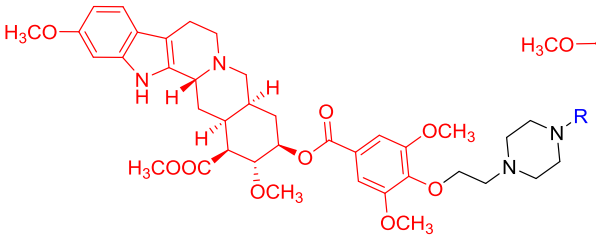

47

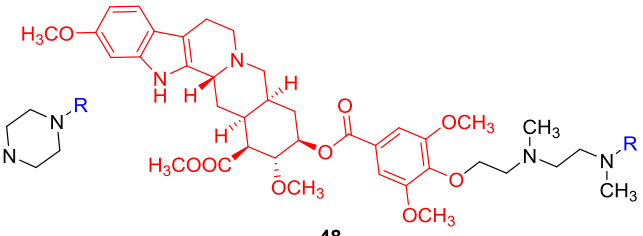

48

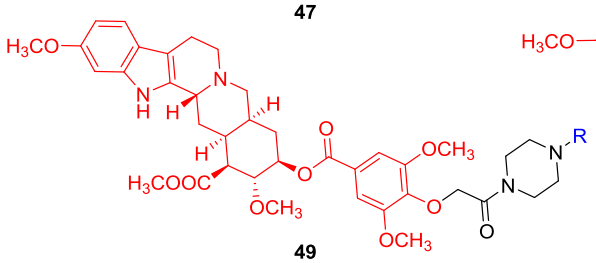

49

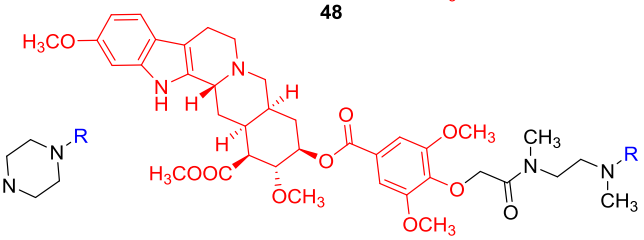

50

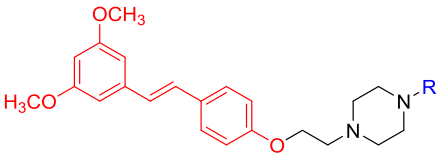

51

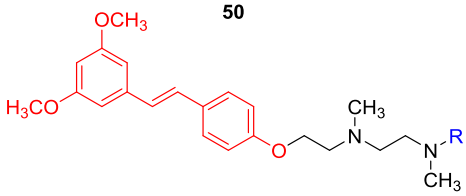

52

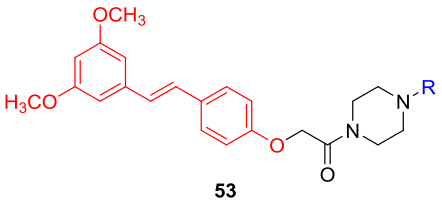

53

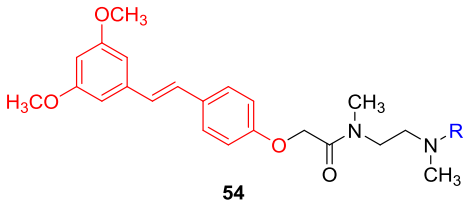

54

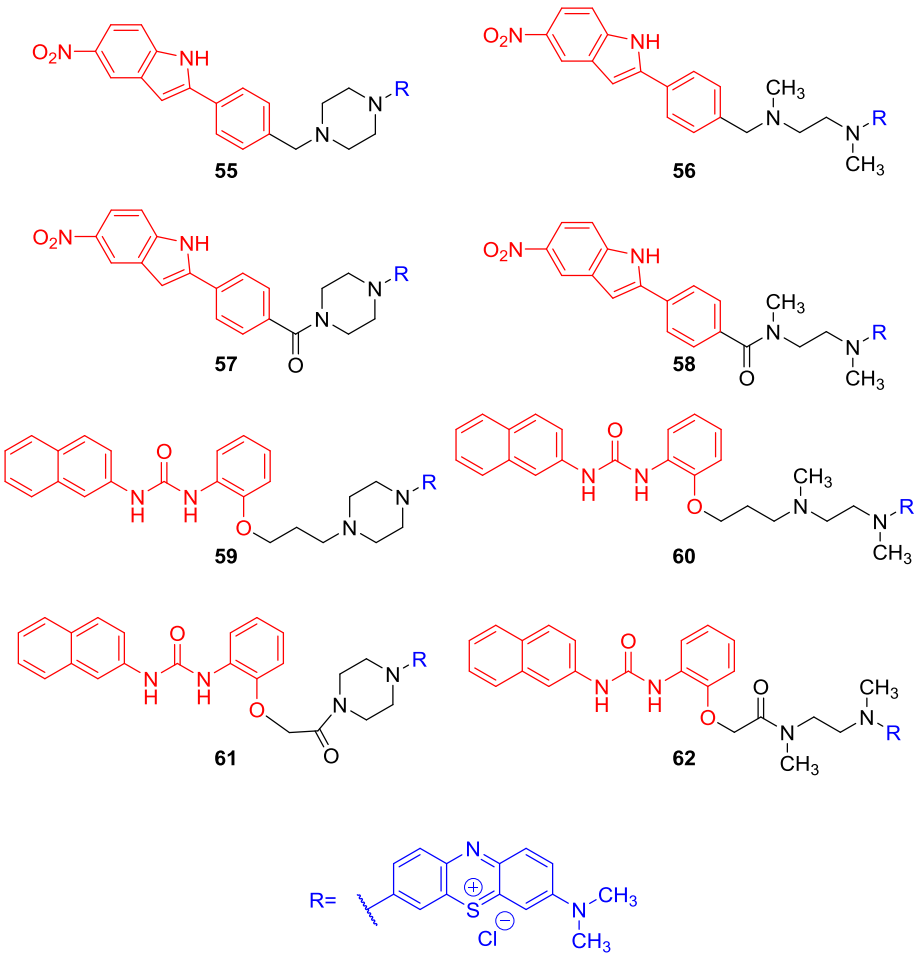

Figure 1.18 Structures of target MB-EPI hybrids. EPI portions are coloured red, linker regions black and the MB moiety blue.

We hypothesized that MB-EPI conjugates **47**-**62** might show enhanced aPDT activity (relative to MB) against *S. aureus*, which carries the NorA pump. In designing the hybrids, it was considered important that only minimal modifications be made to the phenothiazinium core to retain the photochemical properties of MB. In this way hybrids would be more likely to elicit similar spectral properties to MB and be able to undergo analogous Type I and Type II aPDT processes. Substituting the N-$(CH_3)_2$ group at the

C-7 position of MB with alkyl linkages appeared to be the best way to maintain these properties.

At the outset of the project it was not known what effect substituting EPIs with linker moieties to MB so that they could be attached would have on their NorA inhibitory activity. It was therefore considered important to prepare a library of MB-EPI hybrids with different EPIs and linkages to maximise the chances of identifying active hybrid compounds. The effects of attaching large groups to MB on its photochemical properties were also unknown, further justifying the need for a library of hybrids. Additionally, it was considered vital to explore hybrids with a range of physicochemical properties.

Four classes of hybrids carrying four different EPIs were designed giving a total of 16 target hybrids. Two examples from each EPI class were tethered to MB via *N*,*N*'-dimethylethylenediamine linkages. These two differed from each other by incorporating either alkyl or acyl attachments to the EPI. The other two examples from each EPI class carried a piperazine linker, one with an alkyl and one with an acyl attachment to the EPI. Comparing piperazine- versus ethylenediamine-linked hybrids allowed examination of the effects of rigidifying the linker, while exploring alkyl versus acyl attachments allowed modulation of physiochemical properties, especially polarity.

Chapter 2

Synthesis of MB-EPI Hybrids

2.1 General Synthetic Strategy

The synthetic strategy towards MB-EPI hybrids **47**-**62** made use of chemistry reported by Strekowski *et al* for the preparation of asymmetric MB derivatives.[163] Strekowski discovered that reactions of secondary amines with the triiodide salt of *N*,*N*-dimethylaminophenothiazinium **63** installed the amine at the 7-position (Scheme 2.1 (a)). Adapting this chemistry to the synthesis of MB-EPI hybrids required that the requisite EPI-alkyl/acyl-piperazine and EPI-alkyl/acyl-ethylenediamine-based precursors be independently prepared and then reacted with the triiodide salt **63** in the final step (Scheme 2.1 (b)).

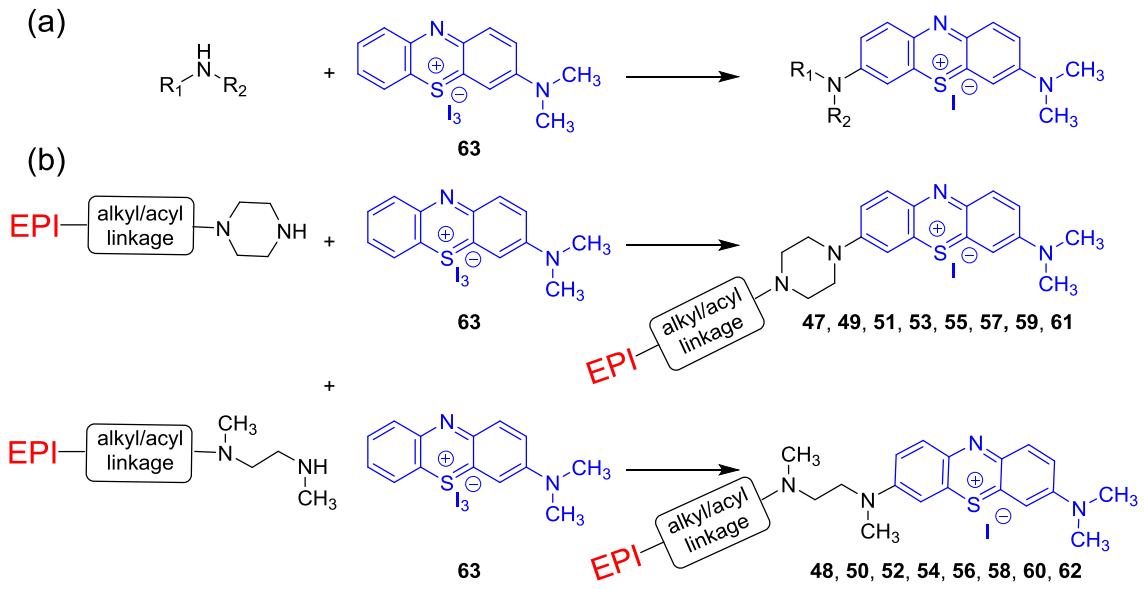

Scheme 2.1 (a) Strekowski's chemistry for the synthesis of asymmetric MB derivatives. (b) Adapting Strekowski's chemistry to the synthesis of MB-EPI hybrids containing piperazine and *N*,*N*'-dimethylethylenediamine-based linkers.

2.2 Synthesis of 3-(dimethylamino)phenothiazine-5-ium triiodide 63

Key intermediate **63** was synthesized via an adaptation of Strekowski's method.[163] In the first step, commercially available phenothiazine **64** was stirred with I_2 in wet chloroform at 5 ^oC for 4 h before being allowed to warm to room temperature. The resulting dark precipitate was washed with large volume of chloroform until no yellow washings were obtained. The tetraiodide salt **65** was obtained in 83% yield after overnight air drying (Scheme 2.2).

The salt **65** was then reacted using Strekowski's procedure with 2 eq of dimethylamine to provide **63** in 24% yield. This method involved stirring **65** for 3 h in MeOH at room temperature.[163] Strekowski reported a 24% yield for this reaction while New and Dolphin reported a 48% yield under the same conditions.[164] It was found that the yield of **63** could be improved to 60% simply by changing the reaction solvent from MeOH to 15% MeOH in $CHCl_3$. This change also yielded the pure product after simple filtration.

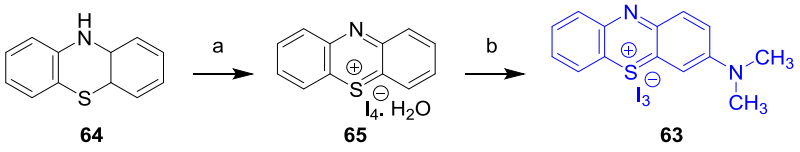

64 **65** **63**

Scheme 2.2 Synthesis of intermediate **63**.
Reagents and Conditions: (a) I_2, $CHCl_3$, rt, 4 h, 83%; (b) $(CH_3)_2NH$, MeOH/$CHCl_3$, rt, 4 h, 60%.

Carrying out this reaction required preparation of a methanolic solution of $NH(CH_3)_2$ of known concentration. This was achieved by bubbling the gas into MeOH over several minutes and determining the exact molar ratio of $NH(CH_3)_2$ to MeOH by

^{1}H NMR. The required volume was then gradually added to a stirring solution of **65** in 15% MeOH in $CHCl_3$ over 4 h at 23 ^oC. Stirring for a further 1 h at room temperature gave the desired product as a dark solid. Reaction progress was monitored by thin layer chromatography (TLC) using a solution containing 3% aqueous $NH_4OAc_{(aq)}$ in MeOH (15:85) as eluent. Under these conditions, the product **63** appeared as a dark spot with R_f = 0.43. A clear and sharp NMR spectrum was obtained for **63** in DMSO-d_6, whereas a poorer spectrum was obtained in D_2O, the NMR solvent reported by Strekowski.

2.3 Synthesis of Reserpine-Containing Intermediates 66, 67, 68 and 69

Selective demethylation of the central methyl ether in the gallic acid portion of reserpine had been reported previously using Lewis acids (BBr_3, $AlCl_3$ and pyridinium chloride Py-HCl) in a variety of solvents, including petroleum ether and EtOAc/HCl.[165] Availability of this phenolic reserpine derivative **70** indicated that MB-EPI hybrids incorporating reserpine should be obtainable by attaching linker moieties via *O*-alkylation.

After testing several reported conditions it was observed that $AlCl_3$ in CH_2Cl_2 provided the best yield of the demethylated reserpine **70**. Adding an excess (~ 50 mol eq) of finely ground $AlCl_3$ in one portion to a stirring solution of reserpine **8** in CH_2Cl_2 and then stirring for an additional 2 h at room temperature afforded **70** in 95% (lit. yield 47%).[165] The structure of **70** was confirmed by ^{1}H NMR and mass spectrometry. The ^{1}H spectrum showed the central phenolic methyl ether at 3.92 ppm had been lost and a peak at *m/z* 595.2671 was observed in the high resolution electrospray mass spectrum (HRESI-MS) corresponding to the expected $C_{32}H_{38}N_2O_9$ $[M+H]^+$ ion for **70**.

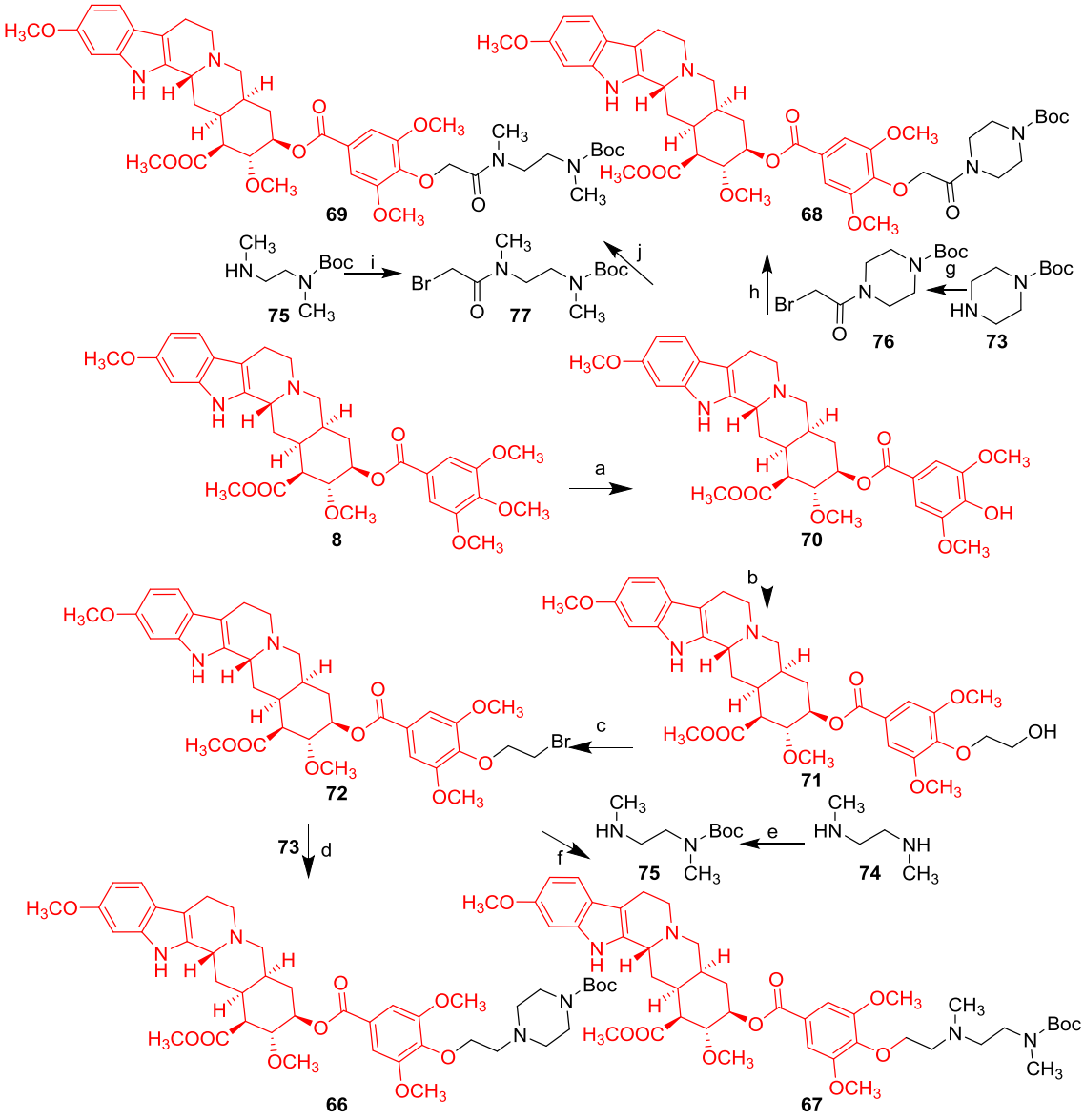

Scheme 2.3 Synthesis of reserpine-containing intermediates **66**, **67**, **68** and **69**

Reagents and Conditions: (a) $AlCl_3$, CH_2Cl_2, rt, 2 h, 95%; (b) 2-bromoethanol, K_2CO_3, DMF, 80 ^oC,16 h, 96%; (c) CBr_4/PPh_3, THF, rt, 3 h, 91%; (d) **73**, Et_3N, THF, reflux, 24 h, 80%; (e) Boc_2O, Et_3N/MeOH, 16 h, 45%; (f) **75**, Et_3N, THF, reflux, 48 h, 75%; (g) Bromoacetyl chloride, *N*,*N*-diethylaniline, acetone, 0 ^oC → rt, 16 h, 35%; (h) **76**, K_2CO_3, DMF, 80 ^oC, 16 h, 64%; (i) Bromoacetyl chloride, *N*,*N*-diethylaniline, acetone, 0 ^oC → rt, 48 h, 40%; (j) **77**, Cs_2CO_3, DMF, 80 ^oC, 24 h 70%.

O-alkylation of **70** with 2-bromoethanol was carried out in the presence of K_2CO_3 in DMF with stirring at 80 ^oC overnight. The desired alcohol **71** was isolated as a yellowish solid after silica gel column chromatography in 96% yield. The structure of **71** was confirmed by ^1H NMR spectroscopy, where two new coupled triplets were observed at 4.25 and 3.73 ppm (J = 10.0 Hz), corresponding to the new CH_2 groups. A peak at *m/z* 639.2844 was observed in the HRESI-MS corresponding to the expected $C_{34}H_{42}N_2O_{10}$ $[M+H]^+$ ion for **71**.

Bromination of alcohol **71** was achieved using standard Appel conditions[166] with CBr_4/PPh_3 in dry THF. Stirring for 3 h at room temperature gave **72** in 91% yield. The compound showed 99% purity by ^1H NMR and the HRESI-MS revealed a peak at *m/z* 701.2645 corresponding to the expected $C_{34}H_{41}BrN_2O_9$ $[M]^+$ ion for **72**.

N-Alkylation of *N*-Boc-piperazine **73** with bromide **72** in dry THF with Et_3N at reflux provided analytically pure **66** in 80% yield after 24 h. The structure of **66** was confirmed by ^1H NMR spectroscopy, where piperazine CH_2 peaks were observed as doublets at 3.41 and 2.56 ppm (J = 8.5 Hz). A peak at *m/z* 807.4188 was observed in the HRESI-MS corresponding to the expected $C_{43}H_{58}N_4O_{11}$ $[M+H]^+$ ion for **66**.

Analogous chemistry was used to prepare reserpine-containing intermediate **67** bearing an *N*-alkyl-*N*,*N*'-dimethylethylenediamine linker. *N*-Boc-*N*,*N*'-dimethylethylenediamine **75** was synthesized from the commercially available *N*,*N*'-dimethylethylenediamine **74** using literature procedure.[167] Briefly, **74** was reacted with Boc_2O in MeOH in the presence of Et_3N and after overnight stirring (monitored by TLC; EtOAc:MeOH:Et_3N, 87:10:3; stained with ninhydrin) the product **75** was isolated in 45% yield after silica gel column chromatography (Scheme 2.3). Reaction of **75** with

bromide **72** in dry THF in the presence of Et_3N at reflux afforded intermediate **67** in 75% (Scheme 2.3). The structure of **67** was confirmed by ^1H NMR spectroscopy, where *N*-methyl peaks were observed at 2.94 and 2.92 ppm as singlets and CH_2 peaks as triplets at 3.22 and 2.55 ppm (J = 10 Hz). A peak at *m/z* 809.4369 was observed in the HRESI-MS corresponding to the expected $C_{43}H_{60}N_4O_{11}$ $[M+H]^+$ ion for **67**.

Similar strategies were applied in the synthesis of intermediates **68** and **69**, which carried amide linkages from the piperazine and *N*,*N*'-dimethylethylenediamine groups to the EPIs. Commercially available *N*-Boc-piperazine **73** and the synthesized *N*-Boc-*N*,*N*'-dimethylethylenediamine **75** were coupled to bromoacetyl chloride in the presence of *N*,*N*-diethylaniline to give **76** and **77** in 35% and 40% yields, respectively. The reactions were carried out by stirring in acetone (0 ^oC to room temperature) for 16 h for **76** and 48 h for **77**.

Intermediates **68** and **69** were synthesized from phenolic reserpine derivative **70** by *O*-alkylation with **76** and **77**, respectively. The reactions were carried out using K_2CO_3 or Cs_2CO_3 in DMF at 80 ^oC and provided respective yields of 64% and 70%. A peak at *m/z* 821.3987 observed in the HRESI-MS corresponded to the expected $C_{43}H_{56}N_4O_{12}$ $[M+H]^+$ ion for **68**. A peak was similarly observed at *m/z* 823.4135 corresponding to the expected $C_{43}H_{58}N_4O_{12}$ $[M+H]^+$ ion for **69**.

2.4 Synthesis of Pterostilbene-Containing Intermediates 78, 79, 80 and 81

Intermediates **80** and **81** were synthesized from the commercially available phenolic pterostilbene derivative **9** by *O*-alkylation reactions using *N*-bromoacetyl-*N*'-Boc-piperazine **76** and *N*-bromoacetyl-*N*'-Boc-*N*,*N*'-dimethylethylenediamine **77**, respectively (Scheme 2.4). The reactions were carried out using K_2CO_3 in DMF at 80 ^oC and gave identical yields of 77%. Intermediate **80** showed a peak at *m/z* 505.2331 in the HRESI-MS, corresponding to the expected $C_{27}H_{34}N_2O_6$ $[M+Na]^+$ ion. A peak at *m/z* 507.2486 was observed for **81**, corresponding to the expected $C_{27}H_{36}N_2O_6$ $[M+Na]^+$ ion.

O-Alkylation of **9** with 2-bromoethanol in the presence of K_2CO_3 afforded the phenoxyethyl alcohol **82** in 90% yield after overnight stirring in DMF at 80 ^oC. The ^1H spectrum of **82** showed two characteristic triplets for the new ethyl group at 4.31 and 3.65 ppm (J = 12 Hz). The Appel reaction was used for bromination of alcohol **82**, where stirring with CBr_4/PPh_3 in THF for 3 h at room temperature afforded bromide **83** in 94% yield. A peak at *m/z* 362.0524 observed in the HRESI-MS corresponded to the expected $C_{18}H_{19}BrO_3$ $[M]^+$ ion for **83** (Scheme 2.4).

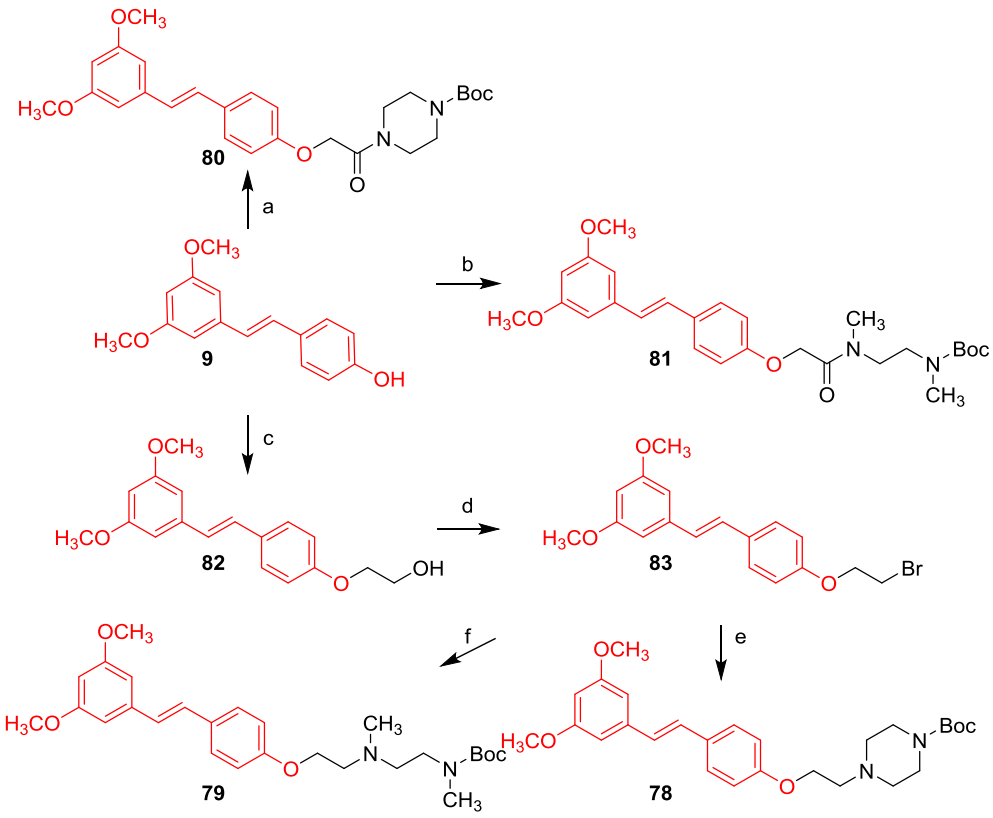

Scheme 2.4 Synthesis of pterostilbene-containing intermediates **78**, **79**, **80** and **81**
Reagents and Conditions: (a) *N*-bromoacetyl-*N*'-Boc-piperazine **76**, K_2CO_3, DMF, 100 ^oC, 48 h, 77%; (b) *N*-bromoacetyl-*N*'-Boc-*N*,*N*'-dimethylethylenediamine **77**, K_2CO_3, DMF, 80 ^oC, 24 h, 77%; (c) 2-bromoethanol, K_2CO_3, DMF, 80 ^oC, 16 h, 90%; (d) CBr_4/PPh_3, THF, rt, 3 h, 94%; (e) *N*-Boc-piperazine, KI (40 mol %), THF, reflux, 48 h, 87%; (f) *N*-Boc-*N*,*N*'-dimethylethylenediamine, K_2CO_3, CH_2Cl_2, reflux, 48 h, 81%.

N-alkylation of *N*-Boc-piperazine and *N*-Boc-*N*,*N*'-dimethylethylenediamine with bromide **83** afforded **78** and **79** in 87% and 81% yields, respectively. The ^1H spectrum of **78** showed characteristic CH_2 signals for piperazine at 3.43 and 2.65 ppm and the Boc CH_3 group at 1.46 ppm. A peak at *m/z* 491.4487 observed in the HRESI-MS corresponded to the expected $C_{27}H_{36}N_2O_5$ $[M+Na]^+$ ion for **78**. For compound **79**, the ^1H spectrum showed characteristic signals for *N*-CH_3 protons at 2.57 and 2.19 ppm and Boc CH_3 protons at 1.45 ppm. Ethyl CH_2 signals were also observed at 3.13 and

2.43 ppm. A peak at *m/z* 493.2364 in the HRESI-MS corresponded to the expected $C_{27}H_{38}N_2O_5$ $[M+Na]^+$ ion for **79**.

2.5 Synthesis of INF55-Containing Intermediates 84, 85, 86 and 87

INF55 methyl ester derivative **88** was synthesized by Naveen Dolla (PhD student in the Kelso Group) using the reported method.[168] Ester **88** was quantitatively reduced to the benzylic alcohol **89** using $NaBH_4$ in THF and bromination of **89** using CBr_4/PPh_3 in Et_2O/THF afforded **90** in 85% yield. The bromination reaction was carried out by stirring at room temperature for 3 h. Purification was achieved by silica gel column chromatography (Scheme 2.5).

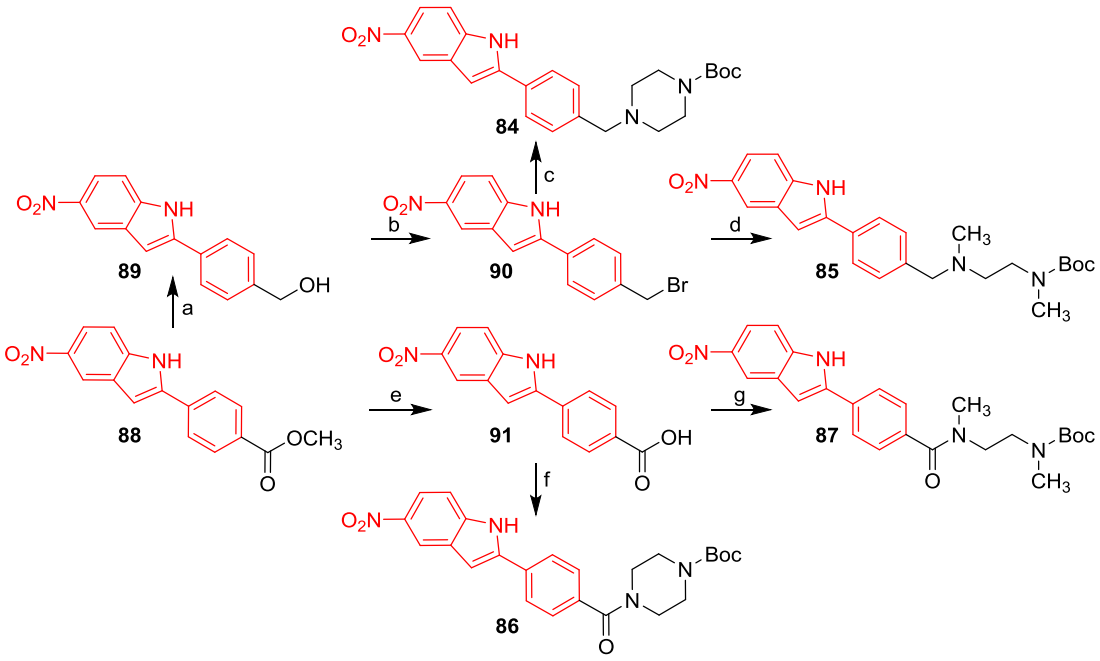

Scheme 2.5 Synthesis of INF55-containing intermediates **84**, **85**, **86** and **87**.
Reagents and Conditions: (a) $NaBH_4$, THF, rt, 24 h, quant.; (b) CBr_4/PPh_3, Et_2O/THF, rt, 3 h, 85%; (c) *N*-Boc-piperazine, KI (45 mol%), THF, reflux, 48 h, 96%; (d) *N*-Boc-*N*,*N*'-dimethylethylenediamine, KI (50 mol%), THF, reflux, 48 h, 78%; (e) NaOH, MeOH/CH_2Cl_2, rt, 30 min, then reflux, overnight, 96% (f) *N*-Boc-piperazine, HATU, DIEA, THF, rt, 5 h, 85%; (g) *N*-Boc-*N*,*N*'-dimethylethylenediamine, HATU, DIEA, THF, rt, 7 h, 78%.

Bromide **90** was reacted separately with commercial *N*-Boc-piperazine and *N*-Boc-*N*,*N*'-dimethylethylenediamine **75** in anhydrous THF in the presence of KI. After 48 h at reflux the alkylated products **84** and **85** were isolated in 96% and 78% yields, respectively, after silica gel column chromatography. The ^{1}H spectrum of **84** showed characteristic CH_2 signals for piperazine at 3.30 and 2.33 ppm and a peak at *m/z* 435.2043 observed in the HRESI-MS corresponded to the expected $C_{24}H_{28}N_4O_4$ $[M-H]^-$ ion. For intermediate **85**, the ^{1}H spectrum showed characteristic signals for the ethyl group at 3.37 and *N*-CH_3 groups at 2.66 ppm and 1.96 ppm. A peak at *m/z* 437.2180 in the HRESI-MS corresponded to the expected $C_{24}H_{30}N_4O_4$ $[M-H]^-$ ion for **85**.

Similar strategies were applied in the synthesis of INF55-containing intermediates **86** and **87** containing amide linkages between the piperazine and *N*,*N*'-dimethylethylenediamine groups and the EPI. INF55 acid derivative **91** was obtained by hydrolysing **90** with NaOH. The crude acid **91** was coupled to *N*-Boc-piperazine and *N*-Boc-*N*,*N*'-dimethylethylenediamine using HATU with diisopropylethylamine (DIPEA) as base. Stirring at room temperature in THF for 5 h and 7 h gave the Boc-protected intermediates **86** and **87** in 85% and 78% yields, respectively. The ^{1}H spectrum of **86** showed characteristic CH_2 signals for piperazine at 3.35 and 2.13 ppm and the ^{13}C spectrum showed a carbonyl signal at 171.1 ppm. A peak at *m/z* 449.1826 observed in the HRESI-MS corresponded to the expected $C_{24}H_{26}N_4O_5$ $[M-H]^-$ ion for **86**. For **87**, the ^{1}H spectrum showed characteristic CH_2 signals for the ethyl group at 3.76-3.32 ppm and *N*-CH_3 signals at 2.76 ppm and 1.67 ppm. The ^{13}C spectrum showed a characteristic signal for the amide carbonyl at 174.0 ppm and a peak at *m/z* 451.1988 observed in the HRESI-MS corresponded to the expected $C_{24}H_{28}N_4O_5$ $[M-H]^-$ ion for **87**.

2.6 Synthesis of INF271-Containing Intermediates 92, 93, 94 and 95

Synthesis of INF271-containing intermediates **92**, **93**, **94** and **95** commenced with the chlorination of 2-naphthoic acid **96** using thionyl chloride (Scheme 2.6).

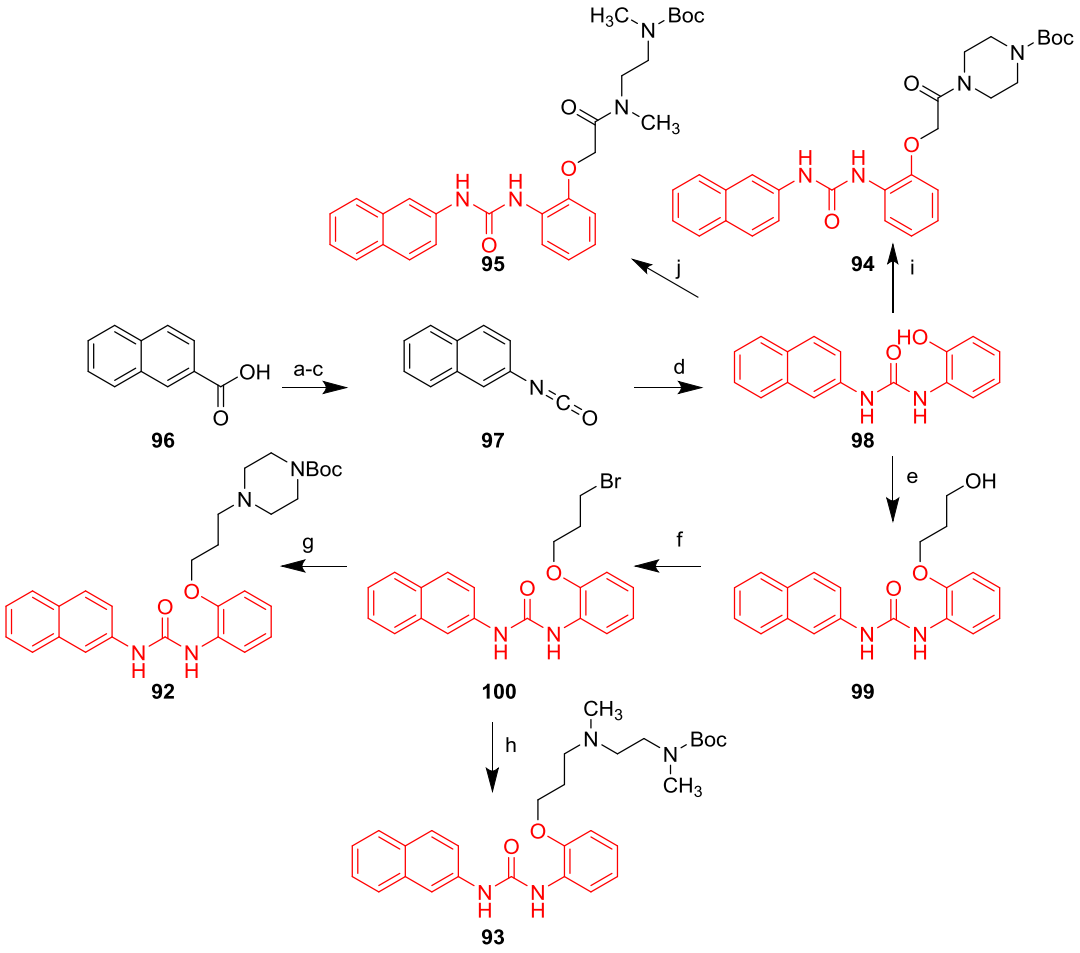

Scheme 2.6 Synthesis of INF271-containing intermediates **92**, **93**, **94** and **95**.
Reagents and Conditions: (a) $SOCl_2$, C_6H_6, reflux, 16 h, 95%; (b) NaN_3, 5% HCl, *N*,*N*-diethylaniline, C_6H_6/H_2O, rt, 16 h, 76%; (c) C_6H_6, reflux, 4 h, quant.; (d) *O*-aminophenol, CH_2Cl_2, rt, 48 h, 80%; (e) 3-bromopropanol, K_2CO_3, DMF, rt, 16 h, 75%; (f) CBr_4/PPh_3, THF, 40 ^oC, 16 h, 85%; (g) *N*-Boc-piperazine **73**, K_2CO_3, KI (25 mol%), THF, reflux, 16 h, 85%; (h) *N*-Boc-*N*,*N*'-dimethylethylenediamine **75**, K_2CO_3 KI (30 mol%), THF, 80 ^oC, 48 h, 85%; (i) *N*-bromoacetyl-*N*'-Boc-piperazine **76**, K_2CO_3, DMF, 80 ^oC, overnight, 66%; (j) *N*-bromoacetyl-*N*'-Boc-*N*,*N*'-dimethylethylenediamine **77**, K_2CO_3, DMF, 80 ^oC, overnight, 80%.

Thionyl chloride was gradually added to the solution of 2-naphthoic acid in benzene before stirring the reaction at reflux overnight. Upon consumption of the starting material (TLC; Pet. Spirit:EtOAc, 50:50) the solvent was evaporated and the residue used without further purification. The crude acyl chloride was reacted with NaN_3/HCl in a two phase solvent system (C_6H_6/H_2O) using the phase transfer catalyst *N*,*N*'-diethylaniline. After stirring overnight at room temperature the desired acyl azide was obtained in 76% yield. Quantitative conversion to isocyanate **97** was then achieved by heating the acyl azide at reflux in benzene for 4 h (Scheme 2.6). These procedures were based on the method reported by Rineh *et al*.[169]

Reaction of 2-naphthylisocyanate **97** with *O*-aminophenol in anhydrous CH_2Cl_2 at room temperature for 48 h afforded the substituted urea **98** in 80% yield. Urea **98** formed as a white precipitate that was filtered, dried under reduced pressure and used without further purification. In cases where *O*-aminophenol starting material was observed in the ^{1}H NMR spectrum of the product the mixture was washed with 1 M HCl. The ^{1}H NMR spectrum of **98** showed characteristic urea NH signals at 9.50 and 8.24 ppm and a peak at *m/z* 277.0973 observed in the HRESI-MS corresponded to the expected $C_{17}H_{14}N_2O_2$ $[M-H]^-$ ion.

O-Alkylation of **98** with 3-bromopropanol was achieved by stirring overnight at room temperature with K_2CO_3 in DMF, affording **99** in 75% yield. The ^{1}H NMR spectrum confirmed alkylation with the appearance of new CH_2 signals at 4.27, 3.65 and 1.97 ppm. A peak at *m/z* 335.1396 observed in the HRESI-MS corresponding to the molecular formula $C_{20}H_{20}N_2O_3$ $[M-H]^-$ supported formation of **99**. Bromination of **99** under Appel conditions using CBr_4/PPh_3 in dry THF at 40 ^oC gave the desired halide

100 in 85% yield after silica gel column chromatography. The ^{1}H NMR spectrum confirmed loss of the OH signal at 4.70 ppm and downfield shifting of the CH_2OH signal from 3.65 to 3.80 ppm, consistent with a CH_2Br signals. A peak at *m/z* 397.0552 observed in the HRESI-MS corresponded to the expected $C_{20}H_{19}BrN_2O_2$ $[M]^-$ ion for **100**.

Reaction of *N*-Boc-piperazine **73** with bromide **100** in the presence of K_2CO_3 and KI (25 mol%) in anhydrous THF afforded **92** in 85% yield after overnight heating at reflux (Scheme 2.6). A peak at *m/z* 505.2834 observed in the HRESI-MS corresponding to the molecular formula $C_{29}H_{36}N_4O_4$ $[M+H]^+$ supported formation of **92**. Intermediate **93** was synthesized by reacting *N*-Boc-*N*,*N*'-dimethylethylenediamine **75** with bromide **100** in the presence of K_2CO_3 and KI (30 mol%) in dry THF. A yield of 85% was obtained after heating overnight at reflux (Scheme 2.6). A peak at *m/z* 507.2971 observed in the HRESI-MS corresponded to the molecular formula $C_{29}H_{38}N_4O_4$ $[M+H]^+$ for **93**.

Alkylation of *N*-bromoacetyl-*N*'-Boc-piperazine **76** and *N*-bromoacetyl-*N*'-Boc-*N*,*N*'-dimethylethylenediamine **77** with the phenolic urea derivative **98** in DMF at 80 ^{o}C in the presence of Cs_2CO_3 gave **94** and **95** in 66% and 80% yields, respectively, after silica gel column chromatography. The ^{1}H NMR spectra for both compounds showed the presence of a Boc CH_3 group at 1.41 ppm. The ^{13}C NMR spectra showed signals for the amide carbonyl groups at 166.0 and 168.2 ppm, consistent with formation of **94** and **95**, respectively. Additional confirmation of the structures was obtained by HRESI-MS, which showed peaks at *m/z* 505.2827 corresponding to the $C_{28}H_{32}N_4O_5$ $[M+H]^+$ ion for **94**, and *m/z* 507.2598, corresponding to the $C_{28}H_{34}N_4O_5$ $[M+H]^+$ ion for **95**.

2.7 Synthesis of MB-EPI Hybrids

Completion of the synthesis of hybrids **47**, **49**, **51**, **53**, **55**, **57**, **59** and **61** with piperazine-based linkers and hybrids **48**, **50**, **52**, **54**, **56**, **58**, **60** and **62** with *N*,*N*'-dimethylethylenediamine-based linkers was achieved using Strekowski's chemistry.[163] The Boc group was quantitatively removed from intermediates **66-69**, **78-81**, **84-87** and **92-95** using TFA in CH_2Cl_2 and the crude products were subsequently reacted with phenothiazinium intermediate **63**. Stirring the deprotected amine with **63** at room temperature for 48-96 h in anhydrous CH_2Cl_2 provided the target hybrids as dark blue powders in modest yields (11-30%). Adequate quantities (25-95 mg) were obtained in all cases for photochemical and biological studies (Chapters 3-4). The quantities of hybrids produced (mg) and yield's for the Strekowski reactions are provided in Tables 2.1 and 2.2.

Table 2.1 Synthesis of hybrids with piperazine-based linkers.

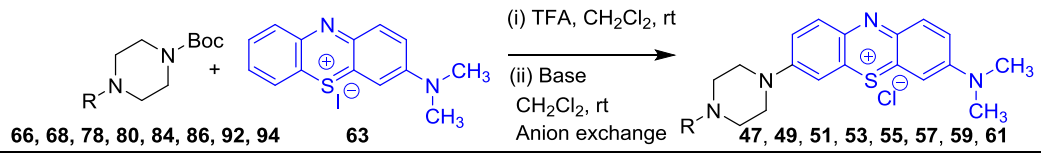

66, 68, 78, 80, 84, 86, 92, 94 **63** **47, 49, 51, 53, 55, 57, 59, 61**

Entry	R	Boc Amine	Base (eq)	Reaction time (hr)	Hybrid (mg), % Yield
1	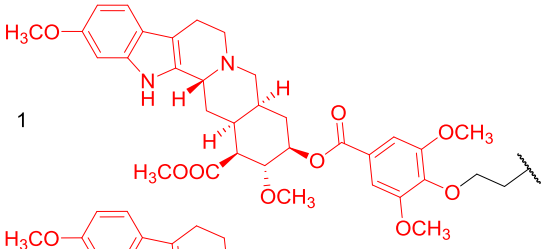	**66**	—	72	**47** (45), 18%
2	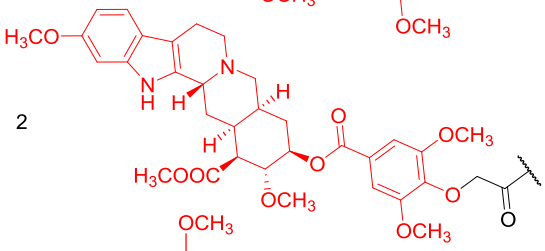	**68**	—	96	**49** (40),14%
3	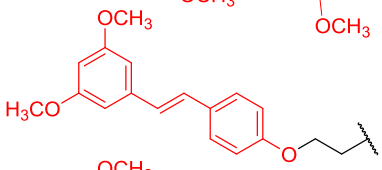	**78**	K_2CO_3 (0.3)	72	**51** (80), 26%
4	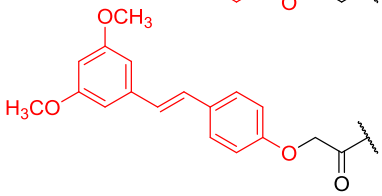	**80**	K_2CO_3 (0.2)	72	**53** (65), 30%
5	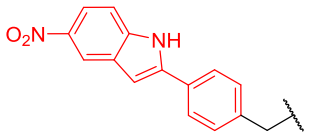	**84**	—	48	**55** (45), 23%
6	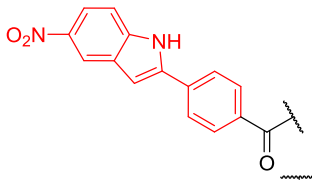	**86**	—	48	**57** (45), 18%
7	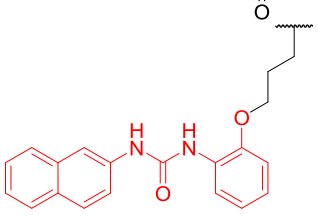	**92**	K_2CO_3 (0.3)	48	**59** (65), 25%
8	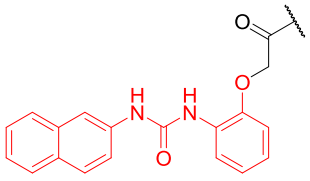	**94**	K_2CO_3 (0.3)	72	**61** (55), 17%

Table 2.2 Synthesis of hybrids with *N*,*N*'-dimethylethylenediamine-based linkers.

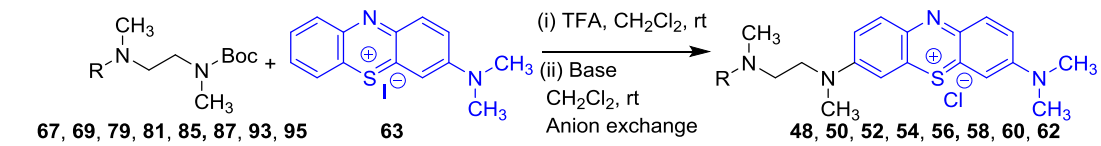

67, **69**, **79**, **81**, **85**, **87**, **93**, **95** **63** **48**, **50**, **52**, **54**, **56**, **58**, **60**, **62**

Entry	R	Boc Amine	Base (eq)	Reaction time (hr)	Hybrid (mg), % Yield
1	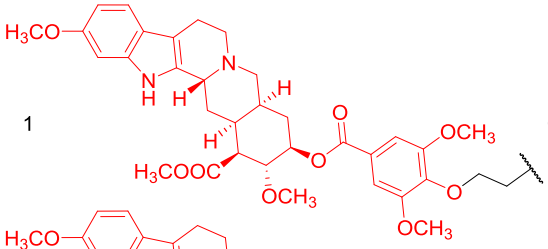	**67**	K_2CO_3 (0.4)	72	**48** (45), 18%
2	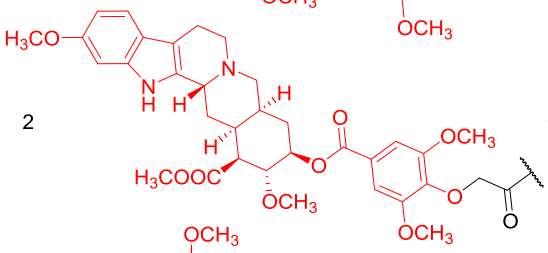	**69**	K_2CO_3 (0.4)	96	**50** (35), 11%
3	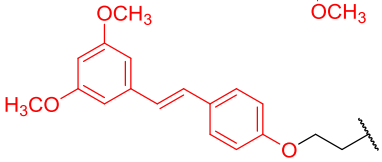	**79**	K_2CO_3 (0.4)	96	**52** (90), 14%
4	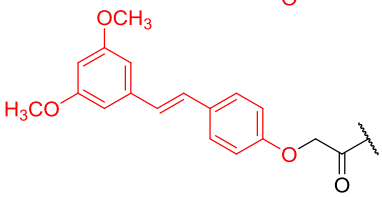	**81**	K_2CO_3 (0.2)	96	**54** (80), 14%
5	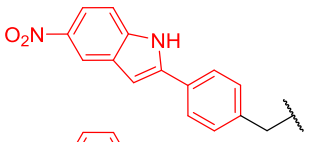	**85**	K_2CO_3	76	**56** (45), 22%
6	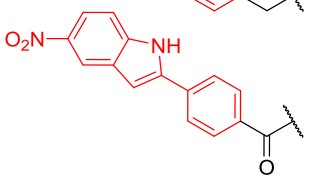	**87**	K_2CO_3	76	**58** (40), 18%
7	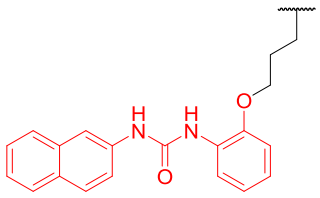	**93**	—	48	**60** (55), 25%
8	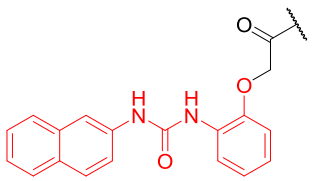	**95**	K_2CO_3 (0.3)	72	**62** (50), 15%

2.7.1 Hybrids with Piperazine-Based Linkers

Synthesis of reserpine-containing hybrids **47** and **49** with piperazine-based linkers was carried out by deprotecting the Boc groups of intermediates **66** and **68** and coupling the resulting amine trifluoroacetate salts to the C-7 position of phenothiazinium precursor **63**. Stirring for 72 h and 96 h, respectively, at room temperature in dry CH_2Cl_2 gave hybrids **47** and **49** as dark blue powders in 18% and 14% yields after preparative TLC and anion exchange to the chloride salt (Table 2.1, Entries 1 and 2). Structures of the hybrids were confirmed by HRESI-MS, which showed a peak at *m/z* 946.4276 corresponding to the $C_{52}H_{61}N_6O_9S$ $[M]^+$ ion for hybrid **47** and a peak at *m/z* 960.4063 corresponding to the $C_{52}H_{59}N_6O_{10}S$ $[M]^+$ for hybrid **49**.

^1H and ^{13}C NMR spectra for **47** and **49** were of poor quality. At this point it was noted that other papers describing related asymmetric phenothiazinium salts failed to report NMR spectra.[170] Y. Lu *et al* reported that changing the counter ion of phenothiazinium gave better NMR spectra, while J. Jahnchen used a mixture of normal and deuterium solvent to reduce peak broadening in the phenothiazinium.[170a,b] The ^1H NMR spectrum of 3-(dimethylamino)phenothiazine-5-ium triiodide **63** was found to be as expected in DMSO-d_6 solution (Figure 2.1A). However, the aromatic region of **47** and **49** showed only broadened phenothiazinium signals in all solvents. The same effect was noted for all other hybrids, except **51**. Figure 2.1B highlights this for a model compound, which contains only phenothiazine aryl protons for clarity, where the phenothiazinium peaks were noticeably broadened. Due to this effect, all hybrids except **51** were unable to be completely characterized by NMR spectroscopy. Nevertheless, all synthesized hybrids showed clean ESI mass spectra that supported their structure and

purity, as exemplified by the ESI-MS of **50** and **57** shown in Figure 2.2. LRESI-MS for some selected hybrids are provided in Appendix 2.1.

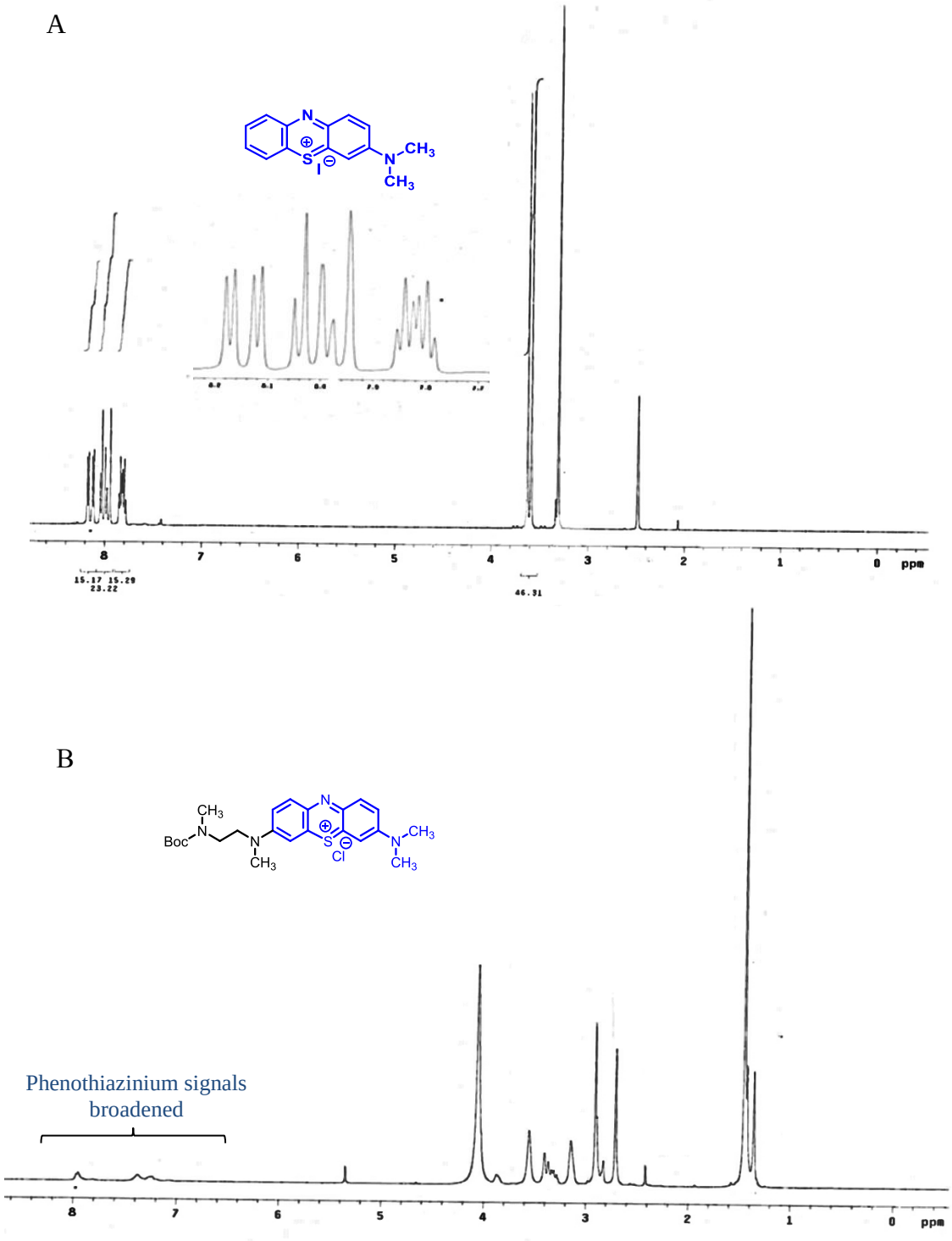

Figure 2.1 (A) ^{1}H NMR spectrum of 3-(dimethylamino)phenothiazine-5-ium triiodide **63** in DMSO-d_6; (B) ^{1}H NMR spectrum of model asymmetric substituted phenothiazinium highlighting the broadened aryl signals. Similar spectra with broadened phenothiazinium signals were observed for all hybrids, except **51**.

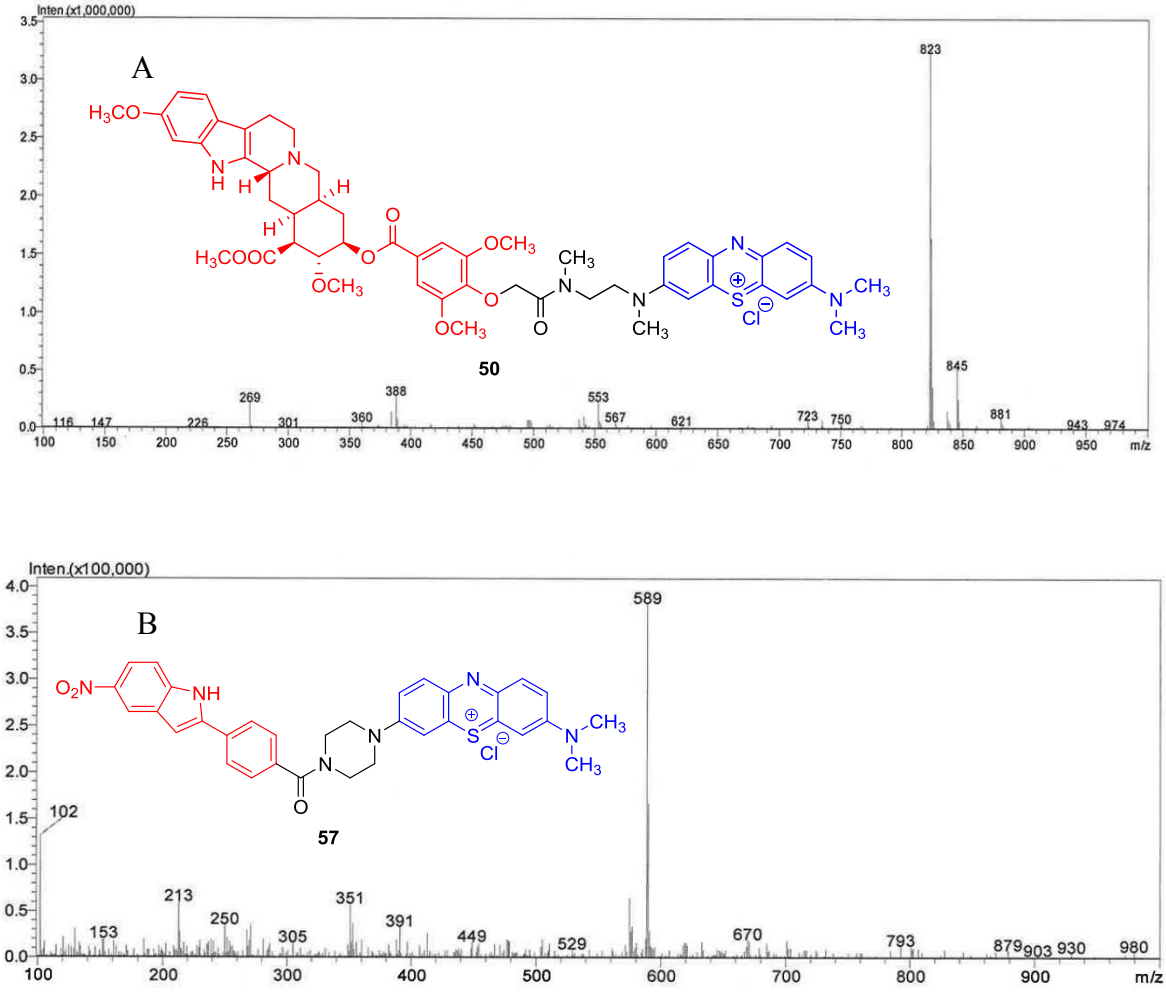

Figure 2.2 LRESI-MS of hybrids **50** and **57**

For unknown reasons the ^{1}H NMR spectrum of hybrid **51** was an exception, clearly showing the phenothiazinium signals in CD_2Cl_2 (Figure 2.3A). The structure of this hybrid was supported by its correct in the LRESI-MS (Figure 2.3B).

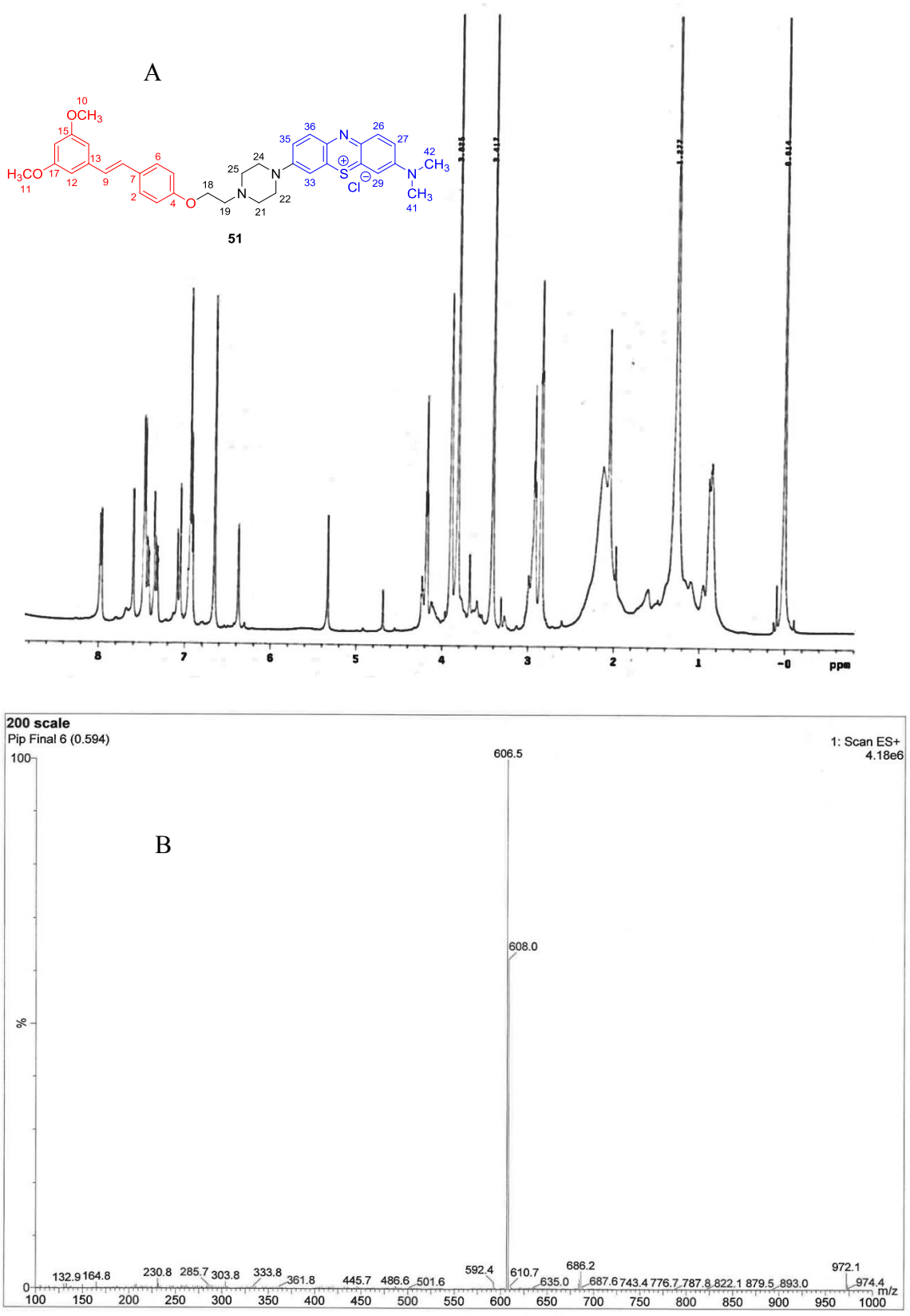

Figure 2.3 (A) ^{1}H NMR spectrum of **51** in CD_2Cl_2 clearly showing the presence of phenothiazinium signals (B) LRESI-MS of **51**.

Pterostilbene-containing intermediates **78** and **80** with piperazine-based linkers were quantitatively deprotected with TFA in dry CH_2Cl_2 by stirring for 3 h at room temperature. The crude residues were submitted to reactions with **63**. After 72 h stirring at room temperature in the presence of K_2CO_3 (0.3 eq and 0.2 eq, respectively) the hybrids **51** and **53** were isolated in 26% and 30% yields after preparative TLC and anion exchange (Table 2.1, Entries 3 and 4). A peak at *m/z* 607.2764 observed in HRESI-MS corresponding to the molecular formula $C_{36}H_{39}N_4O_3S$ $[M]^+$ supported formation of **51**. Hybrid **53** was also confirmed using HRESI-MS, where a peak at *m/z* 621.2546 corresponding to the expected $C_{36}H_{37}N_4O_4S$ $[M]^+$ ion was observed. ^1H NMR spectra lacking phenothiazine peaks were observed for these hybrids.

Synthesis of INF55-containing hybrids with piperazine-based linkers was initiated by quantitatively removing the Boc group from intermediates **84** and **86** by stirring with TFA in dry CH_2Cl_2 at room temperature for 3 h. The resulting amines were reacted with **63** in the standard way to afford hybrids **55** and **57** in 23% and 22% yields, respectively, after preparative TLC and anion exchange (Table 2.1, Entries 5 and 6). The structures were confirmed by HRESI-MS, where a peak at *m/z* 575.2229 corresponding to the $C_{33}H_{31}N_6O_2S$ $[M]^+$ ion for hybrid **55** was observed. A peak at *m/z* 589.2048 corresponding to the $C_{33}H_{29}N_6O_3S$ $[M]^+$ ion was observed for **57**. The ^1H NMR spectra lacked phenothiazine signals for these hybrids.

Synthesis of INF271-containing hybrids with piperazine-based linkers was carried out as above to provide **92** and **94** in 25% and 17% yields, respectively, after preparative TLC and anion exchange resin. A peak at *m/z* 643.2870 observed in the HRESI-MS corresponding to the molecular formula $C_{38}H_{39}N_6O_2S$ $[M]^+$ supported

formation of **92**. Hybrid **94** showed a peak at *m/z* 643.2508 corresponding to the expected $C_{37}H_{35}N_6O_3S$ $[M]^+$ ion. ^1H NMR spectra lacking phenothiazine peaks were observed for these hybrids.

2.7.2 Hybrids with *N,N*'-Dimethylethylenediamine-Based Linkers

Synthesis of reserpine-containing hybrids **48** and **50** was initiated by removing the Boc group from intermediates **67** and **69**. The secondary amines were then coupled to the C-7 position of **63** by stirring in the presence of K_2CO_3 (0.4 eq) at room temperature for 72 h and 96 h, respectively, giving **48** and **50** in 18% and 11% yields after preparative TLC and anion exchange. Structures of the hybrids were confirmed using HRESI-MS, where a peak at *m/z* 948.4423 corresponding to the $C_{52}H_{63}N_6O_{10}S$ $[M]^+$ ion for **48** was observed, as was a peak at *m/z* 961.4199 corresponding to the $C_{52}H_{61}N_6O_{10}S$ $[M]^+$ ion for **50**. Poor ^1H NMR spectra lacking phenothiazine peaks were observed with these hybrids.

Synthesis of pterostilbene-containing hybrids **52** and **54** carrying *N,N*'-dimethylethylenediamine linkers involved Boc-deprotection of **79** and **81**, followed by coupling of the crude amine TFA salts to **63**. Both reactions were stirred at room temperature for 96 h in the presence of K_2CO_3 (0.4 and 0.2 eq, respectively) to give **52** and **54** in 14% yields. Structures of the hybrids were confirmed using HRESI-MS, which showed peaks at *m/z* 609.2901, corresponding to the $C_{36}H_{41}N_4O_3S$ $[M]^+$ ion for **52**, and at *m/z* 623.2703, corresponding to the $C_{36}H_{41}N_4O_3S$ $[M]^+$ ion for **54**. ^1H NMR spectra with broadened phenothiazine peaks were observed with these hybrids.

The Boc-group was quantitatively removed from INF55-containing intermediates **85** and **87** as above before reacting each resulting amine TFA salt with **63**. The coupling reactions were carried out by stirring for 76 h at room temperature in dry CH_2Cl_2, giving hybrids **56** and **58** in identical 18% yields. The structures were confirmed using HRESI-MS, which showed peaks at *m/z* 577.2400, corresponding to the $C_{33}H_{33}N_6O_2S$ $[M]^+$ ion for **56** and *m/z* 591.2183, corresponding to the $C_{33}H_{31}N_6O_3S$ $[M]^+$ ion for **58**.

INF271-containg hybrid **60** was obtained in 25% yield after stirring at room temperature in dry CH_2Cl_2 for 48 h with Boc-deprotected amine **93**. A peak at *m/z* 645.2993 observed in HRESI-MS corresponding to the molecular formula $C_{38}H_{41}N_6O_2S$ $[M]^+$ supported formation of **60**.

Intermediate **95** carrying an amide linkage was deprotected in the usual way and then coupled to the C-7 position of **63**. Hybrid **62** was obtained in 15% after preparative TLC and anion exchange and its structure was confirmed using HRESI-MS, where a peak was observed at *m/z* 645.2663 corresponding to the $C_{37}H_{37}N_6O_3S$ $[M]^+$ ion for **62**.

A total of 16 MB-EPI hybrids were synthesized in this work. All compounds were purified by preparative TLC and converted to chloride salts using a Cl^- anion exchange resin. All coupling reactions were carried out in the absence of light to minimize photodegradation. Hybrids with *N*,*N*'-dimethylethylenediamine linkers tended to be more polar than those with piperazine linkers and more difficult to isolate. More than 35 mg of each hybrid was obtained in pure form for characterization and biological testing.

Chapter 3

Photophysical Characterization and *In Vitro* Photodynamic Activity of Hybrids against *S. aureus*

3.1 UV/Vis Spectrophotometry

The efficiency of aPDT with phenothiazinium PSs is influenced by their UV/Vis absorption properties across the range of wavelengths applied. In general, phenothiazinium PSs must exhibit significant light absorption at wavelengths > 630 nm and show high chemical stability in the presence of visible light. MB shows strong absorbance in the range 550-700 nm, with an intense maximum at λ_{max1} = 668 nm and a shoulder at λ_{max2} = 609 nm.[171]

To be an effective photosensitiser a phenothiazinium must be able to reside for a significant amount of time in the excited triplet state following excitation and intersystem crossing from the exited singlet state. For MB, the triplet excited state is sufficiently populated via conversion both radiatively (fluorescence) and non-radiatively from its relatively long-lived excited singlet state.[172] Relaxation is promoted by structural flexibility in donor-acceptor chromophoric system (i.e. the acceptor being the cationic nucleus and the donors the auxochromic amino groups), while formation of twisted intramolecular charge transfer (TICT) complexes between the phenothiazinium core and amino auxochromes has also been proposed as a relaxation route.[173] This complex allows charge separation and non-radiative relaxation and is particularly strong with *N*-aryl and *N*,*N*-dialkyl auxochromes.[174] For phenothiazinium PSs, benzannelation and the presence of heavy atoms increase the maximum absorption wavelength, while modifications at the phenothiazinium side chains tend to have lesser effects.[173]

When designing hybrids it was considered important to maintain as much of the structural features of MB as possible, making only minimal changes to one of the auxochromes. In this way the hybrids would be expected to maintain the photosensitizer

properties of MB. As discussed in Chapter 1.14, substitution of one of the C-7 *N*-Me groups of MB with *N*-alkyl or piperazinyl linkages was considered the best way to introduce the linker groups without significantly modifying MB's core structure and photophysical properties.

The effects of the structural changes introduced to MB on its absorption properties were examined by comparing the λ_{max1} and λ_{max2} values of hybrids to those of MB. These two maxima arise from the phenothiazinium chromophore, so it was predicted that these would be excellent indicators of whether the structural changes introduced in the hybrids were affecting the absorption properties of the MB portion.

UV/Vis spectra of hybrids **47**-**62** and MB were recorded at the same concentration (10 μM) and at the same temperature (23 ^{o}C) in methanol. The spectra are presented in Figure 3.1. For ease of comparison, the spectra were clustered according to the attached EPI and referred to as, for example, reserpine-containing hybrids (Figure 3.1 (a), compounds **47**-**50**). To facilitate further comparisons between the four different types of linkages, the following colour scheme has been applied in Figure 3.1:

- red = *N*-alkyl piperazine (compounds **47**, **51**, **55**, **59**)
- pink = *N*-acyl piperazine (compounds **49**, **53**, **57**, **61**)
- light blue = *N*-alkyl-*N*,*N'*-dimethylethylenediamine (compounds **48**, **52**, **56**, **60**)
- dark blue = *N*-acyl-*N*,*N'*-dimethylethylenediamine (compounds **50**, **54**, **58**, **62**)

This same colour coding system has also been applied in subsequent figures in the chapter.

a

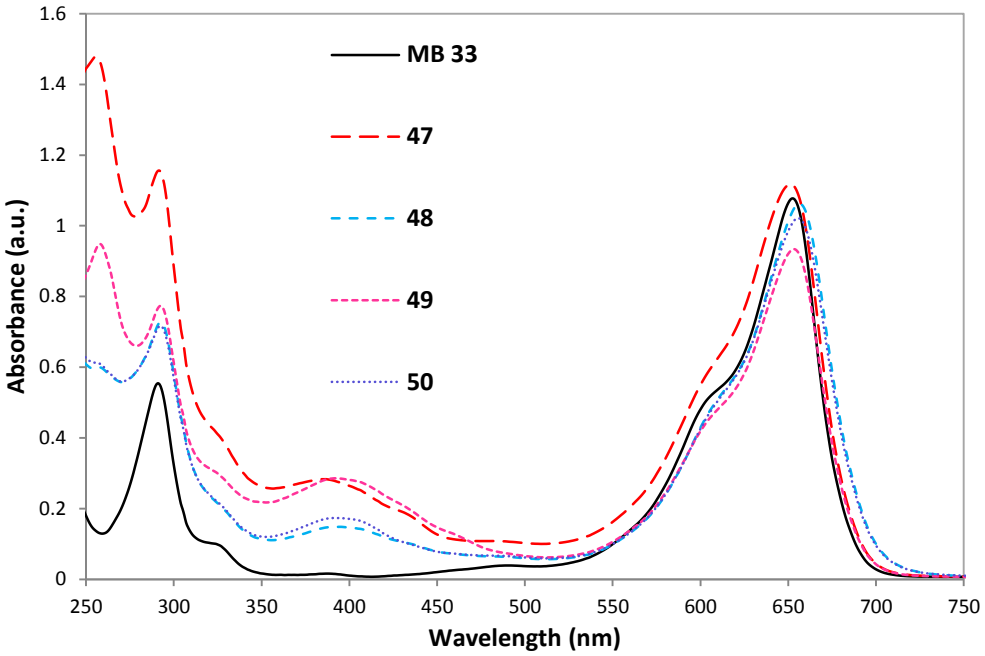
MB 33
47
48
49
50
Absorbance (a.u.)
Wavelength (nm)
0
0.2
0.4
0.6
0.8
1
1.2
1.4
1.6
250
300
350
400
450
500
550
600
650
700
750

b

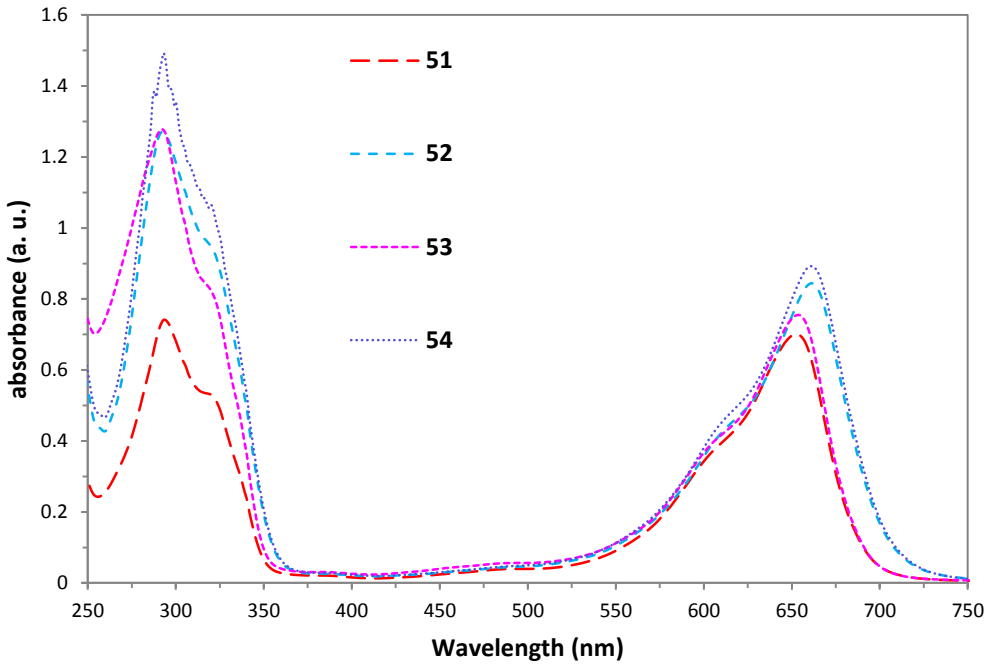
51
52
53
54
absorbance (a. u.)
Wavelength (nm)
0
0.2
0.4
0.6
0.8
1
1.2
1.4
1.6
250
300
350
400
450
500
550
600
650
700
750

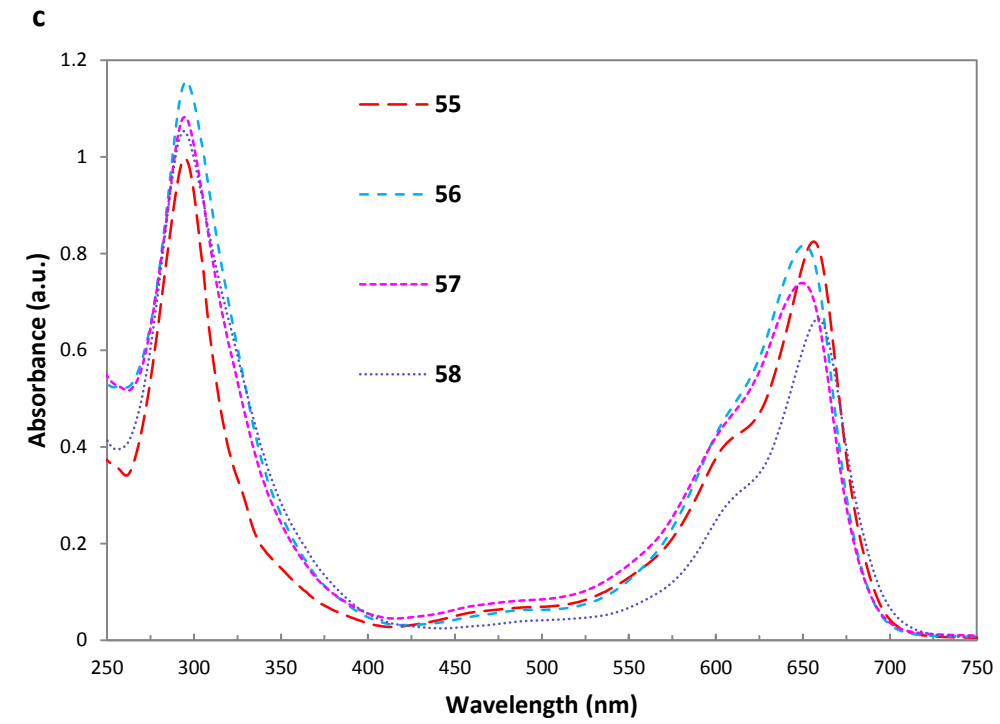

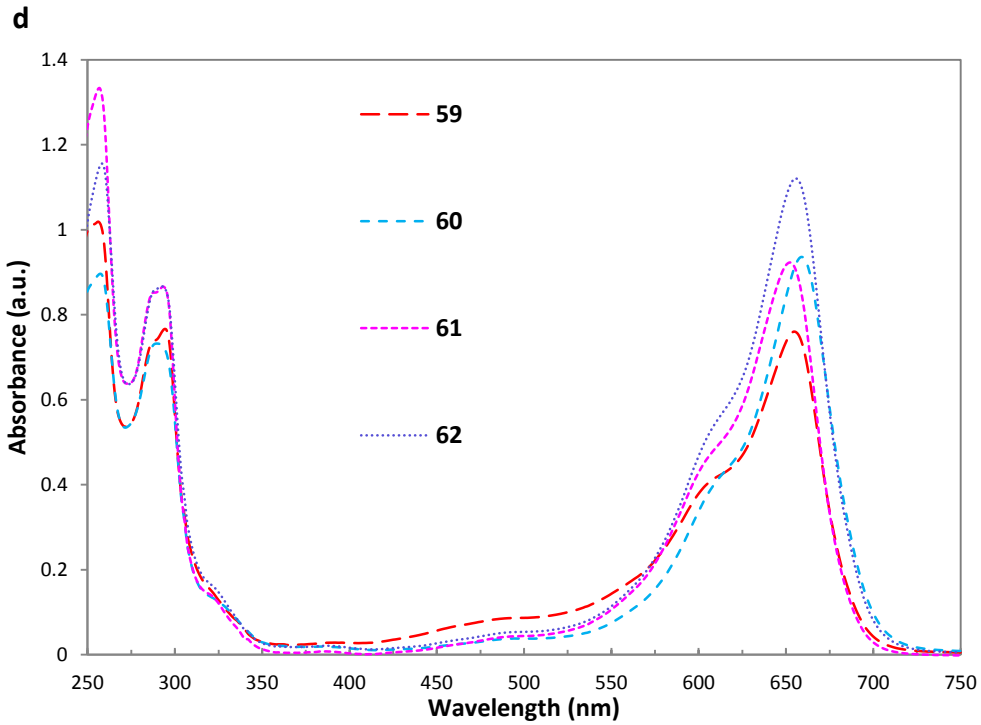

Figure 3.1 UV/Visible absorption spectra of MB **33** and: (a) reserpine-containing hybrids **47**-**50**, (b) pterostilbene-containing hybrids **51**-**54**, (c) INF55-containing hybrids **55**-**58** and (d) INF271-containing hybrids **59**-**62**. All spectra were recorded using 10 µM solutions in MeOH at 23 ^{o}C.

As shown in Figure 3.1, expected changes in lower wavelength bands (250-400 nm) were observed with the different hybrids. These arise from the different EPIs and linker groups attached to MB. The key finding was that the λ_{max1} and λ_{max2} bands arising from the MB portion of the hybrids varied only slightly from MB in wavelength and extinction coefficients across the series. This provided a clear indication that the absorption properties of the MB chromophore had not been drastically changed by introduction of the appended linker-EPI structures. A summary of the λ_{max1}, λ_{max2} and extinction coefficient (log ε) data for MB and hybrids **47**-**62** is provided in Table 3.1.

Under the conditions used, MB showed λ_{max1} = 653 nm and λ_{max2} = 612 nm. The respective extinction coefficients for the two maxima were log ε1 = 4.04 and log ε2 = 3.73. To better visualise the results, the λ_{max} data are presented graphically in Figure 3.2 and the log ε data in Figure 3.3.

Table 3.1 Summary of λ_{max1}, λ_{max2} and extinction coefficient (log ε) data for MB **33** and hybrids **47**-**62**.

Compound	**λ_{max1} [nm](log ε)**	**λ_{max2} [nm](log ε)**
MB	653 (4.04)	612 (3.73)
47	651 (4.05)	609 (3.79)
48	656 (4.02)	616 (3.74)
49	653 (3.97)	610 (3.68)
50	656 (4.00)	614 (3.72)
51	653 (3.84)	615 (3.65)
52	661 (3.93)	613 (3.61)
53	653 (3.91)	612 (3.68)
54	661 (3.95)	610 (3.64)
55	656 (3.91)	613 (3.68)
56	651 (3.91)	611 (3.69)
57	650 (3.86)	609 (3.66)
58	659 (3.82)	613 (3.48)
59	655 (3.88)	611 (3.62)
60	659 (3.97)	614 (3.63)
61	652 (3.96)	610 (3.68)
62	656 (4.05)	611 (3.74)

In Figure 3.2, the λ_{max1} and λ_{max2} values for MB were subtracted from the corresponding values in the hybrids and the differences plotted. All hybrids except **53** showed varying bathochromic (red) or hypsochromic (blue) shifts at both λ_{max1} and λ_{max2}, but the changes were all only small (< 7 nm) and the overall appearance of the bands remained unchanged. No obvious trends were observed with respect to the different EPI-linker groups attached. For instance, hybrids with piperazine-based linkers (red/pink bars) showed no clear trends that distinguish them from *N*,*N'*-dimethylethylenediamine-based linkers (light blue/dark blue bars).

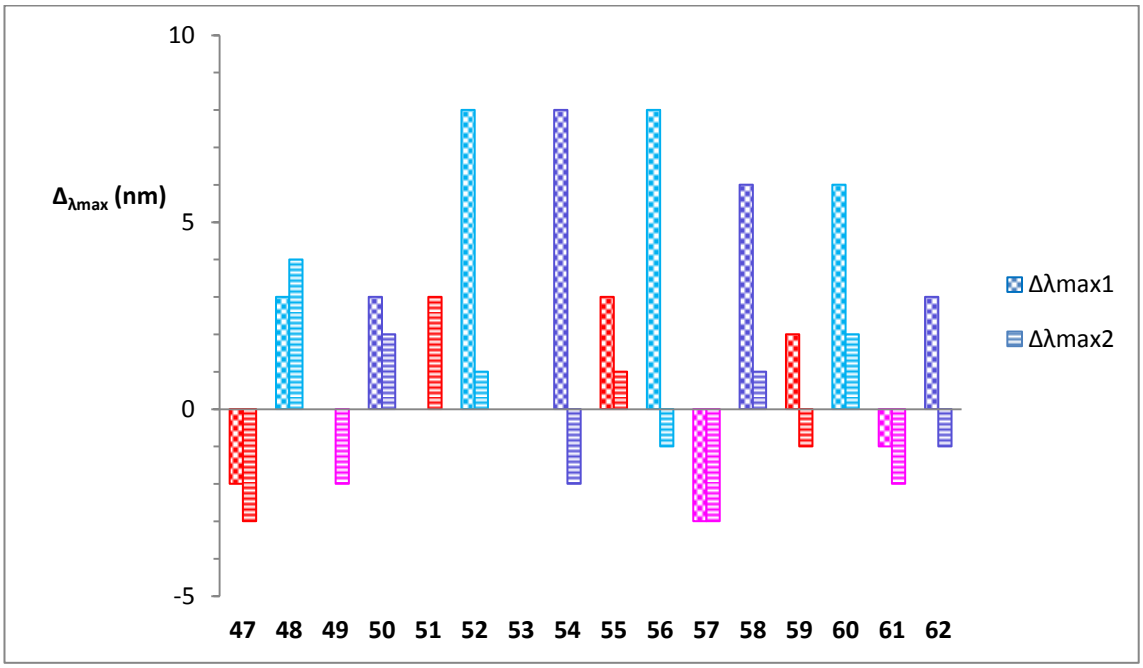

Figure 3.2 λ_{max1} and λ_{max2} data for hybrids **47-62** relative to MB. λ_{max1} and λ_{max2} values for MB were subtracted from the corresponding values for hybrids. Colour coding: red = *N*-alkyl piperazine linker, pink = *N*-acyl piperazine linker, light blue = *N*-alkyl-*N*,*N'*-dimethylethylenediamine linker, dark blue = N-acyl-*N*,*N'*-dimethylethylenediamine linker.

The extinction coefficients at λ_{max1} and λ_{max2} for **47-62** were compared to the equivalent values for MB by subtracting the log ε values for MB from the log ε values for hybrids at the respective maxima and plotting the differences (Figure 3.3).

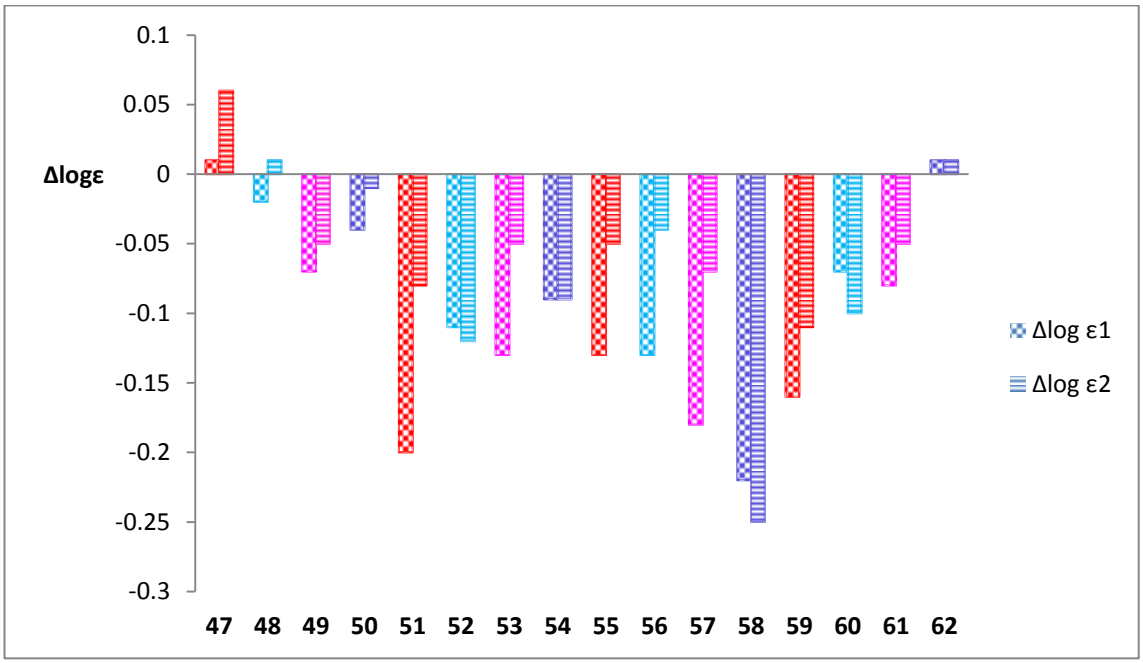

Figure 3.3 Extinction coefficient data for hybrids **47-62** at λ_{max1} (i.e. log ε1) and λ_{max2} (i.e. log ε2). Log ε values for MB (i.e. log ε1 = 4.04, log ε2 = 3.73) were subtracted from the log ε values at the respective maxima of hybrids. Colour coding: red = *N*-alkyl piperazine linker, pink = *N*-acyl piperazine linker, light blue = *N*-alkyl-*N*,*N'*-dimethylethylenediamine linker, dark blue = *N*-acyl-*N*,*N'*-dimethylethylenediamine linker.

Extinction coefficient of the hybrids were mostly lower than MB at both λ_{max1} and λ_{max2}, although the differences were all small (Δlog ε < ± 0.25). The highest Δlog ε values were observed with INF55-containing hybrid **58** (Δlog ε1 = 0.24, Δlog ε2 = 0.21). INF271-containing hybrid **62** closely matched MB showing a Δlog ε1 deviation of almost zero. Minimal Δlog ε changes were also observed in two of the reserpine-containing hybrids **48** and **50**.

In summary, the λ_{max} and log ε data confirmed that introduction of the various linker groups and EPIs to the C7-position of MB to create hybrids **47**-**62** had only a minor impact on the UV/Vis absorbtion properties of the MB chromophore.

3.2 Measurement of $^1O_2$ and •OH Production by Hybrids

As described in Chapter 1.9, when PSs are illuminated with appropriate wavelengths of light they can produce various types of ROS, including singlet oxygen ($^1O_2$), superoxide radical anion, hydrogen peroxide and hydroxyl radical (•OH). Production of these ROS by PSs can be probed experimentally by monitoring the fluorescence emitted by fluorescence-based ROS scavengers. Two such probes, singlet oxygen sensor green (SOSG) and 3'-*p*-(hydroxyphenyl) fluorescein (HPF), can be used for the selective detection of $^1O_2$ and •OH, respectively. Both probes are cell-permeable, relatively insensitive to superoxide and nitric oxide and they are resistant to auto-oxidation processes.[175]

The SOSG probe shows high selectivity for singlet oxygen and is water soluble at mM concentrations. The structure of the probe has not been released by the commercial supplier (Invitrogen) but it is believed to be a bichromophoric molecule incorporating a photoinduced electron transfer (PET) design, comprising a dimethyl anthracene moiety attached to fluorescein (Figure 3.4).

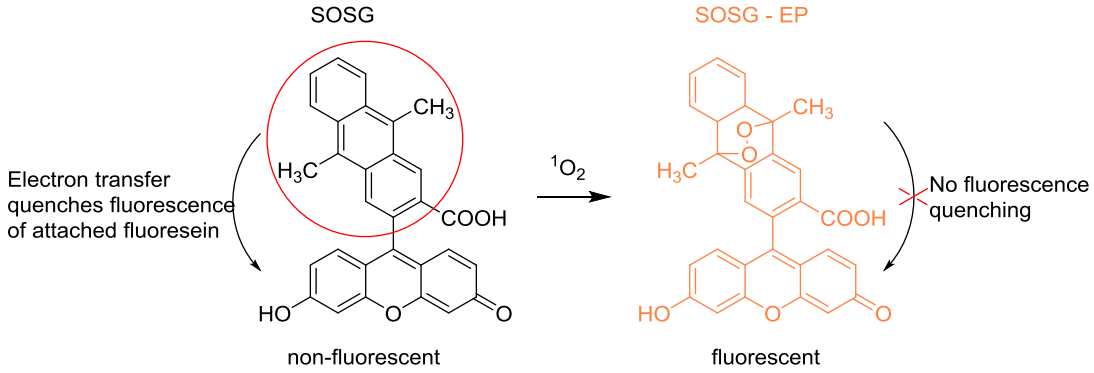

Figure 3.4 SOSG fluorescence only in the presence of $^1O_2$ after forming SOSG - EP.

Photoelectron transfer processes normally quench the fluorescein emission from the SOSG molecule. In the presence of singlet oxygen, the anthracene moiety forms an endoperoxide (SOSG-EP) that disrupts the *p*-dimethylaryl conjugated system, allowing the photoexcited fluorescein derivative to relax via fluorescence. The reaction is irreversible and the fluorescence signal proportional to the singlet oxygen concentration in solution.[176]

The HPF probe was developed by Setsukinai *et al* as a tool for stable and selective detection of •OH.[177] Although a related 3′-*p*-(aminophenyl) fluorescein (APF) probe produces ~ 5-fold more fluorescence than HPF in the presence of •OH, HPF is substantially less sensitive to $^1O_2$, thus making it more selective for •OH and better suited for use in our experiments.[175] In the presence of •OH, the non-fluorescent HPF molecule is oxidized to produce a bright green fluorescent product, with a molecule of *p*-benzoquinone being lost in the process. This chemistry is summarized in Figure 3.5.

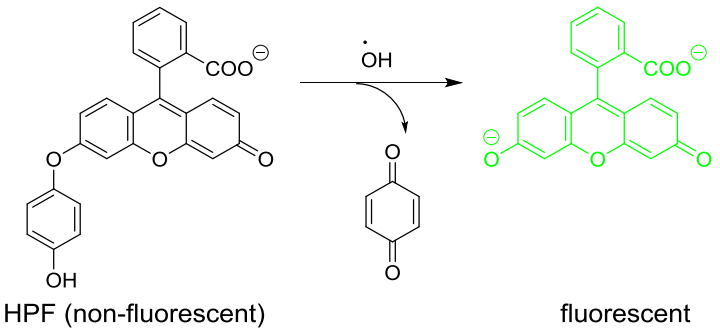

Figure 3.5 Reaction of HPF with •OH produces a green fluorescent molecule.

Cell-free measurements of $^1O_2$ and •OH were performed with the hybrids and probes in 96-well plates, as summarized in Figure 3.6. Solutions containing hybrids **47-62** and the SOSG (1 µM) and HPF (1 µM) probes were prepared in phosphate-buffered saline (PBS, *p*H 11). D_2O was added to increase the life-time and stability of the generated •OH and $^1O_2$.[178] It is known that the relative lifetime of $^1O_2$ in the presence of D_2O is 35 times longer than in H_2O.[179] It is also known that the SOSG and HPF probes are stable in the presence of cells and that there are no significant differences between the amounts of ROS generated by phenothiazinium PSs in the presence or absence of cells.[175] Thus, the $^1O_2$ and •OH measurements obtained here were directly transferable to the cell-based aPDT experiments described later in this Chapter.

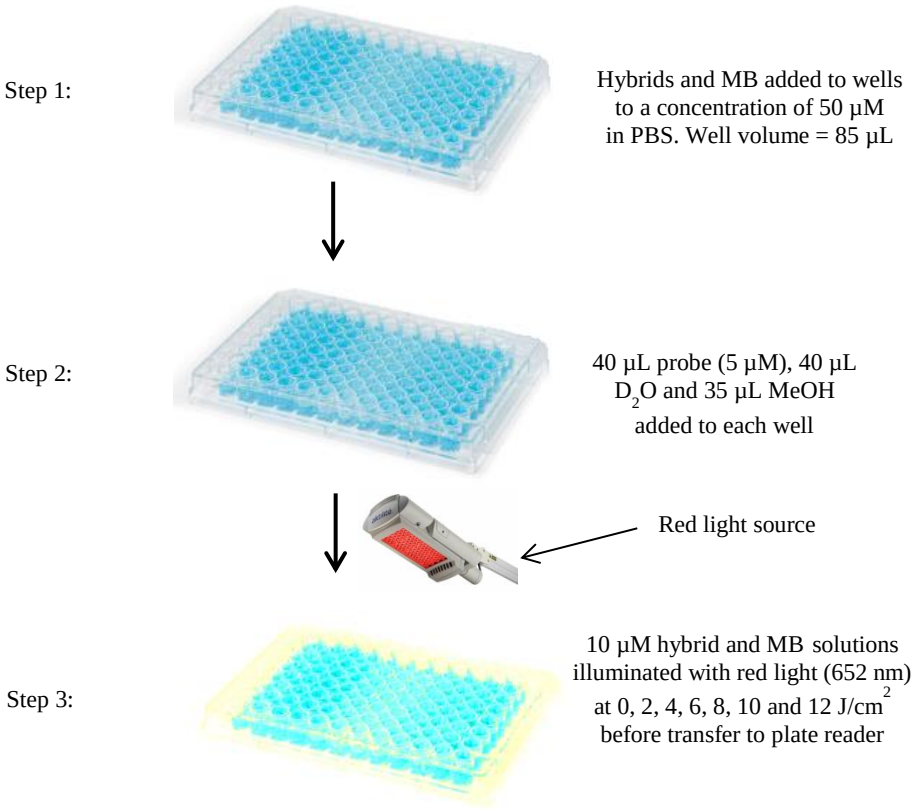

Figure 3.6 Schematic representation of cell-free experiments for the measurement of $^1O_2$ and •OH from hybrids upon illumination with red light.

The final assay solutions containing 10 µM hybrids in a total volume of 200 µL were illuminated with red light (652 nm) at fluences of 0 to 12 J/cm^2. A microplate spectrophotometer was employed for detecting fluorescence from SOSG using the "slow kinetic" mode, with fluorescence emission at 505 nm measured following excitation at 525 nm (2 nm monochromator band pass). For HPF, fluorescence emission was measured at 525 nm after excitation at 492 nm (2 nm monochromator band pass).

The effectiveness of hybrids in aPDT was expected to be influenced by the efficiency of $^1O_2$ and/or •OH production following illumination. The experiments

described were not able to quantitative $^1O_2$ and •OH production but they allowed direct comparison of the ROS-producing efficiencies of the hybrids to MB.

3.2.1 Reserpine-Containing Hybrids

Figure 3.7 shows the relative fluorescence produced by MB and reserpine-containing hybrids **47-50** in the presence of SOSG and HPF. In these experiments, a noncoherent light source with 30 nm-band-pass filters at ranges of 652 ± 15 nm were used for illumination. The total power output provided from the fibre bundle was 300 mW. The plates were arranged to give an irradiance of 100 mW/cm^2. The power (P) in watts was equal to the energy (E) in joules, divided by the time period (t) in seconds:

$$P_{(W)} = E_{(J)} / t_{(s)}$$

So

$$\text{Watt/cm}^2 = \text{joule/cm}^2 \text{ per second}$$

Therefore a 30 second illumination with irradiance of 100 mW/cm^2 over a 3 cm^2 area gave a fluence of 1000 mJ/cm^2 or 1 J/cm^2. Fluences were increased by extending the period of illumination.

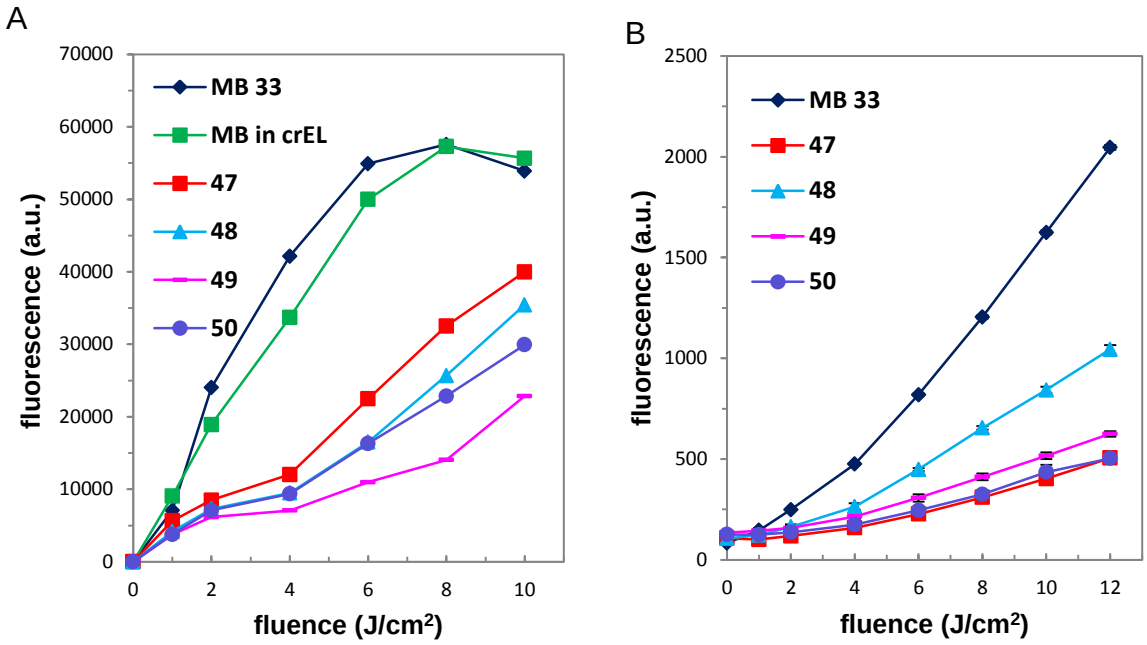

Figure 3.7 Comparison of (A) $^1O_2$ and (B) •OH production by reserpine-containing hybrids **47-50** to **MB** upon illumination with red light (652 nm). Light with power output 300 mW was applied 0.5-5.0 min for ($^1O_2$) and 0.5-6.0 min for (•OH), respectively.

In all cases the reserpine-containing hybrids showed significantly lower levels of $^1O_2$ and •OH production than MB. Indeed, all hybrids except **48** showed very little •OH production. Although much less than MB, the four compounds did produce significant $^1O_2$, with **47** producing the highest levels.

Figure 3.7(A) shows data point for $^1O_2$ production from MB after being formulated in cremophore EL® (CrEL). For later cell-based *in vitro* and *in vivo* experiments it was necessary to identify a suitable aqueous formulation for the hybrids as they were not sufficiently water soluble and organic solvents suitable for the hybrids

(MeOH and CH_2Cl_2) are unsuitable for biological experiments. Identifying a formulation that did not suppress ROS production was therefore considered crucial. As shown in Figure 3.7(A), the data for $^1O_2$ production by MB in CrEL tracked closely with the data for MB in the PBS/MeOH mixture, confirming that CrEL was an excellent formulation for the later *in vitro* and *in vivo* experiments.

Photobleaching is the process whereby photosensitizers decompose during exposure to light. The degree of decomposition usually depends on the light intensity and period of illumination. As the release of $^1O_2$ was measured over a period of 0.5-5.0 min, the $^1O_2$ experiments were able to provide information about photobleaching of hybrids. As shown in Figure 3.7, at fluences of more than 6 J/cm^2 MB showed signs of photobleaching, as evidenced by the flattening of the curve. The reserpine-containing hybrids on the other hand showed no evidence of photobleaching at fluences up to 10 J/cm^2.

3.2.2 Pterostilbene-Containing Hybrids

$^1O_2$ and •OH production by pterostilbene-containing hybrids **51**-**54** is shown in Figure 3.8. As observed with the reserpine-containing compounds, the pterostilbene-based hybrids all showed very little •OH production but they also showed very little $^1O_2$ production. Only hybrid **52** produced significant $^1O_2$ but it was markedly less than MB. No photobleaching effects were evident with **52**.

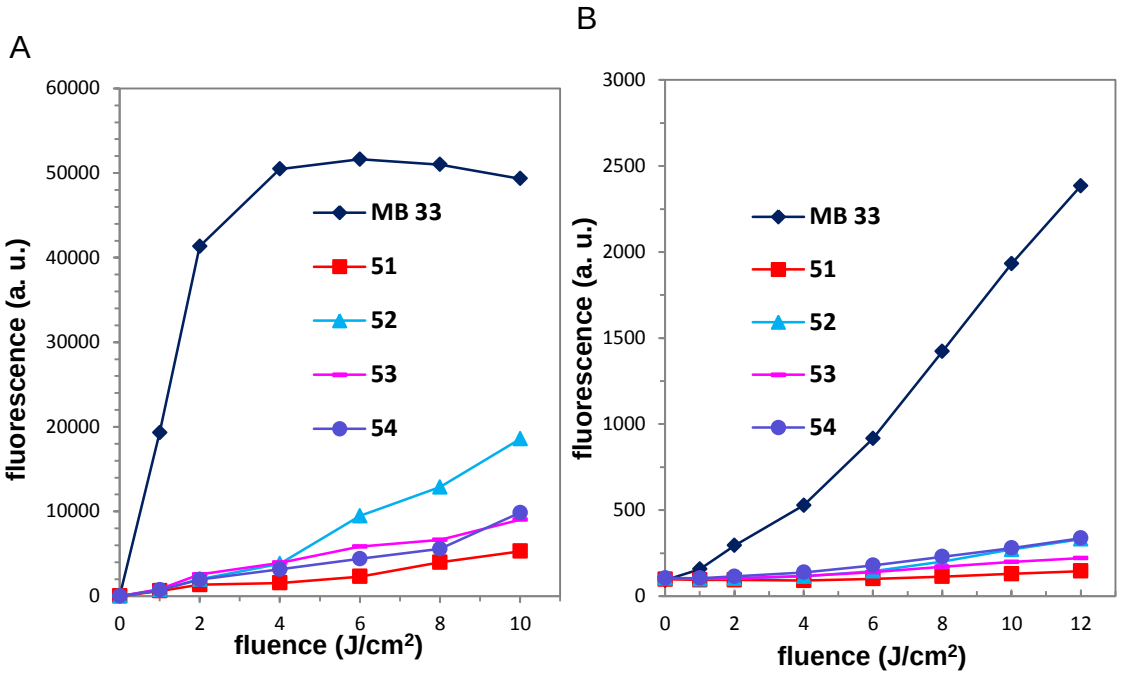

Figure 3.8 Comparison of (A) $^1O_2$ and (B) •OH production by pterostilbene-containing hybrids **51**-**54** to MB.

3.2.3 INF55-Containing Hybrids

$^1O_2$ and •OH production by INF55-containing hybrids **55-58** compared to MB is shown in Figure 3.9. Once again, these hybrids all showed very little •OH production under the experimental conditions. Importantly, while still less than MB, all INF55-containing hybrids showed robust $^1O_2$ production. For example, at 10 J/cm^2 **55** produced 83% of the $^1O_2$ produced by MB at the same fluence.

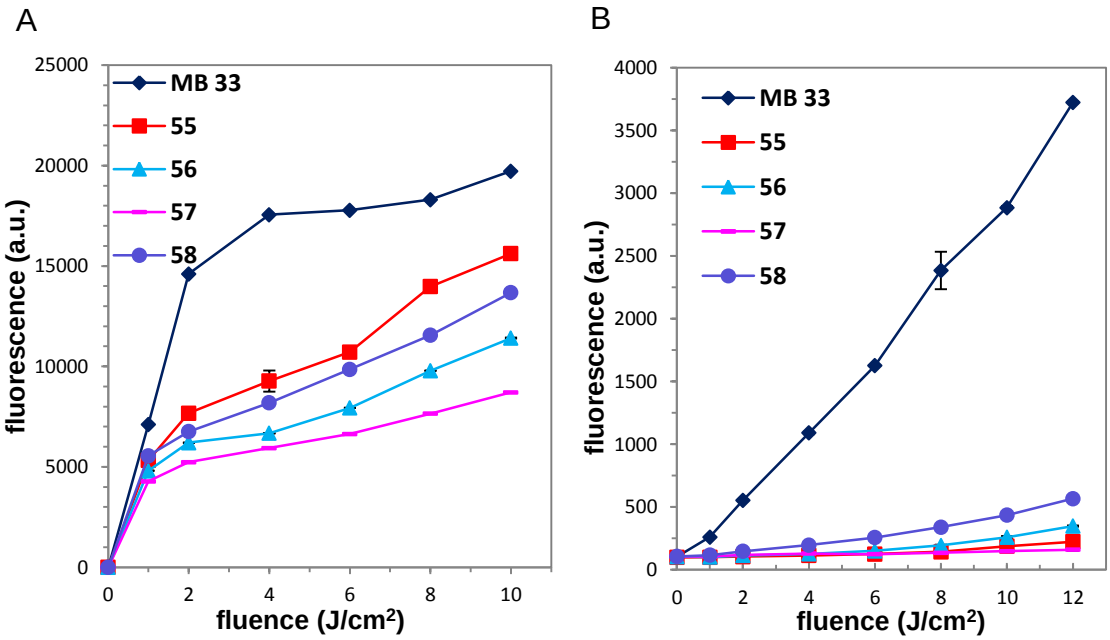

Figure 3.9 Comparison of (A) $^1O_2$ and (B) •OH production by INF55-containing hybrids **55**-**58** to MB.

3.2.4 INF271-Containing Hybrids

$^1O_2$ and •OH production by INF271-containing hybrids compared to MB is shown in Figure 3.10. As observed with the other three classes, these hybrids produced essentially no •OH, although **60** showed evidence of slight •OH production at high fluence. Hybrids **59** and **61** showed minimal $^1O_2$ production relative to MB even at high fluence. At 4 J/cm^2 **60** showed strong $^1O_2$ production, however, the $^1O_2$ did not increase with application of higher fluence, suggesting that photobleaching was occurring. $^1O_2$ production from **62**, on the other hand, steadily increased with higher fluence, indicating the compound is more photostable than **60**. At 10 J/cm^2 **62** produced 86% of the $^1O_2$ produced by MB at the same fluence.

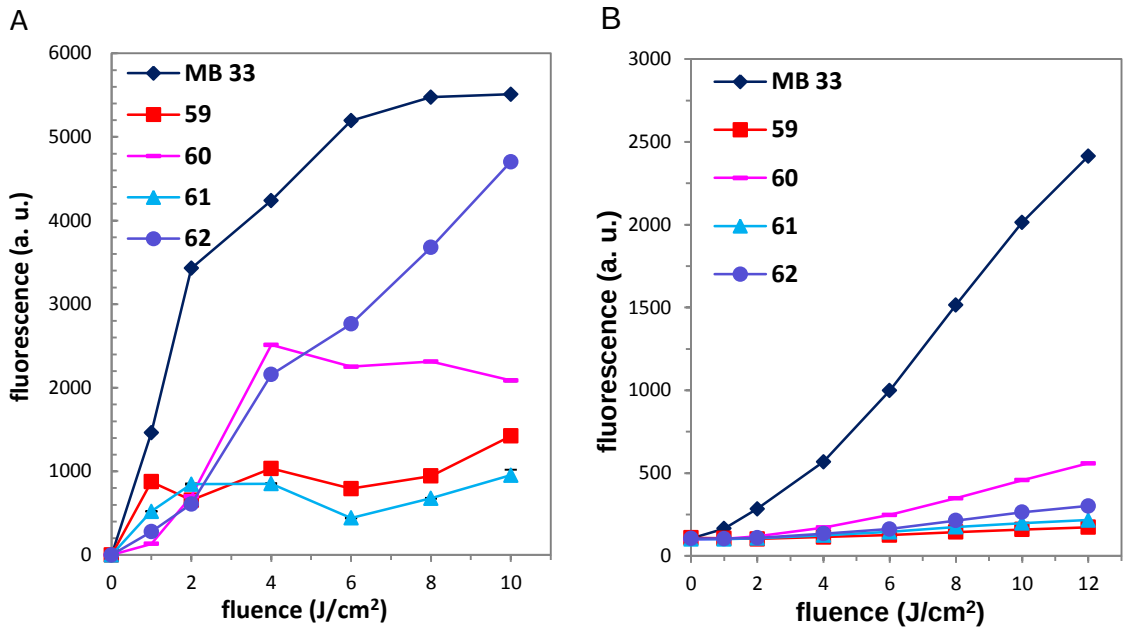

Figure 3.10 Comparison of (A) $^1O_2$ and (B) •OH production by INF271-containing hybrids **59-62** to MB.

3.2.5 Quantum Yields of $^1O_2$ and •OH Production by Hybrids 47-62

While the above analysis provided qualitative comparisons between $^1O_2$ and •OH production by hybrids **47-62** relative to MB a more quantitative treatment was possible based on fluorescence quantum yields. Fluorescence quantum yield is defined as the ratio of the number of photons emitted from a fluorophore to the number of photons absorbed. Relative fluorescence quantum yields in the SOG and HPF assays can be determined by comparing the observed fluorescence for hybrids to MB, which produces a known quantum yield (Φ_Δ (SOG) = 0.52, Φ_Δ (HPF) = 0.46) under the experimental conditions. The quantum yields for hybrids in each assay relative to MB are then calculated using the equation:

$$\Phi_{\Delta} = \Phi_{\Delta MB} \times \frac{Int}{Int_{MB}} \times \frac{1\text{-}10^{-A_{MB}}}{1\text{-}10^{-A}} \times \frac{n^2}{n_{MB}^2}$$

Where *Int* is the area under the emission curve (on a wavelength scale), *A* is optical density at the excitation wavelength and *n* is the refractive index of the solvent. The subscript MB refers to the respective values for methylene blue. Since the same energies of light and the same solvent etc. were used for MB and the hybrids the relative quantum yields could be obtained by measuring the area under the fluorescence curves (Figures 3.7-3.10) and dividing by the area under the MB curve. For each fluorescence curve a best-fit trendline was obtained using polynomial regression and the relative integration calculated over the appropriate fluence range (0-10 J/cm^2 for SOG and 0-12 J/cm^2 for HPF). The fluorescence quantum yields for hybrids **47-62** relative to MB in the SOG and HPF assays are provided in tabular form in Appendix 3.1. The data are presented in graphical form in Figure 3.11 where % Φ_{Δ} relative to MB is presented for hybrids in both assays. The data are colour-coded as described earlier (Chapter 3.1) based on the different linker types.

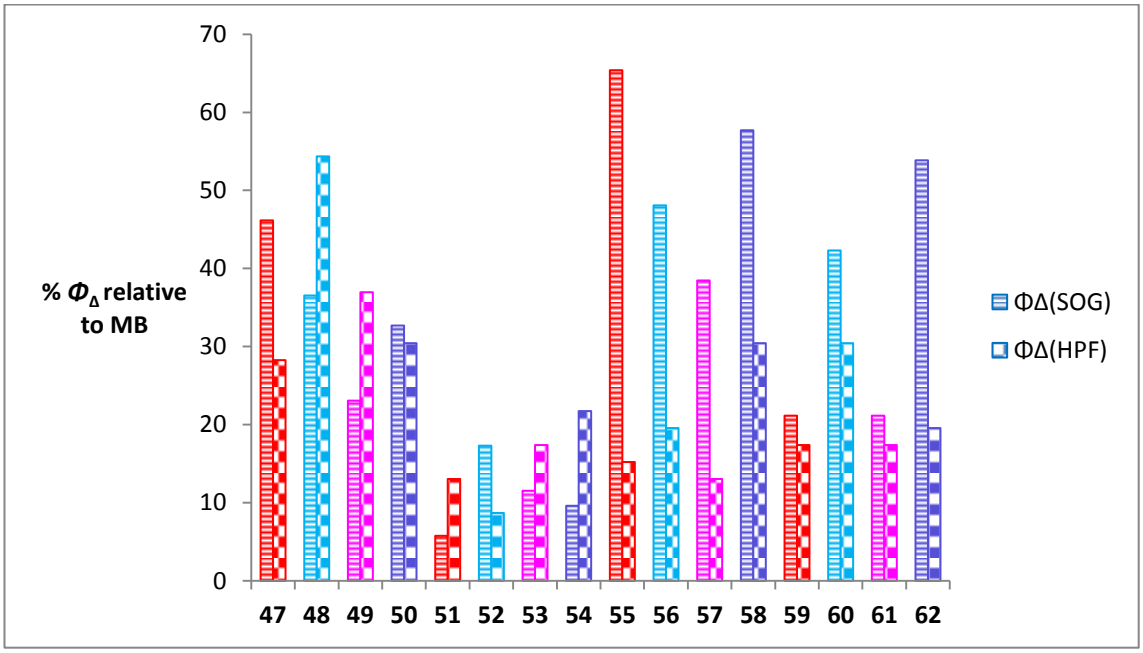

Figure 3.11 Changes in SOG and HPF % quantum yields for hybrids **47**-**62** relative to MB.

Reserpine-containing hybrids **47**-**50** showed $^1O_2$ and •OH quantum yields at around 20-55% of MB. Hybrid **48** showed the highest •OH production at around 55%, while **47** produced the most $^1O_2$ (46%). Pterostilbene-containing hybrids **51**-**54** all showed very low $^1O_2$ and •OH quantum yields (less than 20% relative to MB).

INF55-containing hybrids **55**-**58** showed much higher $^1O_2$ quantum yields than •OH. $^1O_2$ production for **55** at 65% relative to MB was the highest of all the compounds tested. Hybrid **58** also showed strong $^1O_2$ production at about 60% of MB and showed the strongest •OH production in this series at ~ 30 of MB.

INF271-containing hybrid **62** produced the third highest amount of $^1O_2$ relative to MB. Hybrid **60** produced reasonable •OH and $^1O_2$ quantum yields, although the $^1O_2$ generation of this hybrid reduced after 6 J/cm^2 (Figure 3.11), suggesting photobleaching

was occurring with this compound. The significantly higher $^1O_2$ quantum yields relative to •OH quantum yields in the INF55 and INF271-containing hybrid series suggested that these compounds would likely undergo Type II processes when applied in PDT (See Chapter 1.9).

3.3 *In Vitro* Antibacterial Photodynamic Activity

3.3.1 Formulation Vehicle for Hybrids

In the above cell free experiments the hybrids were all significantly soluble in the aqueous PBS/MeOH solutions. For cell-based *in vitro* and *in vivo* aPDT experiments, MeOH was unsuitable as a co-solvent due to its toxicity. It was therefore necessary to identify a formulation vehicle that was both non-toxic and capable of solubilizing the hybrids. Other than MeOH, the best solvents for dissolving the hybrids were found to be CH_2Cl_2 and $CHCl_3$, but these are not miscible with water and were thus unsuitable. A range of commercially available detergents were explored as formulation vehicles for the hybrids.

Encapsulation of reserpine-containing hybrid **49** into micelles was examined, using the detergents tween 60 (T60), cremophor EL (CrEL), triblock copolymers F127 (PL-F127) and poloxamer 388 (POL388). Hybrid **49** was chosen as a representative hybrid for solubility examinations because it was observed to be particularly insoluble in aqueous solution. Micellar solutions of **49** were prepared by initially dissolving the compound in CH_2Cl_2 at 2-3 mM. This solution was added to a 100 mg/mL solution of each detergent in CH_2Cl_2 and the combined mixtures were sonicated until a homogenous solution was obtained. The organic solvent was then removed under

reduced pressure and the remaining thin film of **49** was redissolved in PBS to create a homogenous 500 µM aqueous micellar solution of the compound.

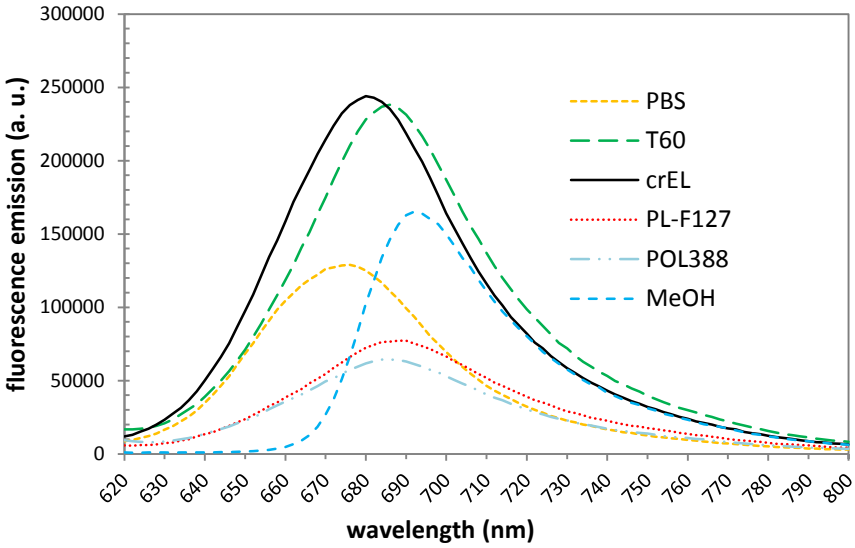

Figure 3.12 Fluorescence emission spectra of hybrid **49** formulated in micelles generated with tween 60 (T60), cremophor EL (CrEL), triblock copolymers F127 (PL-F127) and poloxamer 388 (POL388). Spectra recorded in PBS and MeOH are shown for comparison.

Figure 3.12 shows the fluorescence emission spectra of hybrid **49** in 10 µM micellar solutions. The equivalent spectrum of **49** in PBS and MeOH is shown for comparison. A large increase in the emission intensity at 680 nm was observed for **49** when encapsulated in CrEL and T60 (excitation at 600 nm) compared to the other micelles, PBS and MeOH.

The increased fluorescence observed with CrEL and T60 suggests that these detergents minimise aggregation and are excellent solubilisers for **49**. CrEL is widely used as a formulation or drug delivery vehicle for many poorly water-soluble drugs[180] and is generally considered to be nontoxic.[181] As described on 3.2.1, CrEL was also found to have no effect on $^1O_2$ production from MB. Based on this, CrEL was chosen as

the vehicle for formulating the hybrids in all cell-based experiments (Chapter 3) and *in vivo* studies (Chapter 4).

3.3.2 Preliminary aPDT Screening of Hybrids against MRSA USA300

MRSA USA300 was chosen as a model Gram-positive organism for preliminary screening of hybrids for aPDT activity. USA300 is a major source of community-acquired MRSA infections in the USA, Canada, and Europe[182] and is responsible for major skin and soft-tissue infections,[183] community-acquired pneumonia and catheter-related bloodstream infections.[184] The strain is isogenic with wild-type MRSA making it a good test organism for preliminary screening.

Increasing concentrations of CrEL-formulated hybrids (1-20 μM in PBS) were incubated for 30 min in the dark at room temperature with suspensions of USA300 cells (10^8 CFU/mL). Aliquots were transferred to 96-well plates and illuminated with red light (652 nm) at a fluence of 6 J/cm^2. Remaining colonies were counted after overnight growth and the results plotted as survival fractions at the different concentrations. Dark controls (same procedure without application of red light) were included in all experiments. No significant dark toxicity was observed with any of the hybrids or MB over the concentration range and fluences tested. No differences in dark toxicity of MB were observed when formulated in CrEL compared to PBS/MeOH (Appendix 3.2).

Figure 3.13 shows the photodynamic killing of MRSA USA300 by hybrids **47-62**, grouped according to the attached EPI (e.g. reserpine-containing hybrids etc.). Also shown for comparison is the photodynamic killing by MB under identical conditions. MB showed a dose dependent effect over the concentration range 0-20 μM, producing a

~ 2-log reduction in cell viability at the highest concentration. When MB was formulated in CrEL an additional 1-log killing of cells was observed at the highest concentration (Figure 3.13(A)), suggesting that CrEL potentiates the photodynamic activity of MB. This funding further supported for its use as a formulation vehicle for exploring the aPDT effects of hybrids.

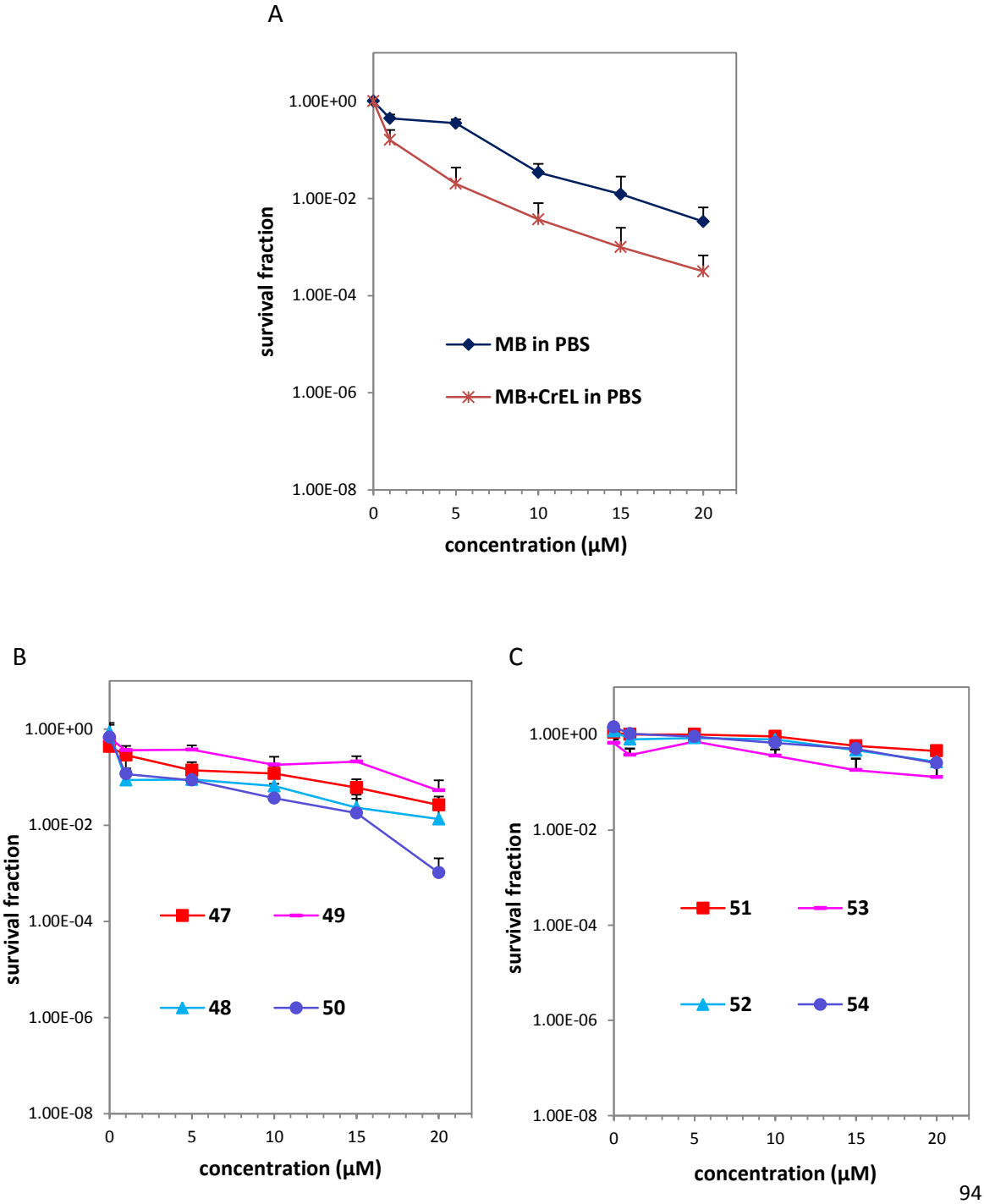

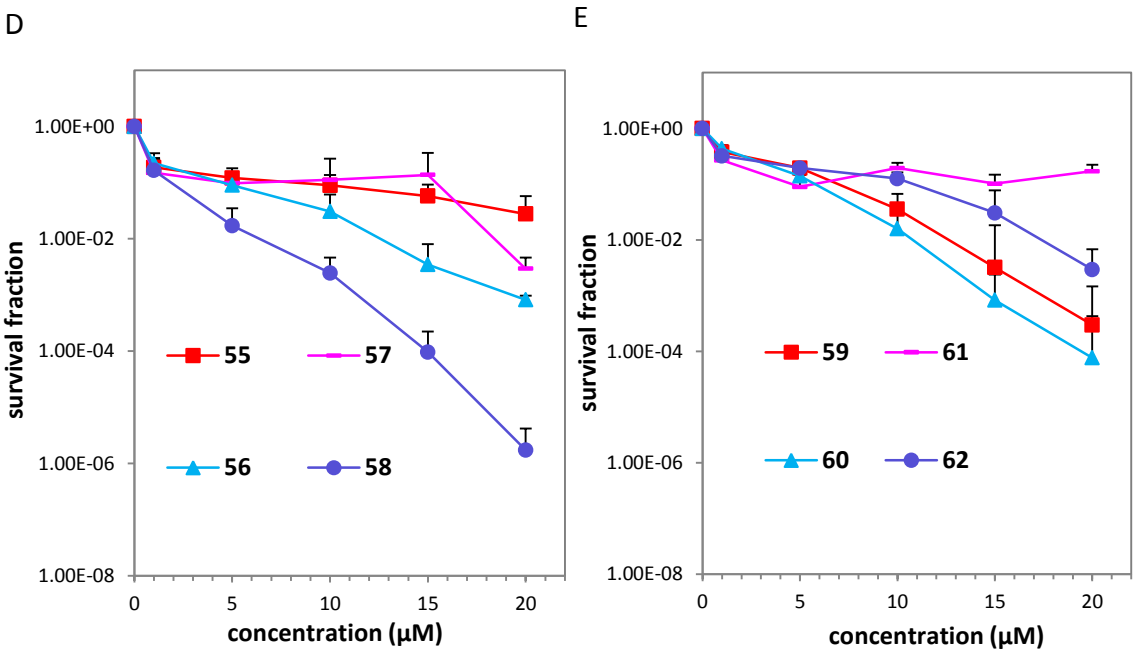

Figure 3.13 Photodynamic inactivation of MRSA USA300 by hybrids **47**-**62**. Cells (10^8 CFU) were incubated for 30 min with CrEL-formulated hybrids at 0-20 µM in PBS and illuminated with 652 nm light (100 mW/cm^2, fluence = 6 J/cm^2). Aliquots were removed from the suspensions after light delivery and CFUs determined after overnight growth in a 37 ^{o}C incubator. The remaining cells were plotted as survival fractions. Data represent the mean of 3-5 independent experiments ± SEM.

Reserpine-containing hybrids **47**-**50** showed very little photodynamic inactivation, except for hybrid **50**, which produced a 2-log reduction in cells at the highest concentration (20 µM, Figure 3.13(B)). Similarly, none of the pterostilbene-containing hybrids **51**-**54** showed significant photodynamic activity (Figure 3.13(C)).

More encouraging results were obtained with INF55-containing hybrids, where compound **58** showed a very strong dose-dependent effect and produced a 6-log reduction in cells at 20 µM. This represented a 3-log increase in killing relative to MB (formulated in CrEL) at the same concentration. Hybrid **56** also showed good dose-

dependency and a 3-log reduction in cells at 20 μM. Hybrids **55** and **57** showed only slight activity (Figure 3.13(D)).

INF271-containing hybrids **59**, **60** and **62** all showed dose-dependent killing, whereas no activity was observed with **61** (Figure 3.13(E)). At 20 μM, **60** produced a 4-log reduction in cells, or 1-log greater than MB (in CrEL). Hybrid **59** showed killing equivalent to MB (in CrEL) while a 2-log kill was observed with **62**.

To facilitate comparisons between the compounds, the data presented in Figure 3.13 were combined into a single figure (Figure 3.14). In this analysis, the 20 μM data points for each compound were expressed as the log reduction in survival. Hybrids **56-58** carrying INF55-based EPIs were clearly active compounds, especially **58**, which showed 3-log greater activity than MB in CrEL. INF271-containing hybrids **59** and **60** were clearly active and **62** also showed some effect. The only other active hybrid **50** (containing an appended reserpine) produced an equivalent effect to MB (in CrEL).

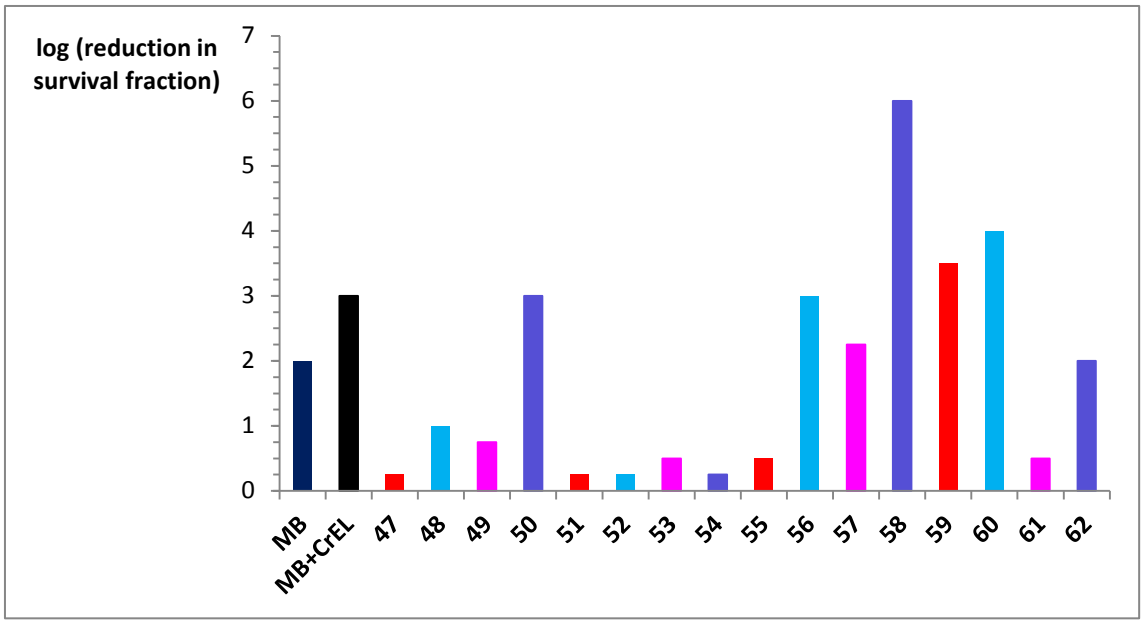

Figure 3.14 Summary of photodynamic inactivation of MRSA USA300 by MB (in PBS and CrEL) and hybrids **47**-**62**.

Examples from each of the four different linker classes were found to show activity, suggesting that the structure of the linker may not be crucial. It was noted, however, that except for **59**, which contained a piperazine-based linker, hybrids that showed the greatest photodynamic inactivation carried *N*,*N*'-dimethylethylenediamine-based linkers. As might be expected, active compounds **56**, **58**, **60** and **62** were strong producers of $^1O_2$ (Figure 3.11) but, surprisingly, hybrid **55**, which was the strongest $^1O_2$ producer (Figure 3.9), showed no photodynamic activity. This observation suggests that strong $^1O_2$ production is not on its own sufficient to create hybrids with potent aPDT activity.

3.3.3 Photodynamic Activity of Hybrids against *S. aureus* Mutants

The above experiments indicated that four hybrids, including two from the INF55-containing series (**56** and **58**) and two from the INF271-containing series (**59** and

60), showed the strongest photodynamic inactivation of MRSA USA300. Based on this, these compounds were advanced to further study of their photodynamic effects against a panel of *S. aureus* strains. To examine whether the photodynamic effects of the chosen hybrids were being influenced by the NorA pump, their aPDT activities were examined in NorA knockout (NorA-), wild-type (WT) and NorA-overexpressing (NorA++) *S. aureus* cells. These strains respectively contain none (or reduced), basal and elevated levels of the NorA pump. MB was included in the experiments for comparison. Tegos *et al* showed that the aPDT activity of MB varies against NorA knockout (K1758), wild-type (8325-4) and NorA-overexpressing (K2361) *S. aureus* cells, where higher NorA expression reduced activity.[154] As explained in Chapter 1.12, this is consistent with MB being a NorA substrate.

In the current experiments, the same three *S. aureus* strains were incubated with the four hybrids (formulated in CrEL) or MB at 20 μM for 30 min before centrifuging and washing to remove compound not taken up into or bound to cells. The cells were then re-suspended in sterile PBS and transferred to 96-well plates and illuminated with 652 nm red light of increasing fluence (0-16 J/cm^2). These solutions were serially diluted from 10^{-1}-10^{-6} to facilitate final CFU counts. Cells were then incubated overnight before performing and determining survival fractions. A summary of the assay is provided in Figure 3.15. The phototoxicity results are shown in Figure 3.16.

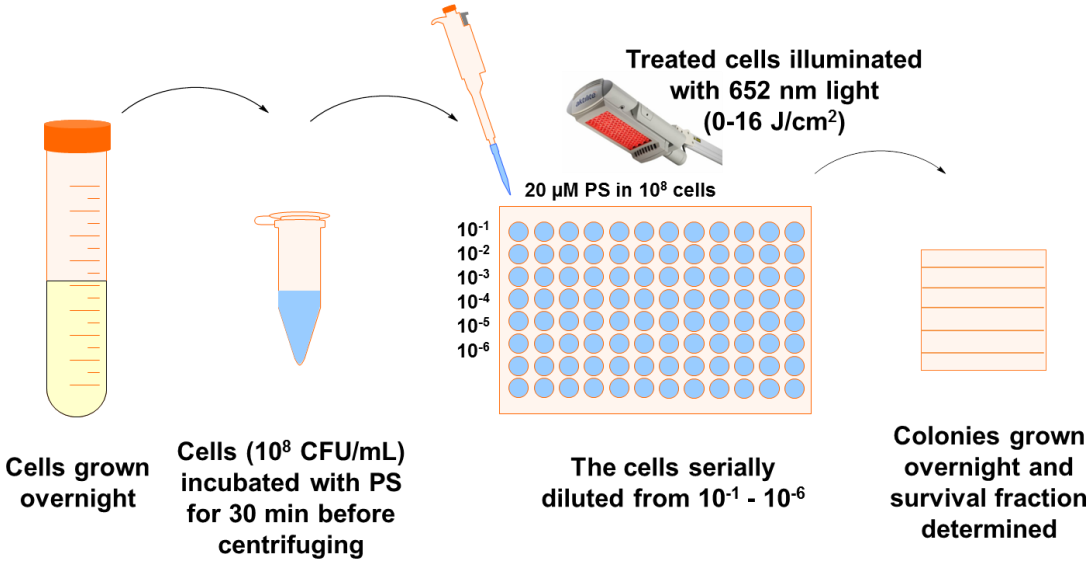

Figure 3.15 Schematic summary of aPDT assay using NorA-, WT and NorA++ *S. aureus* cells.

If our hypothesis was correct and the attached NorA inhibitors (INF55 for **56** and **58** and INF271 for **59** and **60**) in the hybrids were blocking the NorA pump, thereby increasing intracellular concentrations of the attached MB PS and producing increased phototoxicity (Chapter 1.14), the following observations would be expected from these experiments: (1) hybrids should show higher relative phototoxicity compared to MB in the wild-type and NorA++ strains due to the presence of the NorA pump and (2) no change in phototoxicity relative to MB in the NorA- strain.

In agreement with the Tegos study,[154] the NorA- strain showed more than 4-log units of killing in the presence of MB at the maximum fluence 16 J/cm^2, while the wild-type and NorA++ strains showed ~ 2 log lower killing (Figure 3.16 (A)). Phototoxicity against the NorA- strain for the four hybrids was very similar to MB, where they all produced cell kills within 1 log unit of MB at 16 J/cm^2. For the wild-type strain, where MB produced a 2 log kill at 16 J/cm^2, hybrids **56**, **58** and **59** all showed more than 1 log greater killing than MB, while **60** showed equivalent killing to MB. Excitingly, all four

hybrids showed greater killing at 16 J/cm^2 than MB against the NorA++ strain. Collectively these results were in agreement with the proposed hypothesis. A graphical summary of the results is provided in Figure 3.17.

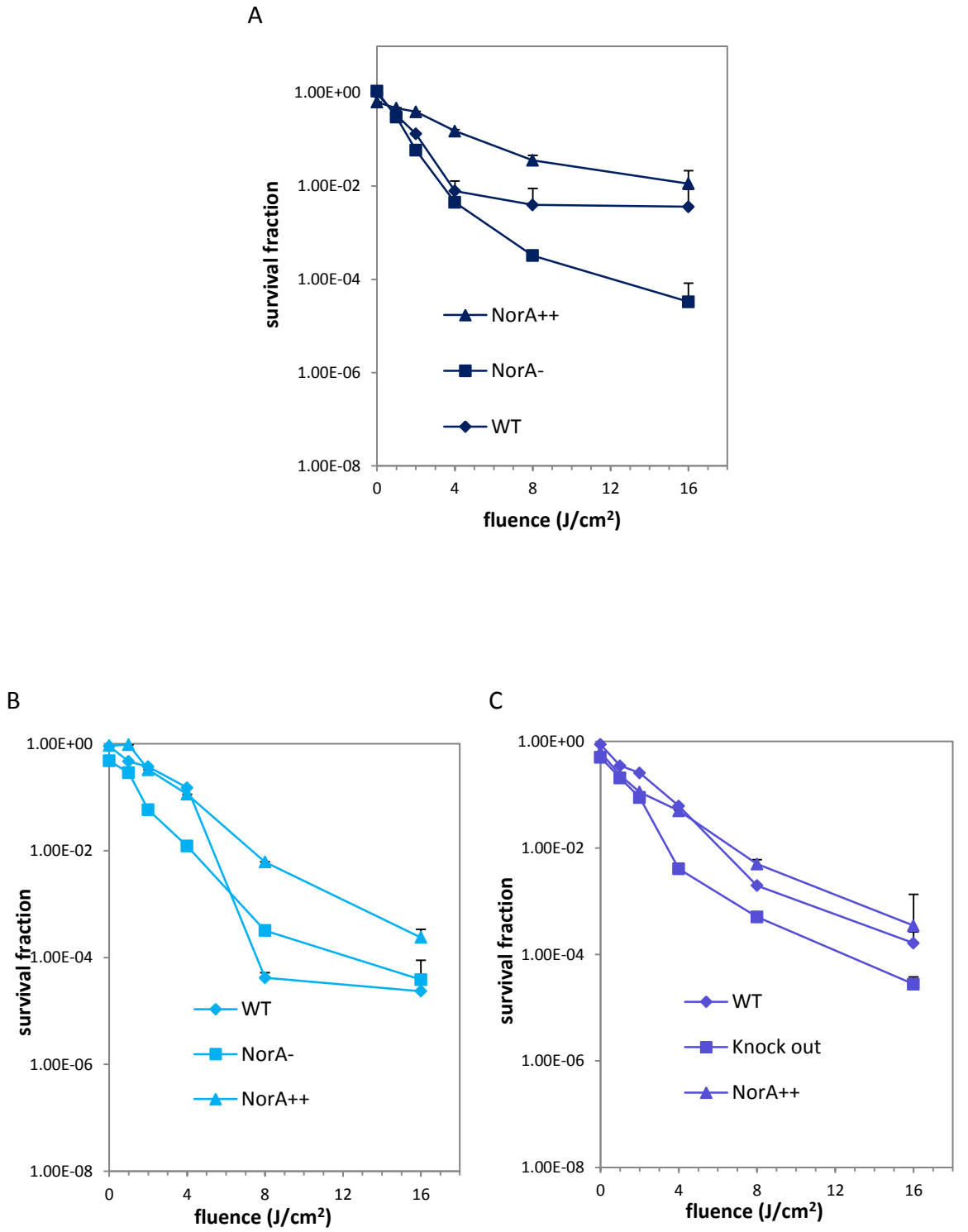

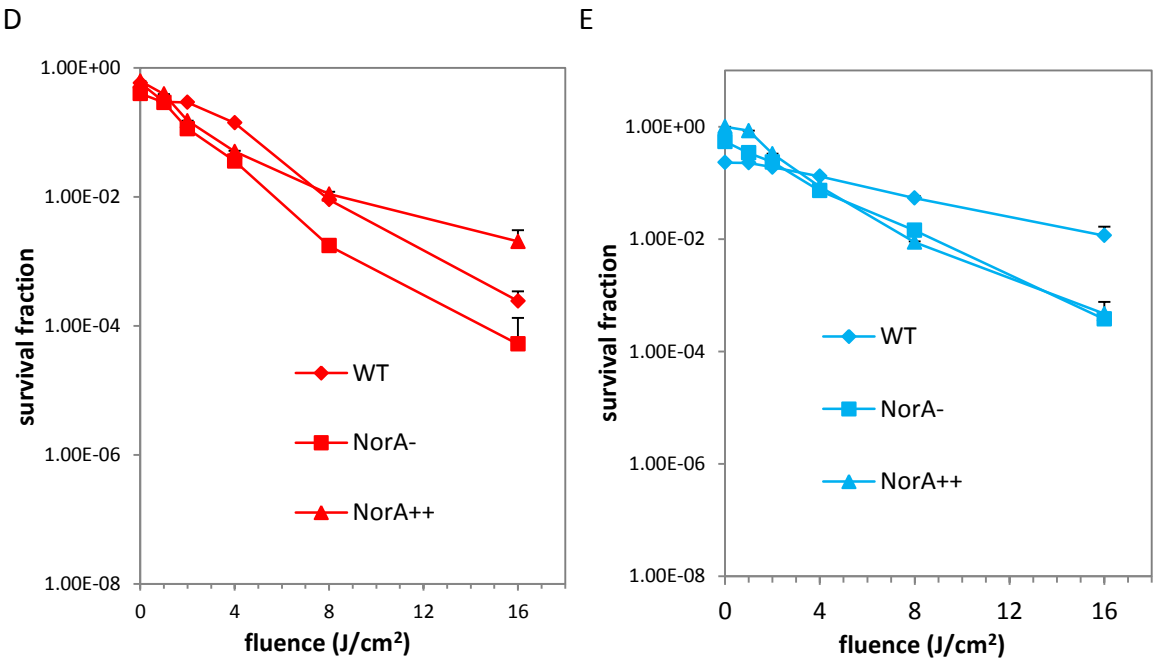

Figure 3.16 Photodynamic inactivation of NorA knockout (NorA-), wild-type (WT), and NorA-overexpressing (NorA++) *S. aureus* strains by: (A) MB, (B) **56**, (C) **58**, (D) **59** and (E) **60**. All compounds were present at 20 µM. Data represent the mean ± SEM from three independent experiments.

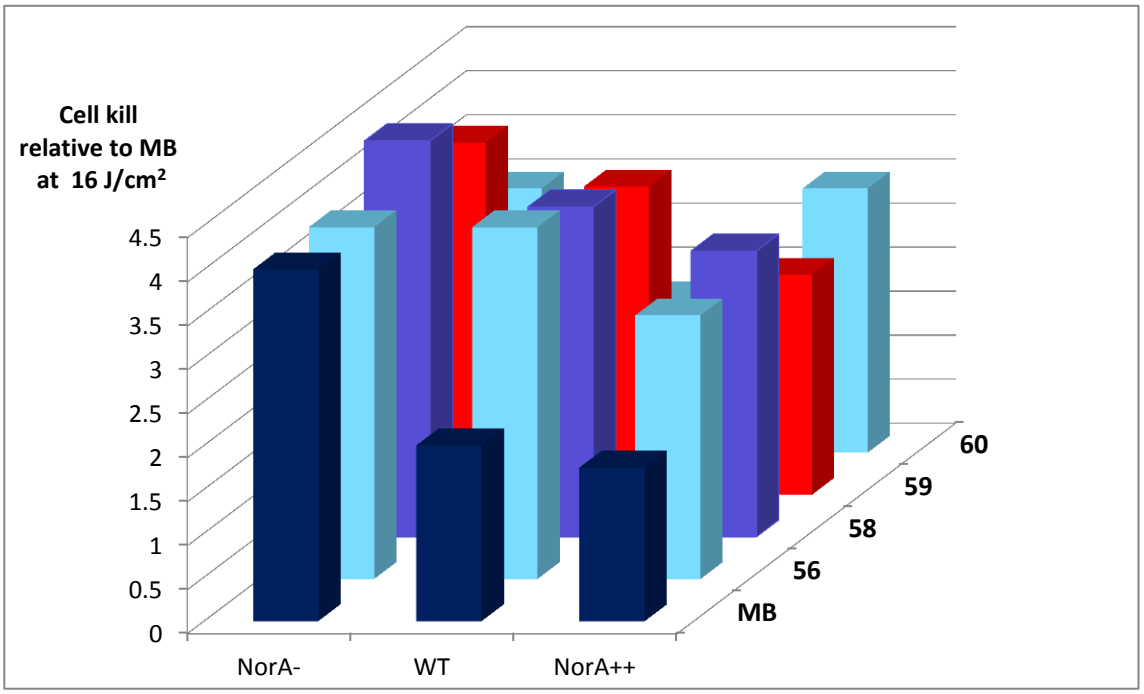

Figure 3.17 Summary of photodynamic inactivation of NorA knockout (NorA-), wild-type (WT) and NorA-overexpressing (NorA++) *S. aureus* strains by MB and hybrids **56**, **58**, **59** and **60**.

3.3.4 Concentration-Dependence of Hybrid Phototoxicity

Three hybrids from the *S. aureus* mutant aPDT experiments, two INF55-containing hybrids **56** and **58** and one INF271-containing hybrid **60**, were advanced to dose-response studies. In these experiments, photodynamic inactivation by each compound was measured at increasing concentrations (0-160 μM) against the *S. aureus* panel (i.e. K1758 NorA-, 8325-4 WT and K2361 NorA++) at a constant fluence of 10 J/cm^2. MB was also included in the experiments for comparison.

Solutions of CrEL/PBS-formulated hybrids (0-160 μM) were incubated for 30 min in the dark with *S. aureus* cells (10^8/mL) at room temperature. The cells were centrifuged and washed before being resuspended in PBS and illuminated with 10 J/cm^2 red light. The centrifuge/washing step served to remove hybrid molecules not contained within the cells or adhered to their surfaces. CFUs were counted after overnight growth and the survival fractions determined. Plots of survival fractions versus concentration as shown in figure 3.18. Dark control experiments were also performed where an identical procedure was followed without application of light. These dark toxicity data are provided in Appendix 3.3.

Surprisingly, MB showed evidence of dark toxicity, especially against the NorA- and NorA++ strains, where it reduced the survival fractions in a dose-dependent manner up to a maximum of 3-4 logs at 160 μM. The three hybrids **56**, **58** and **60** all showed lower dark toxicity than MB, reducing the survival fractions by a maximum of 2 log units at 160 μM. In most instances, however, only 1 log reductions were observed in the dark with the hybrids at this high concentration.

When the light was applied, MB at 80 µM provided a 7 log kill against the NorA$^-$ strain that did not increase as the concentration was raised to 160 µM. MB produce similar results against the WT and NorA++ strains, where ~ 5-7 log kills were observed at 80 µM.

INF271-containing hybrid **60** produced more than 3 log units of killing at 40 µM against the NorA- strain and 4 logs at 80 µM. Increased killing was not observed as the concentration was raised to 160 µM. Similar results were obtained against the WT strain but the NorA++ strain showed higher sensitivity, experiencing a 5 log kill at 80 µM and 7 log at 160 µM.

INF55-containing hybrids **56** and **58** showed very strong and dose-dependent phototoxicity against all three *S. aureus* strains (Figure 18(C) and 18(D), respectively). At 20 µM **56**, a 5-log kill was observed against the NorA- strain essentially complete eradication was observed at 80 µM. The WT strain showed a 5-log kill at 80 µM and 6-log kill at 160 µM. The NorA++ strain showed an impressive 4-log kill at 20 µM and total eradication at 40 µM. Hybrid **58** produced similar results to **56** but with almost complete eradication of the NorA- strain occurring at 40 µM.

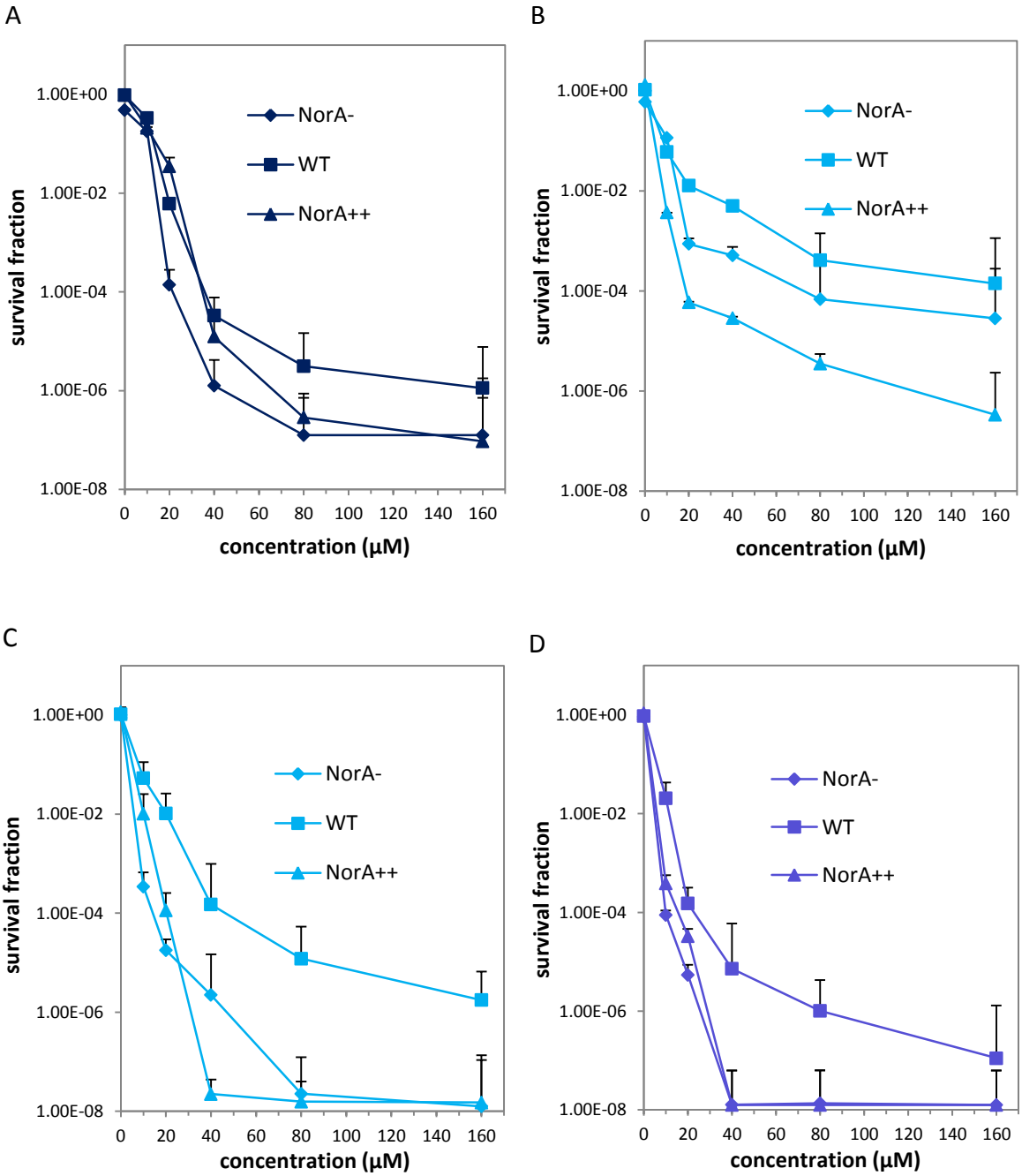

Figure 3.18 Concentration-dependent phototoxicity of (A) MB and hybrids (B) **60**, (C) **56** and (D) **58** against *S. aureus* NorA knockout (NorA-), wild-type (WT) and NorA-overexpressing (NorA++) strains. Data represent the mean ± SEM from 3-4 independent experiments.

3.4 Cell Uptake Studies with Hybrids 56, 58 and 60

Hybrids **56** and **58** showed significantly enhanced cell-killing potency against the NorA- and NorA++ *S. aureus* strains relative to MB, but similar killing to MB against the WT strain. These results conflicted with our design hypothesis, where hybrids would have been expected to produce stronger activity against the WT strain (rather than the NorA- strain) relative to MB.

The role of the NorA pump in the observed activity of hybrids was further probed by measuring the uptake of **56**, **58**, **60** and MB into the NorA-, WT and NorA++ *S. aureus* cells.

Fluorescence versus concentration calibration curves were obtained by measuring the fluorescence of the hybrids and MB across a concentration range (0-3 μM) in the presence of sodium dodecyl sulfate (SDS). To measure compound uptake into cells, 10^8 CFUs were incubated for 30 min with 20 μM hybrids or MB. The cells were centrifuged and washed to remove compound not bound to or taken up into cells and then redissolved in PBS and digested in SDS overnight. The fluorescence of digest solutions was measured and the concentrations of hybrids and MB determined from the calibration curves. The uptake results for hybrid**s 56**, **58** and **60** are summarized in Figure 3.19, with MB included for comparison.

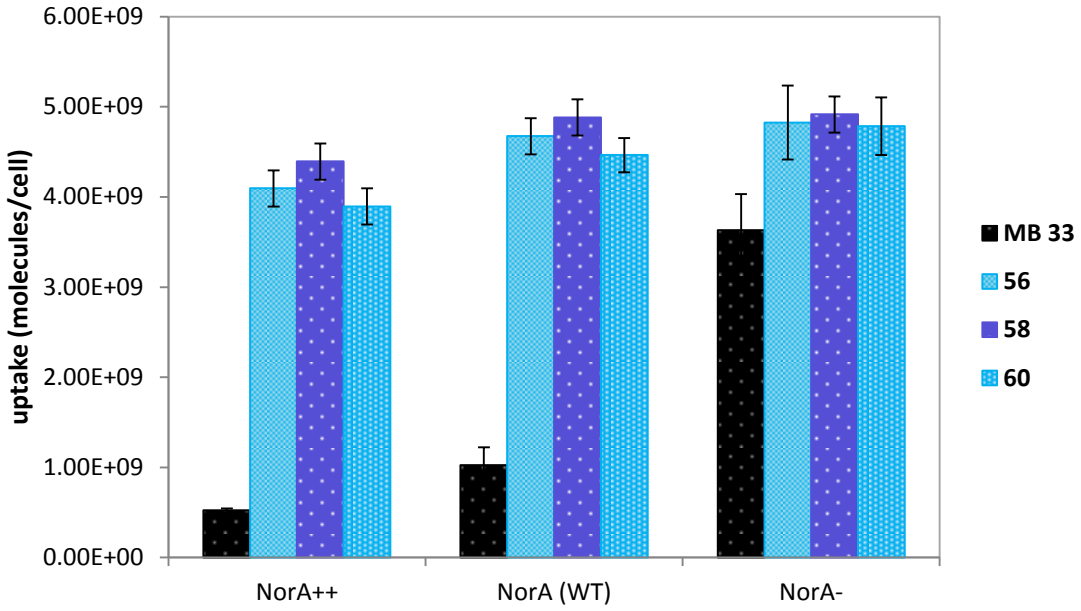

Figure 3.19 Uptake of MB and hybrids **56**, **58** and **60** (molecules per cell) by *S. aureus* NorA knockout (NorA-), wild-type (WT) and NorA-overexpressing (NorA++) strains. Data represent the mean ± SEM from 3-4 independent experiments.

Figure 3.19 shows that uptake of hybrids **56**, **58** and **60** by all three *S. aureus* strains was significantly higher than MB. As expected, MB uptake was greatest in the NorA- strain and least in the NorA++ strain, in alignment with it being a NorA substrate.[154] Approximately 4.7 ± 0.3 x 10^9 molecules of INF55-containing hybrid **56** were taken up per cell by the NorA- strain, or 1.3 times more than MB. Uptake of **56** into the other two strains did not differ appreciably (4.6 ± 0.2 x 10^9 and 4.3 ± 0.2 x 10^9 molecules/cell for WT and NorA++ strains, respectively). The other two hybrids **58** and **60** showed uptake levels essentially identical to those of **56** across the three strains. Observing that **56**, **58** and **60** show identical uptake across the three *S. aureus* strains, despite their differences in NorA expression, suggested that unlike MB, these hybrids are not substrates for the NorA pump. The question of whether the hybrids were also serving to block was addressed next.

3.5 EPI Activity of Hybrids

The NorA pump inhibitory activity of INF55 and INF271 is well characterized[98] but it was unknown whether they retained this activity when part of the hybrids. The effects of the structural changes introduced through incorporation within hybrids on NorA activity were explored by measuring the photodynamic inactivation of *S. aureus* by MB in the presence of INF55, INF271 and various INF55-containing (**84-87**) and INF271-containing (**92-95**) synthetic intermediates that contained just the attached linker groups and no MB moiety. It was reasoned that if the modified EPIs in the synthetic intermediates produced equivalent activity to their parent EPIs then it could be inferred that the structural changes introduced had not significantly impacted their NorA inhibitory effects. NorA++ cells were used for these experiments to maximise the observed differences in photodynamic cell killing by the various MB/EPI treatments.

NorA++ *S. aureus* cells were treated with 10 µM INF55/INF271 or **84-87**/**92-95** and 20 µM solutions of MB added before incubation for 30 min. Cells were then illuminated with increasing fluences of red light (0-16 J/cm^2) and survival fractions determined (as described in Chapter 3.3.2).

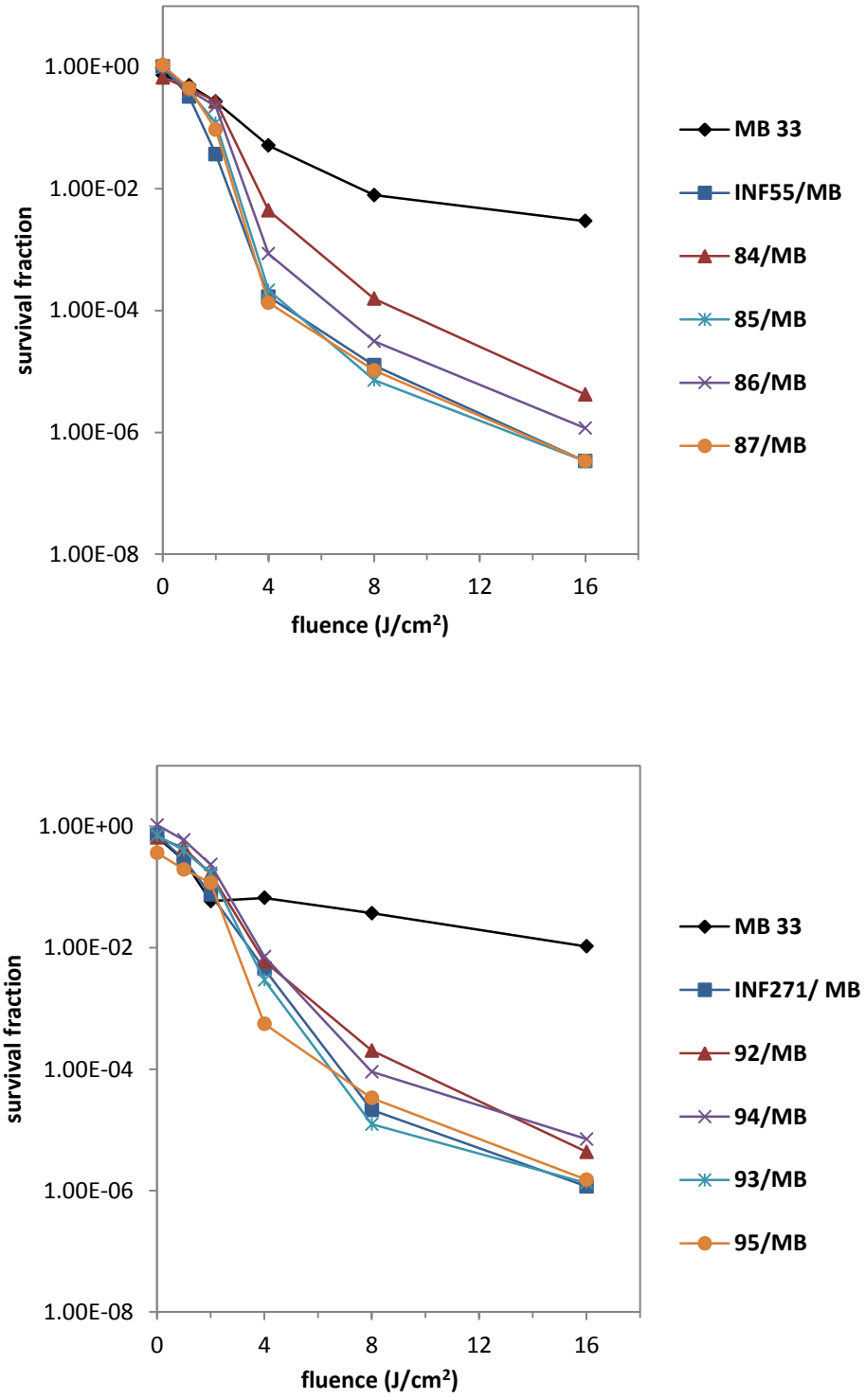

Figure 3.20 Photodynamic inactivation of NorA++ *S. aureus* cells by MB alone and in combination with INF55, INF271, INF55-containing synthetic intermediates **84-87** and INF271-containing intermediates **92-95**. Data represent the mean ± SEM from 3-4 independent experiments.

Figure 3.20 shows that MB produced approximately 2-log units of killing in the absence of EPIs at the maximum fluence of 16 J/cm^2. As expected, introduction of INF55 and INF271 greatly increased cell killing. At 16 J/cm^2 an additional 4 log units of killing were observed with both EPIs. Similar cell kills were observed with the EPI derivatives compared to their parent EPIs, suggesting that the derivatives all retained their ability to block the NorA pump. These results imply that at least some of the increased uptake of **56**, **58** and **60** relative to MB (Figure 3.19) arises from the ability of the appended EPI structures in the hybrids to inhibit the NorA pump, rather than simply because the hybrids are not substrates from the pump.

To support these findings, the pump inhibitory activities of hybrids **56**, **58** and **60** were examined in experiments where they were co-administrated with the antibiotic ciprofloxacin, a well-known NorA substrate.[31c,185] In these experiments, the antibacterial activity of ciprofloxacin was measured (in the dark) and compared to its activity in the presence of MB or the hybrids. A bioluminescent *S. aureus* strain[126b] was used in these experiments, with the level of bioluminescence observed being proportional to the number of surviving cells after treatment. Use of the bioluminescent strain eliminated problems that arise from the deep blue colour of the hybrids and MB interfering with UV/Vis microplate readings.

Bioluminescence of *S. aureus* (100 µL of 10^6 CFU/mL MRSA USA300) was measured after overnight incubation of the cells in the dark with the increasing concentrations of ciprofloxacin, either alone or in the presence of MB (20 µM) or hybrids (10 µM). Bioluminescence versus [ciprofloxacin] curves are shown in Figure 3.21. Ciprofloxacin alone showed dose-dependent cell killing above 0.004 µg/mL and

essentially full eradication at around 0.128 µg/mL. Surprisingly, MB showed some synergic killing with ciprofloxacin in the absence of light. The reasons for this synergy are unknown but one possibility is that MB acts as a competitive substrate for NorA, thus lowering the rate of NorA-mediated ciprofloxacin efflux. The three hybrids **56**, **58** and **60** all strongly potentiated the cell-killing effects of ciprofloxacin.

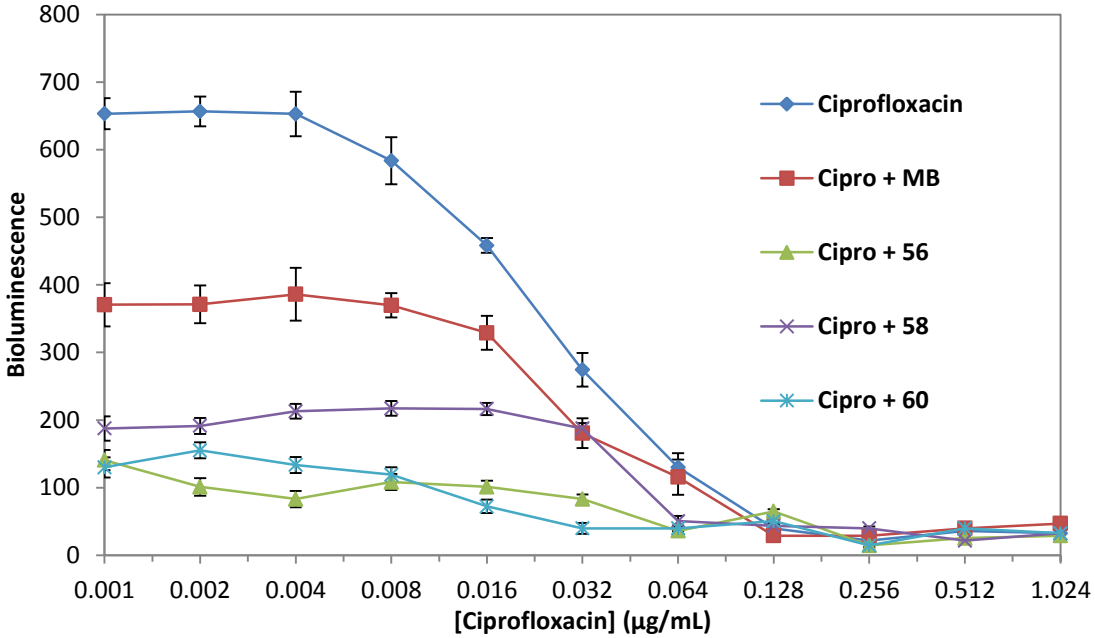

Figure 3.21 Effects of MB and hybrids **56**, **58** and **60** on survival of bioluminescent *S. aureus* cells when coadministered with increasing concentrations of ciprofloxacin. MB was present at 20 µM and the hybrids at 10 µM. Data represent the mean ± SEM from 3-4 independent experiments.

The synergistic effects provided further evidence that these hybrids serve to block the NorA pump and not simply evade its action. Blocking of the pump in these experiments led to increased intracellular concentrations of the antibiotic to potentiating its cell killing effects.

3.6 Summary and Conclusions

In this Chapter the photophysical properties of hybrids were measured and compared with MB. The UV/Visible absorption spectra of MB and all hybrids (Figure 3.1) showed that the λ_{max1} and λ_{max2} bands arising from the MB moiety in the hybrids and their extinction coefficients changed only slightly relative to MB, indicating that the absorption properties of the MB chromophore had not been markedly changed by addition of the appended EPI-linker structures.

SOSG and HPF probes were used to measure production of $^1O_2$ and •OH, respectively, from the hybrids relative to MB. Of the four different classes of hybrids, the reserpine-containing compounds **47**-**50** produced the most •OH, although the level were quite low (Figure 3.11). The same hybrids showed significant production of $^1O_2$. In contrast, pterostilbene-containing hybrids **51**-**54** showed virtually no •OH production and very little $^1O_2$ relative to MB. Examination of the aPDT activity of **47**-**50** and **51**-**54** against the model organism MRSA USA300 revealed that neither the reserpine-containing nor pterostilbene-containing hybrid classes showed any significant activity. Observing •OH and $^1O_2$ production by reserpine-containing hybrids **47**-**50** but no aPDT activity against MRSA USA300 demonstrates that production of ROS is not in itself sufficient to create hybrids with robust aPDT activity.

INF55-containing hybrids **55**-**58** showed only slight •OH production but they all showed stronger production of $^1O_2$. INF271-containing hybrids **59**-**62** also showed very little •OH production and only **60** and **62** showed good $^1O_2$ production. In the MRSA USA300 aPDT assays, INF55-containing hybrids **56** and **58** and INF271-containing hybrids **60** and **62** showed the strongest cell killing effects.

Lack of •OH production while at the same time producing significant amounts of $^1O_2$ is evidence that the aPDT activity observed with **56**, **58**, **60** and **62** was probably arising mostly through Type II mechanisms (See Chapter 1.9). Poor •OH production by all of the hybrids **47**-**62** was probably a result of the many additional hydrogen atoms in the molecules relative to MB. MB contains only strong aryl C-H bonds, whereas the hybrids contain many SP^3 C-Hs, which might be abstracted by •OH to quench the radical.

The two INF55-containing hybrids **56** and **58** and one of the INF271-containing compounds **60** were advanced to experiments examining the dose-dependency of their aPDT effects against the NorA-, WT and NorA++ *S. aureus* strains. Compounds **56** and **58** showed similar effects, with the slightly more potent **58** completely eradicating the NorA- and NorA++ strains at 40 μM and producing a 5-log kill at this concentration against the WT strain. Compound **60** showed similar potency to MB against the NorA++ strain but was less effective than MB against the NorA- and WT strains.

Uptake of **56**, **58** and **60** was explored next with the *S. aureus* panel. The key observation here was that the three compounds showed significantly greater uptake than MB in all strains and showed identical uptake to each other in all three strains. It was concluded that **56**, **58** and **60** were either evading the NorA pump and/or inhibiting the NorA pump.

The question of whether the compounds were blocking and/or evading the NorA pump was addressed by aPDT experiments with combinations of MB and various INF55- and INF271-containing synthetic intermediates. These substituted INF55 and INF271 analogues all strongly potentiated the aPDT activity of MB, confirming that the

structural changes that were introduced into the EPIs did not suppress their EPI activity. These results supported that the increased aPDT activity of **56**, **58** and **60** relative to MB was arising, at least in part, because their EPI portions were serving to block the NorA pump, and the resulting increases in intracellular MB were responsible for increase cell killing.

Further confirmation of the NorA pump-blocking activity of the hybrids was obtained from experiments with bioluminescent *S. aureus* strain and the fluoroquinolone antibiotic ciprofloxacin. Each of the compounds **56**, **58** and **60** showed strong potentiation of ciprofloxacin's antibiotic effects at 10 μM. As ciprofloxacin is a known substrate for the *S. aureus* NorA pump,[31c,185] its potentiation in the presence of the hybrids was further evidence that the compounds block this pump.

In summary, experiments in this Chapter validated the principal around which MB-EPI hybrids were designed for use in aPDT. Hybrid **58**, carrying INF55 as the EPI and an *N*-acyl-*N*,*N'*-dimethylethylenediamine linker to MB, was identified as the most active compound from these studies and advanced to an *in vivo* aPDT MRSA infection model (Chapter 4).

Chapter 4

In Vivo Antimicrobial Photodynamic Activity of Lead Hybrid 58 in a Murine MRSA Wound Infection Model

4.1 Staphylococcus aureus and Humans

S. aureus is a facultative aerobic Gram-positive coccus belonging to the *Staphylococcaceae* family. It is frequently found as a commensal organism in the human respiratory tract and on the skin,[186] but has also been a well-known human pathogen since it was first described by Sir Alexander Ogston in 1880.[187] Production of coagulase and the ability to ferment mannitol are two of the main characteristics that distinguish *S. aureus* from other staphylococci. Mean carriage rates in the general population are around 40% and it is estimated that ~ 20% of the population are carriers and that 60% are occasionally colonised.[188]

S. aureus can cause a spectrum of infections ranging from superficial skin infections to severe, invasive diseases, including bacteraemias.[189] Other organs can also be infected, such as the eye, skin, connective tissues, bones, joints, heart, lungs and gastrointestinal and urinary tracts.[190] *S. aureus* is known to degrade a number of host proteins and tissues through production of a range of enzymes and toxins in its quest for nutrients.[191] These enzymes include haemolysins, proteases, lipases and hyaluronidase. *S. aureus* proteases are able to modulate numerous host immune responses and can interfere with the kallikrein-kinin pathway. This leads to increased vascular permeability, which ensures a plentiful supply of nutrients for the bacteria at the site of infection.[192] *S. aureus* proteases have been implicated in the pathogenesis of skin disorders, such as atopic dermatitis.[193]

In addition to obtaining nutrients, *S. aureus* must also be able to repel constant attacks from the innate and acquired immune systems of its human host. *S. aureus*

produces an extensive array of virulence factors for this purpose. It can produce a variety of toxins and factors that kill leukocytes, inhibit neutrophil chemotaxis, resist phagocytosis, inactivate complement and neutralise host antimicrobial peptides.[194] Many of these virulence factors are multifunctional, for example protein A. This cell wall-associated protein causes release of pro-inflammatory cytokines from monocytes and fibroblasts[195] and also binds to the Fc region of human IgG to disturb antibody opsonisation.[196]

While numerous antibiotics have been used effectively against *S. aureus* infections over many decades, the frequency of these infections has increased gradually with time and has been accompanied by increases in mortality rates.[197] Today, *S. aureus* is the most frequent cause of hospital-acquired infections, including surgical site infections,[198] and is the most common causative agent of skin and soft tissue infections in the North and Latin Americas and Europe.[199] An analysis of the burden of skin and skin-structure infections in the USA caused by *S. aureus* found that these infections are associated with high treatment costs, estimated at ~ $11,000 per patient per episode.[200]

4.2 Methicillin-Resistant *S. aureus* (MRSA)

MRSA was first reported in 1961[201] and has since undergone significant evolutionary changes and epidemiologic expansion.[202] It was so-named because it expresses penicillin-binding proteins (PBPs) that show reduced affinity for penicillins (e.g. methicillin) and other common β-lactam antibiotics.[202] Currently, more than half of nosocomial *S. aureus* infections in many countries are caused by MRSA.[203] In the United States, MRSA accounts for almost 60% of clinical *S. aureus* strains isolated

from intensive care units.[204] Isolates from blood cultures taken from bacteraemia patients in England revealed that the proportion of MRSA infections has increased dramatically there from 5% in 1990 to 40% in 2000.[205] As well as being a major cause of hospital-acquired infections all over the world, MRSA is now widespread in the community, especially in nursing and residential homes.[200b,206] Indeed some MRSA strains are becoming the dominant pathogen in the community (i.e. community-acquired MRSA).[207]

Vancomycin, from the glycopeptide family of antibiotics, has been used extensively in clinical practice for complicated *S. aureus* and other Gram-positive infections over several decades. In the last 20 years, however, concerns have been growing over the increasing minimum inhibitory concentration (MIC) of vancomycin against MRSA.[208] As it is expected that vancomycin resistance will continue to increase in the coming years, it seems only a matter of time before MRSA becomes resistant to this antibiotic. There is thus an urgent need to develop new antibiotics and approaches to replace vancomycin as its effectiveness wanes.

4.3 Skin and Soft Tissue *S. aureus* Infections and their Treatment

S. aureus is the most frequently isolated pathogen from skin and skin-structure infections.[209] Optimal treatment regimes for staphylococcal skin and soft tissue infections are constantly being modified.[210] Due to the high incidence of resistance, β-lactams are no longer an effective treatment choice. Although clindamycin can be effective, its use has been connected with increasing rates of *Clostridium difficile*-associated diarrhoea, leading to concerns about its use in skin infections.[131] Linezolid is

also active against the majority of MRSA strains but it is costly and can be associated with haematological side effects.[211] Doxycycline and minocycline need to be used with caution due to photosensitivity side effects and cannot be used in children under nine due to deposition in teeth and bones. There is also a lack of data to support their efficacy against community-acquired MRSA. Rifampin is another antibiotic that has been shown to be effective against MRSA, but its high frequency generation of resistant mutants requires that it not be used alone.[212] Fluoroquinolones are no longer indicated for the treatment of skin and soft tissue *S. aureus* infections due to resistance.[213]

Vancomycin remains as the antibiotic of choice for invasive staphylococcal infections. In more severe skin and soft tissue infections, tigecycline and daptomycin may also be used,[213] although tigecycline is expensive and both drugs can only be administered intravenously.[214] While several effective therapies have been developed for staphylococcal infections their use is primarily reserved for severe, complicated infections.[215] Because of this and the other problems noted above, especially resistance, there is a continuing need to develop new therapeutics and strategies for treating MRSA and other staphylococcal skin infections.

aPDT presents an attractive alternative due to the ease of applying light to the infected skin surface and because of its effectiveness against resistant organisms (Chapter 1.8). For example, in wound infection operations, which are often complicated by antibiotic-resistant strains of bacteria and account for 25% of all nosocomial infections,[216] aPDT could present a very practical and effective treatment.[217] However, it is unlikely that aPDT could be the only treatment modality employed due to the

severe nature of some of these infections. Nevertheless, it could be useful for lowering the bacterial burden and thus the amount of surgical debridement required.[216]

4.4 aPDT as a Potential Treatment for MRSA Skin Infections

As alluded to above, aPDT is particularly suited to superficial staphylococcal infections due to the accessibility of the infection site and ease of topical application of a photosensitiser and its subsequent illumination.[218] Additionally, the vulnerability of *S. aureus* to toxic photosensitisation is well recognized.[219] Effects of photosensitisation on the activities of virulence factors produced by the pathogen has generated some resent interest.[220]

One of the advantages of aPDT for skin infections is that the treatment can be focussed directly on the infection site using laser light from an optical fibre that produces a beam diameter of only millimetres. This ensures that inadvertent exposure of host tissues to photosensitisation can be minimised. It has been suggested that the specificity of aPDT might be further increased by conjugating antibodies to photosensitizers that target specific antigens on organisms of interest. This approach has been explored, for example, with an IgG-tin(IV) chlorin e6 conjugate.[221] In practice, however, such a strategy would be costly to implement clinically and would require the infecting organism to be properly identified before treatment. While such selectively is very attractive from a scientific perspective, if aPDT does not cause considerable damage to human cells in clinical practice then the need for targeting methods may not be necessary. In support of these simpler and cheaper approaches, treatment of keratinocytes with MB and visible light has been shown not to cause DNA damage, indicating that the treatment is unlikely to be accompanied by genotoxicity.[222]

A number of *in vitro* studies have reported the use of aPDT for inactivating MRSA[223] but there have been relatively few *in vivo* studies. One *in vivo* study explored the effects of aPDT in a skin abrasion wound infection mouse model that made use of a bioluminescent MRSA (Xen31) strain.[126b] This strain allowed real-time monitoring of the infection using a bioluminescence camera. Treatment with a polyethylenimine-(PEI-)ce6 photosensitizing agent (Figure 4.1) and a range of noncoherent red light fluences applied 30 minutes after bacterial inoculation produced up to 2.7 log reductions in MRSA, as measured by loss of bioluminescence from the wounds. Application of aPDT also accelerated wound healing by 8.6 days compared to untreated wound infections.[126b]

In another mouse skin abrasion infection model, a tetracationic Zn(II)phthalocyanine derivative (RLP068/Cl, Figure 4.1) was used as the photosensitizer and shown to inactivate MRSA, inhibit regrowth and accelerate wound healing.[224] In this study, full-thickness wounds of 0.8 cm diameter were established in the subcutaneous back tissue of BALB/c mice and inoculated with 5×10^7 CFU MRSA.[225] Strong bacterial inactivation (> 3 log kill) was observed after two days when mice were treated with the agent and illuminated with visible light. For this *in vivo* study, Complete re-epithelialization was observed in aPDT-treated mice 9 days after therapy.[225]

In a third mouse skin wound EMRSA-16 (epidemic MRSA) infection study, treatment of infected mice with 100 μg/mL MB followed by illumination with 670 nm laser light (total fluence 360 J/cm^2) resulted in a 25-fold reduction in the number of EMRSA-16.[226]

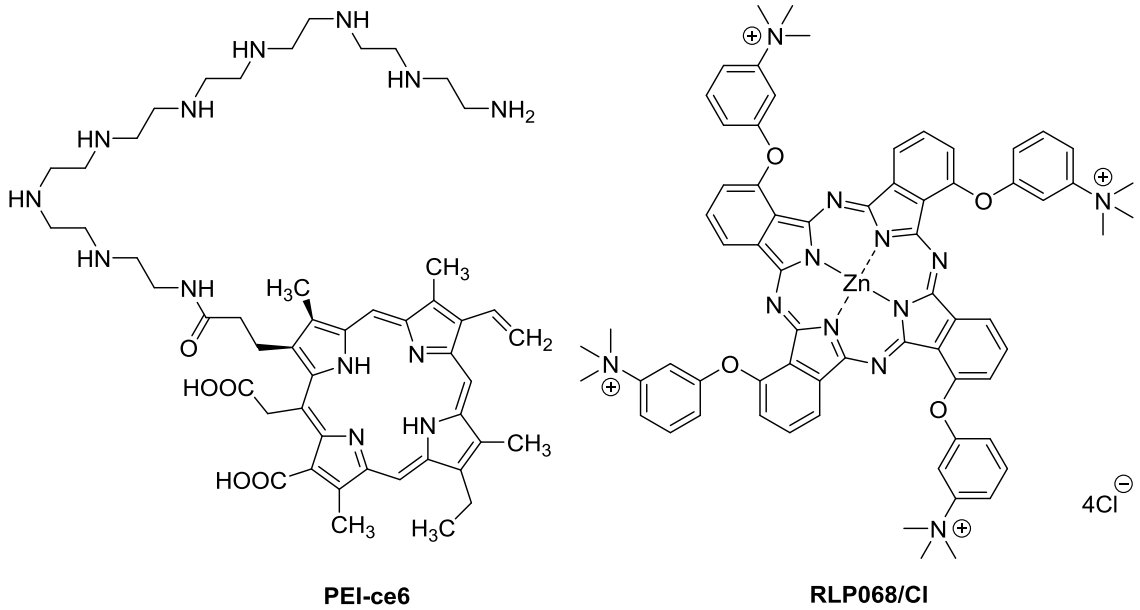

Figure 4.1 Structures of polyethylenimine-ce6 (PEI-ce6) and tetracationic Zn(II) phthalocyanine chloride (RLP068/Cl) photosensitizers used in mouse skin abrasion infection studies.[126b,224]

The effectiveness of aPDT against MRSA arthritis has been tested *in vivo* in a mouse model. MRSA arthritis is a disease affecting joints, where bacteria from the skin are introduced into the joint synovial fluid, usually via percutaneous instrumentation. This study revealed that ~ 30% of intra-articular leukocytes, mainly neutrophils, died immediately after aPDT with photofrin.[227] After 24 h aPDT treatment an additional reduction in the number of intra-articular leukocytes and atrophy of the synovial tissue were observed. Isolated peripheral neutrophils were shown to have significant affinity for photofrin and displayed substantial morphological damage after aPDT.[227] These results suggest that aPDT would probably not be useful in MRSA arthritis because of the damage to intra-articular neutrophils and synovial tissues.

In an attempt to increase bacterial inactivation and reduce damage to host neutrophils, the same group later studied the effects of intra-articular injection of photofrin rather than intravenous administration.[228] Each animal received a knee injection of MRSA (5×10^7 CFU) and after 3 days Photofrin (1 mg) was applied and illuminated 635 nm light as a range of fluences. The maximum reduction of MRSA was achieved at a 20 J/cm^2. Lesser effects were observed at lower fluences.[228] The authors concluded that aPDT for murine MRSA arthritis would require optimised light dosimetry to rapidly inactivate bacteria without affecting neutrophils at the infected site. aPDT with too low a fluence might inactivate insufficient bacteria, whereas too much light could inactivate neutrophils and damage host tissues, allowing bacteria to regrow in an environment where the immune response had been compromised.

An artificial skin construct has been developed for simulating MRSA skin infections.[229] The artificial skin is constructed from human-derived epidermal keratinocytes and dermal fibroblasts, cultured at a media interface to form a stratified model of full-thickness, epithelialized human skin. aPDT with MB in this model produced a strong reduction (> 5 log kill) compared to controls and the effect was sustained over multiple days. Application of MB without light resulted in only a small reduction in MRSA viability.[229]

4.5 aPDT Activity of Lead Hybrid 58 in a Murine MRSA Wound Infection Model

The final part of this thesis work involved examining the aPDT activity of lead hybrid **58** in an *in vivo* murine MRSA wound infection model. Compound **58** was chosen for the study due to its potent *in vitro* aPDT activities, as detailed in Chapter 3, where its superior effects relative to MB were clearly evident. The primary goal of this

in vivo study was to demonstrate that the superior *in vitro* activities of **58** relative to MB translated to a real MRSA infection. The needle scratch model, developed by Dai *et al*,[126b] was chosen for the study. This model reflects the initial colonisation stage of the wound infection process and uses a bioluminescent variant of a strain of MRSA (MRSA Xen 30)[230] that is known to cause wound infections of significant clinical relevance, sometimes with fatal outcomes.[231]

4.5.1 Experiment Protocol and Results

Female BALB/c mice were divided into 5 cohorts (Table 4.1). Group A animals (n = 6) were absolute controls that received no treatment, Group B (n = 6) were dark controls for MB (no light), Group C (n = 6) received aPDT treatment with MB. Group D (n = 6) were dark controls for hybrid **58** (no light) and Group E (n = 6) received aPDT treatment with hybrid **58**.

Table 4.1 Animal cohorts for murine MRSA wound infection study.

Group	Animals	Treatment
A - Absolute control	6	No treatment
B - Dark control for MB	6	MB (40 µL of 200 µM)
C - aPDT with MB	6	MB + light (12, 36, 84, 120 J/cm^2; 652 nm)
D - Dark control for **58**	6	**58** (40 µL of 200 µM)
E - aPDT with **58**	6	**58** + light (12, 36, 84, 108, 120 J/cm^2; 652 nm)

Inoculation of 10^8 CFU MRSA Xen 30 into scratch wounds (using a needle) on the shaved backs of immunosuppressed female BALB/c mice, led to a stable infection, as confirmed by bioluminescence imaging (Figure 4.2, Group A). Pictures were captured using a bioluminescence camera immediately after MRSA inoculation and 30 mins post-inoculation. Light was then applied to the aPDT cohorts (Groups C and E; Time 0) and images were captured for all cohorts after 2, 6, 14, 18 and 20 min. Application of 652 nm light in the aPDT cohorts for these periods corresponded to fluences of 12, 36, 84, 108 and 120 J/cm^2, respectively. Images obtained from a representative animal in Groups A, C and E are shown in Figure 4.2.

	Group A (Absolute Control)	Group C (aPDT with MB)	Group E (aPDT with 58)
Immediately after MRSA inoculation	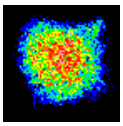	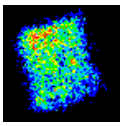	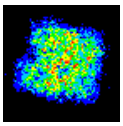
30 min post-inoculation	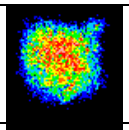	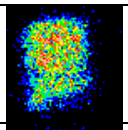	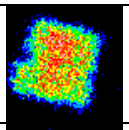
Time = 0	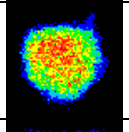	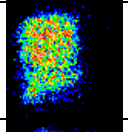	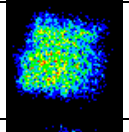
Time = 2 min E = 12 J/cm^2	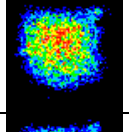	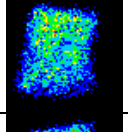	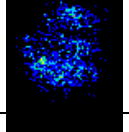
Time = 6 min E = 36 J/cm^2	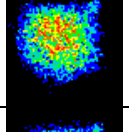	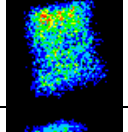	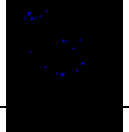
Time = 14 min E = 84 J/cm^2	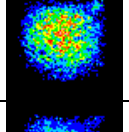	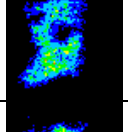	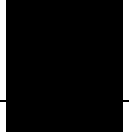
Time = 18 min E = 108 J/cm^2	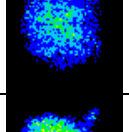	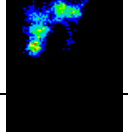	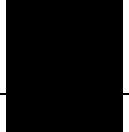
Time = 20 min E = 120 J/cm^2	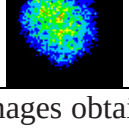	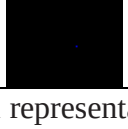	

Figure 4.2 Bioluminescence images obtained from a representative animal in Groups A C and E in the murine MRSA wound infection model. Images were captured post-inoculation and at the times indicated. Application of 652 nm light for these periods in the aPDT Groups C and E corresponded to the fluences indicated. MB in Group C and compound **58** in Group E were applied by delivering 40 µL of 200 µM solutions (formulated in CrEL, see Section 3.3.1) via micropipette directly to the infection site.

The bioluminescence image data from Figure 4.2 is presented graphically in Figure 4.3. These data represent the mean ± SEM of normalized bioluminescence emanating from the wounds of the 6 mice in each cohort. In the absence of photosensitizers (Absolute control – Group A), the relative bioluminescence units

(RLU) decreased only marginally, indicating that infection was stable over the course of the experiment and relatively unaffected by application of light alone.

In the MB dark control (Group B), there was no significant reduction in bioluminescence after 6 min, and after 18 min bioluminescence reduction was less than 0.6 RLU (Appendix 4.1(A)). A clear light dose-dependent response was observed in the aPDT cohort treated with MB (Group C). After 2 min of light application (E = 12 J/cm^2) luminescence was reduced by 45%, which increased to 70% after 6 min (E = 36 J/cm^2). Disappearance of the luminescence signal was observed after 18 min (E = 108 J/cm^2). In Group D, where hybrid **58** was applied without light only a small (0.1 RLU) reduction in luminescence was observed at the highest incubation (Time = 20 min) (Appendix 4.1(B)). In Group E, where aPDT with **58** was applied, a remarkable 98% reduction in luminescence was observed after applying light for only 2 min (E = 12 J/cm^2), and total loss of the luminescence signal was observed after 6 mins (E = 36 J/cm^2).

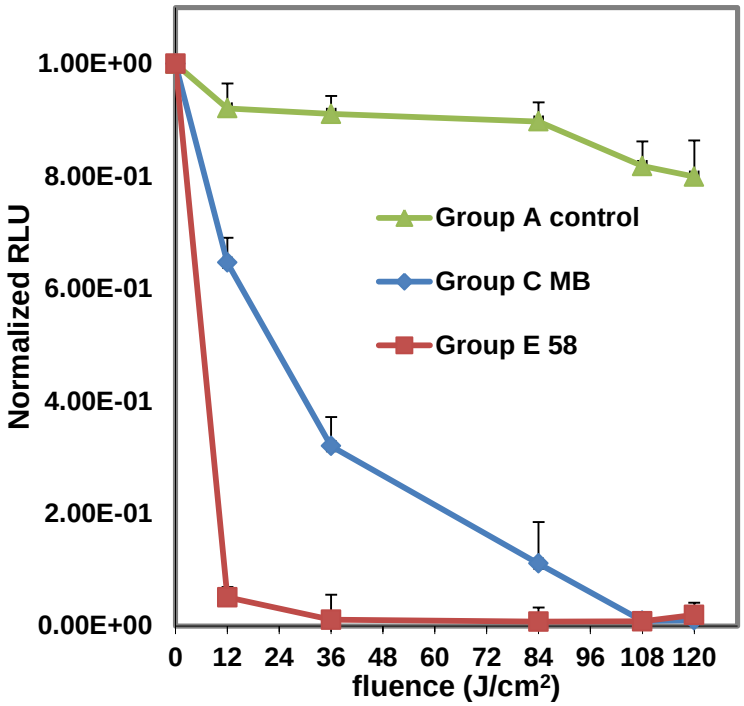

Figure 4.3 Light-dose response (mean ± SEM) for Groups A, C and E in the bioluminescence MRSA wound infection model. Data are presented as normalized relative luminescence units (RLU). Dark control Groups B and D showed only small reductions in RLU at 120 J/cm^2 (Appendix 4.1).

4.5.2 Post-Treatment Monitoring of Infections

Post-treatment monitoring of the bioluminescence signal was carried out daily from the treatment day (Day 0) until to Day 10. As shown in Figure 4.4, a rebound in the bacterial load (as indicated by a 1.6 fold increase in luminescence) was observed in each of the non-aPDT control groups (Group A, B and D) after 1 day. These infections resolved naturally over the course of the following 10 days. For the MB-aPDT cohort (Group C) a smaller (1.3 fold) rebound was observed after 1 day and the infection was completely resolved after 7 days. For the **58**-aPDT cohort (Group E), essentially no

rebound in bacterial load was observed after 1 day and the infection completely resolve after 4 days.

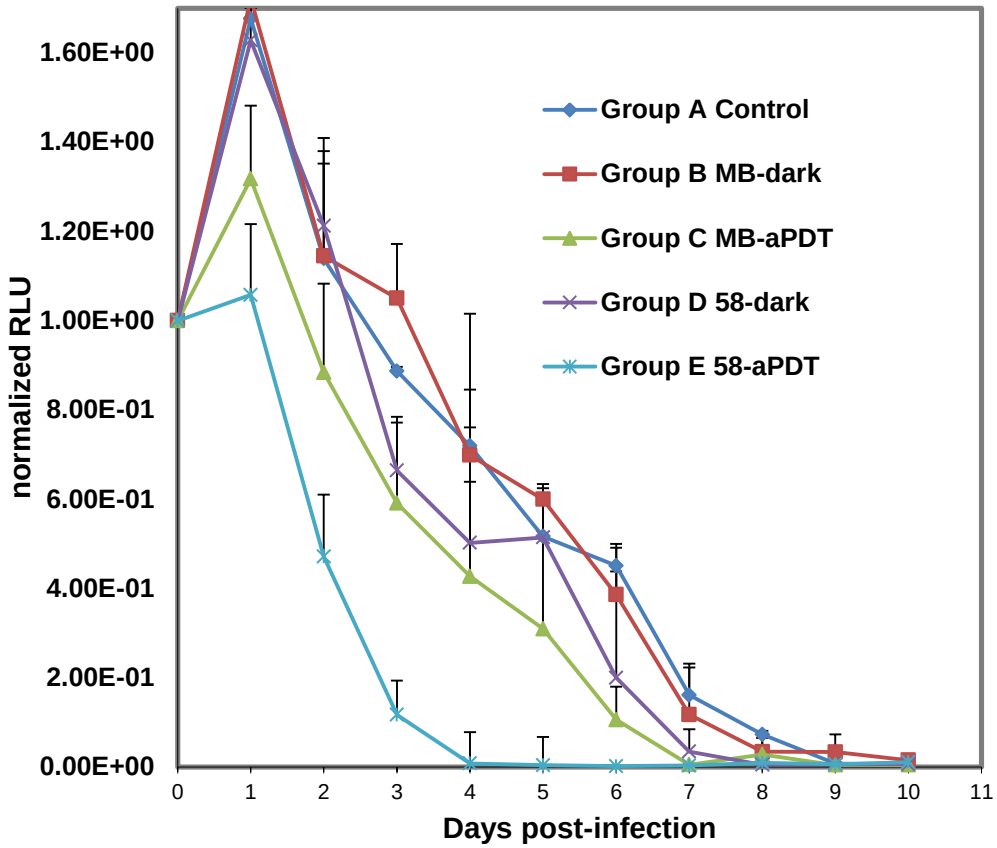

Figure 4.4 Ten day post-treatment monitoring of bacterial loads for Group A-E in the MRSA wound infection study. Luminescence (normalized) emanating from animal infection sites was measured using a luminescence camera. Data represent mean ± SEM obtained from 4-6 animals in each cohort. The luminescence images from which the data were derived (from representative animals in each cohort) are provided in Appendix 4.2.

4.5.4 Wound Healing

During experiments all mice were monitored visually for signs of poor health, suggesting that they might have developed a systemic infection. Weights of animals

were monitored as a proxy for general health. Slight reduction on body weights of animals was included in the formulae used for calculation of total RLU.

Wounds of all animals were also inspected visually for signs of healing. As shown in Figure 4.5, cohorts that received no aPDT treatments (Group A, B and D) showed few signs of wound healing on days 4-6 of the post-treatment monitoring period. In contrast, the MB-aPDT cohort (Group C) showed considerable healing by day 6 and had formed a visible scab by day 7 (not shown). Animals treated with aPDT and **58** (Group E) showed much faster wound healing, with a visible scab formed after only 4 days and the wound visibly healed by Day 6.

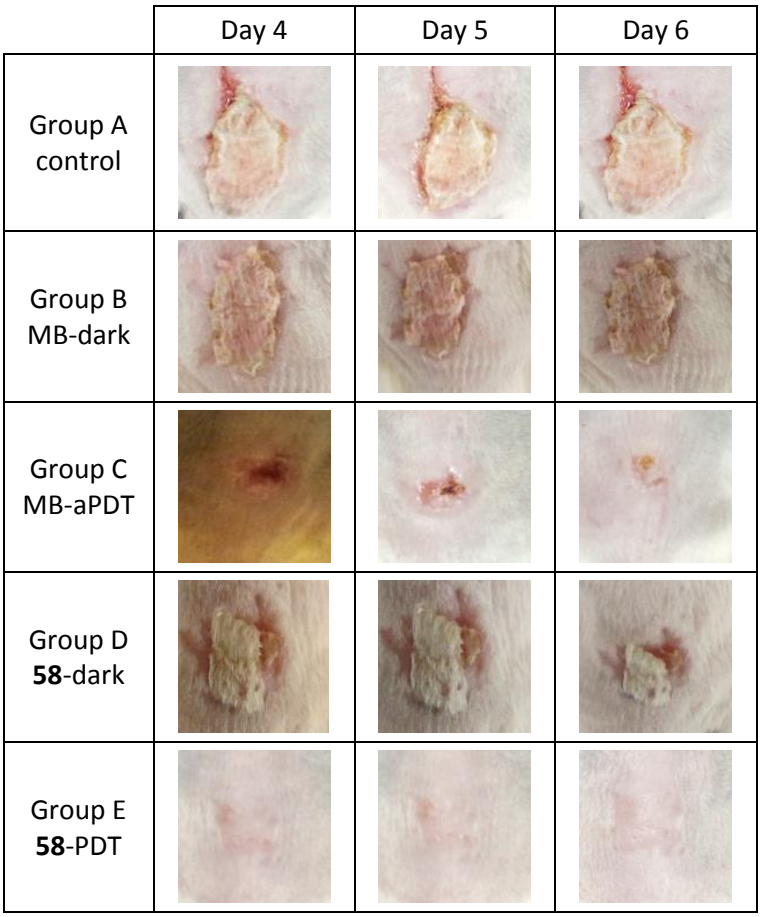

Figure 4.5 Images showing wound healing in representative animals from Groups A-E on Days 4-6 post-treatment.

4.6 Summary and Conclusions

In this Chapter, a mouse skin abrasion wound infection was established by the topical application of an MRSA suspension to superficial scratch wounds on the shaved dorsal surfaces of BALB/c female mice. Use of bioluminescent bacteria allowed real-time monitoring of the extent of the infection in the mice wounds following treatment with MB and lead hybrid **58**. The images captured after aPDT treatments using a 200 μM solution (40 μL) of **58** showed a very strong light-dose response effect, where all bacterial luminescence had disappeared after application of only 36 J/cm^2 of 652 nm light. 3-Fold higher light doses (108 J/cm^2) were required to effect total loss of luminescence using MB at the same concentration.

In the days post-aPDT treatment with **58**, minimal bacterial re-growth was observed and total disappearance of the bioluminescence signal occurred by day 4. Complete loss of bacterial luminescence in dark controls with **58** was not observed until Day 9. For MB, significant bacterial regrowth was observed in the day following aPDT treatment and total disappearance of the bioluminescence signal was not observed until Day 7. The wound healing process after aPDT treatment with **58** occurred earlier (Day 4) than with MB (Day 7), as observed by scab formation in the treated area. Wound healing in Groups treated with MB and **58** alone (i.e. no light) or with no compound treatment did not heal until Days 12-14. These results demonstrated that aPDT with hybrid **58** enhances bacterial inactivation and improves wound healing compared to the parent photosensitizer MB in this infection model. This finding strongly supported our original hypothesis that attachment of an EPI to MB can enhance its aPDT activity.

Chapter 5

Conclusions and Future Directions

This thesis explored novel light-activated antimicrobial photosensitizers as potential new agents for inactivating MDR bacteria using aPDT. The overall goal was to identify an MB-EPI hybrid that showed improved efficacy relative to MB as a potential treatment for superficial, localised infections, such as *S. aureus* skin infections.

Evidence has revealed that MDR pumps contribute to antibiotic resistance by transporting a wide variety of structurally diverse compounds, including the phenothiazinium dye MB.[19] Pharmacological inhibition of pumps, where small molecule inhibitors are used to block pump activity, is one of the strategies that have been investigated to date.[62a] Potentiation of the aPDT effects of MB upon co-incubation of MDR bacterial strains with MB and EPIs had previously been reported.[99a] As discussed in Chapter 1, EPIs can raise the concentration of MB within bacterial cells. Upon irradiation with visible light, MB generates toxic ROS via Type I and II photosensitization processes to kill bacterial cells.

Chapter 1 summarized several issues with using combinations of MB with EPIs and proposed that MB-EPI hybrids could potentially be used to address efflux pump-mediated resistance in aPDT.[154] The concept of MB-EPI hybrids evolved from the reported "dual antimicrobial action" observed with berberine-EPI hybrids (i.e. SS14) that target the NorA pump in *S. aureus*.[162] The physicochemical similarities between berberine and MB and evidence that they are overlapping substrates for various efflux pumps, including NorA, suggested that an analogous MB-EPI hybrids strategy might be successfully applied in aPDT.[99a,154]

In Chapter 2, a convergent synthetic strategy was described for the synthesis of 16 hybrids that conjugated MB to the EPIs reserpine, pterostilbene, INF55 and INF271.

Piperazine and *N*,*N*'-dimethylethylenediamine-based linkers were used to attach the EPIs to MB. Requisite EPI-alkyl/acyl-piperazine and EPI-alkyl/acyl-ethylenediamine-based precursors were prepared and then reacted according to Strekowski's method with a key phenothiazinium common intermediate **63** to form the target hybrids. It was observed that the Strekowski reactions were best carried out in the absence of light to minimise photodegradation. All compounds were purified by preparative TLC, eluting with a very uncommon solvent system (3% $NH_4OAc_{(aq)}$:MeOH 15:85) and subsequently converted to chloride salts using Cl^- anion exchange resin (Chapter 6). Sufficient quantities (25-95 mg) of the final hybrids were obtained for the photophysical and photobiological studies. High resolution mass spectroscopy, NMR and UV/Vis spectroscopy of these hybrids were used to characterize their structures.

As discussed in Chapter 1.14, when designing the hybrids, it was considered crucial that the photosensitization properties of MB be maintained and that this might be achieved by substituting the C-7 *N*-Me groups of MB with *N*-alkyl and piperazinyl linkages. To measure the effects of the structural changes we compared the absorption properties of MB to hybrids by examining the λ_{max1} and λ_{max2} values and extinction coefficients. The λ_{max} and log ε data confirmed that introduction of the various linker groups and EPIs did not significantly impact the absorption properties of the MB chromophore. An interesting observation from these experiments was that the highest $\Delta\log\ \varepsilon_1$ value (0.22), meaning that the compound had the greatest reduction in chromophore absorptivity of all the hybrids relative to MB, was observed with **58**, the compound that was ultimately shown to produce the best activity. It was concluded that absorptivity of the chromophore was not a critical parameter in these hybrids for showing good aPDT activity.

We hypothesized that these light-activated antimicrobial hybrids would show increased effectiveness over the parent PS MB against *S. aureus* in aPDT by generating increased intracellular ROS through inactivation of MDR pumps, namely NorA. Two important assays were performed to explore whether hybrids maintained the PS and EPI properties:

1- Measurement of $^1O_2$ and •OH phototoxic species.
2- Assays to demonstrate retention of efflux pump inhibitory activities.

Production of ROS by PSs can be probed experimentally by fluorescence-based ROS scavengers. SOSG and HPF probes were used to measure production of $^1O_2$ and •OH, respectively, from the hybrids. All hybrids were found to produce less $^1O_2$ and •OH than MB. Reserpine-containing hybrids **47**-**50** showed $^1O_2$ and •OH quantum yields at around 20-55% of MB, with **48** showing the highest •OH production (55%) of all hybrids. Pterostilbene-containing hybrids **51**-**54** all showed $^1O_2$ and •OH quantum yields less than 20% relative to MB. INF55-containing hybrids **55**-**58** and INF271-containing hybrid **59**-**62** generally showed higher $^1O_2$ and •OH quantum yields. $^1O_2$ production for **55**, **56**, **58** and **62** were at 65%, 50%, 60% and 55% relative to MB. It was observed that production of $^1O_2$ was in general stronger than production of •OH, indicating that any observed phototoxicity effects would probably occur via Type II mechanisms.

Aqueous solubilisation of hybrids was achieved by encapsulation in cremophor EL (CrEL). This was determined to be the best detergent out of tween 60 (T60), triblock copolymers F127 (PL-F127) and poloxamer 388 (POL388) for solubilising reserpine-containing hybrid **49**, a particularly insoluble hybrid in aqueous solutions. Due to its

powerful solubilizing effect on **49** and its widespread use as a vehicle for many poorly water-soluble compounds, as well as its low toxicity properties,[180-181] CrEL was chosen as the vehicle for formulating all hybrids in this study.

Preliminary *in vitro* aPDT screening against *S. aureus* USA300 revealed that hybrids **56**, **58**, **59** and **60** showed a better killing than MB at equivalent concentrations and fluence. MB was found to reduce the viability of *S. aureus* USA300 by 2 log units, whereas hybrids **56**, **58**, **59** and **60** showed killing effects of 3-6 logs (Figure 3.14). This result provided the first evidence that some of the hybrids could function as designed; i.e. with the EPI serving to block MDRs and generate higher intracellular concentrations of the attached MB PS and better aPDT cell killing. To support this, MICs were measured with the antibiotic ciprofloxacin, a known MDR substrate for NorA pump in the presence of hybrids and MB in the dark. The MIC of ciprofloxacin was greatly potentiated in the presence of hybrids, leading us to conclude that they are able block MDR pumps in *S. aureus*, specified NorA.

In Chapters 3.3.3, the aPDT activities of the four lead hybrids were explored against NorA knockout (NorA-), wild-type (WT) and NorA-overexpressing (NorA++) mutant *S. aureus* strains. These experiments aimed to obtain further evidence that hybrids show photodynamic effects that were influenced by their action on the NorA pump. aPDT with MB against these strains displayed the hallmarks of it being a substrate for the NorA pump. MB produced a 2 log kill against the NorA++ strain upon irradiation with 16 J/cm^2 of light, and a 4 log reduction was obtained under the same conditions in the NorA- strain. In contrast, phototoxicity of the three hybrids **56**, **58** and **60** remained unchanged (3 log killing) against all three strains, consistent with these

compounds not being substrates for the NorA pumps, and possibly serving to block this pump.

Of the three best hybrids identified from the *in vitro* aPDT experiments, two - contained INF55 (**56** and **58**) and one contained INF271 (i.e. **60**). Hybrids incorporating the natural product EPIs reserpine and pterostilbene showed no aPDT activity, demonstrating the crucial role that molecular structure plays in the activity. The study also demonstrated the importance of linker groups in the structures, where hybrids with piperazine-based linkers (indicated as red/pink data in the Chapter 3 figures) generally showed poorer aPDT activities in comparison to equivalent compounds with *N*,*N'*-dimethylethylenediamine-based linkers (indicated as light blue/dark blue data in the Chapter 3 figures). This was highlighted with INF55-containing hybrids **55**-**58**, where hybrid **58** containing an *N*,*N'*-dimethylethylenediamine linker was found to be the best performing hybrid overall, whereas the equivalent hybrid **55** with a piperazine-based linker showed very little *in vitro* aPDT activity. The better performance of the *N*,*N'*-dimethylethylenediamine linker may arise from its increased flexibity compared to the rigid piperazine linker.

The efflux pump inhibitory activity of **56**, **58** and **60** was explored by measuring uptake of these compounds into WT, NorA- and NorA++ *S. aureus* cells. The hybrids showed identical uptake in all three strains, consistent with them not being NorA substrates.

aPDT concentration response experiments with NorA++ *S. aureus* cells identified hybrid **58** as a highly potent lead. At 40 μM this hybrid showed complete eradication of cells at 10 J/cm^2 fluence (Figure 3.18). Under the same conditions, MB

produced a 5 log kill. It was also noted that, increasing the concentration of MB to 160 μM did not lead to complete eradication, as was observed with **58**. On the basis of all of the photophysical an *in vitro* aPDT experiments hybrid **58** was advanced to an *in vivo* aPDT infection model.

A murine MRSA wound infection model was used to study the *in vivo* activity of lead hybrid **58**.[232] This model reflects the early stages of an infectious process, i.e. initial colonisation of a wound by a potential pathogen. Infections were established by inoculating scratch wounds on the dorsal surfaces of mice with bioluminescence MRSA. MRSA was found to be highly susceptible to photodynamic killing by **58**, where irradiation with 36 J/cm^2 of 652 nm light in the presence of 200 μM **58** resulted in complete disappearance of luminescent MRSA. A 3-fold higher light dose (108 J/cm^2) was required for the same effects using MB at the same concentration. Post-treatment monitoring of the bacterial loads showed that total disappearance of the bioluminescence signal had occurred by Day 4 with **58**, which was not observed until Day 7 with MB. Significant bacterial regrowth had occurred one day after treatment with MB but this rebound growth was not observed with **58**.

This study has demonstrated that Gram-positive bacteria are susceptible to hybrid-photosensitization and low light energies were found to kill the bacteria. It has been reported that higher light energies are often necessary to kill the Gram-negative species.[233] It would be of interest to explore the activity of **58** against Gram-negative, e.g. *P. aeruginosa*, in future experiments, and it would be worthwhile using higher light fluences in these studies.

MB has been used clinically and is known to show low toxicity towards normal cells.[234] In this thesis it was shown that the effects of **58** occur at lower concentration than MB, suggesting it would likely show little toxicity in humans. The low irradiation times required for the successful killing of bacteria and reduction of their virulence potential are attractive features for the clinical setting, where short treatment durations would cause less discomfort to patients and minimise damage to host tissues. Further investigations are needed to fully understand the toxicity of these hybrids.

As shown in chapter 2, a library of four compounds using four different linker groups were synthesized for each EPI used in this study. The importance of linker group as well as EPIs was revealed by this study. Hybrids **55** and **58** have the same EPI but different linker group and the result shows that hybrid **58** with *N,N'*-dimethylethylenediamine linker showed 4 logs killing of *S. aureus* NorA-overexpressing whilst the hybrids **55** with piperazine linker group did not reveal any activity. Further pharmacophore study need to perform to find the best non-cleavable or any possibility of using cleavable linker groups for these hybrids.

Chapter 6

Experimental

6.1 Experimental Procedure - Chemistry

6.1.1 Chemistry - General

All reactions were performed under an argon atmosphere in flame or oven-dried glassware with magnetic stirring unless otherwise stated. Pterostilbene was purchased from ChromaDex (NV, USA). Reserpine, IRA-904 quaternary ammonium Cl^- anion exchange resin and all other commercial reagents were purchased from Sigma-Aldrich (St. Louis, MO) and used without further purification, unless otherwise noted. Anhydrous acetonitrile and toluene were obtained using a PureSolv system. *N*,*N*-dimethylformamide (DMF) was dried over barium oxide and distilled under reduced pressure onto 4Å molecular sieves. Anhydrous tetrahydrofuran (THF) and diethyl ether (Et_2O) were freshly distilled from sodium benzophenone ketyl. All other solvents were of analytical reagent (AR) grade and used as received. The term petroleum spirit refers to petroleum spirit within the boiling range 40-60 ^oC.

Reaction monitoring was performed using thin layer chromatography (TLC) analysis on Merck Silica Gel 60 F_{254} (0.2 mm) aluminium plates. Purification by flash column chromatography used silica gel 60 (230-400 mesh, Merck) with the indicated eluents. Purification of hybrids **47**-**62** was performed using Merck 60 F_{254} preparative TLC plates (1000 µm).

Melting points were determined on a Buchi digital M-560 melting point apparatus and are uncorrected. ^1H and ^{13}C NMR spectra were recorded on either Varian Unity-300 MHz or Varian-Inova-500 MHz spectrometers in deuterated solvents. Spectra were referenced internally using the chemical shifts of solvent resonances

relative to TMS. UV/Vis spectra were recorded on a Shimadzu UV-1700 PharmaSpec UV/Vis spectrophotometer. Infrared spectra were obtained as neat samples using an Avator ESP spectrometer. Low resolution electrospray ionisation mass spectra (EI-LCMS) were measured using a Shimadzu LC-MS (2010) spectrophotometer. High resolution electrospray ionisation mass spectroscopy (HRESI-MS) were recorded using a factory modified Waters QToF Ultima^{TM} Spectrometer (Wyntheshawe, UK).

6.1.2 Synthesis of 3-(Dimethylamino)phenothiazin-5-ium triiodide 63

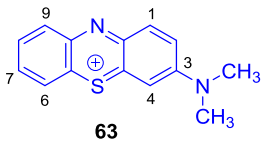

63

Dimethylamine in methanol (6.2 g, 11.9 mmol) was added dropwise to a solution of phenothiazin-5-ium tetraiodide hydrate **65** (5.0 g, 6.90 mmol) in 80 mL chloroform at room temperature. The reaction was stirred for 5 h while monitoring by TLC (3% $NH_4OAc_{(aq)}$/MeOH, 15:85). The resulting precipitate was filtered, washed with chloroform and air dried to give **63** (205 mg, 60%) as a dark blue solid. TLC R_f (3% $NH_4OAc_{(aq)}$/MeOH, 15:85) = 0.28; Mp 144 -145 ºC. ^{1}H NMR (500 MHz, $(CD_3)_2SO$) δ 8.18 (dd, J = 8.0, 1.6 Hz, 1H, H9), 8.13 (dd, J = 8.0, 1.6 Hz, 1H, H6), 8.06 (d, J = 10.0 Hz, 1H, H1), 7.98 (dd, J = 10.0, 2.4 Hz, 1H, H2), 7.94 (d, J = 2.4 Hz, 1H, H4), 7.82 (m, 2H, H7, H8), 3.64 and 3.60 (2s, 6H, $N(CH_3)_2$); ^{13}C NMR (125 MHz, $(CD_3)_2SO$) δ 156.1, 144.1, 139.8, 139.6, 138.0, 134.6, 133.2, 129.8, 126.3, 126.1, 125.8, 109.7, 43.4, 42.9; IR (neat) ν 2800, 1617, 1559, 1489, 1429, 1411, 1252, 1118, 1078, 887, 835, 772 cm^{-1}; HRESI-MS: *m/z* calcd for $[C_{14}H_{13}N_2S]$ 241.2051, found 241.2067.

6.1.3 Synthesis of Piperazine and N,N'-Dimethylethylenediamine Linkers

Tert-butyl 4-(2-bromoacetyl)piperazine-1-carboxylate 76

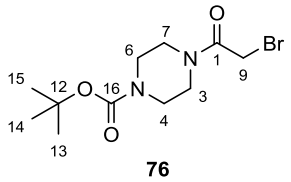

76

Bromoacetylchloride (500 g, 3.2 mmol) was added dropwise during 30 min to a solution of *tert*-butyl piperazine-1-carboxylate (500 mg, 2.7 mmol) and K_2CO_3 (2.0 g, 14.6 mmol) in 50 mL anhydrous THF. The reaction was stirred for 12 h while monitoring by TLC (Pet. spirit:EtOAc, 50:50). The reaction mixture was concentrated and the residue re-dissolved in CH_2Cl_2. The organic layer was washed with water and brine, dried over anhydrous Na_2SO_4 and concentrated. The crude residue was purified by silica gel column chromatography (30% EtOAc/Pet, Spirit) to afford **77** (250 mg, 35%) as an off-white solid. TLC R_f (Pet. spirit:EtOAc, 50:50) = 0.48; Mp 114 -115 ºC. ^{1}H NMR (500 MHz, $CDCl_3$) δ 3.85 (s, 2H, H9), 3.62-3.42 (m, 8H, H3, H4, H6, H7), 1.45 (s, 9H, H13, H14, H15); ^{13}C NMR (125 MHz, $CDCl_3$) δ 165.1, 154.3, 80.4, 46.5 (2C), 41.9 (2C), 28.3 (3C), 25.6; IR (neat) ν 1762, 1723, 1560, 1498, 1429, 1413, 1250, 1120 cm^{-1}; HRESI-MS: *m/z* calcd for $C_{11}H_{19}{}^{79}BrN_2O_3$) 306.0581, found 306.0590.

Tert-butyl (2-(2-bromo-N-methylacetamido)ethyl)(methyl) carbamate 77

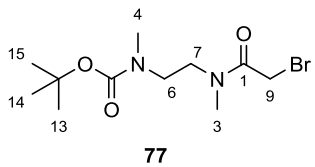

77

Bromoacetylchloride (500 g, 3.2 mmol) was added dropwise during 30 min to a solution of *tert*-butyl methyl(2-(methylamino)ethyl)carbamate (500 mg, 2.7 mmol) and K_2CO_3 (1.2 g, 8.7 mmol) in 30 mL anhydrous CH_2Cl_2. The reaction was stirred for 16 h while monitoring by TLC (Pet. spirit:EtOAc, 50:50). The reaction mixture was concentrated and the residue re-dissolved in CH_2Cl_2. The organic layer was washed

with water and brine, dried over anhydrous Na_2SO_4 and concentrated. The crude residue was purified by silica gel column chromatography (30% EtOAc/Pet, Spirit) to afford **77** (330 mg, 40%) as an off-white solid. TLC R_f (Pet. spirit:EtOAc, 50:50) = 0.46; Mp 129 -131 ºC. ^{1}H NMR (500 MHz, $CDCl_3$) δ 4.26 (s, 2H, H9), 3.46 (t, 2H, H7), 3.28 (t, 2H, H6), 3.25 (s, 3H, H3), 2.89 (s, 3H, H4), 1.45 (s, 9H, H13, H14, H15); ^{13}C NMR (125 MHz, $CDCl_3$) δ 165.3, 153.9, 79.6, 51.8, 47.5, 35.3, 34.9, 28.2 (3C), 27.6; IR (neat) ν 1752, 1717, 1559, 1489, 1429, 1411, 1252, 1118 cm^{-1}; HRESI-MS: *m/z* calcd for $C_{11}H_{21}$ $^{79}BrN_2O_3$) 308.0535, found 308.0552.

6.1.4 Synthesis of Reserpine-Containing Intermediates

Methyl (1*S*,2*R*,3*R*,4a*S*,13b*R*,14a*S*)-3-((4-hydroxy-3,5-dimethoxy benzoyl)oxy)-2,11-dimethoxy-1,2,3,4,4a,5,7,8,13,13b,14,14a-dodecahydroindolo [2',3':3,4]pyrido[1,2-b]isoquinoline-1-carboxylate 70[165]

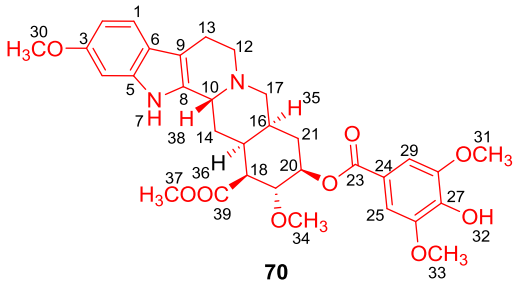

70

Aluminium chloride (1.0 g, 7.63 mmol) was added in one portion to a stirring solution of reserpine **8** (100 mg, 0.16 mmol) in dry CH_2Cl_2 (20 mL) at room temperature. The reaction was stirred for 2 h while monitoring by TLC (EtOAc). The reaction was quenched by addition of 5% aqueous HCl (15 mL) and the mixture diluted with CH_2Cl_2 (30 mL) and the layers separated. The aqueous layer was extracted twice more with CH_2Cl_2 and the combined organic fractions were washed with water and brine, dried over anhydrous $MgSO_4$ and concentrated to yield **70** (90 mg, 95%) as a yellowish solid. TLC R_f (EtOAc) = 0.45; Mp 154-156 ºC; ^{1}H NMR (500 MHz, $CDCl_3$) δ 7.54 (br s, 1H, H7), 7.33 (s, 2H, H25, H29),7.31 (d, J = 10.0 Hz,

1H, H1), 6.88 (s, 1H, H4), 6.78 (d, *J* = 10.0 Hz, 1H, H2), 4.97 (sextet, *J* = 4.5 Hz, 1H, H20), 4.74 (app s, 1H, H19), 3.98 (t, *J* = 10.0 Hz, 1H, H38), 3.92 (s, 6H, H31, H33), 3.86 (s, 3H, H30), 3.81 (s, 3H, H37), 3.50 (s, 3H, H34), 3.28 (d, *J* = 7.1 Hz, 2H, H17), 3.21 (d, *J* = 7.1 Hz, 1H, H18), 2.95 (sextet, *J* = 7.1 Hz, 1H, H36) 2.77-2.45 (m, 5H, H14, H21, H35), 2.15-1.95 (m, 4H, H12, H13); ^{13}C NMR (125 MHz, $CDCl_3$) δ 172.4 (C39), 165.6 (C23), 156.7 (C3), 146.8 (C26, C28), 139.7 (C5, C8), 137.1 (C27), 121.2 (C24), 120.87 (C6, C9), 118.6 (C1), 109.7 (C2), 106.8 (C25, C29), 95.3 (C4), 60.7 (C19, C20), 56.9 (C30, C31, C33), 55.9 (C34), 54.5 (C0), 52.2 (C37), 51.4 (C18), 50.9 (C17), 48.5 (C12), 33.2 (C36), 31.3 (C35), 29.4 (C36), 23.7 (C21), 16.3 (C13); IR (neat) ν 3736, 2921, 1732, 1691, 1550, 1436, 1181, 1118 cm^{-1}; HRESI-MS: *m/z* calcd for [$C_{32}H_{38}N_2O_9$] 595.2656, found 595.2671.

Methyl (1S,2R,3R,4aS,13bR,14aS)-3-((4-(2-hydroxyethoxy)-3,5-dimethoxy benzoyl) oxy)-2,11-dimethoxy-1,2,3,4,4a,5,7,8,13,13b,14,14a-dodecahydroindolo[2',3':3,4] pyrido[1,2-b]isoquinoline-1-carboxylate 71

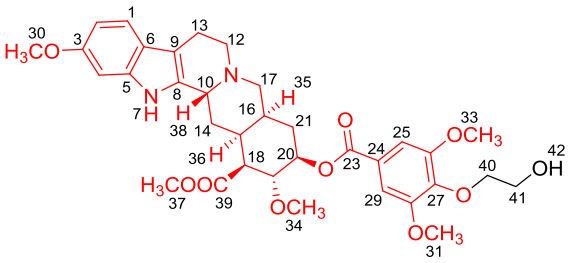

71

The phenolic reserpine **70** (100 mg, 17 mmol) was dissolved in dry DMF (5 mL) in a 25 mL flame-dried round bottom flask under Ar and K_2CO_3 (1.00 g, 17.8 mmol) was added. The mixture was stirred at room temperature for 30 min before adding 2-bromoethanol (50 mg, 40 mmol) and warming to 80 ^{o}C. After overnight stirring and monitoring by TLC (EtOAc) the reaction mixture was concentrated and the residue re-dissolved in CH_2Cl_2. The organic layer was washed with water and brine, dried over anhydrous Na_2SO_4 and concentrated.

The crude residue was purified by silica gel column chromatography (60% EtOAc/Pet, Spirit) to afford **71** (100 mg, 96%) as a yellow solid. TLC R_f (EtOAc) = 0.38; Mp 121-123 ºC; ^{1}H NMR (500 MHz, $CDCl_3$) δ 7.58 (br s, 1H, H7), 7.33 (m, 3H, H25, H29, H1), 6.84 (app d, J = 2 Hz, 1H, H4), 6.78 (d, J = 10.0 Hz, 2.0 Hz, 1H, H2), 5.05 (sextet, J = 4.5 Hz, 1H, H20), 4.47 (app s, 1H, H19), 4.25 (t, J = 10.0 Hz, 2H, H40), 3.92 (s, 6H, H31, H33), 3.89 (t, J = 10.0 Hz, 1H, H38), 3.84 (s, 3H, H30), 3.82 (s, 3H, H37), 3.73 (t, J = 10.0 Hz, 2H, H41), 3.50 (s, 3H, H34), 3.18 (d, J = 7.1 Hz, 2H, H17), 3.05 (d, J = 7.1 Hz, 1H, H18), 2.96 (sextet, J = 7.1 Hz, 1H, H36) 2.70 (dd, J = 10.0 Hz, 5.0 Hz, 2H, H14), 2.52-2.27 (m, 3H, H21, H35), 2.15-1.95 (m, 4H, H12, H13) ; ^{13}C NMR (125 MHz, $CDCl_3$) δ 171.8 (C39), 165.8 (C23), 156.4 (C3), 149.2 (C26, C28), 140.1 (C5, C8), 137.5 (C27), 121.5 (C24), 120.84 (C6, C9), 118.3 (C1), 109.2 (C2), 106.5 (C25, C29), 94.9 (C4), 69.8 (C40), 60.7 (C19, C20), 59.5 (C41), 56.9 (C30, C31, C33), 55.9 (C34), 54.5 (C0), 52.2 (C37), 51.4 (C18), 50.9 (C17), 48.5 (C12), 33.2 (C36), 31.3 (C35), 29.4 (C36), 23.7 (C21), 16.3 (C13) ; IR (neat) ν 3741, 2918, 1731, 1688, 1553, 1437, 1182, 1121 cm^{-1}; HRESI-MS: *m/z* calcd for [$C_{34}H_{42}N_2O_{10}$] 639.2839, found 639.2844.

Methyl (1S,2R,3R,4aS,13bR,14aS)-3-((4-(2-bromoethoxy)-3,5-dimethoxybenzoyl) oxy)-2,11-dimethoxy-1,2,3,4,4a,5,7,8,13,13b,14,14a-dodeca-hydroindolo[2',3': 3,4] pyrido[1,2-b]isoquinoline-1-carboxylate 72

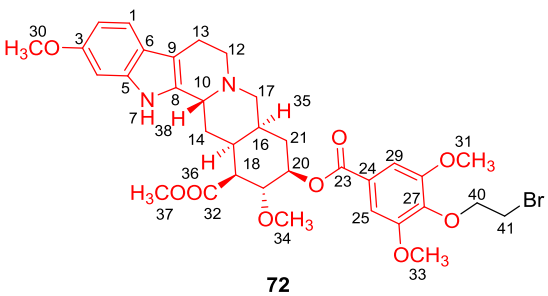

72

O-alkylated reserpine alcohol **71** (100 mg, 0.16 mmol) was dissolved in dry THF (20 mL) in a 50 mL flame-dried round bottom flask under Ar. CBr_4 (200 mg, 0.60 mmol)

was added and the mixture stirred at room temperature for 10 min before adding PPh_3 (100 mg, 0.38 mmol) in one portion. Stirring was continued at room temperature for a further 3 h while monitoring by TLC (Pet. spirit:EtOAc, 70:30). The solvent was evaporated and the residue purified by silica gel column chromatography using a gradient (Pet. spirit:EtOAc, 60:40 → 100% EtOAc) to give **72** (98 mg, 91%) as a yellow-brown solid. TLC R_f (Pet. spirit:EtOAc, 60:40) = 0.55; Mp 140-143 ºC; ^{1}H NMR (500 MHz, $CDCl_3$) δ 7.58 (br s, 1H, H7), 7.32 (m, 3H, H25, H29, H1), 6.85 (app d, *J* = 2.0 Hz, 1H, H4), 6.78 (d, *J* = 10.0 Hz , 2.0 Hz, 1H, H2), 5.10 (sextet, *J* = 4.5 Hz, 1H, H20), 4.75 (t, *J* = 10.0 Hz, 2H, H40), 3.91 (s, 7H, H31, H33, H19), 3.77 (app t, 7H, H30, H37, H38), 3.63 (t, *J* = 10.0 Hz, 2H, H41), 3.52 (s, 3H, H34), 3.18 (d, *J* = 7.1 Hz, 2H, H17), 3.05 (d, *J* = 7.1 Hz, 1H, H18), 2.97 (sextet, *J* = 7.1 Hz, 1H, H36) 2.73 (dd, *J* = 10.0 Hz, 5.0 Hz, 2H, H14), 2.54-2.22 (m, 3H, H21, H35), 2.12-1.88 (m, 4H, H12, H13); ^{13}C NMR (125 MHz, $CDCl_3$) δ 172.1 (C39), 165.4 (C23), 156.6 (C3), 149.0 (C26, C28), 140.5 (C5, C8), 137.0 (C27), 122.0 (C24), 120.2 (C6, C9), 118.8 (C1), 109.0 (C2), 106.0 (C25, C29), 94.7 (C4), 69.3 (C40), 60.2 (C19, C20), 57.2 (C30, C31, C33), 56.1 (C34), 54.5 (C0), 52.0 (C37), 51.1 (C18), 51.2 (C17), 48.2 (C12), 33.0 (C36), 31.6 (C41), 31.1 (C35), 29.6 (C36), 23.9 (C21), 18.1 (C13); IR (neat) ν 3744, 2916, 1734, 1683, 1558, 1437, 1183, 1119 cm^{-1}; HRESI-MS: *m/z* calcd for $[C_{34}H_{41}BrN_2O_9]$ 701.2633, found 701.2645.

Methyl (1S,2R,3R,4aS,13bR,14aS)-3-((4-(2-(4-(tert-butoxy carbonyl) piperazin-1-yl)ethoxy)-3,5-dimethoxybenzoyl)oxy)-2,11-dimethoxy-1,2,3,4,4a,5,7,8,13,13b,14, 14a-dodecahydroindolo[2',3':3,4]pyrido[1,2-b]isoquin- oline-1-carboxylate 66

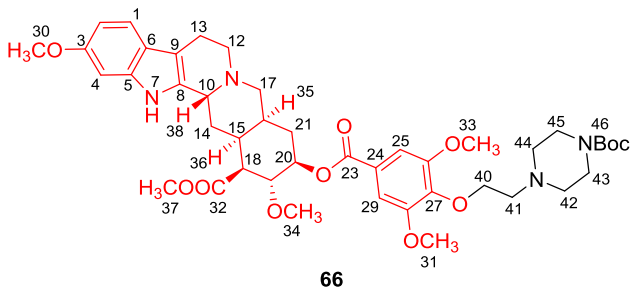

66

Bromide **72** (200 mg, 0.28 mmol) was dissolved in dry THF (25 mL) in a 50 mL flame-dried round bottom flask under Ar and *N*-Boc-piperazine (150 mg, 0.78 mmol) and triethylamine (500 mg, 5.0 mmol) were successively added. A reflux condenser was attached and the mixture heated at 100 ^{o}C with stirring 16 h while monitoring by TLC (60% EtOAc/Pet. spirit). The solvent was evaporated and the residue purified by silica gel column chromatography (Pet. spirit:EtOAc, 50:50) to provide **66** (184 mg, 80%) as a yellow-brown solid. TLC R_f (Pet. spirit:EtOAc, 60:40) = 0.25; Mp 170-172 ^{o}C; ^{1}H NMR (500 MHz, $CDCl_3$) δ 7.55 (br s, 1H, H7), 7.31 (m, 3H, H25, H29, H1), 6.78 (app d, J = 2.0 Hz, 1H, H4), 6.69 (d, J = 10.0 Hz, 2.0 Hz, 1H, H2), 5.03 (sextet, J = 4.5 Hz, 1H, H20), 4.46 (app s, 1H, H19), 4.27 (t, J = 10.0, 2H, H40), 3.90 (s, 6H, H31, H33), 3.87 (t, J = 10.0 Hz, 1H, H38), 3.83 (s, 3H, H30), 3.80 (s, 3H, H37), 3.71 (t, J = 10.0 Hz, 2H, H41), 3.50 (s, 3H, H34), 3.41 (app dd, J = 8.5 Hz, 4H, H43, H45), 3.18 (d, J = 7.1 Hz, 2H, H17), 3.08 (d, J = 7.1 Hz, 1H, H18), 2.94 (sextet, J = 7.1 Hz, 1H, H36) 2.68 (dd, J = 10.0 Hz, 5.0 Hz, 2H, H14), 2.56 (app dd, J = 8.5 Hz, 4H, H42, H44), 2.50-2.24 (m, 3H, H21, H35), 2.18-1.92 (m, 4H, H12, H13), 1.45 (s, 9H, H46); ^{13}C NMR (125 MHz, $CDCl_3$) δ 172.1 (C32), 166.0 (C23), 158.8 (C46), 156.2 (C3), 148.9 (C26, C28), 138.8 (C5, C8), 137.3 (C27), 121.2 (C24), 120.82 (C6, C9), 118.1 (C1), 109.0 (C2), 106.3 (C25, C29), 94.5 (C4), 79.4 (C46), 69.8 (C40), 68.5 (C10), 60.6 (C19, C20), 59.1

(C41), 57.2 (C30, C31, C33), 56.1(C42, C44), 56.1 (C34), 52.0 (C37), 51.6 (C18), 51.1 (C17), 48.8 (C12), 45.8 (C43, C45), 33.0 (C15), 32.0 (C14), 31.5 (C14), 29.2 (C36), 27.9 (C46), 23.7 (C21), 16.3 (C13); IR (neat) ν 3741, 2935, 2794, 1700, 1695, 1457, 1418, 1248, 1152 cm^{-1}; HRESI-MS: *m/z* calcd for [$C_{43}H_{58}N_4O_{11}$] 807.4180, found 807.4188.

Methyl (1S,2R,3R,4aS,13bR,14aS)-3-((4-(2-(4-(tert-butoxy carbonyl)piperazin-1-yl)-2-oxoethoxy)-3,5-dimethoxybenzoyl)oxy)-2,11-dimethoxy-1,2,3,4,4a,5,7,8,13,13b,14,14a-dodecahydroindolo[2',3':3,4]pyrido[1,2-b]isoquin-oline-1-carboxylate 68

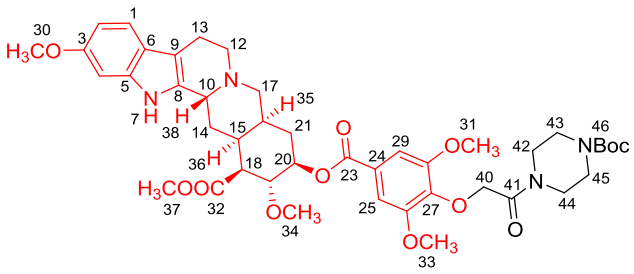

68

Phenolic reserpine **70** (50 mg, 0.08 mmol) was dissolved in DMF (7 mL) in a 25 mL flame-dried round bottom flask under Ar and K_2CO_3 (250 mg, 1.79 mmol) was added. The mixture was stirred for 20 min before *N*-bromoacetyl-*N*'-Boc-piperazine **76** (40 mg, 0.13 mmol) was added in one portion. The mixture was stirred at 80 ^oC for 48 h while monitoring by TLC (EtOAc:MeOH, 95:5). The solvent was evaporated and the residue purified by silica gel column chromatography to yield **68** (43 mg, 64%) as a brown solid. TLC R_f (EtOAc:MeOH, 95:5) = 0.25; Mp 138-141 ^oC; ^1H NMR (500 MHz, $CDCl_3$) δ 7.64 (br s, 1H, H7), 7.35 (m, 3H, H25, H29, H1), 6.82 (s, 1H, H4), 6.77 (d, *J* = 15.0 Hz, 1H, H2), 5.05 (sextet, *J* = 4.5 Hz, 1H, H20), 4.68 (s, 2H, H40), 4.44 (app s, 1H, H19), 3.88 (s, 6H, H31, H33), 3.86 (t, *J* = 10.0 Hz, 1H, H38), 3.85 (s, 3H, H30), 3.81 (s, 3H, H37), 3.76 (app dd, *J* = 8.5 Hz, 4H, H42, H44), 3.63 (app dd, *J* = 8.5 Hz, 4H, H43, H45), 3.48 (s, 3H, H34), 3.19 (d, *J* = 7.1 Hz, 2H, H17), 3.07 (d, *J* = 7.1 Hz,

1H, H18), 2.94 (sextet, *J* = 7.1 Hz, 1H, H36) 2.69 (dd, *J* = 10.0 Hz, 5.0 Hz, 2H, H14), 2.56-2.24 (m, 3H, H21, H35), 2.13-1.85 (m, 4H, H12, H13), 1.48 (s, 9H, H46); ^{13}C NMR (125 MHz, $CDCl_3$) δ 172.0 (C32), 168.2 (41), 165.6 (C23), 158.5 (C46), 156.0 (C3), 148.8 (C26, C28), 138.9 (C5, C8), 137.2 (C27), 121.1 (C24), 120.8 (C6, C9), 118.2 (C1), 109.1 (C2), 106.1 (C25, C29), 94.3 (C4), 79.2 (C46), 68.4 (C10), 65.7 (C40), 60.5 (C19, C20), 57.1 (C30, C31, C33), 56.0 (C34), 52.4 (C37), 51.9 (C43, C45), 51.5 (C18), 51.0 (C17), 50.6 (C42, C44), 48.6 (C12), 33.1 (C15), 31.8 (C14), 31.4 (C14), 29.1 (C36), 27.8 (C46), 23.8 (C21), 16.1 (C13); IR (neat) ν 3340, 2931, 2844, 1707, 1694, 1458, 1415, 1211, 1125 cm^{-1}; HRESI-MS: m/z calcd for [$C_{43}H_{56}N_4O_{12}$] 821.3973, found 821.3987.

Methyl (1S,2R,3R,4aS,13bR,14aS)-3-((4-(2-((2-((tert-butoxy carbonyl) (methyl) amino)ethyl)(methyl)amino)ethoxy)-3,5-dimethoxybenzoyl) oxy)-2,11-dimethoxy-1,2,3,4,4a,5,7,8,13,13b,14,14a-dodecahydroindolo[2',3':3,4] pyrido[1,2-b]isoquinol one-1-carboxylate 67

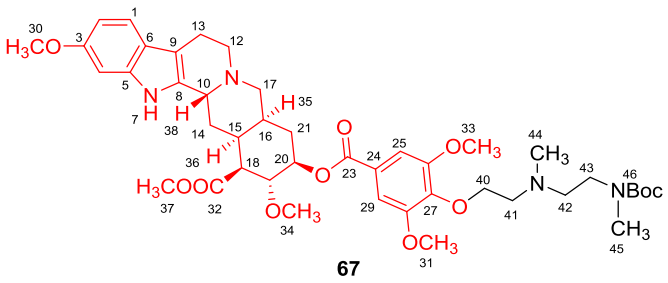

67

Bromide **72** (200 mg, 0.28 mmol) was dissolved in dry THF (20 mL) in a 50 mL flame-dried round bottom flask under Ar and *N*-Boc-*N*,*N*'-dimethylethylenediamine **75** (150 mg, 0.78 mmol) was added followed by triethylamine (500 mg, 5.0 mmol). A reflux condenser was attached and the mixture warmed to 100 ^{o}C and stirred for 16 h while monitoring by TLC (Pet. spirit:EtOAc 60:40). The mixture was concentrated and the residue purified by a silica gel column chromatography using 30%

EtOAc/Pet. spirit to provide **67** (172 mg, 75%) as a brown solid. TLC R_f (Pet. spirit:EtOAc 60:40) = 0.23; Mp 188-191 ºC; ^{1}H NMR (500 MHz, $CDCl_3$) δ 7.60 (br s, 1H, H7), 7.24 (m, 3H, H25, H29, H1), 6.91 (app d, *J* = 2.0 Hz, 1H, H4), 6.78 (d, *J* = 10.0 Hz, 2.0 Hz, 1H, H2), 5.04 (sextet, *J* = 4.5 Hz, 1H, H20), 4.54 (app s, 1H, H19), 4.21 (t, *J* = 10.0, 2H, H40), 3.89 (s, 6H, H31, H33), 3.86 (t, *J* = 10.0 Hz, 1H, H38), 3.81 (s, 3H, H30), 3.79 (s, 3H, H37), 3.71 (t, *J* = 10.0 Hz, 2H, H41), 3.48 (s, 3H, H34), 3.22 (t, *J* = 10.0 Hz, 2H, H43), 3.16 (d, *J* = 7.1 Hz, 2H, H17), 3.03 (d, *J* = 7.1, 1H, H18), 2.96 (sextet, *J* = 7.1 Hz, 1H, H36) 2.94 (s, 3H, H45), 2.92 (S, 3H, H44), 2.68 (dd, *J* = 10.0 Hz, 5.0 Hz, 2H, H14), 2.55 (t, *J* = 10.0 Hz, 2H, H42), 2.49-2.22 (m, 3H, H21, H35), 2.16-1.90 (m, 4H, H12, H13), 1.44 (s, 9H, H46); ^{13}C NMR (125 MHz, $CDCl_3$) δ 171.6 (C32), 165.8 (C23), 158.5 (C46), 156.0 (C3), 149.1 (C26, C28), 139.0 (C5, C8), 137.1 (C27), 121.0 (C24), 120.4 (C6, C9), 117.6 (C1), 108.7 (C2), 105.9 (C25, C29), 94.1 (C4), 79.2 (C46), 69.5 (C40), 68.1 (C10), 60.4 (C19, C20), 59.0 (C41), 57.0 (C30, C31, C33), 56.1 (C34), 55.3 (C42), 52.6(C43), 51.8 (C37), 51.4 (C18), 50.8 (C17), 48.6 (C12), 46.7 (C44), 36.8 (C45), 32.6 (C15), 31.6 (C14), 29.1 (C36), 28.4 (C46), 23.6 (C21), 16.1 (C13); IR (neat) ν 3419, 2941, 1709, 1684, 1458, 1330, 1216, 1158 cm^{-1}; HRESI-MS: *m/z* calcd for [$C_{43}H_{60}N_4O_{11}$] 809.4337, found 809.4369.

Methyl (1S,2R,3R,4aS,13bR,14aS)-3-((4-(2-((2-((tert-butoxycarbonyl)(methyl) amino)ethyl)(methyl)amino)-2-oxoethoxy)-3,5-dimethoxyben-zoyl)oxy)-2,11-dimethoxy-1,2,3,4,4a,5,7,8,13,13b,14,14a-dodecahydroindolo[2' ,3':3,4]pyrido[1,2-b]isoquinoline-1-carboxylate 69

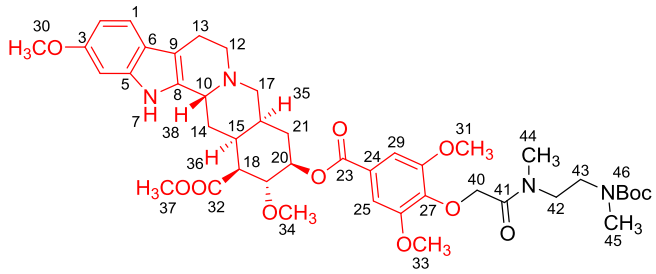

69

The phenolic reserpine derivative **70** (50 mg, 0.08 mmol) was dissolved in dry DMF (7 mL) in a 50 mL oven-dried round bottom flask under Ar and K_2CO_3 (250 mg, 1.79 mmol) was added. The mixture was stirred at room temperature for 30 min before adding *N*-bromoacetyl-*N*'-Boc-*N*,*N*'-dimethylethylenediamine **77** (40 mg, 0.13 mmol) in one portion. The reaction mixture was heated to 80 ^{o}C and stirred for 48 h while monitoring by TLC (EtOAc:MeOH, 95:5). The solvent was evaporated and the residue purified by silica gel column chromatography using a gradient (100% EtOAc → 5% MeOH/EtOAc) to give **69** (47 mg, 70%) as a brown solid. TLC R_f (EtOAc:MeOH, 95:5) = 0.20; Mp 103-105 ^{o}C; ^{1}H NMR (500 MHz, $CDCl_3$) δ 7.63 (br s, 1H, H7), 7.36-7.28 (m, 3H, H25, H29, H1), 6.91 (app d, J = 1.0 Hz, 1H, H4), 6.78 (d, J = 10.0 Hz, 1.0 Hz, 1H, H2), 5.04 (sextet, J = 4.5 Hz, 1H, H20), 4.68 (s, 2H, H40), 4.51 (app s, 1H, H19), 3.89 (s, 6H, H31, H33), 3.84 (s, 3H, H30), 3.81 (s, 3H, H37), 3. 68 (app s, 1H, H38), 3.49 (s, 3H, H34), 3.40 (t, J = 10.0 Hz, 2H, H43), 3.17 (d, J = 7.1 Hz, 2H, H17), 3.03 (d, J = 7.1 Hz, 1H, H18), 2.94 (s, 3H, H45), 2.92 (S, 3H, H44), 2.88 (sextet, J = 7.1 Hz, 1H, H36), 2.70 (dd, J = 10.0 Hz, 5.0 Hz, 2H, H14), 2.55 (t, J = 10.0 Hz, 2H, H42), 2.49-2.22 (m, 3H, H21, H35), 2.16-1.90 (m, 4H, H12, H13), 1.44 (s, 9H, H46); ^{13}C NMR (125 MHz, $CDCl_3$) δ 171.4 (C32), 166.4 (C41), 165.3 (C23), 158.2 (C46), 156.1

(C3), 149.3 (C26, C28), 139.0 (C5, C8), 136.0 (C27), 121.5 (C24), 119.3 (C6, C9), 117.4 (C1), 108.4 (C2), 104.7 (C25, C29), 93.0 (C4), 79.5 (C46), 69.0 (C40), 67.4 (C10), 60.2 (C19, C20), 56.8 (C30, C31, C33), 56.0 (C34), 53.3 (C43), 52.4 (C42), 51.6 (C37), 51.3 (C18), 50.7 (C17), 48.5 (C12), 43.7 (C45), 36.6 (C44), 32.5 (C15), 31.8 (C14), 29.1 (C36), 28.3 (C46), 23.3 (C21), 16.3 (C13); IR (neat) ν 3291, 2935, 2828, 2162, 1704, 1696, 1458, 1415, 1213, 1126 cm^{-1}; HRESI-MS: *m/z* calcd for $[C_{43}H_{58}N_4O_{12}]$ 823.4129, found 823.4135.

6.1.5 Synthesis of Pterostilbene-Containing Intermediates

(*E*)-2-(4-(3,5-Dimethoxystyryl)phenoxy)ethan-1-ol 82

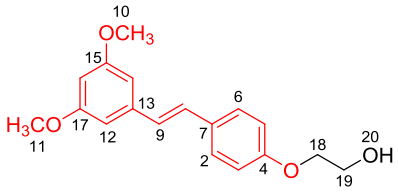

82

To a solution of pterostilbene **9** (300 mg, 1.1 mmol) in anhydrous DMF (10 mL) in a 25 mL flame-dried round bottom flask under Ar was added K_2CO_3 (260 mg, 1.1 mmol) and the mixture was stirred at room temperature for 20 min. 2-Bromoethanol (300 mg, 2.5 mmol) was added dropwise over 10 min and the reaction mixture warmed to 80 ^oC and stirred for 16 h while monitoring by TLC (Pet. spirit:EtOAc, 50:50). The solvent was evaporated under reduce pressure and the residue re-dissolved in CH_2Cl_2. The organic layer was washed successively with water and brine, dried over anhydrous Na_2SO_4 and concentrated. The crude residue was purified by silica gel column chromatography using 10% EtOAc/Pet. spirit to afford **82** (280 mg, 90%) as an off-white powder. TLC R_f (Pet. spirit:EtOAc, 50:50) = 0.45; Mp 83-84 ^oC; ^1H NMR (500 MHz, CD_3OD) δ 7.46 (d, J = 10.0 Hz, 2H, H6, H2), 7.05 (d, J = 15.8 Hz, 1H, H9), 6.93 (m, 3H, H3, H5, H8), 6.67 (s, 2H, H12, H14), 6.38 (s, 1H, H16), 4.31 (t, J = 12.0 Hz, 2H, H18), 3.78 (s, 6H, H10, H11), 3.65 (t, J = 14.0 Hz, 2H,

H19); ^{13}C NMR (125 MHz, CD_3OD) δ 162.6 (C4), 161.8 (C15, C17), 141.5 (C13), 130.8 (C2, C6), 128.3 (C9), 127.9 (C8), 114.9 (C3, C5), 105.0 (C12, C14), 100.4 (C16), 69.7 (C18), 60.9 (C19), 54.8 (C10, C11); IR (neat) ν 3671, 2927, 2348, 1586, 1146, 1129, 1110 cm^{-1}; HRESI-MS: *m/z* calcd for [$C_{18}H_{19}NaO_4$] 322.1181, found 322.1189.

(*E*)-1-(4-(2-Bromoethoxy)styryl)-3,5-dimethoxybenzene 83

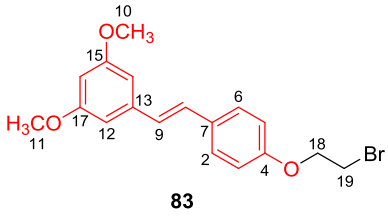

83

To a solution of alcohol **82** (200 mg, 0.67 mmol) in anhydrous THF (25 mL) in a 50 mL flame-dried round bottom flask under Ar was added CBr_4 (850 mg, 2.5 mmol). PPh_3 (262 mg, 1.0 mmol) was then added in one portion and the reaction stirred for 3 h at room temperature while monitoring by TLC (Pet. spirit:EtOAc, 50:50). The solvent was evaporated and the residue re-dissolved in EtOAc. The organic layer was washed successively with water and brine, dried over anhydrous $MgSO_4$ and concentrated. The crude residue was purified by silica gel column chromatography to afford **83** (225 mg, 94%) as an off-white foam. TLC R_f (Pet. spirit:EtOAc, 50:50) = 0.69; Mp 76-77 ºC; ^{1}H NMR (500 MHz, CD_3OD) δ 7.45 (d, J = 10.0 Hz, 2H, H6, H2), 7.08 (d, J = 15.8 Hz, 1H, H9), 6.95 (m, 3H, H3, H5, H8), 6.66 (s, 2H, H12, H14), 6.35 (s, 1H, H16), 4.30 (t, J = 12.0 Hz, 2H, H18), 3.76 (s, 6H, H10, H11), 3.63 (t, J = 14.0 Hz, 2H, H19); ^{13}C NMR (125 MHz, CD_3OD) δ 161.9 (C4), 161.5 (C15, C17), 141.0 (C13), 130.8 (C2, C6), 127.8 (C9), 127.9 (C8), 115.2 (C3, C5), 106.1 (C12, C14), 99.8 (C16), 69.5 (C18), 60.8 (C19), 55.01 (C10, C11) ; IR (neat) ν 2928, 2346, 1583, 1145, 1122, 1115 cm^{-1}; HRESI-MS: *m/z* calcd for [$C_{18}H_{19}BrO_3$] 362.0518, found 362.0524.

***Tert*-butyl (*E*)-4-(2-(4-(3,5-dimethoxystyryl)phenoxy)ethyl)piperazine-1-carboxylate 78**

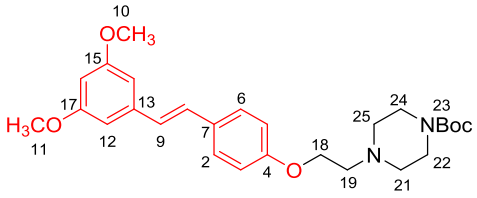

78

To a solution of bromide **83** (150 mg, 0.41 mmol) in anhydrous THF (30 mL) in a 50 mL oven-dried round bottom flask under Ar was added KI (300 mg, 1.80 mmol). *N*-Boc-piperazine (120 mg, 0.63 mol) was then added in one portion, a reflux condenser attached and the reaction heated at 100 ^{o}C with stirring for 48 h while monitoring by TLC (Pet. spirit:EtOAc, 50:50). The solvent was evaporated and the residue re-dissolved in EtOAc (50 mL). The organic layer was washed successively with water and brine, dried over anhydrous Na_2SO_4 and concentrated. The crude residue was purified by silica gel column chromatography using a gradient (10 → 15% EtOAc/Pet. Spirit) to give **78** (166 mg, 87%) as an off-white solid. TLC R_f (Pet. spirit:EtOAc, 50:50) = 0.30; Mp 103-105 ºC; ^{1}H NMR (500 MHz, $CDCl_3$) δ 7.40 (d, J = 10.0 Hz, 2H, H6, H2), 7.12 (d, J = 15.8 Hz, 1H, H9), 6.90 (m, 3H, H3, H5, H8), 6.70 (s, 2H, H12, H14), 6.38 (s, 1H, H16), 4.31 (t, J = 12.0 Hz, 2H, H18), 3.75 (s, 6H, H10, H11), 3.43 (dd, J = 7.5 Hz, 4H, H22, H24), 3.65 (t, J = 14.0 Hz, 2H, H19), 2.65 (dd, J = 7.5 Hz, 4H, H21, H25), 1.46 (s, 9H, H23) ; ^{13}C NMR (125 MHz, $CDCl_3$) δ 161.4 (C23), 160.8 (C15, C17), 159.9 (C4), 141.5 (C13), 131.6 (C2, C6), 128.1 (C9), 127.6 (C8), 115.0 (C3, C5), 106.0 (C12, C14), 100.4 (C16), 76.8 (C23), 69.4 (C18), 58.9 (C19), 57.6 (C21, C25), 54.5 (C10, C11), 47.4 (C22, C24), 28.9 (C23); IR (neat) ν 2934, 2836, 1685, 1584, 1513, 1425, 1248, 1145 cm^{-1}; HRESI-MS: *m/z* calcd for [$C_{27}H_{36}N_2O_5$] 491.4463, found 491.4487.

***Tert*-butyl (E)-4-(2-(4-(3,5-dimethoxystyryl)phenoxy)acetyl) piperazine-1-carboxy late 80**

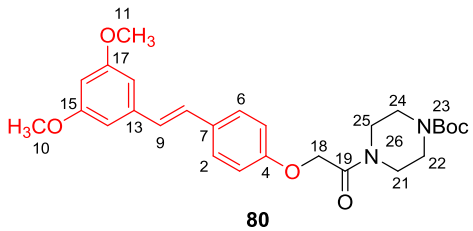

80

To a solution of phenolic pterostilbene **9** (256 mg, 1.0 mmol) in anhydrous DMF (10 mL) in a 25 mL oven-dried round bottom flask under Ar was added K_2CO_3 (552 mg, 4.0 mmol). *N*-bromoacetyl-*N*'-Boc-piperazine **76** (460 mg, 1.5 mmol) was then added in one portion and a reflux condenser attached and the reaction stirred at 100 ^oC for 48 h while monitoring by TLC (pet. Spirit:EtOAc, 50:50). The solvent was evaporated and the residue redissolved in CH_2Cl_2 (50 mL). The organic layer was washed successively with water and brine, dried over anhydrous $NaSO_4$ and concentrated. The crude residue was purified by silica gel column chromatography using 15% EtOAc/Pet. spirit to afford **80** (371 mg, 77%) as an off-white solid. TLC R_f (Pet. spirit:EtOAc, 55:45) = 0.42; Mp 52-53 ^oC; ^1H NMR (500 MHz, $CDCl_3$) δ 7.44 (d, J = 10.0 Hz, 2H, H6, H2), 7.11 (d, J = 15.8 Hz, 1H, H9), 7.05-6.86 (m, 3H, H3, H5, H8), 6.63 (app d, J = 1.5 Hz, 2H, H12, H14), 6.37 (s, 1H, H16), 4.71 (s, 2H, H18), 3.81 (s, 6H, H10, H11), 3.57 (dd, J = 7.5 Hz, 4H, H21, H25), 3.42 (dd, J = 7.5 Hz, 4H, H22, H24), 1.46 (s, 9H, H23); ^{13}C NMR (125 MHz, $CDCl_3$) δ 166.8 (C19), 161.2 (C15, C17), 157.6 (C4), 154.7 (C23), 139.7 (C13), 131.1 (C7), 128.6 (C9), 128.1 (C2, C6), 127.5 (C8), 115.0 (C3, C5), 104.5 (C12, C14), 100.0 (C16), 80.6 (C23), 68.2 (C18), 55.6 (C10, C11), 45.6 (C22, C24), 42.2 (C21, C25), 28.6 (C23); IR (neat) ν 2930, 2886, 1684, 1651, 1589, 1510, 1436, 1232, 1219 cm^{-1}; HRESI-MS: *m/z* calcd for [$C_{27}H_{34}N_2O_6$] 505.2315, found 505.2331.

***Tert*-butyl (*E*)-(2-((2-(4-(3,5-dimethoxystyryl)phenoxy)ethyl) (methyl)amino)ethyl) (methyl)carbamate 79**

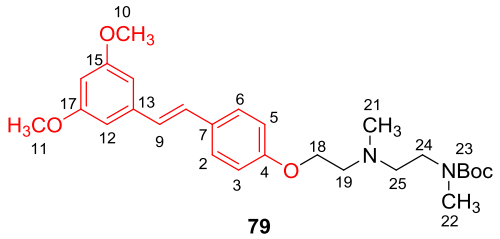

79

To a stirring solution of pterostilbene alkyl bromide **83** (150 mg, 0.41 mol) in anhydrous CH_2Cl_2 (30 mL) in a 50 mL oven-dried round bottom flask under Ar was added K_2CO_3 (250 mg, 1.80 mmol). *N*-Boc-*N*,*N*'-dimethylethylenediamine **75** (120 mg, 0.63 mol) was then added in one portion, a reflux condenser attached and the reaction heated at 60 ^oC for 48 h while monitoring by TLC (Pet. spirit:EtOAc, 50:50). The cooled reaction mixture was diluted with CH_2Cl_2 (30 mL) and the organic layer washed successively with water and brine, dried over anhydrous Na_2CO_3 and concentrated. The crude residue was purified by silica gel column chromatography using a gradient (15% EtOAc/Pet. spirit to 100% EtOAc) to provide **79** (154 mg, 81%) as a pale yellow solid. TLC R_f (Pet. spirit:EtOAc, 50:50) = 0.27; Mp 131-135 ºC; ^{1}H NMR (500 MHz, $CDCl_3$) δ 7.44 (d, J = 10.0 Hz, 2H, H6, H2), 7.14 (d, J = 15.8 Hz, 1H, H9), 7.06-6.90 (m, 3H, H3, H5, H8), 6.65 (s, 2H, H12, H14), 6.37 (s, 1H, H16), 4.29 (t, J = 12.0 Hz, 2H, H18), 3.75 (s, 6H, H10, H11), 3.13 (t, J = 7.5 Hz, 2H, H24), 2.75 (t, J = 7.1 Hz, 2H, H19), 2.57 (s, 3H, H22), 2.43 (3, J = 7.1 Hz, 2H, H25), 2.19 (s, 3H, H21), 1.45 (s, 9H, H23); ^{13}C NMR (125 MHz, $CDCl_3$) δ 161.2 (C23), 160.7 (C15, C17), 159.6 (C4), 141.0 (C13), 131.3 (C2, C6), 128.0 (C9), 127.2 (C8), 114.7 (C3, C5), 105.5 (C12, C14), 99.8 (C16), 78.1 (C23), 67.9 (C18), 58.9 (C19), 56.2 (C25), 54.4 (C10, C11), 53.1 (C24), 46.4 (C22), 37.5 (C21), 28.7 (C23); IR (neat) ν 2944, 2861, 1687, 1585, 1511, 1422, 1247, 1125 cm^{-1}; HRESI-MS: *m/z* calcd for [$C_{27}H_{38}N_2O_5$] 493.2356, found 493.2364.

***Tert*-butyl (E)-(2-(2-(4-(3,5-dimethoxystyryl)phenoxy)-N-methyl acetamido)ethyl) (methyl)carbamate 81**

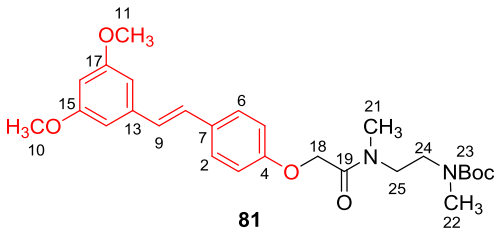

81

To a stirring solution of phenolic pterostilbene **9** (256 mg, 1.0 mmol) in anhydrous DMF (10 mL) in a 25 mL oven-dried round bottom flask under Ar was added K_2CO_3 (552 mg, 4.0 mmol). *N*-bromoacetyl-*N*'-Boc-*N*,*N*'-dimethylethylenediamine **77** (460 mg, 1.5 mmol) was added in one portion, a reflux condenser attached and the reaction heated at 80 ^oC for 24 h while monitoring by TLC (Pet. spirit:EtOAc, 50:50). The reaction mixture was concentrated and the residue redissolved in CH_2Cl_2 (30 mL). The organic layer was washed successively with water and brine, dried over anhydrous $MgSO_4$ and concentrated. The residue was purified by silica gel column chromatography using a gradient (Pet. spirit:EtOAc, 85:15 to 100% EtOAc) to afford **81** (255 mg, 77%) as a pale yellow solid. TLC R_f (Pet. spirit:EtOAc, 50:50) = 0.27; Mp 118-120 ^oC; ^1H NMR (500 MHz, $CDCl_3$) δ 7.41 (d, J = 18.0 Hz, 2H, H6, H2), 7.07-6.86 (m, 4H, H3, H5, H8, H9), 6.64 (s, 2H, H12, H14), 6.38 (s, 1H, H16), 4.69 (d, J = 18.0 Hz, 2H, H18), 3.82 (s, 6H, H10, H11), 3.54 (t, J = 8.5 Hz, 2H, H25), 3.39 (t, J = 8.5 Hz, 2H, H24), 3.10 (s, 3H, H21), 2.86 (s, 3H, H22), 1.45 (s, 9H, H23); ^{13}C NMR (125 MHz, $CDCl_3$) δ 167.8 (C19), 160.9 (C15, C17), 157.7 (C4), 155.9 (C23), 139.6 (C13), 130.8 (C7), 128.5 (C9), 127.8 (C2, C6), 127.0 (C8), 114.9 (C3, C5), 104.4 (C12, C14), 97.7 (C16), 79.8 (C23), 67.1 (C18), 55.3 (C10, C11), 47.4 (C24), 45.5 (C25), 34.8 (C21, C22), 28.4 (C23); IR (neat) ν 2935, 2831, 1684, 1659, 1590, 1509, 1457, 1204, 1173, 1148 cm^{-1}; HRESI-MS: *m/z* calcd for $[C_{27}H_{36}N_2O_6]$ 507.2471, found 507.2486.

6.1.6 Synthesis of INF55-Containing Intermediates

2-(4-(Bromomethyl)phenyl)-5-nitro-1H-indole 90

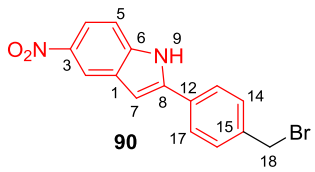

To a solution of the methyl ester **88** (80 mg, 0.27 mmol) in dry THF (5.0 mL) under Ar was added $NaBH_4$ (50 mg, 1.3 mmol) and the reaction stirred at room temperature while monitoring by TLC (pet. Spirit:EtOAc, 50:50). After 24 h the reaction was quenched by slow addition of sat. NH_4Cl (aq) until bubbling ceased. The mixture was diluted with water (50 mL) and extracted with EtOAc (4 x 50 mL). The combined organic layers were dried over anhydrous $MgSO_4$ and concentrated to give benzylic alcohol **89** (85%) as a bright yellow powder. TLC R_f (Pet. spirit:EtOAc, 50:50) = 0.42; Mp 215-218 ^oC; ^1H NMR (500 MHz, $(CD_3)_2CO$) δ 11.37 (br.s, 1H, H9), 8.53 (s, 1H, H2), 8.04 (d, J = 8.5 Hz, 1H, H5), 7.89 (d, J = 8.5 Hz, 2H, H13, H17), 7.59 (d, J = 8.5 Hz, 1H, H4), 7.51 (d, 2H, J = 8.5 Hz, H14, H16), 7.17 (s, 1H, H7), 4.72 (s, 2H, H18); ^{13}C NMR (125 MHz, $(CD_3)_2CO$) δ 146.3 (C6), 143.1 (C15), 141.2 (C8), 140.1 (C12), 131.5 (C3), 130.9 (C14, C16), 130.0 (C1), 125.8 (C13, C17), 119.1 (C4), 118.4 (C5), 110.6 (C2), 101.7 (C7), 64.3 (C18). The alcohol **89** (30 mg, 0.10 mmol) and CBr_4 (100 mg, 0.30 mmol) were added to a flame-dried 25 mL round bottom flask followed by anhydrous Et_2O/THF (1:1, 5 mL). The mixture was stirred at room temperature for 30 min before PPh_3 (80 mg, 0.31 mmol) was added in one portion. The reaction was stirred at room temperature for 3 h while monitoring by TLC (Pet. spirit:EtOAc, 70:30). The solvent was evaporated and the residue purified by silica gel column chromatography using Pet. spirit:EtOAc 90:10 to yield **90** (30 mg, 94%) as a yellow powder. TLC R_f (Pet. spirit:EtOAc, 50:50) = 0.91; Mp 198-199 ^oC; ^1H NMR (500 MHz, $(CD_3)_2CO$) δ 10.14

(br.s, 1H, H9), 9.27 (s, 1H, H2), 8.05 (d, 1H, *J* = 8.5 Hz, H5), 7.91 (d, 2H, *J* = 7.5 Hz, H4), 7.61-7.57 (m, 4H, H13, H14, H16, H17), 6.92 (s, 1H, H7), 4.51 (s, 2H, H18); ^{13}C NMR (125 MHz, $(CD_3)_2CO$) δ 143.0 (C6), 142.1 (C8), 138.3 (C15), 137.6 (C10), 135.8 (C12), 132.5 (C3), 129.5 (C14, C16), 129.2 (C7), 125.8 (C13, C17), 113.7 (C4), 112.2 (C5), 98.6 (C11), 33.3 (C2). HRESI-MS: *m/z* calcd for $[C_{15}H_{11}BrN_2O_2]$ 330.0018, found 330.0023.

Tert-butyl 4-(4-(5-nitro-1H-indol-2-yl)benzyl)piperazine-1-carboxylate 84

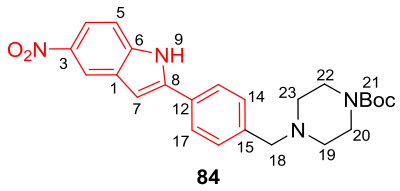

84

Bromide **90** (70 mg, 0.21 mmol) was dissolved in anhydrous THF (25 mL) under Ar and KI (175 mg, 1.1 mmol) added. The mixture was stirred at room temperature for 30 min before adding *N*-Boc-piperazine (100 mg, 0.53 mmol) in one portion. The reaction was then heated at reflux for 48 h while monitoring by TLC (Pet. spirit:EtOAc, 70:30). The mixture was concentrated and the residue purified by silica gel column chromatography using Pet. spirit:EtOAc 85:15 to afford **84** (89 mg, 96%) as a yellow solid. TLC R_f (Pet. spirit:EtOAc, 70:30) = 0.43; Mp 208-210 ºC; ^{1}H NMR (500 MHz, $(CD_3)_2SO$) δ 12.25 (br.s, 1H, H9), 8.53 (s, 1H, H2), 7.89 (d, *J* = 7.5 Hz, 2H, H5), 7.84 (d, *J* = 8.5 Hz, 2H, H13, H17), 7.53 (d, *J* = 7.5 Hz,1H, H4), 7.42 (d, *J* = 8.5, 2H, H14, H16), 7.15 (s, 1H, H7), 3.51 (s, 2H, H18), 3.30 (m, 4H, H20, H22), 2.33 (m, 4H, H19, H23), 1.37 (s, 9H, H21) ; ^{13}C NMR (125 MHz, $(CD_3)_2SO$) δ 155.0 (C21), 142.4 (C6), 141.2 (C15), 139.9 (C8), 139.0 (C12), 130.2 (C3), 130.0 (C14, C16), 128.7 (C1), 125.5 (C13, C17), 118.0 (C4), 117.7 (C5), 110.9 (C2), 101.6 (C7), 70.9 (C21), 62.7 (C18), 53.0 (C19, C23, C20, C22), 28.6 (C21) ; IR (neat) ν 3272, 2969, 2811, 2769,

1663, 1520, 1476, 1330, 1318, 1216, 1158 cm^{-1}; HRESI-MS: *m/z* calcd for $[C_{24}H_{28}N_4O_4]$ 435.2032, found 435.2043.

4-(5-nitro-1H-indol-2-yl)benzoic acid 91

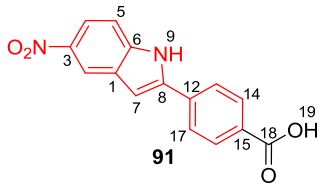

To a solution of methyl ester **88** (250 mg, 0.84 mmol) in MeOH/CH_2Cl_2 (10:90 v/v, 40 mL) was added methanolic NaOH (3 N, 2.5 mL). The mixture was stirred at room temperature for 30 min before attaching a reflux condenser and heating the reaction overnight at reflux while monitoring by TLC (CH_2Cl_2:MeOH, 90:10). The solvent was removed under reduced pressure and the residue redissolved in water (100 mL). The aqueous layer was washed with CH_2Cl_2 (2 x 60 mL) and the *p*H reduced to 2-3 by dropwise addition of 5% HCl. The aqueous layer was extracted with CH_2Cl_2 (3 x 50 mL). The combined organic layers were washed with water and brine, dried over anhydrous $MgSO_4$ and concentrated to give **91** (230 mg, 96%) as a yellow powder. TLC R_f (CH_2Cl_2:MeOH, 90:10) = 0.21; Mp 138-139 ºC; ^{1}H NMR (500 MHz, $(CD_3)_2SO$) δ 12.41 (s, 1H, H9), 8.56 (s, 1H, H2), 8.02 (m, 5H, H5, H13, H14, H16, H17), 7.57 (d, J = 10.0 Hz, 1H, H4),7.31 (s, 1H, H7); ^{13}C NMR (125 MHz, $(CD_3)_2CO$) δ 174.2 (C18), 148.3 (C6), 143.1 (C15), 141.2 (C8), 140.1 (C12), 131.5 (C3), 130.9 (C14, C16), 130.0 (C1), 125.8 (C13, C17), 119.1 (C4), 118.4 (C5), 110.6 (C2), 101.7 (C7); IR (neat) ν 3420, 3233, 2891, 2787, 2771, 1793, 1518, 1473, 1321, 1317, 1210, 1151 cm^{-1}; HRESI-MS: *m/z* calcd for $[C_{15}H_{10}N_2O_4]$ 281.0689, found 281.0680.

***Tert*-butyl 4-(4-(5-nitro-1H-indol-2-yl)benzoyl)piperazine-1-carboxylate 86**

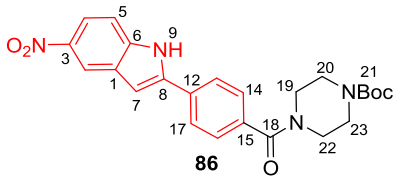

86

The acid **91** (20 mg, 0.07 mmol) was dissolved in anhydrous THF (10 mL) under Ar and DIEA (9.0 mg, 0.07 mmol) added. *N*-Boc-piperazine (16 mg, 0.08 mmol) and HATU (35 mg, 0.09 mmol) were then successively added and the reaction stirred at room temperature for 5 h while monitoring by TLC (Pet. spirit:EtOAc, 30:70). The solvent was removed under reduced pressure and the residue redissolved in CH_2Cl_2. The organic layer was washed with 5% aqueous HCl, water and brine and then dried over anhydrous Na_2SO_4 and concentrated. The crude residue was purified by silica gel column chromatography using Pet. spirit:EtOAc 60:40 to afford **86** (26 mg, 85%) as a yellow solid. TLC R_f (Pet. spirit:EtOAc, 30:70) = 0.50; Mp 210-12 ºC; ^{1}H NMR (500 MHz, $(CD_3)_2CO$) δ 11. 05 (br.s, 1H, H9), 8.58 (s, 1H, H2), 8.06 (d, J = 7.5 Hz, 1H, H5), 7.99 (d, J = 8.5 Hz, 2H, H13, H17), 7.74 (d, J = 8.5, 2H, H14, H16), 7.60 (d, J = 8.5 Hz,1H, H4), 7.27 (s, 1H, H7), 3.35 (m, 4H, H19, H22), 2.13 (m, 4H, H20, H23), 1.43 (s, 9H, H21); ^{13}C NMR (125 MHz, $(CD_3)_2CO$) δ 171.1 (C18), 151.8 (C21), 147.5 (C6), 142.5 (C15), 140.6 (C8), 139.0 (C12), 131.4 (C3), 130.8 (C14, C16), 129.5 (C1), 125.9 (C13, C17), 119.1 (C4), 118.3 (C5), 110.5 (C2), 101.8 (C7), 68.2 (C21), 46.0 (C20, C23), 40.4 (C19, C22), 29.3 (C21); IR (neat) ν 3267, 2957, 2795, 2768, 1701, 1663, 1521, 1475, 1322, 1312, 1215, 1119 cm^{-1}; HRESI-MS: *m/z* calcd for $[C_{24}H_{26}N_4O_5]$ 449.1825, found 449.1826.

Tert-butyl methyl(2-(methyl(4-(5-nitro-1H-indol-2-yl)benzyl)amino)ethyl) carbamate 85

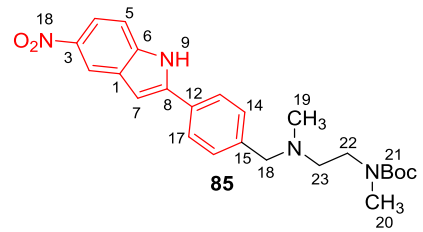

85

Bromide **90** (80 mg, 0.24 mmol) was dissolved in anhydrous THF (25 mL) under Ar in a 50 mL oven-

dried round bottom flask. KI (200 mg, 1.12 mmol) was added and the mixture stirred at room temperature for 30 min before adding *N*-Boc-*N*,*N*'-dimethylethylenediamine **75** (100 mg, 0.53 mmol) in one portion. A reflux condenser was attached and the reaction heated to reflux for 48 h while monitoring by TLC (Pet. spirit:EtOAc, 70:30). The solvent was evaporated and the residue purified by silica gel column chromatography using a gradient from Pet. spirit:EtOAc 60:40 to 100% EtOAc to yield **85** (63 mg, 78%) as a yellow solid. TLC R_f (Pet. spirit:EtOAc, 70:30) = 0.23; Mp 118-120 ºC; ^{1}H NMR (500 MHz, $(CD_3)_2SO$) δ 12.26 (br.s, 1H, H9), 8.55 (s, 1H, H2), 8.00-7.82 (m, 3H, H5, H13, H17), 7.60-7.38 (m, 3H, H4, H14, H16), 7.21 (s, 1H, H7), 4.00 (s, 2H, H18), 3.37 (m, 4H, H23, H22), 2.66 (s, 3H, H20), 1.96 (s, 3H, H19), 1.36 (s, 9H, H21); ^{13}C NMR (125 MHz, $(CD_3)_2SO$) δ 158.8 (C21), 142.1 (C6), 141.2 (C15), 140.0 (C8), 139.7 (C12), 129.9 (C3), 129.6 (C14, C16), 128.6 (C1), 125.3 (C13, C17), 117.8 (C4), 117.5 (C5), 110.7 (C2), 101.2 (C7), 79.4 (C21), 62.0 (C23), 47.1 (C22), 42.7 (C19), 35.0 (C20), 28.4 (C21); IR (neat) ν 3268, 2961, 2810, 2776, 1668, 1523, 1475, 1396, 1330, 1317, 1211, 1153 cm^{-1}; HRESI-MS: *m/z* calcd for $[C_{24}H_{30}N_4O_4]$ 437.2189, found 437.2180.

***Tert*-butyl methyl(2-(N-methyl-4-(5-nitro-1H-indol-2 yl)benzamido)ethyl) carbamate 87**

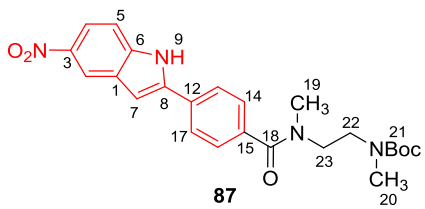

87

The acid **91** (20 mg, 0.07 mmol) was dissolved in anhydrous THF (9 mL) under Ar in a 25 mL flame-dried round bottom flask. DIEA (9.0 mg, 0.07 mmol), *N*-Boc-piperazine (16 mg, 0.088 mmol) and HATU (35 mg, 0.09 mmol) were successively added and the reaction stirred at room

temperature for 7 h while monitoring by TLC (pet. Spirit:EtOAc, 70:30). The solvent was evaporated and the residue redissolved in CH_2Cl_2 (30 mL). The organic layer was washed with 5% aqueous HCl, water and brine, dried over anhydrous Na_2SO_4 and concentrated. The crude residue was purified by silica gel column chromatography using a gradient from Pet. spirit:EtOAc 60:40 to 100% EtOAc to provide **87** (23 mg, 78%) as a yellow solid. TLC R_f (Pet. spirit:EtOAc, 70:30) = 0.45; Mp 162-164 ºC; ^{1}H NMR (500 MHz, $CDCl_3$) δ 12.20 (br.s, 1H, H9), 8.57 (s, 1H, H2), 7.61 (d, J = 11.5 Hz, 2H, H13, H17), 7.49 (d, 1H, H5), 7.43-7.27 (m, 3H, H4, H14, H16), 6.91 (d, J = 11.4 Hz,1H, H7), 3.76-3.32 (m, 4H, H23, H22), 2.76 (s, 3H, H20), 1.68 (s, 3H, H19), 1.46 (s, 9H, H21); ^{13}C NMR (125 MHz, $CDCl_3$) δ 174.0 (C18), 157.0 (C21), 142.0 (C6), 140.4 (C15), 139.8 (C8), 139.1 (C12), 129.1 (C3), 128.1 (C14, C16), 127.5 (C1), 125.2 (C13, C17), 116.9 (C4), 116.3 (C5), 110.3 (C2), 101.2 (C7), 79.8 (C21), 61.9 (C23), 47.1 (C22), 43.1 (C19), 36.8 (C20), 28.5 (C21); IR (neat) ν 3233, 2981, 2790, 1697, 1675, 1598, 1472, 1398, 1332, 1317, 1166, 1028 cm^{-1}; HRESI-MS: *m/z* calcd for [$C_{24}H_{28}N_4O_5$] 451.1981, found 451.1988.

6.1.7 Synthesis of INF271-Containing Intermediates

1-(2-hydroxyphenyl)-3-(naphthalen-2-yl)urea 98

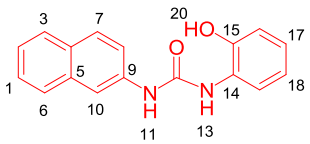

98

O-Aminophenol (4.0 g, 36.7 mmol) was added to a solution of 2-naphthaleneisocyanate **97** (4.00 g, 23.6 mmol) in dry CH_2Cl_2 (100 mL) in one portion. The reaction was stirred at room temperature for 48 h while monitored by TLC (Pet. spirit:EtOAc, 50:50). The white precipitate was filtered, washed with dry CH_2Cl_2:Et_2O, 50:50 (2 x 100 mL) and dried *in vacuo*. The residue was additionally washed with 1M aqueous HCl in cases where *O*-

aminophenol was observed in the ^{1}H NMR spectrum of the product. Compound **98** (5.20 g, 80%) was obtained as an off-white powder. TLC R_f (Pet. spirit:EtOAc, 50:50) = 0.48; Mp 163-165 ºC; ^{1}H NMR (500 MHz, $(CD_3)_2SO$) δ 9.98 (s, 1H, H20), 9.50 (s, 1H, H11), 8.24 (s, 1H, H13), 8.12 (s, 1H, H10), 8.08 (d, 1H, J = 9.8 Hz, H3), 7.82 (d, J = 10.0 Hz, 1H, H6), 7.80 (d, J = 10.0 Hz, 1H, H19), 7.78 (d, J = 10.0 Hz, 1H, H8), 7.45, 7.40 (dd, J = 10.0 Hz, 2H, H1, H2), 7.33 (d, J = 9.8 Hz, 1H, H17), 6.86 (d, J = 10.0 Hz,1H, H7), 6.96, 6.98 (dd, J = 10.0 Hz, 2H, H16, H18); ^{13}C NMR (125 MHz, $(CD_3)_2SO$) δ 153.3 (C12), 146.3 (C15), 138.3 (C9), 134.5 (C5), 129.7 (C4), 129.1 (C3), 128.5 (C14), 128.1 (C17), 127.6 (C1), 127.0 (C6), 122.5 (C2), 120.1 (C19), 119.3 (C8), 115.1 (C10), 113.6 (C16); IR (neat) ν 3669, 3316, 2978, 2923, 1701, 1654, 1602, 1534, 1460, 1250, 1220 cm^{-1}; HRESI-MS: *m/z* calcd for $[C_{17}H_{14}N_2O_2]$ 277.0977, found 277.0973.

1-(2-(3-Hydroxypropoxy)phenyl)-3-(naphthalen-2-yl)urea 99

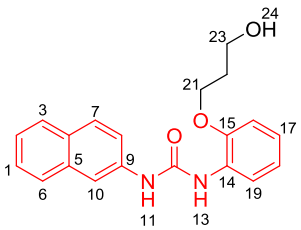

99

Phenolic urea **98** (1.0 g, 3.6 mmol) and KOH (1.20 g, 8.63 mmol) were added to a 50 mL oven-dried round bottom flask under argon. Anhydrous DMF (7 mL) was added and the mixture cooled to 0 ^{o}C before adding 3-bromopropanol (600 mg, 4.3 mmol) over 20 min. The reaction was stirred at room temperature for 16 h while monitoring by TLC (Pet. spirit:EtOAc, 50:50). The DMF was evaporated and the residue purified by silica gel column chromatography using a gradient of EtOAc:Pet. spirit 30:70 to 100% EtOAc. The product isolated was redissolved in EtOAc (250 mL) and washed with 1 M KOH and brine. The organic layer was dried over anhydrous $MgSO_4$ and concentrated to yield **99** (904 mg, 75%) as

an off-white powder. TLC R_f (Pet. spirit:EtOAc, 50:50) = 0.32; Mp 145-146 ºC; ^{1}H NMR (500 MHz, $(CD_3)_2SO$) δ 9.62 (s, 1H, H11), 8.18 (d, J = 7.5 Hz, 1H, H19), 8.15 (s, 1H, H13), 8.14 (s, 1H, H10), 7.84 (d, J = 7.4 Hz, 1H, H6), 7.80 (dd, J = 7.5 Hz, 2H, H8, H3), 7.51 (d, J = 7.5 Hz, 1H, H7), 7.43 (t, J = 7.5 Hz, 1H, H2), 7.34 (t, J = 7.5 Hz, 1H, H1), 7.02 (d, J = 7.5 Hz,1H, H16), 6.92 (dd, J = 7.5 Hz, 2H, H17, H18), 4.70 (s, J = 6.5 Hz, 1H, H24), 4.27 (t, J = 6.5 Hz, 2H, H21), 3.65 (t, J = 6.5 Hz, 2H, H23), 1.97 (q, J = 6.5 Hz, 2H, H22); ^{13}C NMR (125 MHz, $(CD_3)_2SO$) δ 155.4 (C15), 149.9 (C12), 140.3 (C9), 136.6 (C5), 131.9 (C6), 131.6 (C14), 131.3 (C7), 130.3 (C17), 129.85 (C4), 129.2 (C3), 126.8 (C1), 124.8 (C2), 123.3 (C18), 122.4 (C8), 121.7 (C19), 116.2 (C10), 114.6 (C16) 68.4 (C21), 60.3 (C23) 34.9 (C22); IR (neat) ν 3672, 3318, 2977, 2921, 1699, 1653, 1601, 1534, 1461, 1251, 1222 cm^{-1}; HRESI-MS: *m/z* calcd for $[C_{20}H_{20}N_2O_3]$ 335.1396, found 335.1402.

1-(2-(3-Bromopropoxy)phenyl)-3-(naphthalen-2-yl)urea 100

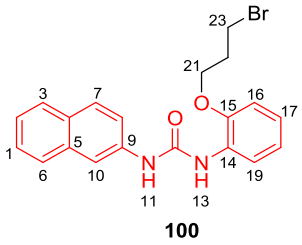

100

CBr_4 (3.10 g, 9.0 mmol) was added to a solution of alcohol **99** (800 mg, 2.4 mmol) in dry THF (30mL) in a 50 mL flame-dried round bottom flask under Ar. After 30 min stirring at room temperature PPh_3 (2.50 g, 9.5 mmol) was added in one portion and stirring continued at room temperature for a further 16 h. The solvent was removed under reduced pressure and the residue redissolved in CH_2Cl_2 (45 mL). The organic layer was washed with 1% KOH, water and brine and dried over anhydrous Na_2SO_4. The crude residue was purified by silica gel column chromatography using Pet. spirit:EtOAc 90:10 to afford **100** (800 mg, 85%) as grey crystals. TLC R_f (Pet. spirit:EtOAc, 50:50) = 0.76; Mp 122-123 ºC; ^{1}H NMR (500 MHz, $(CD_3)_2SO$) δ 9.58 (s,

1H, H11), 8.17 (d, *J* = 7.5 Hz, 1H, H19), 8.13 (s, 1H, H13), 8.11 (s, 1H, H10), 7.84 (d, *J* = 7.5 Hz, 1H, H6), 7.81 (dd, *J* = 7.4 Hz, 2H, H8, H3), 7.52 (d, *J* = 7.5 Hz, 1H, H7), 7.45 (t, *J* = 7.5 Hz, 1H, H2), 7.36 (t, *J* = 7.5 Hz, 1H, H1), 7.05 (d, *J* = 7.6 Hz, 1H, H16), 6.94 (dd, J = 7.4 Hz, 2H, H17, H18), 4.18 (t, *J* = 6.5 Hz, 2H, H21), 3.80 (t, *J* = 6.5 Hz, 2H, H23), 2.35 (q, *J* = 6.5 Hz, 2H, H22); ^{13}C NMR (125 MHz, $(CD_3)_2SO$) δ 156.1 (C15), 149.7 (C12), 139.9 (C9), 136.3 (C5), 132.8 (C6), 131.9 (C14), 131.0 (C7), 129.5 (C17), 129.0 (C4), 128.8 (C3), 126.9 (C1), 124.7 (C2), 123.0 (C18), 121.9 (C8), 120.9 (C19), 115.8 (C10), 114.01 (C16) 64.8 (C21), 34.5 (C23) 29.1 (C22); IR (neat) ν 3317, 2996, 2927, 1696, 1655, 1602, 1534, 1250, 1221 cm^{-1}; HRESI-MS: *m/z* calcd for $[C_{20}H_{19}BrN_2O_2]$ 397.0552, found 397.0566.

1-(Naphthalen-2-yl)-3-(2-(3-(piperazin-1-yl)propoxy)phenyl)urea 92

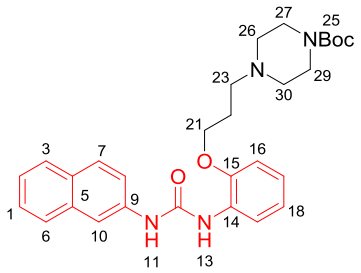

92

Bromide **100** (200 mg, 0.5 mmol), *N*-Boc-piperazine (200 mg, 1.1 mmol), K_2CO_3 (800 mg, 5.75 mmol) and KI 400 mg, 2.39 mol) were successively added to a 50 mL oven-dried round bottom flask under Ar. Dry THF (30 mL) was then added, a reflux condenser attached and the mixture stirred at 80 ^{o}C for 48 h. The reaction mixture was concentrated *in vacuo* and the residue redissolved in EtOAc (200 mL). The organic layer was washed with water and brine, dried over anhydrous Na_2SO_4 and concentrated. The crude residue was purified by silica gel column chromatography using a gradient (Pet. spirit:EtOAc, 50:50 to 100% EtOAc) to afford **92** (214 mg, 85%) as a brown powder. TLC R_f (Pet. spirit:EtOAc, 50:50) = 0.28; Mp 98-100 ^{o}C; ^{1}H NMR (500 MHz, $(CD_3)_2SO$) δ 8.90 (s, 1H, H11), 8.28 (d, *J* = 7.5, 1H, H19), 8.09 (s, 1H, H13), 7.76 (d, *J* = 7.5 Hz, 3H, H3, H6, H8), 7.11 (s,

1H, H10), 7.46 (d, *J* = 7.6 Hz, 1H, H7), 7.43 (d, *J* = 7.5 Hz, 2H, H1), 7.36 (d, *J* = 7.5 Hz, 1H, H2), 7.08 (d, *J* = 7.4 Hz, 1H, H16), 6.9-6.10 (d, *J* = 7.6 Hz, 1H, H18), 6.94 (d, *J* = 7.5 Hz, 1H, H17), 4.73 (t, *J* = 7.1 Hz, 2H, H21), 3.63 (t, *J* = 7.1 Hz, 2H, H27), 3.44 (dd, J = 7.1 Hz, 4H, H26, H29), 3.65 (t, *J* = 7.1, 2H, H30), 2.17 (t, *J* = 7.1 Hz, 2H, H23), 1.83 (q, *J* = 7.1 Hz, 2H, H22), 1.47 (s, 9H, H25); ^{13}C NMR (125 MHz, $(CD_3)_2SO$) δ 155.6 (C15), 154.7 (C40), 152.9 (C12), 135.4 (C9), 133.7 (C5), 129.9 (C7), 127.8 (C17), 126.8 (C4), 126.5 (C3), 125.3 (C1), 124.6 (C6), 124.3 (C14), 121.4 (C2), 120.5 (C18), 119.9 (C8, C19), 116.7 (C10), 112.9 (C16), 79.8 (C36), 73.1 (C21), 58.2 (C23), 56.7 (C26, C30), 46.2 (C27, C29), 28.4 (C37, C38, C39), 27.7 (C25); IR (neat) ν 3327, 2979, 2930, 2741, 1690, 1601, 1528, 1449, 1248, 1233, 1193, 1164, 1117 cm^{-1}; HRESI-MS: *m/z* calcd for $[C_{29}H_{36}N_4O_4]$ 505.2815, found 505.2834.

Tert-butyl 4-(2-(2-(3-(naphthalen-2-yl)ureido)phenoxy)acetyl)piperazine-1-carboxylate 94

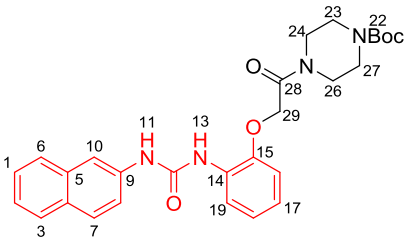

94

To a solution of the phenolic urea **98** (200 mg, 0.72 mmol) in dry DMF (5 mL) in a 50 mL oven-dried round bottom flask under Ar was added Cs_2CO_3 (800 mg, 2.5 mmol). The mixture was stirred at 40 ^{o}C for 30 min before *N*-bromoacetyl-*N'*-Boc-piperazine **76** (200 mg, 0.65 mmol) in dry DMF (3 mL) was added dropwise over 5 min. The reaction was stirred at 80 ^{o}C for 16 h while monitoring by TLC (Pet. spirit:EtOAc, 50:50). The solvent was removed *in vacuo* and the residue redissolved in EtOAc. The organic phase was washed with water and brine, dried over anhydrous Na_2SO_4 and concentrated. The crude residue was purified by silica gel column chromatography using a gradient (Pet. spirit:EtOAc, 50:50 to 100% EtOAc

followed by EtOAc:MeOH, 95:5) to yield **94** (237 mg, 66%) as an off-white powder. R_f (pet. Spirit:EtOAc, 50:50) = 0.48; Mp 243-244 ºC; ^{1}H NMR (500 MHz, $(CD_3)_2SO$) δ 9.57 (s, 1H, H11), 8.36 (s, 1H, H13), 8.15 (d, *J* = 7.5 Hz, 1H, H19), 7.78 (d, 1H, *J* = 7.5 Hz, H3), 7.76 (d, *J* = 7.5 Hz, 1H, H6), 7.72 (dd, *J* = 7.5 Hz, 2H, H7, H8), 7.38, 7.43 (dt, *J* = 7.4 Hz, 2H, H1,H2), 7.32 (d, *J* = 7.5 Hz, 1H, H17), 6.94-6.98 (m, *J* = 7.5 Hz, 3H, H10, H16, H18), 4.51 (s, 2H, H29), 3.68-3.31 (m, J = 7.11, 4H, H23, H24), 3.01 (s, 1H, H27), 2.93 (s, 1H, H26), 1.41 (s, 9H, H22); ^{13}C NMR (125 MHz, $(CD_3)_2SO$) δ 166.0 (C28), 153.7 (C22, C=O), 152.5 (C12), 146.8 (C15), 138.4 (C9), 137.5 (C5), 133.8 (C4), 129.0 (C14), 128.4 (C7), 127.5 (C17), 127.3 (C3), 126.8 (C1), 126.3 (C6), 123.8 (C2), 121.7 (C18), 121.1 (C19), 119.4 (C8),114.8 (C10), 113.2 (C16), 79.1 (C22), 66.5 (C27), 54.8 (C23), 43.8 (C26), 41.1 (24), 36.2 (C29), 27.9 (C22); IR (neat) ν 3363, 2984, 2925, 1707, 164, 1629, 1601, 1540, 1507, 1430, 1241, 1232, 1193, 1158, 1128, 1119 cm^{-1}; HRESI-MS: *m/z* calcd for [$C_{28}H_{32}N_4O_5$] 505.2833, found 505.2827.

Tert-butyl methyl(2-(methyl(3-(2-(3-(naphthalen-2-yl)ureido)phenoxy)propyl) amino)ethyl)carbamate 93

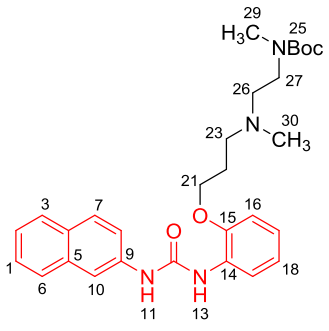

93

Bromide **100** (200 mg, 0.50 mmol), *N*-Boc-*N,N'*-dimethylethylenediamine **75** (200 mg, 1.0 mmol), K_2CO_3 (850 mg, 6.11 mmol) and KI (450 mg, 2.69 mmol) were added to a 50 mL flame-dried round bottom flask under Ar followed by dry THF (40 mL). The reaction was stirred for 48 h at 80 ºC while monitoring by TLC (Pet. spirit:EtOAc, 50:50). The solvent was evaporated and the residue redissolved in EtOAc (50 mL). The organic layer was washed with 5% aqueous HCl, water and brine before being dried

over anhydrous Na_2SO_4 and concentrated. The crude residue was purified by silica gel column chromatography using a gradient (Pet. spirit:EtOAc, 70:30 to 100% EtoAc followed by EtOAc:MeOH, 90:10) to yield **93** (215 mg, 85%) as a pale yellow powder. TLC R_f (Pet. spirit:EtOAc, 50:50) = 0.28; Mp 94-97 ºC; ^{1}H NMR (500 MHz, $(CD_3)_2SO$) δ 9.27 (s, 1H, H11), 8.35 (s, 1H, H13), 7.85 (d, *J* = 7.5 Hz, 1H, H19), 7.78 (d, *J* = 7.5 Hz, 1H, H3), 7.71 (d, *J* = 7.5 Hz, 1H, H6), 7.54 (d, *J*= 7.5 Hz, 1H, H8), 7.45 (d, *J* = 7.5 Hz, 2H, H1), 7.42 (d, *J* = 7.5 Hz, 1H, H7), 7.40 (d, *J* = 7.5 Hz, 1H, H2), 7.20 (d, *J* = 7.5 Hz, 1H, H16), 7.16 (s, 1H, H10), 7.10 (d, *J* = 7.5 Hz, 1H, H18), 7.08 (d, *J* = 7.5 Hz, 1H, H17), 4.04 (t, *J* = 7.1 Hz, 2H, H21), 3.27 (s, 4H, H29), 3.06 (t, *J* = 7.1 Hz, 3H, H27), 2.53 (t, *J* = 7.1 Hz, 2H, H26), 2.46 (t, *J* = 7.1 Hz, 2H, H23), 2.18 (s, 3H, H30), 1.82 (q, *J* = 7.1 Hz, 2H, H22), 1.42 (s, 9H, H37, H38, H39); ^{13}C NMR (125 MHz, $(CD_3)_2SO$) δ 155.6 (C15), 154.7 (C40), 152.9 (C12), 135.4 (C9), 133.7 (C5), 129.9 (C7), 127.8 (C17), 126.8 (C4), 126.5 (C3), 125.3 (C1), 124.6 (C6), 124.3 (C14), 121.4 (C2), 120.5 (C18), 119.9 (C8, C19), 116.7 (C10), 112.9 (C16), 79.8 (C36), 73.1 (C21), 55.6 (C26), 55.4 (C23), 52.4 (27), 46.9 (C30), 36 (C29), 28.4 (C37, C38, C39), 27.4 (C22); IR (neat) ν 3360, 2974, 2931, 2802, 1689, 1654, 1600, 1533, 1449, 1249, 1231, 1193, 1159, 1117 cm^{-1}; HRESI-MS: *m/z* calcd for $[C_{29}H_{38}N_4O_4]$ 507.2971, found 507.2964.

Tert-butyl methyl(2-(N-methyl-2-(2-(3-(naphthalen-2-yl)ureido)phenoxy) acetamido)ethyl)carbamate 95

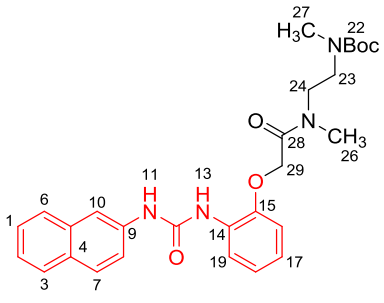

95

To a stirring solution of the phenolic urea **98** (200 mg, 0.72 mmol) in dry DMF (5 mL) in a 50 mL oven-dried round bottom flask under Ar was added Cs_2CO_3 (1.0 g, 3.06 mmol). The mixture was stirred at 40 ºC for 30

min before adding *N*-bromoacetyl-*N*'-Boc-*N*,*N*'-dimethylethylenediamine **77** (200 mg, 0.64 mmol) in DMF (3 mL) was added dropwise over 5 min. The reaction was heated to 80 ^{o}C and stirred while monitoring by TLC (Pet. spirit:EtOAc, 50:50). The solvent was removed and the residue redissolved in EtOAc. The organic layer was washed with water and brine and the aqueous layer back-extracted with EtOAc (50 mL). The pooled organic fractions were dried over anhydrous $MgSO_4$ and concentrated. The crude residue was purified by silica gel column chromatography using a gradient (Pet. spirit:EtOAc, 70:30 to 100% EtoAc followed by EtOAc:MeOH, 95:5) to afford **95** (290 mg, 80%) as an off-white powder. TLC R_f (Pet. spirit:EtOAc, 50:50) = 0.22; Mp 110-113 ºC; ^{1}H NMR (500 MHz, $(CD_3)_2SO$) δ 8.70 (s, 1H, H11), 8.50 (s, 1H, H13), 8.43 (d, *J* = 7.5 Hz, 1H, H19), 8.22 (s, 1H, H10), 7.81-7.72 (m, *J* = 7.5 Hz, 3H, H3, H6, H2), 7.42 (dd, *J* = 7.4 Hz, 2H, H7, H8), 7.33 (t, *J* = 7.4 Hz, 1H, H1), 7.04 (t, *J* = 7.5 Hz, 1H, H17), 6.95 (t, *J* = 7.5 Hz, 1H, H18), 6.81 (d, *J* = 7.5 Hz, 1H, H16), 4.52 (s, 2H, H29), 3.70-3.30 (m, *J* = 7.11, 4H, H23, H24), 3.1 (s, 1H, H27), 2.95 (s, 1H, H26), 1.41 (s, 9H, H22); ^{13}C NMR (125 MHz, $(CD_3)_2SO$) δ 168.2 (C28), 160.1 (C22), 157.3 (C12), 153.2 (C15), 146.2 (C9), 137.4 (C5), 134.5 (C7), 132.2 (C4), 130.0 (C14), 128.6 (C17), 127.6 (C3), 126.4 (C1), 124.2 (C6), 122.9 (C2), 121.9 (C18), 119.7 (C19), 119.2 (C8), 114.4 (C10), 111.8 (C16), 79.6 (C36), 73.2 (C21), 55.9 (C26), 55.4 (C23), 52.3 (27), 46.8 (C30), 36.0 (C29), 28.5 (C37, C38, C39), 27.5 (C22); IR (neat) ν 3363, 2977, 2930, 1704, 1648, 1629, 1601, 1533, 1506, 1454, 1249, 1229, 1193, 1155, 1155, 1115 cm^{-1}; HRESI-MS: *m/z* calcd for $[C_{28}H_{34}N_4O_5]$ 507.2607, found 507.2598.

6.1.8 Synthesis of Reserpine-Containing Hybrids

General Procedure for the Synthesis of Hybrids 47-62. The general procedure is exemplified using the synthesis of 3-(4-(2-(4-((((1S,2R,3R,4aS,13bR,14aS)-2,11-dimethoxy-1-(methoxycarbonyl)-1,2,3, 4 ,4a,5,7,8,13,13b,14,14a-dodecahydroindolo

[2',3':3,4] pyrido[1,2-b]isoquinolin-3-yl)oxy)carbonyl)-2,6-dimethoxyphenoxy)ethyl) piperazin-1-yl)-7-(dimethylamino) phenothiazin-5-ium chloride **47**

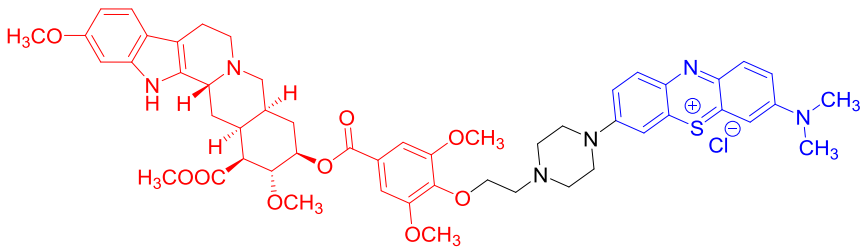

47

The Boc-protected intermediate **66** (80 mg, 0.07 mmol) was dissolved in CH_2Cl_2 (25 mL) in a 50 mL round bottom flask under Ar and cooled to 0 ^oC. TFA (5 mL) was added in one portion and the reaction allowed to warm to room temperature with stirring while monitoring by TLC (Pet. spirit:EtOAc, 40:60). Upon consumption of the starting material the reaction was quenched with water and extracted with CH_2Cl_2 (3 x 30 mL). The pooled organic fractions were dried over anhydrous $MgSO_4$ and concentrated under reduced pressure. The crude amine TFA salt was redissolved in dry CH_2Cl_2 (15 mL) in a 25 mL oven-dried round bottom flask under Ar and 3-dimethylaminophenothiazin-5-ium triiodide **63** (120 mg, 0.19 mmol, 0.9 eq) was added in one portion. The reaction was stirred at room temperature for 72 h while monitoring

by TLC (3% $NH_4OAc_{(aq)}$:MeOH, 15:85). K_2CO_3 was added in cases where the reaction showed little or no progress after overnight stirring. The completed reaction was concentrated and the residue purified by preparative TLC using 3% $NH_4OAc_{(aq)}$/MeOH 15:85. The dark blue product obtained was dissolved in dry MeOH (25 mL) and stirred at room temperature with quaternary ammonium chloride-anion exchange resin (350 mg, 10% w/w). After 1 h the mixture was filtered through a plug of cotton and the filtrate concentrated to give **47** (15.3 mg, 18%) as a dark blue powder. The light-sensitive compound was stored in a vial under Ar wrapped in aluminium foil at -20 °C. TLC R_f (3% $NH_4OAc_{(aq)}$:MeOH 15:85) = 0.03; Mp > 250 °C; UV (MeOH): 292 (log ε 5.06, λ_{max}), 3.29 (log ε 4.59), 386 (log ε 4,45), 510 (log ε 4.00, λ_{min}), 610 (log ε 4.80), 651 (log ε 5.04, λ_{max}) nm; IR (neat) ν 3419, 2926, 2843, 1708, 1591, 1459, 1387, 1330, 1222, 1126 cm^{-1}; L HRESI-MS: *m/z* calcd for $[C_{52}H_{61}N_6O_9S]$ 946.4299, found 946.4276.

3-(4-(2-(4-((((1S,2R,3R,4aS,13bR,14aS)-2,11-dimethoxy-1-(methoxycarbonyl)-1,2,3,4,4a,5,7,8,13,13b,14,14a-dodecahydroindolo[2',3':3,4]pyrido[1,2-b]isoquinolin-3-yl)oxy)carbonyl)-2,6-dimethoxyphenoxy)acetyl)piperazin-1-yl)-7-(dimethylamino)phenothiazin-5-ium chloride 49

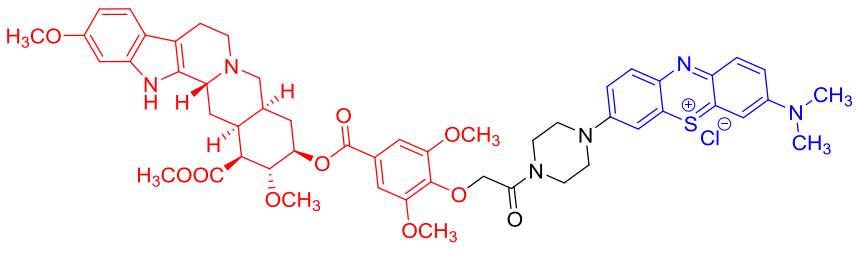

49

The general procedure was used with Boc-protected intermediate **68** (80 mg, 0.01 mmol). Stirring at room temperature for 96 h yielded **49** (13.6 mg, 14%) as a dark blue

powder after preparative TLC and anion exchange. TLC R_f (3% $NH_4OAc_{(aq)}$:MeOH 15:85) = 0.02; Mp > 250 ºC; UV (MeOH): 292 (log ε 4.88, λ_{max}), 3.27 (log ε 4.46), 392 (log ε 4,45), 512 (log ε 3.79, λ_{min}), 609 (log ε 4.67), 653 (log ε 4.97, λ_{max}) nm; IR (neat): 3744, 2933, 2845, 1714, 1700, 1592, 1458, 1384, 1329, 1209, 1179, 1152 cm^{-1}; HRESI-MS: *m/z* calcd for [$C_{52}H_{59}N_6O_{10}S$] 960.4092, found 960.4063.

3-((2-((2-(4-((((1S,2R,3R,4aS,13bR,14aS)-2,11-dimethoxy-1-(methoxycarbonyl)-1,2,3,4,4a,5,7,8,13,13b,14,14a-dodecahydroindolo[2',3':3,4]pyrido[1,2-b]isoquin olin-3-yl)oxy)carbonyl)-2,6-dimethoxyphenoxy)ethyl)(methyl)amino)ethyl)(methyl) amino)-7-(dimethylamino)phenothiazin-5-ium chloride 48

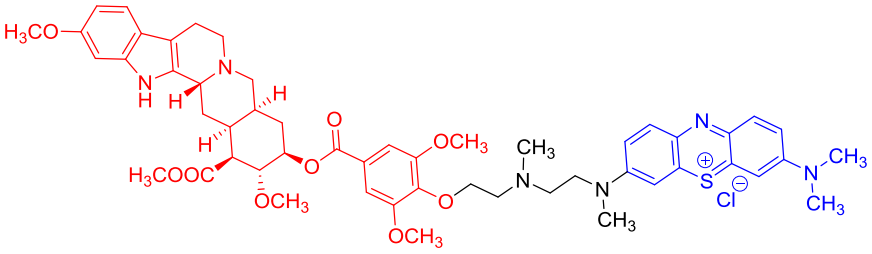

48

The general procedure was used with Boc-protected intermediate **67** (100 mg, 0.12 mmol). Stirring for 72 h at room temperature in the presence of K_2CO_3 (0.4 eq) afforded **48** (22 mg, 18%) as a dark blue powder after preparative TLC and anion exchange. TLC R_f (3% $NH_4OAc_{(aq)}$:MeOH 15:85) = 0.03; Mp = 212-214 ºC; UV (MeOH): 292 (log ε 4.86, λ_{max}), 327 (log ε 4.31), 392 (log ε 4.17), 512 (log ε 3.75, λ_{min}), 609 (log ε 4.70), 656 (log ε 5.02, λ_{max}) nm; IR (neat) ν 3416, 2931, 2870, 1709, 1594, 1454, 1383, 1327, 1229, 1216 1123 cm^{-1}; HRESI-MS: *m/z* calcd for [$C_{52}H_{63}N_6O_9S$] 948.4456, found 948.4423.

3-((2-(2-(4-((((1S,2R,3R,4aS,13bR,14aS)-2,11-dimethoxy-1-(methoxycarbonyl)-1,2,3,4,4a,5,7,8,13,13b,14,14a-dodecahydroindolo[2',3':3,4]pyrido[1,2-b]isoquinolin-3-yl)oxy)carbonyl)-2,6-dimethoxyphenoxy)-N-methylacetamido)ethyl)(methyl)amino)-7-(dimethylamino)phenothiazin-5-ium chloride 50

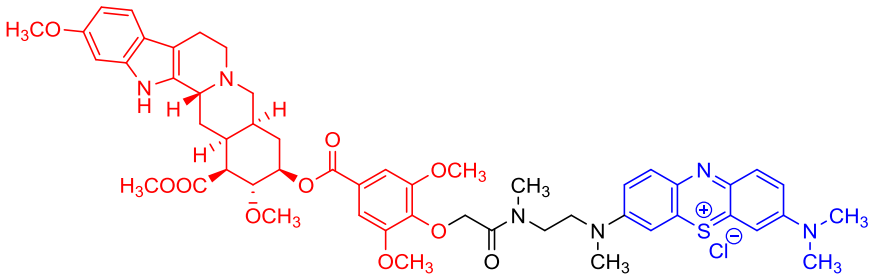

50

The general procedure was used with Boc-protected intermediate **69** (90 mg, 0.11 mmol). Stirring for 96 h at room temperature in the presence of K_2CO_3 (0.4 eq) afforded **50** (12 mg, 11%) as a dark blue powder after preparative TLC and anion exchange. TLC R_f (3% $NH_4OAc_{(aq)}$:MeOH 15:85) = 0.02; Mp > 250 ºC; UV (MeOH): 292 (log ε 4.85, λ_{max}), 329 (log ε 4.29), 392 (log ε 4.23), 512 (log ε 3.77, λ_{min}), 609 (log ε 4.70), 656 (log ε 5.00, λ_{max}) nm; IR (neat) ν 3363, 2926, 2848, 1716, 1710, 1594, 1462, 1387, 1330, 1217, 1183, 1124 cm^{-1}; HRESI-MS: *m/z* calcd for $[C_{52}H_{61}N_6O_{10}S]$ 961.4170, found 961.4199.

6.1.9 Synthesis of Pterostilbene-Containing Hybrids

(*E*)-3-((2-((2-(4-(3,5-dimethoxystyryl)phenoxy)ethyl)(methyl) amino)ethyl)(methyl) amino)-7-(dimethylamino)phenothiazin-5-ium chloride 51

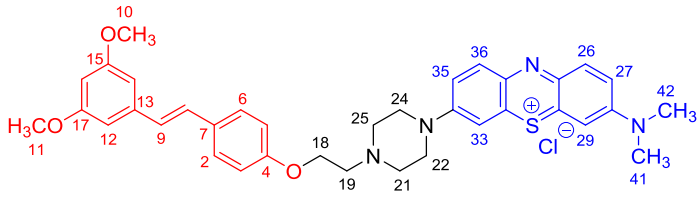

51

The general procedure was used with Boc-protected intermediate **78** (100 mg, 0.21 mmol). Stirring at room temperature for 72 h in the presence of K_2CO_3 (0.3 eq) afforded **51** (35 mg, 26%) as a dark blue powder after preparative TLC and anion exchange. TLC R_f (3% $NH_4OAc_{(aq)}$:MeOH 15:85) = 0.03; Mp = 162-163 ºC; ^{1}H NMR (500 MHz, CD_2Cl_2) δ 7.98 (dd, J = 8.0, 1.6 Hz, 1H, H36), 7.44 (d, J = 10.0 Hz, 2H, H6, H2), 7.42 (dd, J = 8.0, 1.6 Hz, 1H, H33), 7.37 (d, J = 10.0 Hz, 1H, H26), 7.35 (dd, J = 10.0, 2.4 Hz, 1H, H27), 7.08 (d, J = 2.4 Hz, 1H, H29), 6.86 (m, 5H, H35, H9, H3, H5, H8), 6.67 (s, 2H, H12, H14), 6.38 (s, 1H, H16), 4.31 (t, J = 12.0 Hz, 2H, H18), 3.75 (s, 6H, H10, H11), 3.64 and 3.60 (2s, 6H, $N(CH_3)_2$), 2.95 (t, J = 14.0 Hz, 2H, H19), 2.93 (dd, J = 7.5 Hz, 4H, H22, H24), 2.08 (dd, J = 7.5 Hz, 4H, H21, H25); ^{13}C NMR (125 MHz, $(CD_3)_2SO$) δ ^{13}C NMR (125 MHz, CD_2Cl_2) δ 161.4, 158.8, 139.9, 139.1, 130.5, 128.8, 128.1, 126.9, 122.2, 119.8, 115.10, 106.7, 106.4, 104.5, 99.9, 66.3, 60.9, 57.0, 55.6, 54.2, 54.0, 48.4, 30.0, 28.9; UV (MeOH): 294 (log ε 4.86, λ_{max}), 323 (log ε 4.70), 415 (log ε 4.10, λ_{min}), 612 (log ε 4.60), 655 (log ε 4.84, λ_{max}) nm; IR (neat) ν 2921, 1589, 1386, 1146, 1129, 1110 cm^{-1}; HRESI-MS: *m/z* calcd for [$C_{36}H_{39}N_4O_3S$] 607.2743, found 607.2764.

(*E*)-3-(4-(2-(4-(3,5-dimethoxystyryl)phenoxy)acetyl)piperazin-1-yl)-7-(dimethyl amino)phenothiazin-5-ium chloride 53

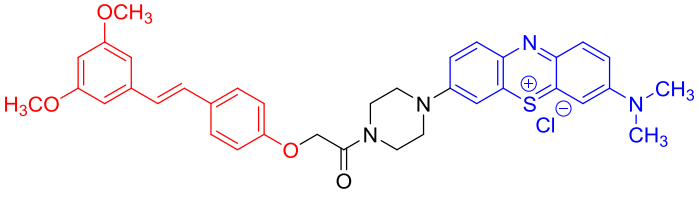

53

The general procedure was used with Boc-protected intermediate **80** (60 mg, 0.12 mmol). Stirring

at room temperature for 72 h in the presence of K_2CO_3 (0.2 eq) yielded **53** (25 mg, 30%) as a dark blue powder after preparative TLC and anion exchange. TLC R_f (3% $NH_4OAc_{(aq)}$:MeOH 15:85) = 0.04; Mp = 85-87 ºC; UV (MeOH): 292 (log ε 5.10, λ_{max}), 320 (log ε 4.91), 412 (log ε 3.37, λ_{min}), 615 (log ε 4.64), 654 (log ε 4.87, λ_{max}) nm; IR (neat) ν 3261, 2921, 1589, 1386, 1146, 1129, 1110 cm^{-1}; HRESI-MS: *m/z* calcd for $[C_{36}H_{37}N_4O_4S]$ 621.2536, found 607.2546.

(*E*)-3-((2-((2-(4-(3,5-dimethoxystyryl)phenoxy)ethyl)(methyl) amino)ethyl)(methyl) amino)-7-(dimethylamino)phenothiazin-5-ium chloride 52

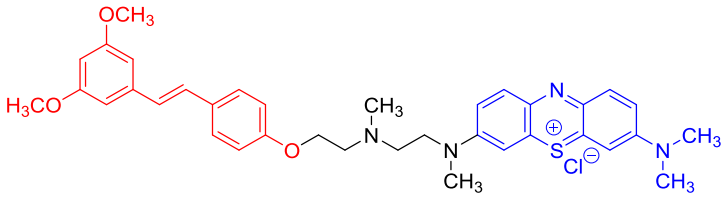

52

The general procedure was used with Boc-protected intermediate **79** (70 mg, 0.15 mmol). Stirring for 72 h at room temperature in the presence of K_2CO_3 (0.4 eq) provided **52** (27 mg, 28%) as a dark blue powder after preparative TLC and anion exchange. TLC R_f (3% $NH_4OAc_{(aq)}$:MeOH 15:85) = 0.02; Mp = 178-180 ºC; UV (MeOH): 293 (log ε 5.10, λ_{max}), 324 (log ε 4.95), 413 (log ε 3.26, λ_{min}), 611 (log ε 4.63), 661 (log ε 4.92, λ_{max}) nm; IR (neat) ν 2919, 2848, 1589, 1455, 1386, 1174, 1145, 1137 cm^{-1}; HRESI-MS: *m/z* calcd for $[C_{36}H_{41}N_4O_3S]$ 609.2899, found 609.2901.

(*E*)-3-((2-(2-(4-(3,5-dimethoxystyryl)phenoxy)-N-methylacetamido)ethyl)(methyl) amino)-7-(dimethylamino)phenothiazin-5-ium chloride 54

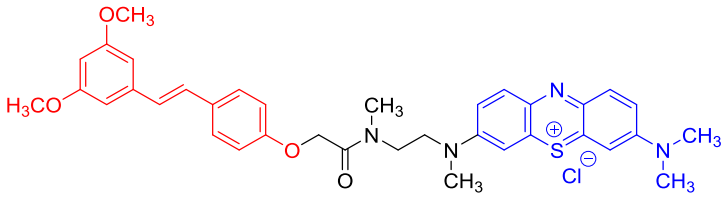

54

The general procedure was used with Boc-protected

intermediate **81** (80 mg, 0.16 mmol). Stirring for 48 h at room temperature in the presence of K_2CO_3 (0.2 eq) afforded **54** (28 mg, 26%) as a dark blue powder after preparative TLC and anion exchange. TLC R_f (3% $NH_4OAc_{(aq)}$:MeOH 15:85) = 0.02; Mp = 194-196 ºC; UV (MeOH): 293 (log ε 5.17, λ_{max}), 324 (log ε 4.99), 415 (log ε 3.29, λ_{min}), 613 (log ε 4.67), 661 (log ε 4.95, λ_{max}) nm; IR (neat) ν 2938, 2842, 1664, 1589, 1456, 1203, 1149, 1065, 1055 cm^{-1}; HRESI-MS: *m/z* calcd for $[C_{36}H_{41}N_4O_3S]$ 623.2692, found 623.2703.

6.1.10 Synthesis of INF55-Containing Hybrids

3-(Dimethylamino)-7-(4-(4-(5-nitro-1H-indol-2-yl)benzyl)piperazin-1-yl)phenothiazine-5-ium chloride 55

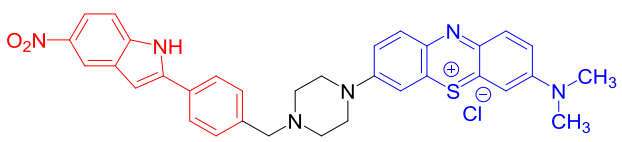

55

The general procedure was used with Boc-protected intermediate **84** (90 mg, 0.20 mmol). Stirring at room temperature for 48 h gave **55** (29 mg, 23%) as a dark blue powder after preparative TLC and anion exchange. TLC R_f (3% $NH_4OAc_{(aq)}$:MeOH 15:85) = 0.04; Mp > 250 ºC; UV (MeOH): 295 (log ε 4.99, λ_{max}), 415 (log ε 3.43, λ_{min}), 610 (log ε 4.62), 656 (log ε 4.91, λ_{max}) nm; IR (neat) ν 3205, 2924, 1683, 1591, 1517, 1472, 1387, 1329, 1220, 1134, 1045; HRESI-MS: *m/z* calcd for $[C_{33}H_{31}N_6O_2S]$ 575.2229, found 575.2236.

3-(Dimethylamino)-7-(methyl(2-(methyl(4-(5-nitro-1H-indol-2-yl)benzyl)amino)ethyl)amino)phenothiazin-5-ium chloride 57

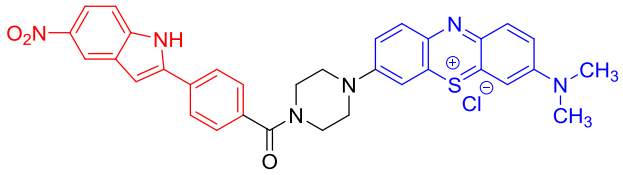

57

The general procedure was used with Boc-protected intermediate **86** (100 mg, 0.23 mmol). Stirring at room temperature for 76 h in the presence of K_2CO_3 (0.3 eq) provided **57** (25 mg, 18%) as a dark blue powder after preparative TLC and anion exchange. TLC R_f (3% $NH_4OAc_{(aq)}$:MeOH 15:85) = 0.03; Mp > 250 ºC; UV (MeOH): 297 (log ε 5.06, λ_{max}), 419 (log ε 3.49, λ_{min}), 609 (log ε 4.68), 651 (log ε 4.91, λ_{max}) nm; IR (neat) ν 3305, 2975, 2922, 1695, 1558, 1553, 1549, 1540, 1472, 1409, 1400, 1331, 1220, 1134 cm^{-1}; HRESI-MS: *m/z* calcd for $[C_{33}H_{33}N_6O_2S]$ 577.2386, found 577.2400.

3-(Dimethylamino)-7-(4-(4-(5-nitro-1H-indol-2-yl)benzoyl)piperazin-1-yl)phenol thiazine-5-ium chloride 56

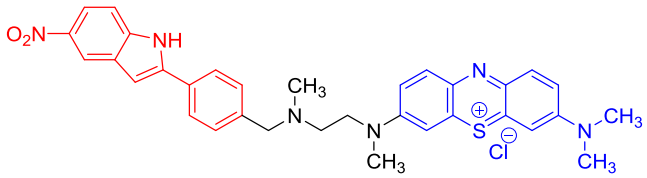

56

The general procedure was used with Boc-protected intermediate **85** (80 mg, 0.18 mmol). Stirring at room temperature for 48 h yielded **56** (25 mg, 22%) as dark blue powder after preparative TLC and anion exchange. TLC R_f (3% $NH_4OAc_{(aq)}$:MeOH 15:85) = 0.02; Mp > 250 ºC; UV (MeOH): 295 (log ε 5.03, λ_{max}), 415 (log ε 3.65, λ_{min}), 609 (log ε 4.66), 650 (log ε 4.86, λ_{max}) nm; IR (neat) ν 3245, 2922, 2850, 1663, 1591, 1519, 1458, 1386, 1329, 1230, 1219, 1135 cm^{-1}; HRESI-MS: *m/z* calcd for $[C_{33}H_{29}N_6O_3S]$ 589.2022, found 589.2048.

3-(Dimethylamino)-7-(methyl(2-(N-methyl-4-(5-nitro-1H-indol-2-yl)benzamido) ethyl)amino)phenothiazin-5-ium chloride 58

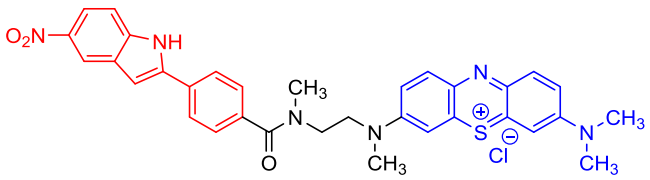

58

The general procedure was used with Boc-protected intermediate **87** (120 mg, 0.26 mmol). Stirring at room temperature for 76 h in the presence of K_2CO_3 (0.4 eq) afforded **58** (30 mg, 18%) as a dark blue powder after preparative TLC and anion exchange. TLC R_f (3% $NH_4OAc_{(aq)}$:MeOH 15:85) = 0.02; Mp > 250 ºC; UV (MeOH): 294 (log ε 5.02, λ_{max}), 413 (log ε 3.39, λ_{min}), 610 (log ε 4.46), 659 (log ε 4.82, λ_{max}) nm; IR (neat) ν 3240, 2921, 2853, 1665, 1591, 1516, 1456, 1387, 1328, 1226, 1218, 1130 cm^{-1}; HRESI-MS: *m/z* calcd for $[C_{33}H_{31}N_6O_3S]$ 591.2175, found 591.2183.

6.1.11 Synthesis of INF271-Containing Hybrids

3-(Dimethylamino)-7-(4-(3-(2-(3-(naphthalen-2-yl)ureido)phenoxy)propyl) piperazin-1-yl)phenothiazin-5-ium chloride 59

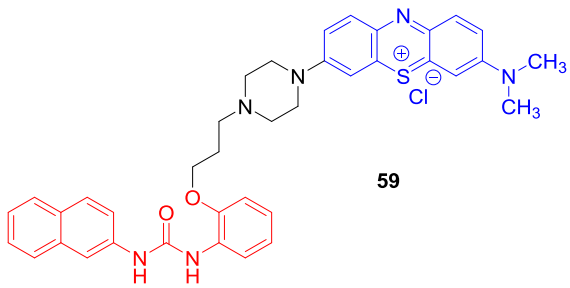

59

The general procedure was used with Boc-protected intermediate **92** (100 mg, 0.19 mmol). Stirring at room temperature for 48 h afforded **59** (34 mg, 25%) as a dark blue powder after preparative TLC and anion exchange. TLC R_f (3% $NH_4OAc_{(aq)}$:MeOH, 15:85) = 0.04; Mp > 250 ºC; UV (MeOH): 287 (log ε 4.86), 295 (log ε 4.88, λ_{max}), 323 (log ε 4.14), 368 (log ε 3.37, λ_{min}), 608 (log ε 4.61), 655 (log ε 4.88, λ_{max}) nm; IR (neat) ν 3355, 2972, 2921, 2740, 1704, 1595, 1458, 1353, 1136, 1127, 1118 cm^{-1}; HRESI-MS: *m/z* calcd for $[C_{38}H_{39}N_6O_2S]$ 643.2855, found 643.2870.

3-(Dimethylamino)-7-(4-(2-(2-(3-(naphthalen-2-yl)ureido)phenoxy)acetyl) piperazin-1-yl)phenothiazin-5-ium chloride 61

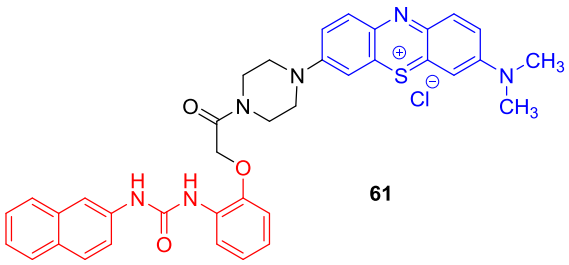

61

The general procedure was used with Boc-protected intermediate **94** (90 mg, 0.18 mmol). Stirring at room temperature for 72 h with K_2CO_3 (0.3 eq) yielded **61** (21 mg, 17%) as a dark blue powder after preparative TLC and anion exchange. TLC R_f (3% $NH_4OAc_{(aq)}$:MeOH 15:85) = 0.03; Mp 228-231 ºC; UV (MeOH): 289 (log ε 4.93), 293 (log ε 4.94, λ_{max}), 324 (log ε 4.10), 410 (log ε 2.04, λ_{min}), 608 (log ε 4.67), 652 (log ε 4.96, λ_{max}) nm; IR (neat) ν 3324, 2989, 2923, 2738, 1700, 1653, 1593, 1458, 1386, 1215, 1196, 1136, 1127 cm^{-1}; HRESI-MS: *m/z* calcd for $[C_{37}H_{35}N_6O_3S]$ 643.2491, found 643.2508.

3-(Dimethylamino)-7-(methyl(2-(methyl(3-(2-(3-(naphthalen-2-yl)ureido)phenoxy)propyl)amino)ethyl)amino)phenothiazin-5-ium chloride 60

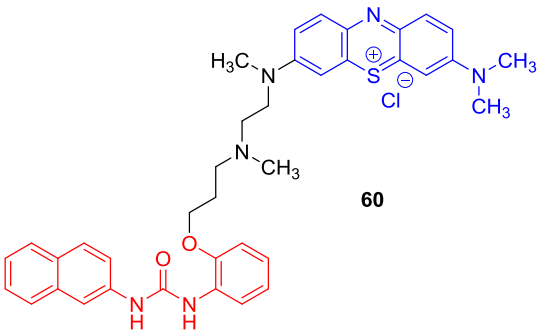

60

The general procedure was used with Boc-protected intermediate **93** (100 mg, 0.19 mmol). Stirring at room temperature for 48 h provided **60** (34 mg, 25%) as a dark blue powder after preparative TLC and anion exchange. TLC R_f (3% $NH_4OAc_{(aq)}$:MeOH 15:85) = 0.03; Mp = 239-241 ºC; UV

(MeOH): 290 (log ε 4.86), 327 (log ε 4.06), 415 (log ε 3.03, λ_{min}), 610 (log ε 4.60), 659 (log ε 4.97, λ_{max}) nm; IR (neat) ν 3299, 2968, 2925, 2710, 1700, 1593, 1450, 1386, 1327, 1231, 1195, 1136, 1126, 1117 cm^{-1}; HRESI-MS: *m/z* calcd for [$C_{38}H_{41}N_6O_2S$] 645.3012, found 645.2993.

3-(Dimethylamino)-7-(methyl(2-(N-methyl-2-(2-(3-(naphthalen-2-yl)ureido) phenoxy)acetamido)ethyl)amino)phenothiazin-5-ium chloride 62

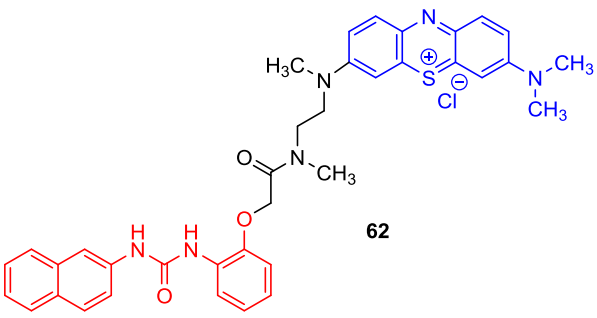

62

The general procedure was used with Boc-protected intermediate **95** (80.0 mg, 0.16 mmol). Stirring at room temperature for 72 h with K_2CO_3 (0.3 eq) afforded hybrid **62** (15 mg, 15%) as a dark blue powder after preparative TLC and anion exchange. TLC R_f (3% $NH_4OAc_{(aq)}$:MeOH 15:85) = 0.02; Mp = 246-248 ºC; UV (MeOH): 293 (log ε 4.93, λ_{max}), 325 (log ε 4.16), 413 (log ε 3.09, λ_{min}), 610 (log ε 4.73), 656 (log ε 5.05, λ_{max}) nm; IR (neat) ν 3311, 2968, 2923, 2851, 2736, 1706, 1654, 1593, 1457, 1387, 1327, 1231, 1192, 1136, 1126, 1119 cm^{-1}; HRESI-MS: *m/z* calcd for [$C_{37}H_{37}N_6O_3S$] 645.2648, found 645.2663.

6.2 Experimental Procedures - Photochemical and *In Vitro* Studies

6.2.1 Microbial Strains and Culture Conditions

The following bacterial strains were used: *S. aureus* 8325-4 (wild-type), K1902 (8325-4, NorA-), K2378 (NorA++), *S. aureus* Community Associated (CA)-MRSA USA300 (Human isolate/Clinical Microbiology, MGH). The NorA-overexpressing

strain K2378 was obtained from Prof Kim Lewis at Northeastern University, Boston. All other strains were obtained from Dr George Tegos at The University of New Mexico.

Bacterial cells were cultured in Mueller-Hinton Broth (MHB) or brain heart infusion (BHI) medium at 37 °C with shaking at 100 rpm. Cell growth was assessed using an Evolution 300 UV/Vis Spectrophotometer (Thermo Scientific, Waltham, MA). Cultures were grown to an optical density (OD_{600}) of 0.6, corresponding to a bacterial cell density of 10^8 CFU/mL, and then washed and resuspended in phosphate-buffered saline (PBS) (Dulbecco) at 2×10^9 CFU/mL. Cell growth was assessed using a spectrophotometer (Shimadzu, Mini 1240) measuring absorbance at 600 nm (OD_{600}).

6.2.2 Chemicals

Purified H_2O was produced in-house (Milli-Q Water Purification System, Millipore). D_2O (99.8%) was obtained from Cambridge Isotope Laboratories (Apeldoorn, The Netherlands). Ciprofloxacin was obtained from the Massachusetts General Hospital Pharmacy and MB was obtained from Sigma-Aldrich (St. Louis, MO).

6.2.3 Photosensitizers and Light Source

Stock solutions of MB and the synthesized hybrids were prepared in phosphate-buffered saline (PBS) (2 mM) after encapsulation in Cremophore EL (CrEL) (See Chapter 6.2.5). For all photodynamic experiments, the stock solutions were stored for a maximum of 2 weeks at 4°C in the dark. For UV/Vis experiments, stock solutions of PS (10 μM) in methanol were prepared immediately prior to use.

A noncoherent light source with interchangeable fiber bundles (LC122; LumaCare, London, United Kingdom) was employed in all photodynamic experiments. Thirty nanometre band-pass filters at ranges of 652 ± 15 nm were used for both MB and hybrids. The total power output provided from the fibre bundle was 300 mW and plates were positioned to give an irradiance of 100 mW/cm^2.

6.2.4 ROS Generation Assay

Cell-free ROS assays were performed in 96-well plates. SOSG and HPF probes (Molecular Probes Invitrogen^{TM}) were prepared as 5 µM stocks in MeOH before use. Solutions of hybrids and MB in PBS were added to each well to give 50 µM solutions in a volume of 85 µL. Probe solutions (40 µL) and deuterium oxide (40 µL) were then added followed by MeOH (35 µL) to produce a final volume of 200 µL, with compounds present at 10 µM. Plates were illuminated with light delivered in increasing doses (1-10 J/cm^2 for SOG and 1-12 J/cm^2 for HPF). A microplate spectrophotometer (Spectra Max M5, Molecular Devices) was used to monitor the fluorescence signals in the "slow kinetic" mode. For HPF, fluorescence emission at 525 nm was measured upon excitation at 492 nm using a 2 nm monochromator band pass for both excitation and emission. With SOSG, the corresponding values were 505 nm and 525 nm, respectively. Data are expressed as mean ± SEM from three independent experiments, each performed in quadruplicate to sextuplicate.

6.2.5 Preparation of Micellar Solutions of Compounds

Triblock copolymers F127 (PL-F127) and poloxamer 388 (POL388) were purchased from BASF chemical company. Cremophor EL (CrEL) and Tween 60 (T60)

were obtained from Sigma-Aldrich. Micellar suspensions were prepared by mixing solutions containing 2-3 mM hybrids or MB in CH_2Cl_2 with 500 mL of detergent solution (100 mg/mL) in dry CH_2Cl_2. An additional 2 mL of CH_2Cl_2 was added and the mixtures stirred and sonicated until a homogenous solution was obtained. The final detergent /compounds ratios were ~ 250:1. The solvent was then removed *in vacuo* and the resulting dry film redissolved in 1 mL of sterile PBS with agitation. The micellar suspensions were filtered through a 0.22 μm mixed-cellulose-ester (MCE) filter under sterile conditions.

6.2.6 Photodynamic Studies

Bacterial suspensions in PBS (10^8 cells/mL) were incubated with CrEL-formulated hybrids in PBS (1-20 μM) in the dark at room temperature for 30 min. The suspensions were centrifuged at 12,000 rpm and then washed twice with sterile PBS before being placed into wells of a 96-well microtiter plate (Fisher Scientific) and illuminated with light at room temperature. Fluences ranged from 0-20 J/cm^2 at 100 mW/cm^2. Contents of the wells were mixed before sampling, with aliquots being serially diluted 10-fold in PBS to give 10^{-1}-10^{-6}-fold dilutions. The diluted samples were streaked horizontally onto square BHI agar plates, as described by Jett *et al.*[235] Plates were incubated at 37 °C overnight and CFUs counted. The limit of detection in these experiments was 8 log units of killing.

6.2.7 Cell Uptake Studies

Bacterial suspensions (10^8 cells/mL) were incubated in PBS in the dark at room temperature for 30 min with hybrids at the same final concentrations (20 μM) used for

the photodynamic experiments. Incubations were carried out in triplicate. The cell suspensions were centrifuged (9000 rpm) and the supernatants aspirated. The cells were then washed twice with sterile PBS (1 mL) and centrifuged. Cell pellets were digested in 3 mL of sodium dodecyl sulfate (SDS) solution (10% in PBS) for at least 24 h or until homogenous solutions were obtained. Fluorescence of the extracts was measured using a spectrofluorometer (FluoroMax3; SPEX Industries, Edison, N.J.). The excitation wavelength for both MB and hybrids was 650 nm and the emission range was 655 to 720 nm. Calibration curves were prepared from samples of the pure hybrids and MB (dissolved at equivalent concentrations in SDS) and used for determination of hybrid concentrations in the cell extracts. Uptake values were obtained by dividing the number of nanomoles of PS in the extract by the number of CFUs obtained by serial dilution, with the number of PS molecules/cell then being calculated using Avogadro's number.

6.2.8 MIC Determinations with Ciprofloxacin

The pump inhibitory activities of hybrids and MB were determined by MIC measurements in sterile 96-well, black-sided plates using bioluminescence rather than traditional turbidity measurements. A bioluminescent *S. aureus* suspension (MRSA USA300, 100 µL containing 10^6 CFU/mL) was incubated at 37 °C for 15 h with vigorous shaking in the dark with 100 µL ciprofloxacin alone (dilution series from 0.001 to 1.024 µg/mL) and ciprofloxacin in the presence of 100 µL MB (20 µM) and 100 µL (10 µM) of hybrids **56**, **58** and **60**. The luminescence was monitored using a luminescence plate reader (MicroBeta Trilux 1450; PerkinElmer Life and Analytical

Sciences Inc., Wellesley, MA). MIC values were plotted from 3-4 independent experiments.

6.3 Murine MRSA Wound Infection Experiments

6.3.1 Photosensitizers, Light Source and Bacterial Species

Methylene blue (MB) was purchased from Sigma (UK). Stock solutions of MB and hybrid **58** were freshly prepared as Cremophor EL Micelles in sterile PBS (see Chapter 6.2.5 for details) to a final concentration of 200 μM. A noncoherent light source (LC122; LumaCare, London, UK) with interchangeable fibre bundles and 30 nm band-pass filters (652 ± 15 nm) was used for all experiments. Power output from the fibre bundle was 300 mW. The spot was positioned at a constant distance from the wound to give an irradiance of 100 mW over the 1 cm^2 wound area.

Bioluminescent MRSA (Xen 30)[230] was obtained from the Dai Lab (Wellman Center for Photomedicine). Cultures were prepared by growing overnight in brain heart infusion (BHI) at 37 °C with 100 rpm orbital shaking. Bacterial growth was assessed with an Evolution 300 UV/Vis Spectrophotometer (Thermo Scientific, Waltham, MA). Optical density (OD) at 600 nm of 0.8 corresponded to a bacterial cell density of 10^8 CFU/mL. Cells were washed and re-suspended in PBS and used at a density of 10^8 CFU/mL.

6.3.2 Animal Preparation and Infection

Six to eight week old adult female BALB/c mice (Charles River Laboratories, Wilmington, MA) weighing 17-21 g were used in the study. Animals were housed one per cage and maintained on a 12-hour light/dark cycle with *ad libitum* access to food

and water. All procedures were approved by the Subcommittee on Research Animal Care (IACUC) (Massachusetts General Hospital) and met guidelines of the US National Institutes of Health (NIH). Mice were administered cyclophosphamide at 4 days and 1 day prior to MRSA inoculation. The first dose was 150 mg/kg and the second dose 100 mg/kg (both injected i.p.). Cyclophosphamide reduces peripheral blood neutrophils to <100/μL blood, making mice more vulnerable to infection.[224]

Mice were anesthetized with i.p. injections of a ketamine/xylazine cocktail and their dorsal surfaces shaved. Skin abrasion wounds were introduced on the dorsal surfaces using a 28-gauge needle (Micro-Fine IV, Becton Dickinson, Franklin Lakes, NJ), creating 6 x 6 crossed scratch lines covering on area of 1 cm^2. The scratches were applied such that they damaged only the stratum corneum and upper-layer of the epidermis (i.e. not the dermis). Five minutes after wounding, a 40 μL aliquot was taken from a suspension containing 10^8 CFU/mL bioluminescent MRSA (Xen 30) in PBS and inoculated over the scratched areas using a micropipette.

6.3.3 Bioluminescence Imaging

A Hamamatsu Photonics KK (Bridgewater, NJ) bioluminescence imaging system was used in the study.[126b] The setup consisted of an intensified charge-coupled-device (ICCD), camera (C2400-30H; Hamamatsu), camera controller, imaging box, image processor (C5510-50; Hamamatsu) and a color monitor (PVM 1454Q; Hamamatsu). Light-emitting diodes were mounted inside the imaging box to supply light for dimensional imaging of the sample. This setup allowed a grayscale background image of each mouse to be captured. Using the photo-counting mode, clear images were obtained at very low-light levels through detection and integration of individual

photons. Luminescence emanating from bacteria was captured using an integration time of 2 min with a maximum setting on the image-intensifier control module.

ARGUS software (Hamamatsu) was used to present luminescence images as false-colour images superimposed on the grayscale background image. The software calculated total pixel values (relative luminescence units RLU) from the luminescence images of the infected wound areas. Wounds were observed daily and photographs captured using a Nikon Coolpix L20 camera until wounds had healed. Wound area analysis was performed using ImageJ software.

Prior to imaging, mice were anesthetized by i.p. injections of a ketamine/xylazine cocktail. The mice were placed on an adjustable stage in the specimen chamber and their infected areas positioned directly under the camera. A grayscale background image of each wound was taken followed by a photon count of the same region. This total wound photon count was obtained as relative luminescence units (RLUs) and displayed in a false-color scale ranging from pink (most intense) to blue (least intense).

6.3.4 Application of aPDT

Photosensitizers MB and **58** (40 µL of 200 µM stock solutions) were added to infection sites of animals in Groups B-E 30 minutes after bacterial inoculation. Fifteen minutes after addition of PS (time to allow compounds to bind/penetrate bacteria) the mice were again imaged to quantify any dark toxicity of the PS. Mice were illuminated with light from a non-coherent light source as described above, receiving total light doses of 120 J/cm^2 delivered in aliquots in periods of 2, 4, 8, 4 and 2 min for a total of

20 min. Bioluminescence imaging were captured after each light dose (12, 36, 84, 108 and 120 J/cm^2). Dark controls (animals receiving PS without light treatment) were assessed at the times corresponding to light delivery in the aPDT treatment groups. Control Group A received light and no PS, with images capture at the same time intervals as other groups.

References

(1) Xie, C.; Taylor, D. M.; Howden, B. P.; Charles, P. G. P. *Intern Med J* **2012**, *42*, e157.

(2) (a) O'Fallon, E.; Schreiber, R.; Kandel, R.; D'Agata, E. M. C. *Infect Control Hosp Epidemiol* **2009**, *30*, 1172. (b) Pop-Vicas, A.; Mitchell, S. L.; Kandel, R.; Schreiber, R.; D'Agata, E. M. C. *J Am Geriatr Soc* **2008**, *56*, 1276.

(3) WHO Geneva 2014; Vol. 2014.

(4) Dennis, B. a. V., Brian In *Washington Post*, 2013.

(5) CDC; CDC: Atlanta, 2013; Vol. 2013.

(6) (a) Roland, K. L.; Esther, C. R.; Spitznagel, J. K. *J Bacteriol* **1994**, *176*, 3589. (b) Boyle-Vavra, S.; Labischinski, H.; Ebert, C. C.; Ehlert, K.; Daum, R. S. *Antimicrob Agents Chemother* **2001**, *45*, 280.

(7) Crowe, S. A.; Dossing, L. N.; Beukes, N. J.; Bau, M.; Kruger, S. J.; Frei, R.; Canfield, D. E. *Nature* **2013**, *501*, 535.

(8) Gonzales, R. D.; Schreckenberger, P. C.; Graham, M. B.; Kelkar, S.; DenBesten, K.; Quinn, J. P. *The Lancet* **2001**, *357*, 1179.

(9) David N. Gilbert, R. J. G., Helen W. Boucher, Geroge H. Talbot, Brad Spellberg, John E. Edwards Jr, W. Michael Scheld, John S. Bradley and John G. Bartlett *Clin Infect Dis* **2010**, *50*, 1081.

(10) Bockstael, K.; Van Aerschot, A. *Cent Eur J Med* **2009**, *4*, 141.

(11) Bush, K.; Jacoby, G. A. *Antimicrob Agents Chemother* **2010**, *54*, 969.

(12) Poole, K. *Cell Mol Life Sci* **2004**, *61*, 2200.

(13) Nordmann, P.; Dortet, L.; Poirel, L. *Trends Mol Med* **2012**, *18*, 263.

(14) Bugg, T. D. H.; Wright, G. D.; Dutka-Malen, S.; Arthur, M.; Courvalin, P.; Walsh, C. T. *Biochemistry* **1991**, *30*, 10408.

(15) McMurry, L.; Petrucci, R. E., Jr.; Levy, S. B. *Proc Natl Acad Sci USA* **1980**, *77*, 3974.

(16) Van Bambeke, F.; Balzi, E.; Tulkens, P. M. *Biochem Pharmacol* **2000**, *60*, 457.

(17) Lomovskaya, O.; Watkins, W. J. *Curr Med Chem* **2001**, *8*, 1699.

(18) Ren, Q.; Paulsen, I. T. *PLoS Comput Biol* **2005**, *1*, 19.

(19) Singh, M.; Jadaun, G. P. S.; Ramdas; Srivastava, K.; Chauhan, V.; Mishra, R.; Gupta, K.; Nair, S.; Chauhan, D. S.; Sharma, V. D.; Venkatesan, K.; Katoch, V. M. *Indian J Med Res* **2011**, *133*, 535.

(20) Nikaido, H. *Clin Infect Dis* **1998**, *27*, S32.

(21) Piddock, L. J. V. *Clin Microbiol Rev* **2006**, *19*, 382.

(22) Eijkelkamp, B. A.; Hassan, K. A.; Paulsen, I. T.; Brown, M. H. *Microbial Efflux Pumps: Current Research*; Caister Academic Press, 2013.

(23) Tegos, G. P.; Haynes, M.; Strouse, J. J.; Khan, M. M. T.; Bologa, C. G.; Oprea, T. I.; Sklar, L. A. *Curr Pharm Des* **2011**, *17*, 1291.

(24) McAleese, F., Petersen, P, Ruzin, A, Dunman, PM, Murphy, E, Projan, SJ, Bradford, PA. *Antimicrob Agents Chemother* **2005**, *49*, 1865.

(25) Narui, K., Noguchi, N, Wakasugi, K, Sasatsu, M. *Biol Pharm Bull* **2002**, *25*, 1533.

(26) (a) Brown, M., Skurray, RA. *J Mol Microbiol Biotechnol* **2001**, *3*, 163. (b) Xu, Z., O'Rourke, BA, Skurray, RA, Brown, MH. *J Biol Chem* **2006**, *281*, 792.

(27) Jin, J., Guffanti, AA, Bechhofer, DH, Krulwich, TA. *J Bacteriol* **2002**, *184*, 4722.

(28) (a) Lewis, K. *J Mol Microbiol Biotechnol* **2001**, *3*, 247. (b) Tegos, G., Stermitz, F.R., Lomovskaya, O., Lewis, K. *Antimicrob Agents Chemother* **2002**, *46*, 3133.

(29) De Marco, C. E.; Cushing, L. A.; Frempong-Manso, E.; Seo, S. M.; Jaravaza, T. A. A.; Kaatz, G. W. *Antimicrob Agents Chemother* **2007**, *51*, 3235.

(30) Dawson, R. J. P.; Locher, K. P. *Nature* **2006**, *443*, 180.
(31) (a) Neyfakh, A. A. *Antimicrob Agents Chemother* **1992**, *36*, 484. (b) Neyfakh, A. A.; Borsch, C. M.; Kaatz, G. W. *Antimicrob Agents Chemother* **1993**, *37*, 128. (c) Kaatz, G. W.; Seo, S. M.; Ruble, C. A. *Antimicrob Agents Chemother* **1993**, *37*, 1086. (d) Ng, E. Y. W.; Trucksis, M.; Hooper, D. C. *Antimicrob Agents Chemother* **1994**, *38*, 1345.
(32) Jonas, B. M.; Murray, B. E.; Weinstock, G. M. *Antimicrob Agents Chemother* **2001**, *45*, 3574.
(33) (a) Kumar, S.; Varela, M. F. *Int J Mol Sci* **2012**, *13*, 4484. (b) Singh, K. V.; Malathum, K.; Murray, B. E. *Antimicrob Agents Chemother* **2001**, *45*, 263.
(34) Gill, M. J.; Brenwald, N. P.; Wise, R. *Antimicrob Agents Chemother* **1999**, *43*, 187.
(35) Piddock, L. J. V.; Johnson, M. M.; Simjee, S.; Pumbwe, L. *Antimicrob Agents Chemother* **2002**, *46*, 808.
(36) Ambrose, K. D.; Nisbet, R.; Stephens, D. S. *Antimicrob Agents Chemother* **2005**, *49*, 4203.
(37) (a) Lomovskaya, O.; Zgurskaya, H. I.; Bostian, K. A.; Lewis, K. *Bacterial Resistance to Antimicrobials (2nd Edition)*; CRC Press LLC, 2008. (b) Tseng, T.-T.; Gratwick, K. S.; Kollman, J.; Park, D.; Nies, D. H.; Goffeau, A.; Saier, M. H., Jr. *J Mol Microbiol Biotechnol* **1999**, *1*, 107.
(38) (a) Cuthbertson, L.; Mainprize, I. L.; Naismith, J. H.; Whitfield, C. *Microbiol Mol Biol Rev* **2009**, *73*, 155. (b) Higgins, M. K.; Bokma, E.; Koronakis, E.; Hughes, C.; Koronakis, V. *Proc Nati Acad Sci USA* **2004**, *101*, 9994.
(39) Gotoh, N.; Tsujimoto, H.; Tsuda, M.; Okamoto, K.; Nomura, A.; Wada, T.; Nakahashi, M.; Nishino, T. *Antimicrob Agents Chemother* **1998**, *42*, 1938.
(40) Poole, K.; Srikumar, R. *Curr Top Med Chem (Hilversum Neth)* **2001**, *1*, 59.
(41) Poole, K. *Front Microbiol* **2011**, *2*, 65.
(42) (a) Ma, D.; Cook, D. N.; Alberti, M.; Pon, N. G.; Nikaido, H.; Hearst, J. E. *Mol Microbiol* **1995**, *16*, 45. (b) Pan, W.; Spratt, B. G. *Mol Microbiol* **1994**, *11*, 769.
(43) Adewoye, L.; Sutherland, A.; Srikumar, R.; Poole, K. *J Bacteriol* **2002**, *184*, 4308.
(44) Poole, K. *J Mol Microbiol Biotechnol* **2001**, *3*, 255.
(45) Aendekerk, S.; Diggle, S. P.; Song, Z.; Hoiby, N.; Cornelis, P.; Williams, P.; Camara, M. *Microbiology (Reading, U. K.)* **2005**, *151*, 1113.
(46) Symmons, M. F.; Bokma, E.; Koronakis, E.; Hughes, C.; Koronakis, V. *Proc Natl Acad Sci USA* **2009**, *106*, 7173.
(47) (a) Nikaido, H. *Curr Opin Microbiol* **1998**, *1*, 516. (b) Nikaido, H., Zgurskaya HI. *Curr Opin Infect Dis* **1999**, *12*, 529.
(48) (a) Mazzariol, A.; Tokue, Y.; Kanegawa, T. M.; Cornaglia, G.; Nikaido, H. *Antimicrob Agents Chemother* **2000**, *44*, 3441. (b) Oethinger, M.; Kern, W. V.; Jellen-Ritter, A. S.; McMurry, L. M.; Levy, S. B. *Antimicrob Agents Chemother* **2000**, *44*, 10. (c) Webber, M. A.; Piddock, L. J. V. *Antimicrob Agents Chemother* **2001**, *45*, 1550.
(49) (a) Yu, E., McDermott, G, Zgurskaya, HI, Nikaido, H, Koshland, DE Jr. *Science* **2003**, *300*, 976. (b) Fernandes, P.; Ferreira, B. S.; Cabral, J. M. S. *Int J Antimicrob Agents* **2003**, *22*, 211.
(50) Ziha-Zarifi, I.; Llanes, C.; Kohler, T.; Pechere, J.-C.; Plesiat, P. *Antimicrob Agents Chemother* **1999**, *43*, 287.
(51) Eaves, D. J.; Ricci, V.; Piddock, L. J. *Antimicrob Agents Chemother* **2004**, *48*, 1145.
(52) (a) Baucheron, S.; Tyler, S.; Boyd, D.; Mulvey, M. R.; Chaslus-Dancla, E.; Cloeckaert, A. *Antimicrob Agents Chemother* **2004**, *48*, 3729. (b) Giraud, E.; Cloeckaert, A.; Kerboeuf, D.; Chaslus-Dancla, E. *Antimicrob Agents Chemother* **2000**, *44*, 1223. (c) Piddock, L. J.

V.; White, D. G.; Gensberg, K.; Pumbwe, L.; Griggs, D. J. *Antimicrob Agents Chemother* **2000**, *44*, 3118. (d) Nishino, K.; Latifi, T.; Groisman, E. A. *Mol Microbiol* **2006**, *59*, 126.

(53) (a) Lin, J.; Sahin, O.; Michel, L. O.; Zhang, Q. *Infect Immun* **2003**, *71*, 4250. (b) Pumbwe, L.; Randall, L. P.; Woodward, M. J.; Piddock, L. J. V. *Antimicrob Agents Chemother* **2005**, *49*, 1289.

(54) Pumbwe, L.; Randall, L. P.; Woodward, M. J.; Piddock, L. J. V. *J Antimicrob Chemother* **2004**, *54*, 341.

(55) (a) Dowson, C. G.; Jephcott, A. E.; Gough, K. R.; Spratt, B. G. *Mol Microbiol* **1989**, *3*, 35. (b) Spratt, B. G. *Nature* **1988**, *332*, 173.

(56) (a) Delahay, R. M.; Robertson, B. D.; Balthazar, J. T.; Shafer, W. M.; Ison, C. A. *Microbiology* **1997**, *143*, 2127. (b) Hagman, K. E.; Lucas, C. E.; Balthazar, J. T.; Snyder, L.; Nilles, M.; Judd, R. C.; Shafer, W. M. *Microbiology* **1997**, *143*, 2117.

(57) Veal, W. L.; Nicholas, R. A.; Shafer, W. M. *J Bacteriol* **2002**, *184*, 5619.

(58) Plorde, K. R. C. G. R. N. A. W. L. D. J. *Sherris Medical Microbiology*; McGraw Hill: New York, 2004.

(59) Oethinger, M. O., B.; Levy, S. B.; ; Patent, U. S., Ed. U.S, **2004**.

(60) (a) Mahamoud, A.; Chevalier, J.; Alibert-Franco, S.; Kern, W. V.; Pagès, J.-M. *J Antimicrob Chemother* **2007**, *59*, 1223. (b) Van Bambeke, F. P., J.- M.; Lee, V. J In *Front Anti-Infect Drug Discovery*; Benthanm e books: Pakistan, **2010**; Vol. 1.

(61) González-Lamothe, R.; Mitchell, G.; Gattuso, M.; Diarra, M.; Malouin, F.; Bouarab, K. *Int J Mol Sci* **2009**, *10*, 3400.

(62) (a) Tegos, G. P.; Haynes, M.; Strouse, J. J.; Khan, M. M.; Bologa, C. G.; Oprea, T. I.; Sklar, L. A. *Curr Pharm Des* **2011**, *17*, 1291. (b) Bohnert, J. A.; Szymaniak-Vits, M.; Schuster, S.; Kern, W. V. *J Antimicrob Chemother* **2011**, *66*, 2057.

(63) Renau, T. E.; Léger, R.; Yen, R.; She, M. W.; Flamme, E. M.; Sangalang, J.; Gannon, C. L.; Chamberland, S.; Lomovskaya, O.; Lee, V. J. *Bioorg Med Chem Lett* **2002**, *12*, 763.

(64) Barrett, J. *Curr Opin Investig Drugs* **2001**, *2*, 212.

(65) (a) Pages, J. M.; Sandrine, A. F.; Mahamoud, A.; Bolla, J. M.; Davin-Regli, A.; Chevalier, J.; Garnotel, E. *Curr Top Med Chem* **2010**, *10*, 1848. (b) Pages, J. M.; Amaral, L. *Biochim Biophys Acta* **2009**, *5*, 826.

(66) (a) Seeger, M. A.; Diederichs, K.; Eicher, T.; Brandstatter, L.; Schiefner, A.; Verrey, F.; Pos, K. M. *Curr Drug Targets* **2008**, *9*, 729. (b) Renau, T. E.; Leger, R.; Flamme, E. M.; She, M. W.; Gannon, C. L.; Mathias, K. M.; Lomovskaya, O.; Chamberland, S.; Lee, V. J.; Ohta, T.; Nakayama, K.; Ishida, Y. *Bioorg Med Chem Lett* **2001**, *11*, 663.

(67) Lomovskaya, O.; Bostian, K. A. *Biochem Pharmacol* **2006**, *71*, 910.

(68) (a) Matsumoto, Y.; Hayama, K.; Sakakihara, S.; Nishino, K.; Noji, H.; Iino, R.; Yamaguchi, A. *PLoS One* **2011**, *6*, 0018547. (b) Askoura, M.; Mottawea, W.; Abujamel, T.; Taher, I. *Libyan J Med* **2011**, *13*.

(69) (a) Russo-Marie, F.; Roederer, M.; Sager, B.; Herzenberg, L. A.; Kaiser, D. *Proc Natl Acad Sci USA* **1993**, *90*, 8194. (b) Yang, N. C.; Hu, M. L. *Anal Biochem* **2004**, *325*, 337. (c) Fieldler, F.; Hinz, H. *Eur J Biochem* **1994**, *222*, 75.

(70) Matsumoto, Y., Hayama, K, Sakakihara, S, Nishino, K, Noji, H, Iino, R, Yamaguchi, A. *PLoS One* **2011**, *6*, e18547.

(71) (a) Nakayama, K.; Ishida, Y.; Ohtsuka, M.; Kawato, H.; Yoshida, K. I.; Yokomizo, Y.; Hosono, S.; Ohta, T.; Hoshino, K.; Ishida, H.; Yoshida, K.; Renau, T. E.; Léger, R.; Zhang, J. Z.; Lee, V. J.; Watkins, W. J. *Bioorg Med Chem Lett* **2003**, *13*, 4201. (b) Nakayama, K.; Ishida, Y.; Ohtsuka, M.; Kawato, H.; Yoshida, K. I.; Yokomizo, Y.; Ohta, T.; Hoshino, K.; Otani, T.; Kurosaka, Y.; Yoshida, K.; Ishida, H.; Lee, V. J.; Renau, T. E.; Watkins, W. J. *Bioorg Med Chem Lett* **2003**, *13*, 4205. (c) Nakayama, K.; Kawato, H.; Watanabe, J.;

Ohtsuka, M.; Yoshida, K. I.; Yokomizo, Y.; Sakamoto, A.; Kuru, N.; Ohta, T.; Hoshino, K.; Yoshida, K.; Ishida, H.; Cho, A.; Palme, M. H.; Zhang, J. Z.; Lee, V. J.; Watkins, W. J. *Bioorg Med Chem Lett* **2004**, *14*, 475. (d) Nakayama, K.; Kuru, N.; Ohtsuka, M.; Yokomizo, Y.; Sakamoto, A.; Kawato, H.; Yoshida, K. I.; Ohta, T.; Hoshino, K.; Akimoto, K.; Itoh, J.; Ishida, H.; Cho, A.; Palme, M. H.; Zhang, J. Z.; Lee, V. J.; Watkins, W. J. *Bioorg Med Chem Lett* **2004**, *14*, 2493. (e) Yoshida, K.-i.; Nakayama, K.; Ohtsuka, M.; Kuru, N.; Yokomizo, Y.; Sakamoto, A.; Takemura, M.; Hoshino, K.; Kanda, H.; Nitanai, H.; Namba, K.; Yoshida, K.; Imamura, Y.; Zhang, J. Z.; Lee, V. J.; Watkins, W. J. *Bioorg Med Chem* **2007**, *15*, 7087.

(72) Nakashima, R., Sakurai, K, Yamasaki, S, Hayashi, K, Nagata, C, Hoshino, K, Onodera, Y, Nishino, K, Yamaguchi, A. *Nature* **2013**, *500*, 102.

(73) (a) Cherigo, L.; Pereda-Miranda, R.; Fragoso-Serrano, M.; Jacobo-Herrera, N.; Kaatz, G. W.; Gibbons, S. *J Nat Prod* **2008**, *71*, 1037. (b) Kumar, A.; Khan, I. A.; Koul, S.; Koul, J. L.; Taneja, S. C.; Ali, I.; Ali, F.; Sharma, S.; Mirza, Z. M.; Kumar, M.; Sangwan, P. L.; Gupta, P.; Thota, N.; Qazi, G. N. *J Antimicrob Chemother* **2008**, *61*, 1270. (c) Timmer, A.; Gunther, J.; Rucker, G.; Motschall, E.; Antes, G.; Kern, W. V. *Cochrane Database Syst Rev* **2008**, *16*.

(74) Jankun, J.; Selman, S. H.; Swiercz, R.; Skrzypczak-Jankun, E. *Nature* **1997**, *387*, 561.

(75) Sudano Roccaro, A.; Blanco, A. R.; Giuliano, F.; Rusciano, D.; Enea, V. *Antimicrob Agents Chemother* **2004**, *48*, 1968.

(76) Kurincic, M.; Klancnik, A.; Smole Mozina, S. *Microb Drug Resist* **2012**, *18*, 492.

(77) Parthasarathy, M. R.; Ranganathan, K. R.; Sharma, D. K. *Phytochemistry* **1979**, *18*, 506.

(78) (a) Stermitz, F. R.; Tawara-Matsuda, J.; Lorenz, P.; Mueller, P.; Zenewicz, L.; Lewis, K. *J Nat Prod* **2000**, *63*, 1146. (b) Park, J. H.; Hur, H. J.; Woo, J. S.; Lee, H. J. *Eur J Pharm Sci* **2012**, *45*, 296.

(79) Kang, H. K.; Kim, H. Y.; Cha, J. D. *Biotechnol J* **2011**, *6*, 1397.

(80) Poisson, J.; LE HIR, A.; GOUTAREL, R.; JANOT, M. M. *[Isolation of reserpine from roots of Rauwolfia vomitoria Afz.]*, 1954.

(81) Juranka, P. F.; Zastawny, R. L.; Ling, V. *Faseb J* **1989**, *3*, 2583.

(82) Neyfakh, A. A.; Bidnenko, V. E.; Chen, L. B. *Proc Natl Acad Sci USA* **1991**, *88*, 4781.

(83) Kaatz, G. W.; Seo, S. M. *Antimicrob Agents Chemother* **1995**, *39*, 2650.

(84) Schmitz, F. J.; Fluit, A. C.; Luckefahr, M.; Engler, B.; Hofmann, B.; Verhoef, J.; Heinz, H. P.; Hadding, U.; Jones, M. E. *J Antimicrob Chemother* **1998**, *42*, 807.

(85) (a) Brenwald, N. P.; Gill, M. J.; Wise, R. *J Antimicrob Chemother* **1997**, *40*, 458. (b) Markham, P. N. *Antimicrob Agents Chemother* **1999**, *43*, 988.

(86) Pages, J. M.; Masi, M.; Barbe, J. *Trends Mol Med* **2005**, *11*, 382.

(87) (a) Kriengkauykiat, J.; Porter, E.; Lomovskaya, O.; Wong-Beringer, A. *Antimicrob Agents Chemother* **2005**, *49*, 565. (b) Beyer, R.; Pestova, E.; Millichap, J. J.; Stosor, V.; Noskin, G. A.; Peterson, L. R. *Antimicrob Agents Chemother* **2000**, *44*, 798. (c) Piddock, L. J.; Johnson, M.; Ricci, V.; Hill, S. L. *Antimicrob Agents Chemother* **1998**, *42*, 2956. (d) Brenwald, N. P.; Gill, M. J.; Wise, R. *Antimicrob Agents Chemother* **1998**, *42*, 2032.

(88) Belofsky, G.; Percivill, D.; Lewis, K.; Tegos, G. P.; Ekart, J. *J Nat Prod* **2004**, *67*, 481.

(89) Lechner, D.; Gibbons, S.; Bucar, F. *J Antimicrob Chemother* **2008**, *62*, 345.

(90) Belofsky, G.; Percivill, D.; Lewis, K.; Tegos, G. P.; Ekart, J. *J Nat Prod* **2004**, *67*, 481.

(91) Aeschlimann, J. R.; Dresser, L. D.; Kaatz, G. W.; Rybak, M. J. *Antimicrob Agents Chemother* **1999**, *43*, 335.

(92) Aeschlimann, J. R.; Kaatz, G. W.; Rybak, M. J. *J Antimicrob Chemother* **1999**, *44*, 343.

(93) (a) Mullin, S.; Mani, N.; Grossman, T. H. *Antimicrob Agents Chemother* **2004**, *48*, 4171. (b) Germann, U. A.; Ford, P. J.; Shlyakhter, D.; Mason, V. S.; Harding, M. W. *Anticancer Drugs* **1997**, *8*, 141.
(94) Germann, U. A.; Shlyakhter, D.; Mason, V. S.; Zelle, R. E.; Duffy, J. P.; Galullo, V.; Armistead, D. M.; Saunders, J. O.; Boger, J.; Harding, M. W. *Anticancer Drugs* **1997**, *8*, 125.
(95) Leitner, I.; Nemeth, J.; Feurstein, T.; Abrahim, A.; Matzneller, P.; Lagler, H.; Erker, T.; Langer, O.; Zeitlinger, M. *J Antimicrob Chemother* **2011**, *66*, 834.
(96) Gibbons, S.; Oluwatuyi, M.; Kaatz, G. W. *J Antimicrob Chemother* **2003**, *51*, 13.
(97) Fox, E.; Bates, S. E. *Expert Rev Anticancer Ther* **2007**, *7*, 447.
(98) Markham, P. N.; Westhaus, E.; Klyachko, K.; Johnson, M. E.; Neyfakh, A. A. *Antimicrob Agents Chemother* **1999**, *43*, 2404.
(99) (a) Tegos, G. P.; Masago, K.; Aziz, F.; Higginbotham, A.; Stermitz, F. R.; Hamblin, M. R. *Antimicrob Agents Chemother* **2008**, *52*, 3202. (b) Ambrus, J. I.; Kelso, M. J.; Bremner, J. B.; Ball, A. R.; Casadei, G.; Lewis, K. *Bioorg Med Chem Lett* **2008**, *18*, 4294. (c) Bremner, J. B.; Kelso, M. J. *Synth Commun* **2010**, *40*, 3561. (d) Samosorn, S.; Tanwirat, B.; Muhamad, N.; Casadei, G.; Tomkiewicz, D.; Lewis, K.; Suksamrarn, A.; Prammananan, T.; Gornall, K. C.; Beck, J. L.; Bremner, J. B. *Bioorg Med Chem* **2009**, *17*, 3866. (e) Tomkiewicz, D.; Casadei, G.; Larkins-Ford, J.; Moy, T. I.; Garner, J.; Bremner, J. B.; Ausubel, F. M.; Lewis, K.; Kelso, M. J. *Antimicrob Agents Chemother* **2010**, *54*, 3219.
(100) Markham, P. N.; Mulhearn, D. C.; Neyfakh, A. A.; Crich, D.; Jaber, M.-R.; Johnson, M. E.; Influx, Inc., USA . 2000.
(101) Fournier dit Chabert, J.; Marquez, B.; Neville, L.; Joucla, L.; Broussous, S.; Bouhours, P.; David, E.; Pellet-Rostaing, S.; Marquet, B.; Moreau, N.; Lemaire, M. *Bioorg Med Chem* **2007**, *15*, 4482.
(102) Samosorn, S.; Bremner, J. B.; Ball, A.; Lewis, K. *Bioorg Med Chem* **2006**, *14*, 857.
(103) Ambrus, J. I.; Kelso, M. J.; Bremner, J. B.; Ball, A. R.; Casadei, G.; Lewis, K. *Bioorg Med Chem Lett* **2008**, *18*, 4294.
(104) Stermitz, F. R.; Scriven, L. N.; Tegos, G.; Lewis, K. *Planta Med* **2002**, *68*, 1140.
(105) Morel, C.; Stermitz, F. R.; Tegos, G.; Lewis, K. *J Agric Food Chem* **2003**, *51*, 5677.
(106) (a) Renau, T. E.; Leger, R.; Filonova, L.; Flamme, E. M.; Wang, M.; Yen, R.; Madsen, D.; Griffith, D.; Chamberland, S.; Dudley, M. N.; Lee, V. J.; Lomovskaya, O.; Watkins, W. J.; Ohta, T.; Nakayama, K.; Ishida, Y. *Bioorg Med Chem Lett* **2003**, *13*, 2755. (b) Kaatz, G. W.; Seo, S. M.; O'Brien, L.; Wahiduzzaman, M.; Foster, T. J. *Antimicrob Agents Chemother* **2000**, *44*, 1404.
(107) Tegos, G.; Stermitz, F. R.; Lomovskaya, O.; Lewis, K. *Antimicrob Agents Chemother* **2002**, *46*, 3133.
(108) German, N.; Wei, P.; Kaatz, G. W.; Kerns, R. J. *Eur J Med Chem* **2008**, *43*, 2453.
(109) (a) Triesscheijn, M.; Baas, P.; Schellens, J. H.; Stewart, F. A. *Oncologist* **2006**, *11*, 1034. (b) Luksiene, Z. *Medicina* **2003**, *39*, 1137.
(110) (a) Musser, D. A.; Wagner, J. M.; Weber, F. J.; Datta-Gupta, N. *Res Commun Chem Pathol Pharmacol* **1980**, *28*, 505. (b) Dvorak, H. F.; Orenstein, N. S.; Carvalho, A. C.; Churchill, W. H.; Dvorak, A. M.; Galli, S. J.; Feder, J.; Bitzer, A. M.; Rypysc, J.; Giovinco, P. *J Immunol* **1979**, *122*, 166.
(111) (a) Dvorak, H. F.; Dvorak, A. M.; Manseau, E. J.; Wiberg, L.; Churchill, W. H. *J Natl Cancer Inst* **1979**, *62*, 1459. (b) Freitas, I. *J Photochem Photobiol B* **1990**, *7*, 359.
(112) (a) Lipson, R. L.; Baldes, E. J.; Olsen, A. M. *J Thorac Cardiovasc Surg* **1961**, *42*, 623. (b) Schwartz S, A. K., Vermund H; Bull, U. M. M., Ed.; Uni Minnesota Med Bull: Minnesota, 1955; Vol. 27.

(113) Modell, J.; Schwartz, S. *Proc Soc Exp Biol Med* **1964**, *116*, 399.
(114) Dougherty, T. J.; Gomer, C. J.; Henderson, B. W.; Jori, G.; Kessel, D.; Korbelik, M.; Moan, J.; Peng, Q. *J Natl Cancer Inst* **1998**, *90*, 889.
(115) Dougherty, T. J. *J Clin Laser Med Surg* **1996**, *14*, 219.
(116) Pass, H. I. *J Natl Cancer Inst* **1993**, *85*, 443.
(117) (a) Hudson, R.; Carcenac, M.; Smith, K.; Madden, L.; Clarke, O. J.; Pelegrin, A.; Greenman, J.; Boyle, R. W. *Br J Cancer* **2005**, *92*, 1442. (b) Konan, Y. N.; Gurny, R.; Allemann, E. *J Photochem Photobiol B* **2002**, *66*, 89.
(118) Jori, G.; Fabris, C.; Soncin, M.; Ferro, S.; Coppellotti, O.; Dei, D.; Fantetti, L.; Chiti, G.; Roncucci, G. *Lasers Surg Med* **2006**, *38*, 468.
(119) (a) Meisel, P.; Kocher, T. *J Photochem Photobiol B* **2005**, *79*, 159. (b) Zeina, B.; Greenman, J.; Purcell, W. M.; Das, B. *Br J Dermatol* **2001**, *144*, 274.
(120) Cassell, G. H.; Mekalanos, J. *JAMA* **2001**, *285*, 601.
(121) Raab, O. *Z Biol* **1900**, *39*, 524.
(122) Cope, Z. *Med Hist* **1958**, *2*, 163.
(123) Maisch, T. *Lasers Med Sci* **2007**, *22*, 83.
(124) (a) Wainwright, M. *J Antimicrob Chemother* **1998**, *42*, 13. (b) Wilson, M.; Yianni, C. *J Med Microbiol* **1995**, *42*, 62. (c) Tavares, A.; Carvalho, C. M.; Faustino, M. A.; Neves, M. G.; Tome, J. P.; Tome, A. C.; Cavaleiro, J. A.; Cunha, A.; Gomes, N. C.; Alves, E.; Almeida, A. *Mar Drugs* **2010**, *8*, 91.
(125) (a) Lounis, B.; Deich, J.; Rosell, F. I.; Boxer, S. G.; Moerner, W. E. *J Phy Chem B* **2001**, *105*, 5048. (b) Flors, C.; Fryer, M. J.; Waring, J.; Reeder, B.; Bechtold, U.; Mullineaux, P. M.; Nonell, S.; Wilson, M. T.; Baker, N. R. *J Exp Bot* **2006**, *57*, 1725. (c) Ragas, X.; Jimenez-Banzo, A.; Sanchez-Garcia, D.; Batllori, X.; Nonell, S. *Chem Commun* **2009**, *28*, 2920.
(126) (a) Costa, L.; Tome, J. P.; Neves, M. G.; Tome, A. C.; Cavaleiro, J. A.; Faustino, M. A.; Cunha, A.; Gomes, N. C.; Almeida, A. *Antiviral Res* **2011**, *91*, 278. (b) Dai, T.; Tegos, G. P.; Zhiyentayev, T.; Mylonakis, E.; Hamblin, M. R. *Lasers Surg Med* **2010**, *42*, 38. (c) Luksiene, Z.; Zukauskas, A. *J Appl Microbiol* **2009**, *107*, 1415.
(127) Hamblin, M. R.; Hasan, T. *Photochem Photobiol Sci* **2004**, *3*, 436.
(128) Demidova, T. N.; Hamblin, M. R. *Antimicrob Agents Chemother* **2005**, *49*, 2329.
(129) Hamblin, M. R.; Hasan, T. *Photochem Photobiol Sci* **2004**, *3*, 436.
(130) Korytowski, W.; Bachowski, G. J.; Girotti, A. W. *Photochem Photobiol* **1992**, *56*, 1.
(131) Rineh, A.; Kelso, M. J.; Vatansever, F.; Tegos, G. P.; Hamblin, M. R. *Expert Rev Anti Infect Ther* **2014**, *12*, 131.
(132) Girotti, A. W. *Photochem Photobiol* **1990**, *51*, 497.
(133) (a) Bonnett, R. *Chem Soc Rev* **1995**, *24*, 19. (b) Wainwright, M. *Int J Antimicrob Agents* **2003**, *21*, 510.
(134) Pervaiz, S.; Olivo, M. *Clin Exp Pharmacol Physiol* **2006**, *33*, 551.
(135) (a) Zhang, Y.; Aslan, K.; Previte, M. J. R.; Geddes, C. D. *Proc Natl Acad Sci USA* **2008**, *105*, 1798. (b) Hideg, É. *Cent Eur J Biol* **2008**, *3*, 273.
(136) Taniguchi, S.; Suzuki, N.; Masuda, M.; Hisanaga, S.; Iwatsubo, T.; Goedert, M.; Hasegawa, M. *J Biol Chem* **2005**, *280*, 7614.
(137) (a) Wainwright, M. *Biotech Histochem* **2003**, *78*, 147. (b) Lambrecht, B.; Mohr, H.; Knuver-Hopf, J.; Schmitt, H. *Vox Sang* **1991**, *60*, 207. (c) Bachmann, B.; Knuver-Hopf, J.; Lambrecht, B.; Mohr, H. *J Med Virol* **1995**, *47*, 172. (d) Muller-Breitkreutz, K.; Mohr, H. *J Med Virol* **1998**, *56*, 239. (e) Mohr, H.; Bachmann, B.; Klein-Struckmeier, A.; Lambrecht, B. *Photochem Photobiol* **1997**, *65*, 441.

(138) Ragas, X.; Jimenez-Banzo, A.; Sanchez-Garcia, D.; Batllori, X.; Nonell, S. *Chem Commun* **2009**, 2920.
(139) (a) Kiesslich, T.; Gollmer, A.; Maisch, T.; Berneburg, M.; Plaetzer, K. *Biomed Res Int* **2013**, *840417*, 16. (b) Moreira, L. M.; Romani, A. P.; Severino, D.; de Oliveira, H. P. M.; Lyon, J. P.; Rodrigues, M. R. *Phenotiazinium Dyes as Photosensitizers (PS) in Photodynamic Therapy (PDT): Spectroscopic Properties and Photochemical Mechanisms*; INTECH Open Access Publisher, 2012.
(140) (a) Perussi, J. R. *Química Nova* **2007**, *30*, 988. (b) Orth, K.; Ruck, A.; Beck, G.; Stanescu, A.; Beger, H. G. *Chirurg* **1995**, *66*, 1254. (c) Andreazza, N. L.; de Lourenco, C. C.; Siqueira, C. A. T.; Sawaya, A. C. H. F.; Lapinski, T. F.; Gasparetto, A.; Khouri, S.; Zamuner, S. R.; Munin, E.; Salvador, M. J. *Curr Drug Targets* **2013**, *14*, 1015. (d) Barbosa, A. F. S.; Sangiorgi, B. B.; Galdino, S. L.; Pitta, I. R.; Barral Netto, M.; Correia, N. A.; Pinheiro, A. L. B. *Proc SPIE* **2012**, *8211*, 82110N/1. (e) Nagata, J. Y.; Hioka, N.; Kimura, E.; Batistela, V. R.; Terada, R. S. S.; Graciano, A. X.; Baesso, M. L.; Hayacibara, M. F. *Photodiagn Photodyn Ther* **2012**, *9*, 122.
(141) (a) Floyd, R. A.; Schneider, J. E., Jr.; Dittmer, D. P. *Antiviral Res* **2004**, *61*, 141. (b) Wainwright, M. *Int J Antimicrob Agents* **2000**, *16*, 381.
(142) (a) Harris, F.; Chatfield, L. K.; Phoenix, D. A. *Curr Drug Targets* **2005**, *6*, 615. (b) Biel, M. A.; Pedigo, L.; Gibbs, A.; Loebel, N. *Int Forum Allergy Rhinol* **2013**, *3*, 468. (c) Hasebe, A.; Ishikawa, I.; Shamsul, H. M.; Ohtani, M.; Segawa, T.; Saeki, A.; Tanizume, N.; Oouchi, M.; Okagami, Y.; Okano, T.; Shibata, K. *Photomed Laser Surg* **2013**, *31*, 125. (d) Biel, M. A.; Sievert, C.; Usacheva, M.; Teichert, M.; Balcom, J. *Int Forum Allergy Rhinol* **2011**, *1*, 329. (e) Taraszkiewicz, A.; Fila, G.; Grinholc, M.; Nakonieczna, J. *Biomed Res Int* **2013**, *150653*, 23.
(143) Wainwright, M.; Phoenix, D. A.; Gaskell, M.; Marshall, B. *J Antimicrob Chemother* **1999**, *44*, 823.
(144) Demidova, T. N.; Hamblin, M. R. *Int J Immunopathol Pharmacol* **2004**, *17*, 245.
(145) Martin, J. P.; Logsdon, N. *Arch Biochem Biophys* **1987**, *256*, 39.
(146) (a) Wainwright, M. *Anticancer Agents Med Chem* **2008**, *8*, 280. (b) Tardivo, J. P.; Del Giglio, A.; de Oliveira, C. S.; Gabrielli, D. S.; Junqueira, H. C.; Tada, D. B.; Severino, D.; de Fatima Turchiello, R.; Baptista, M. S. *Photodiagn Photodyn Ther* **2005**, *2*, 175. (c) Junqueira, H. C.; Severino, D.; Dias, L. G.; Gugliotti, M. S.; Baptista, M. S. *Phys Chem Chem Phys* **2002**, *4*, 2320. (d) Severino, D.; Junqueira, H. C.; Gugliotti, M.; Gabrielli, D. S.; Baptista, M. S. *Photochem Photobiol* **2003**, *77*, 459. (e) Impert, O.; Katafias, A.; Kita, P.; Mills, A.; Pietkiewicz-Graczyk, A.; Wrzeszcz, G. *Dalton Trans* **2003**, 348. (f) Ehrhardt, K.; Davioud-Charvet, E.; Ke, H.; Vaidya, A. B.; Lanzer, M.; Deponte, M. *Antimicrob Agents Chemother* **2013**, *57*, 2114.
(147) (a) Bergmann, K.; O'Konski, C. T. *J Phys Chem* **1963**, *67*, 2169. (b) Lee, C.; Sung, Y. W.; Park, J. W. *J Phys Chem B* **1999**, *103*, 893.
(148) Severino, D.; Junqueira, H. C.; Gugliotti, M.; Gabrielli, D. S.; Baptista, M. S. *Photochem Photobiol* **2003**, *77*, 459.
(149) (a) Bonneau, R.; Pottier, R.; Bagno, O.; Joussot-Dubien, J. *Photochem Photobiol* **1975**, *21*, 159. (b) Havelcová, M.; Kubát, P.; Němcová, I. *Dyes Pigments* **1999**, *44*, 49.
(150) Kandela r, K.; Bartlett, J. A.; Indig, G. L. *Photochem Photobiol Sci* **2002**, *1*, 309.
(151) Bunting, J. R. *Photochem Photobiol* **1992**, *55*, 81.
(152) (a) Petrat, F.; Pindiur, S.; Kirsch, M.; de Groot, H. *J Biol Chem* **2003**, *278*, 3298. (b) Petrat, F.; Pindiur, S.; Kirsch, M.; de Groot, H. *Arch Biochem Biophys* **2003**, *412*, 207.
(153) Yu, D. S.; Chang, S. Y.; Ma, C. P. *J Urol* **1993**, *149*, 1198.
(154) Tegos, G. P.; Hamblin, M. R. *Antimicrob Agents Chemother* **2006**, *50*, 196.

(155) Lewis, K.; Ausubel, F. M. *Nat Biotech* **2006**, *24*, 1504.
(156) Boberek, J. M.; Stach, J.; Good, L. *PLoS One* **2010**, *5*, e13745.
(157) (a) Hsieh, P. C.; Siegel, S. A.; Rogers, B.; Davis, D.; Lewis, K. *Proc Natl Acad Sci USA* **1998**, *95*, 6602. (b) Lewis, K. *Curr Biol* **1999**, *9*, R403.
(158) Stermitz, F. R.; Lorenz, P.; Tawara, J. N.; Zenewicz, L. A.; Lewis, K. *Proc Natl Acad Sci USA* **2000**, *97*, 1433.
(159) Lynch, A. S. *Biochem Pharmacol* **2006**, *71*, 949.
(160) (a) Ball, A. R.; Casadei, G.; Samosorn, S.; Bremner, J. B.; Ausubel, F. M.; Moy, T. I.; Lewis, K. *ACS Chem Biol* **2006**, *1*, 594. (b) Charifson, P. S.; Grillot, A. L.; Grossman, T. H.; Parsons, J. D.; Badia, M.; Bellon, S.; Deininger, D. D.; Drumm, J. E.; Gross, C. H.; LeTiran, A.; Liao, Y.; Mani, N.; Nicolau, D. P.; Perola, E.; Ronkin, S.; Shannon, D.; Swenson, L. L.; Tang, Q.; Tessier, P. R.; Tian, S. K.; Trudeau, M.; Wang, T.; Wei, Y.; Zhang, H.; Stamos, D. *J Med Chem* **2008**, *51*, 5243.
(161) Bremner, J. B.; Ambrus, J. I.; Samosorn, S. *Curr Med Chem* **2007**, *14*, 1459.
(162) Ball, A. R.; Casadei, G.; Samosorn, S.; Bremner, J. B.; Ausubel, F. M.; Moy, T. I.; Lewis, K. *ACS Chem Biol* **2006**, *1*, 594.
(163) Strekowski, L.; Hou, D. F.; Wydra, R. L.; Schinazi, R. F. *J Heterocycl Chem* **1993**, *30*, 1693.
(164) New, O. M.; Dolphin, D. *Eur J Org Chem* **2009**, *2009*, 2675.
(165) Negi, A. S.; Chattopadhyay, S. K.; Srivastava, S.; Bhattacharya, A. K.; Council of Scientific and Industrial Research, India . 2006.
(166) Appel, R. *Angew Chem Int Ed* **1975**, *14*, 801.
(167) Schafer, M.; Schmitz, C.; Facius, R.; Horneck, G.; Milow, B.; Funken, K. H.; Ortner, J. *Photochem Photobiol* **2000**, *71*, 514.
(168) Bremner, J. B.; Kelso, M. J. *Synth Commun* **2010**, *40*, 3561.
(169) (a) Shafiee, A.; Rineh, A.; Kebriaeezadeh, A.; Foroumadi, A.; Sheibani, V.; Afarinesh, M. R. *Med Chem Res* **2009**, *18*, 758. (b) Rineh, A.; Mahmoodi, N.; Abdollahi, M.; Foroumadi, A.; Sorkhi, M.; Shafiee, A. *Arch Pharm (Weinheim Ger)* **2007**, *340*, 409.
(170) (a) Lu, Y.-T.; Arai, C.; Ge, J.-F.; Ren, W.-S.; Kaiser, M.; Wittlin, S.; Brun, R.; Lu, J.-M.; Ihara, M. *Dyes Pigments* **2011**, *89*, 44. (b) Jahnchen, J.; Purwanto, M. G.; Weisz, K. *Biopolymers* **2005**, *79*, 335. (c) Mark, W.; Katie, M.; Ciara, L.; M, G. R. *Dyes Pigments* **2009**, *82*, 387. (d) Wainwright, M.; Giddens, R. M. *Dyes Pigments* **2003**, *57*, 245. (e) Raj, M. M.; Dharmaraja, A.; Kavitha, S. J.; Panchanatheswaran, K.; Lynch, D. E. *Inorganica Chimica Acta* **2007**, *360*, 1799.
(171) Redmond, R. W.; Gamlin, J. N. *Photochem Photobiol* **1999**, *70*, 391.
(172) Frimberger, A. E.; Moore, A. S.; Cincotta, L.; Cotter, S. M.; Foley, J. W. *Clin Cancer Res* **1998**, *4*, 2207.
(173) Wainwright, M.; Mohr, H.; Walker, W. H. *J Photochem Photobiol B* **2007**, *86*, 45.
(174) Cincotta, L.; Foley, J. W.; Cincotta, A. H. *Photochem Photobiol* **1987**, *46*, 751.
(175) Price, M.; Reiners, J. J.; Santiago, A. M.; Kessel, D. *Photochem Photobiol* **2009**, *85*, 1177.
(176) Forkink, M.; Smeitink, J. A. M.; Brock, R.; Willems, P. H. G. M.; Koopman, W. J. H. *Biochimica et Biophysica Acta (BBA) - Bioenergetics* **2010**, *1797*, 1034.
(177) Setsukinai, K.; Urano, Y.; Kakinuma, K.; Majima, H. J.; Nagano, T. *J Biol Chem* **2003**, *278*, 3170.
(178) (a) Ogilby, P. R.; Foote, C. S. *J Am Chem Soc* **1981**, *103*, 1219. (b) Lindig, B. A.; Rodgers, M. A. J.; Schaap, A. P. *J Am Chem Soc* **1980**, *102*, 5590.
(179) Merkel, P. B.; Kearns, D. R. *J Am Chem Soc* **1972**, *94*, 1029.

(180) Zhao, F. K.; Chuang, L. F.; Israel, M.; Chuang, R. Y. *Biochem Biophys Res Commun* **1989**, *159*, 1359.
(181) Sparreboom, A.; Loos, W. J.; Verweij, J.; de Vos, A. I.; van der Burg, M. E.; Stoter, G.; Nooter, K. *Anal Biochem* **1998**, *255*, 171.
(182) Diep, B. A.; Gill, S. R.; Chang, R. F.; Phan, T. H.; Chen, J. H.; Davidson, M. G.; Lin, F.; Lin, J.; Carleton, H. A.; Mongodin, E. F.; Sensabaugh, G. F.; Perdreau-Remington, F. *Lancet* **2006**, *367*, 731.
(183) Moran, G. J.; Krishnadasan, A.; Gorwitz, R. J.; Fosheim, G. E.; McDougal, L. K.; Carey, R. B.; Talan, D. A. *N Engl J Med* **2006**, *355*, 666.
(184) Seybold, U.; Kourbatova, E. V.; Johnson, J. G.; Halvosa, S. J.; Wang, Y. F.; King, M. D.; Ray, S. M.; Blumberg, H. M. *Clin Infect Dis* **2006**, *42*, 647.
(185) Kaatz, G. W.; Moudgal, V. V.; Seo, S. M. *J Antimicrob Chemother* **2002**, *50*, 833.
(186) Minegishi, Y.; Saito, M.; Nagasawa, M.; Takada, H.; Hara, T.; Tsuchiya, S.; Agematsu, K.; Yamada, M.; Kawamura, N.; Ariga, T.; Tsuge, I.; Karasuyama, H. *J Exp Med* **2009**, *206*, 1291.
(187) Ogston, A. *J Anato Physio* **1882**, *17*, 24.
(188) Kluytmans, J.; van Belkum, A.; Verbrugh, H. *Clin Microbiol Rev* **1997**, *10*, 505.
(189) Alekshun, M. N.; Levy, S. B. *Biochem Pharmacol* **2006**, *71*, 893.
(190) Wertheim, H. F.; Melles, D. C.; Vos, M. C.; van Leeuwen, W.; van Belkum, A.; Verbrugh, H. A.; Nouwen, J. L. *Lancet Infect Dis* **2005**, *5*, 751.
(191) Dinges, M. M.; Orwin, P. M.; Schlievert, P. M. *Clin Microbiol Rev* **2000**, *13*, 16.
(192) Travis, J.; Potempa, J.; Maeda, H. *Trends Microbiol* **1995**, *3*, 405.
(193) Miedzobrodzki, J.; Kaszycki, P.; Bialecka, A.; Kasprowicz, A. *Eur J Clin Microbiol Infect Dis* **2002**, *21*, 269.
(194) Garcia-Lara, J.; Needham, A. J.; Foster, S. J. *FEMS Immunol Med Microbiol* **2005**, *43*, 311.
(195) Fournier, B.; Philpott, D. J. *Clin Microbiol Rev* **2005**, *18*, 521.
(196) Forsgren, A.; Sjoquist, J. *J Immunol* **1966**, *97*, 822.
(197) Naber, C. K. *Clin Infect Dis* **2009**, *48*, S231.
(198) (a) Deshpande, L. M.; Jones, R. N. *Clin Microbiol Infect* **2003**, *9*, 1120. (b) Casey, A. L.; Lambert, P. A.; Elliott, T. S. *Int J Antimicrob Agents* **2007**, *29*, S23.
(199) Moet, G. J.; Jones, R. N.; Biedenbach, D. J.; Stilwell, M. G.; Fritsche, T. R. *Diagn Microbiol Infect Dis* **2007**, *57*, 7.
(200) (a) Marton, J. P.; Jackel, J. L.; Carson, R. T.; Rothermel, C. D.; Friedman, M.; Menzin, J. *Curr Med Res Opin* **2008**, *24*, 2821. (b) Gould, I. M. *Lancet* **2006**, *368*, 824.
(201) Barber, M. *J Clin Pathol* **1961**, *14*, 385.
(202) Deresinski, S. *Clin Infect Dis* **2005**, *40*, 562.
(203) Jean, S. S.; Hsueh, P. R. *Int J Antimicrob Agents* **2011**, *37*, 291.
(204) Noskin, G. A.; Rubin, R. J.; Schentag, J. J.; Kluytmans, J.; Hedblom, E. C.; Smulders, M.; Lapetina, E.; Gemmen, E. *Arch Intern Med* **2005**, *165*, 1756.
(205) Johnson, A. P.; Pearson, A.; Duckworth, G. *J Antimicrob Chemother* **2005**, *56*, 455.
(206) (a) Ayliffe , C. M., Cookson BD *J Hosp Infect* **1998**, *39*, 253. (b) Ayliffe, G. *J Hosp Infect* **1995**, *31*, 245.
(207) Miller, L. G.; Diep, B. A. *Clin Infect Dis* **2008**, *46*, 752.
(208) (a) Gould, I. M. *Int J Antimicrob Agents* **2008**, *31*, 1. (b) Sakoulas, G.; Moellering Jr, R. C. *Clin Infect Dis* **2008**, *46*, S360.
(209) Frazee, B. W.; Lynn, J.; Charlebois, E. D.; Lambert, L.; Lowery, D.; Perdreau-Remington, F. *Ann Emerg Med* **2005**, *45*, 311.

(210) Pérez Rodríguez, M. T. *Empirical hospital treatment regimes for skin and soft tissue infections. Clinical guidelines and real empirical practice*; Sociedade Galega de Medicina Interna (SOGAMI), 2014.
(211) Watkins, R. R.; Lemonovich, T. L.; File, T. M. *Core Evid* **2012**, *7*, 131.
(212) Osburne, M. S.; Murphy, C. K.; Rothstein, D. M. *J Antibiot* **2006**, *59*, 303.
(213) Daum, R. S. *N Engl J Med* **2007**, *357*, 380.
(214) Merlino, J. I.; Malangoni, M. A. *Cleve Clin J Med* **2007**, *74*, S21.
(215) Raghavan, M.; Linden, P. K. *Drugs* **2004**, *64*, 1621.
(216) Dai, T.; Tegos, G. P.; Lu, Z.; Huang, L.; Zhiyentayev, T.; Franklin, M. J.; Baer, D. G.; Hamblin, M. R. *Antimicrob Agents Chemother* **2009**, *53*, 3929.
(217) Lipovsky, A.; Nitzan, Y.; Lubart, R. *Lasers Surg Med* **2008**, *40*, 509.
(218) Wainwright, M.; Phoenix, D. A.; Laycock, S. L.; Wareing, D. R.; Wright, P. A. *FEMS Microbiol Lett* **1998**, *160*, 177.
(219) Nakonieczna, J.; Michta, E.; Rybicka, M.; Grinholc, M.; Gwizdek-Wisniewska, A.; Bielawski, K. *BMC Microbiol* **2010**, *10*, 323.
(220) Tubby, S.; Wilson, M.; Nair, S. P. *BMC Microbiol* **2009**, *9*, 1471.
(221) (a) Embleton, M. L.; Nair, S. P.; Cookson, B. D.; Wilson, M. *J Antimicrob Chemother* **2002**, *50*, 857. (b) Embleton, M. L.; Nair, S. P.; Heywood, W.; Menon, D. C.; Cookson, B. D.; Wilson, M. *Antimicrob Agents Chemother* **2005**, *49*, 3690.
(222) Zeina, B.; Greenman, J.; Corry, D.; Purcell, W. M. *Br J Dermatol* **2003**, *148*, 229.
(223) (a) Fu, X. J.; Fang, Y.; Yao, M. *Biomed Res Int* **2013**, *159157*, 28. (b) Li, X.; Guo, H.; Tian, Q.; Zheng, G.; Hu, Y.; Fu, Y.; Tan, H. *J Surg Res* **2013**, *184*, 1013. (c) Tseng, S. P.; Hung, W. C.; Chen, H. J.; Lin, Y. T.; Jiang, H. S.; Chiu, H. C.; Hsueh, P. R.; Teng, L. J.; Tsai, J. C. *J Microbiol Immunol Infect* **2015**, *10*, 00020. (d) Yin, R.; Wang, M.; Huang, Y. Y.; Landi, G.; Vecchio, D.; Chiang, L. Y.; Hamblin, M. R. *Free Radic Biol Med* **2015**, *79*, 14.
(224) Vecchio, D.; Dai, T.; Huang, L.; Fantetti, L.; Roncucci, G.; Hamblin, M. R. *J Biophotonics* **2013**, *6*, 733.
(225) Simonetti, O.; Cirioni, O.; Orlando, F.; Alongi, C.; Lucarini, G.; Silvestri, C.; Zizzi, A.; Fantetti, L.; Roncucci, G.; Giacometti, A.; Offidani, A.; Provinciali, M. *Br J Dermatol* **2011**, *164*, 987.
(226) Zolfaghari, P. S.; Packer, S.; Singer, M.; Nair, S. P.; Bennett, J.; Street, C.; Wilson, M. *BMC Microbiol* **2009**, *9*.
(227) Tanaka, M.; Kinoshita, M.; Yoshihara, Y.; Shinomiya, N.; Seki, S.; Nemoto, K.; Morimoto, Y. *Photochem Photobiol* **2010**, *86*, 403.
(228) Tanaka, M.; Kinoshita, M.; Yoshihara, Y.; Shinomiya, N.; Seki, S.; Nemoto, K.; Hamblin, M. R.; Morimoto, Y. *Lasers Surg Med* **2011**, *43*, 221.
(229) Street, C. N.; Pedigo, L.; Gibbs, A.; Loebel, N. G. Progress in Biomedical Optics and Imaging - Proceedings of SPIE, 2009.
(230) Ragàs, X.; Sánchez-García, D.; Ruiz-González, R.; Dai, T.; Agut, M.; Hamblin, M. R.; Nonell, S. *J Med Chem* **2010**, *53*, 7796.
(231) Kuklin, N. A.; Pancari, G. D.; Tobery, T. W.; Cope, L.; Jackson, J.; Gill, C.; Overbye, K.; Francis, K. P.; Yu, J.; Montgomery, D.; Anderson, A. S.; McClements, W.; Jansen, K. U. *Antimicrob Agents Chemother* **2003**, *47*, 2740.
(232) Dai, T.; Kharkwal, G. B.; Tanaka, M.; Huang, Y. Y.; Bil de Arce, V. J.; Hamblin, M. R. *Virulence* **2011**, *2*, 296.
(233) Sperandio, F. F.; Huang, Y. Y.; Hamblin, M. R. *Recent Pat Antiinfect Drug Discov* **2013**, *8*, 108.

(234) Tardivo, J. P.; Del Giglio, A.; de Oliveira, C. S.; Gabrielli, D. S.; Junqueira, H. C.; Tada, D. B.; Severino, D.; de Fátima Turchiello, R.; Baptista, M. S. *Photodiagn Photodyn Ther* **2005**, *2*, 175.
(235) Jett, B. D.; Hatter, K. L.; Huycke, M. M.; Gilmore, M. S. *BioTechniques* **1997**, *23*, 648.

Appendices

Appendix 2.1 LRESI-MS of some selected hybrids.

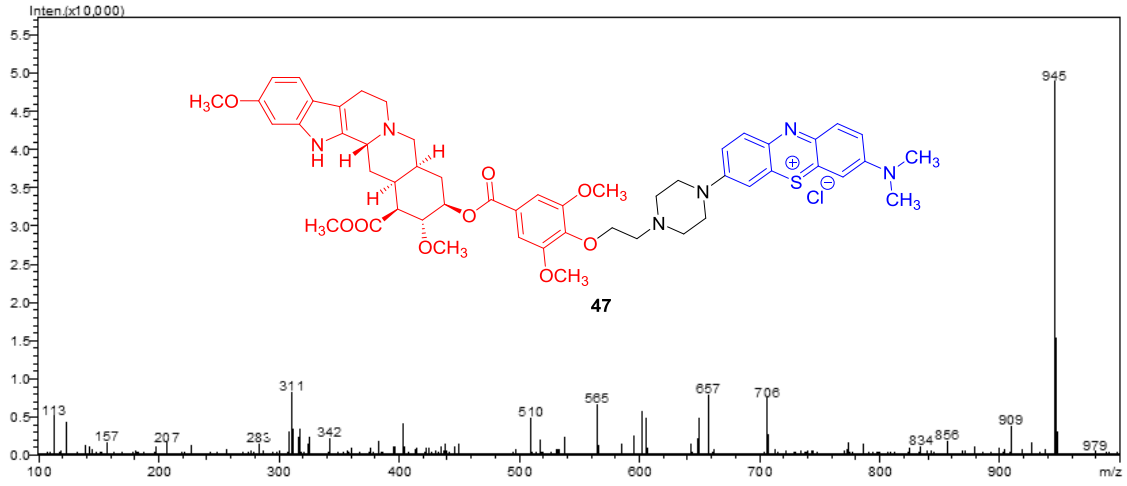

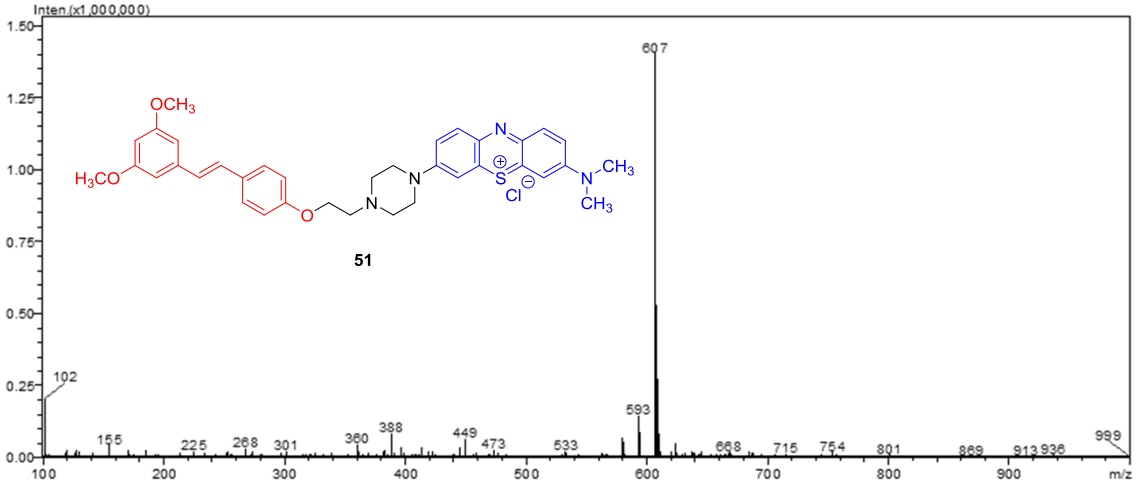

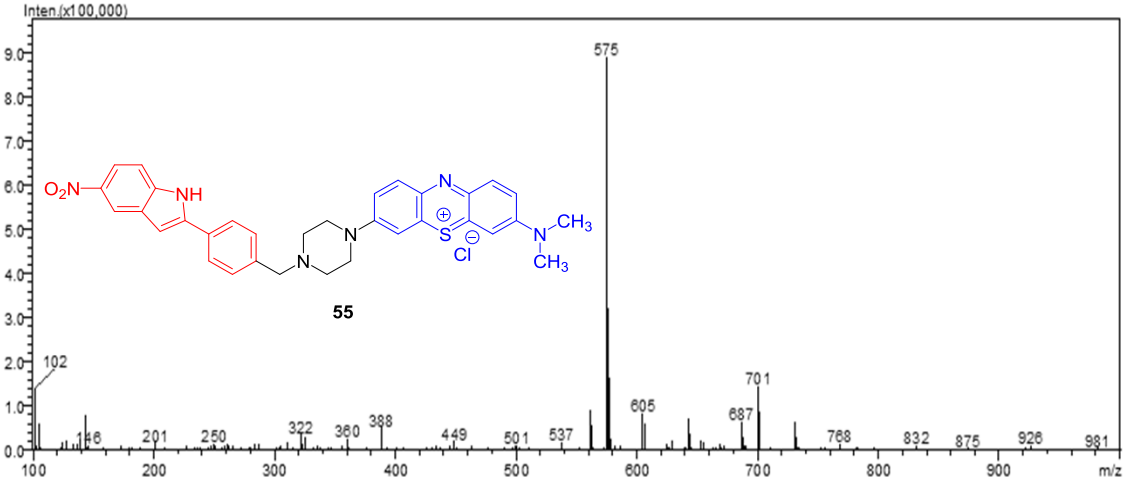

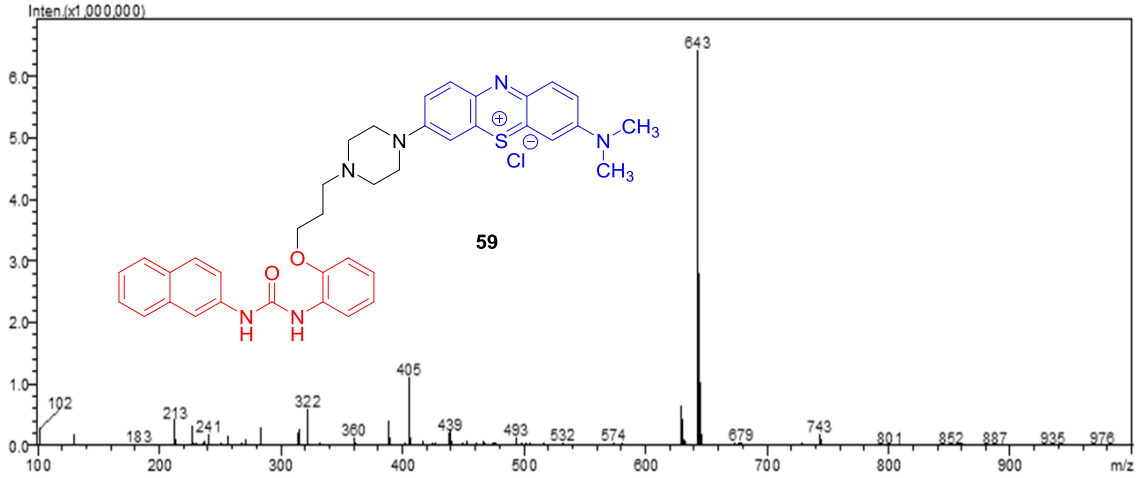
Inten.(x1,000,000)
643
405
322
102
213
241
183
360
439
493
532
574
679
743
801
852
887
935
976
m/z
59

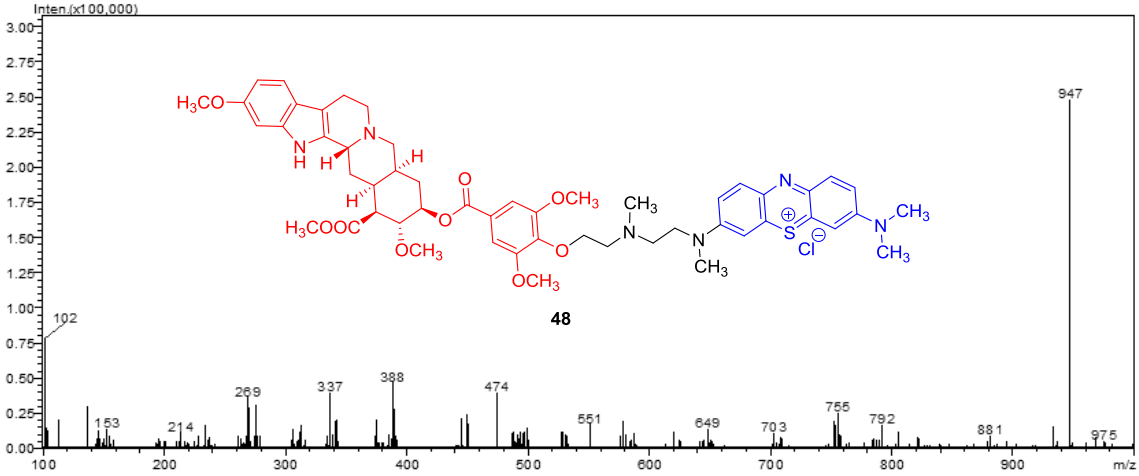
Inten.(x100,000)
947
102
269
337
388
474
153
214
551
649
703
755
792
881
975
m/z
48

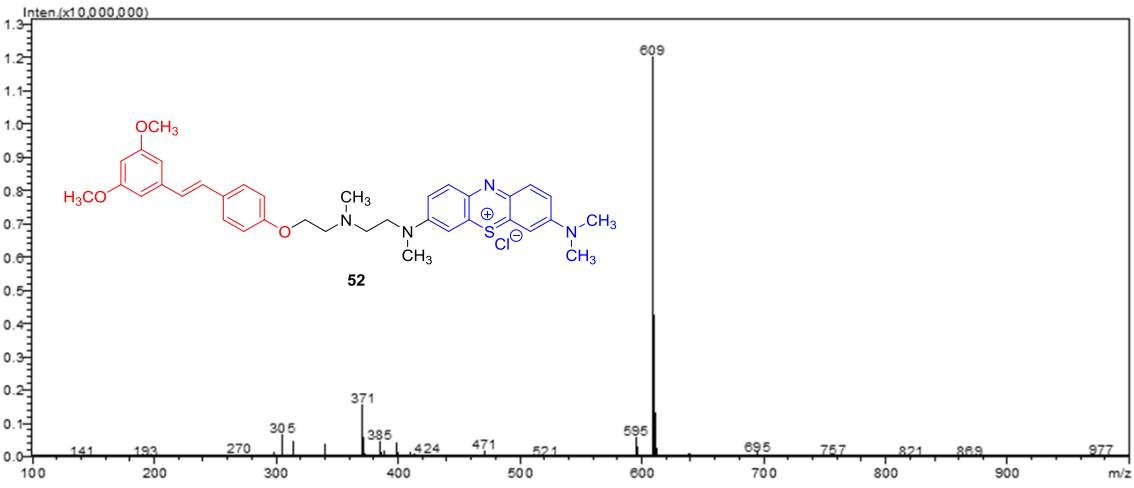
Inten.(x10,000,000)
609
371
305
385
141
193
270
424
471
521
595
695
757
821
869
977
m/z
52

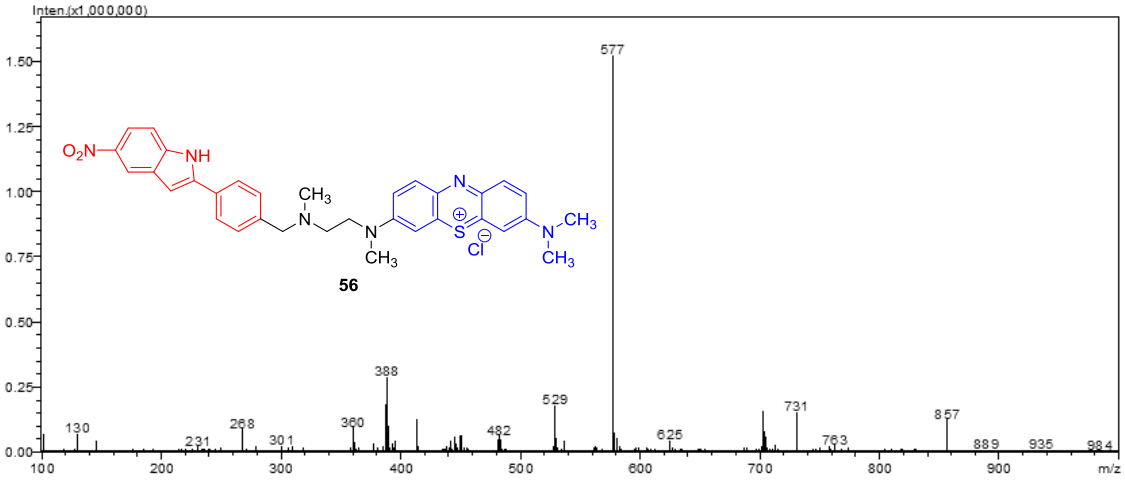
Inten.(x1,000,000)
577
388
529
731
857
56
m/z

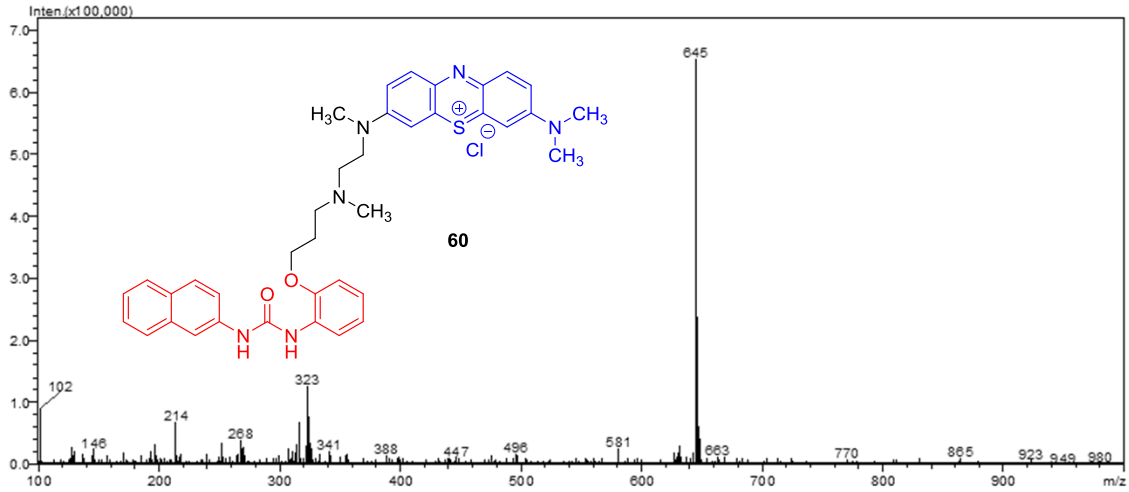
Inten.(x100,000)
645
323
102
214
60
m/z

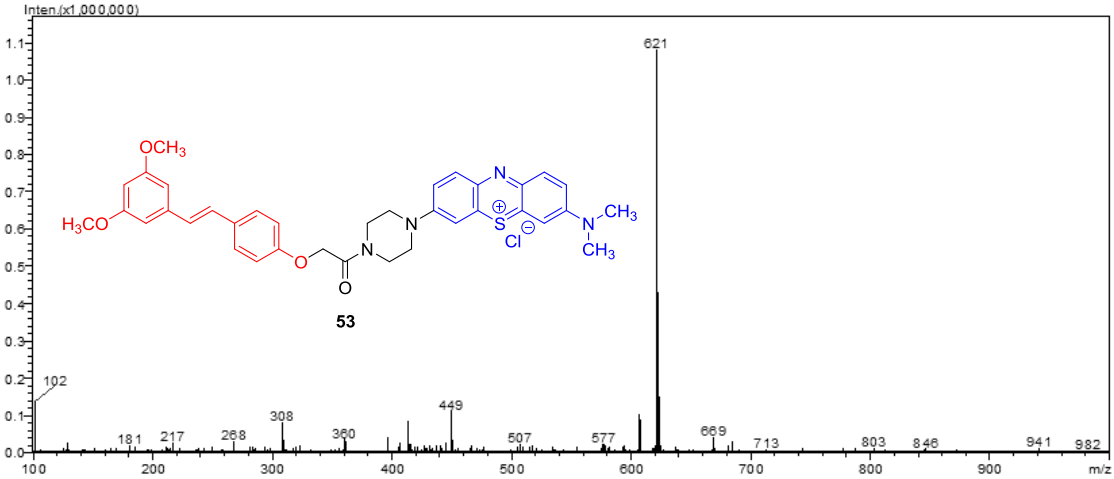
Inten.(x1,000,000)
621
102
449
53
m/z

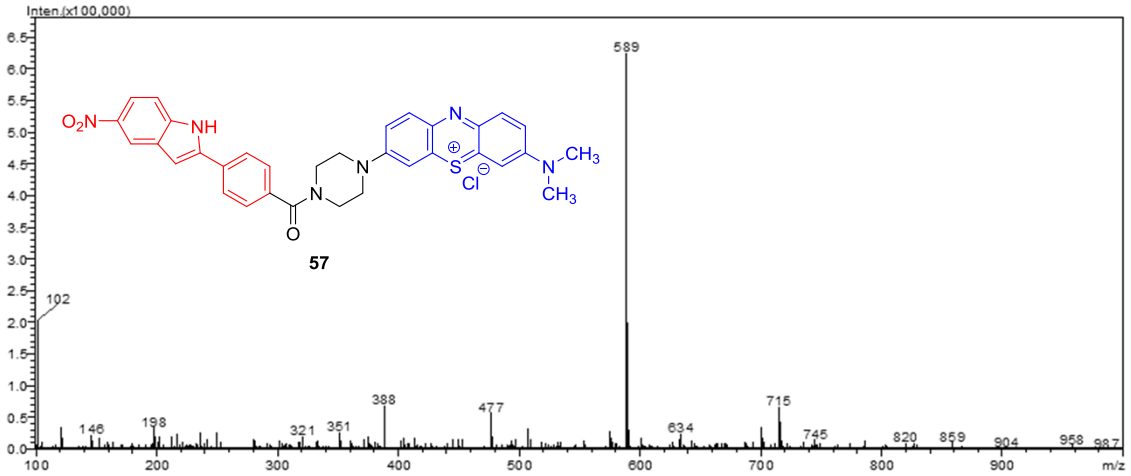
Inten.(x100,000)
589
102
146
198
321
351
388
477
634
715
745
820
859
904
958
987
m/z
57

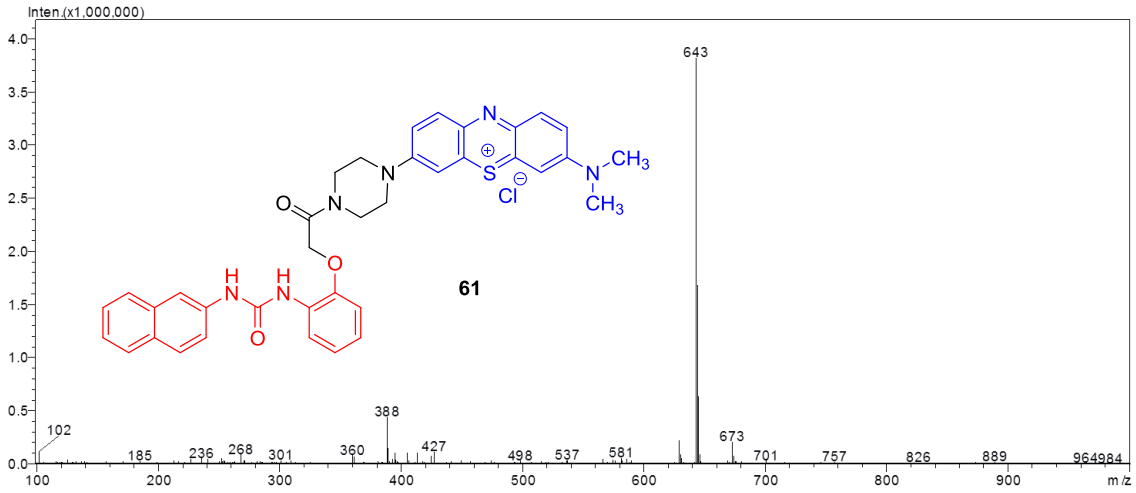
Inten.(x1,000,000)
643
102
185
236
268
301
360
388
427
498
537
581
673
701
757
826
889
964984
m/z
61

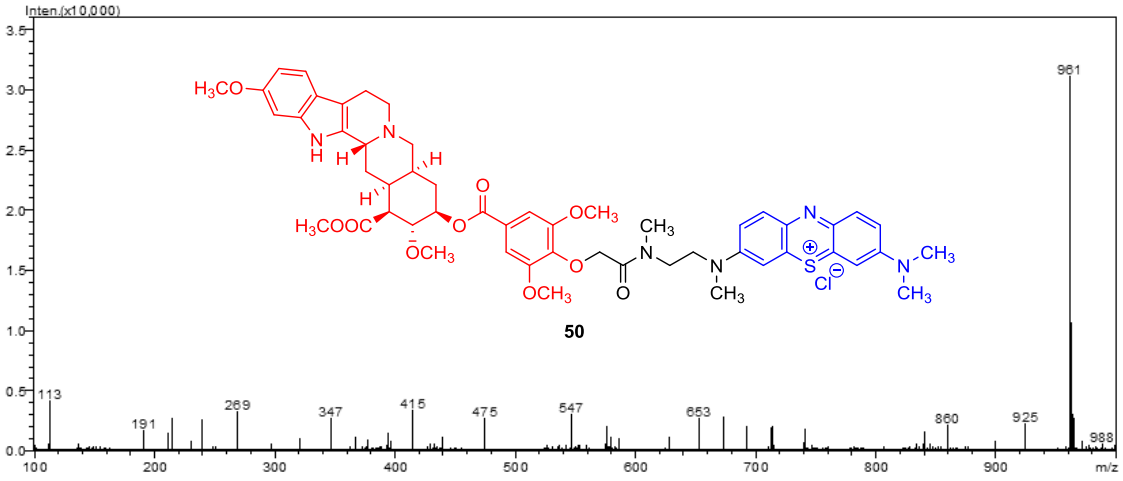
Inten.(x10,000)
961
113
191
269
347
415
475
547
653
860
925
988
m/z
50

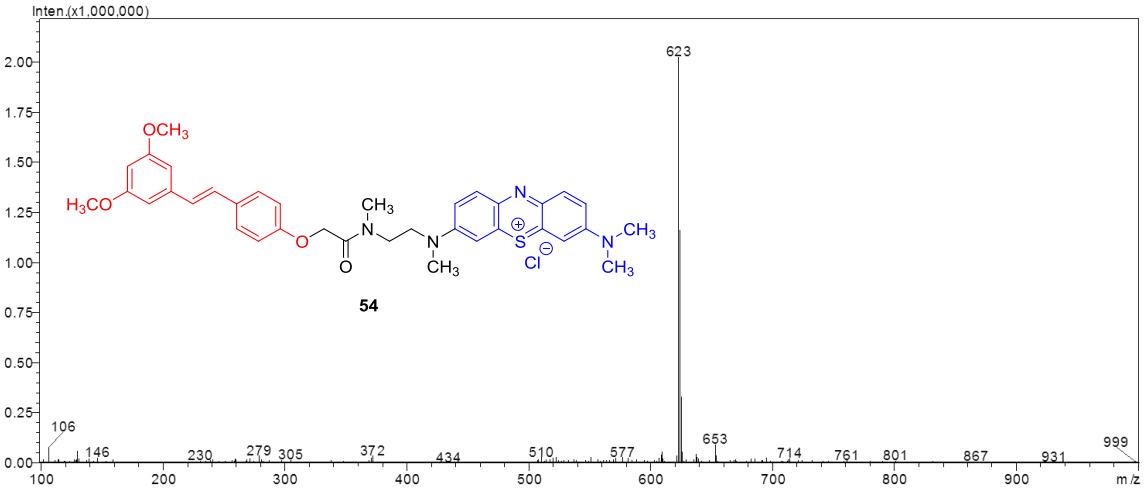
Inten.(x1,000,000)
623
106
146
230
279
305
372
434
510
577
653
714
761
801
867
931
999
m/z
54

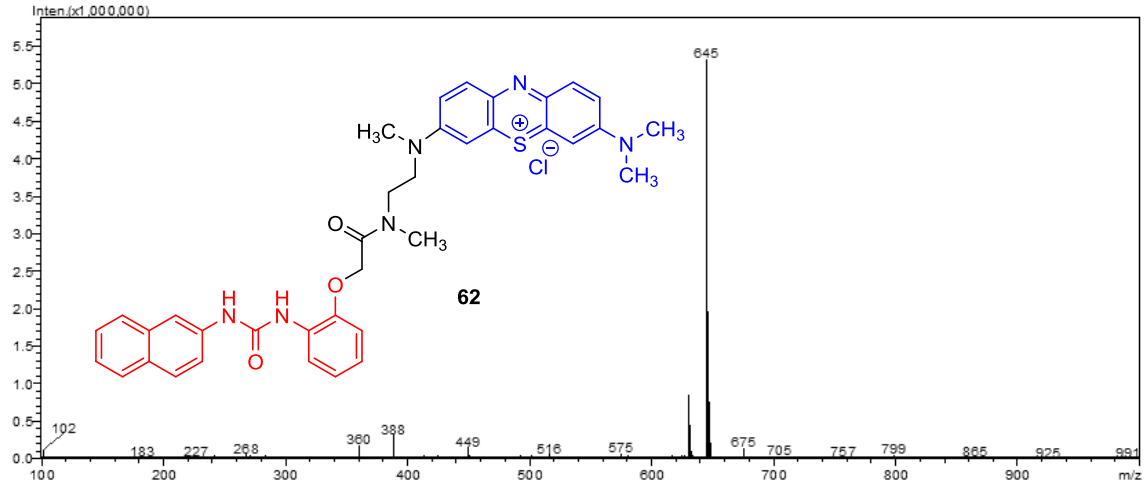
Inten.(x1,000,000)
645
102
183
227
268
360
388
449
516
575
675
705
757
799
865
925
991
m/z
62

Appendix 3.1 SOG and HPF quantum yields for MB and hybrids **47**-**62**.

Compound	Φ_Δ(SOG)	Φ_Δ(HPF)
MB	0.52	0.46
47	0.24	0.13
48	0.19	0.25
49	0.12	0.17
50	0.17	0.14
51	0.03	0.06
52	0.09	0.04
53	0.06	0.08
54	0.05	0.10
55	0.34	0.07
56	0.25	0.09
57	0.20	0.06
58	0.30	0.14
59	0.11	0.08
60	0.22	0.14
61	0.11	0.08
62	0.28	0.09

Appendix 3.2 Dark toxicity of MB and hybrids **47-62** against *S. aureus* MRSA USA300. Cells (10^8 per mL) were incubated for 30 min with CrEL-formulated hybrids at 0-20 µM in PBS and subsequently illuminated with 652 nm light (fluence 6 J/cm^2). CFUs were determined after overnight growth at 37 ^{o}C and survival fractions calculated. Data represent the mean of 3-5 independent experiments ± SEM.

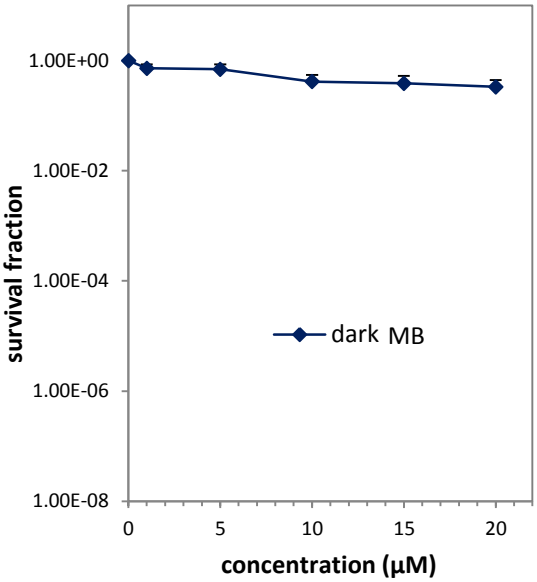

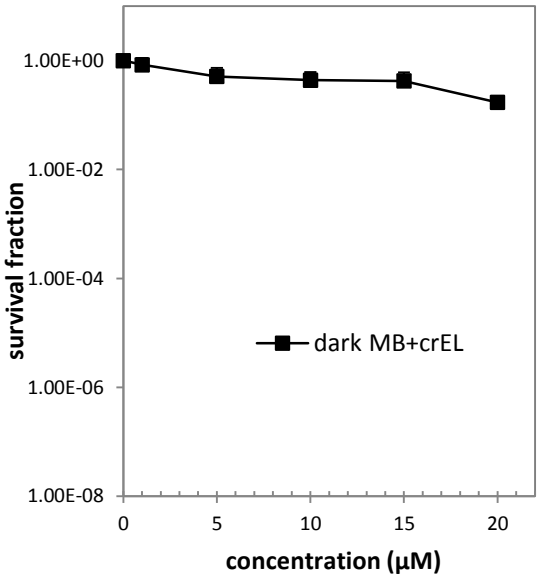

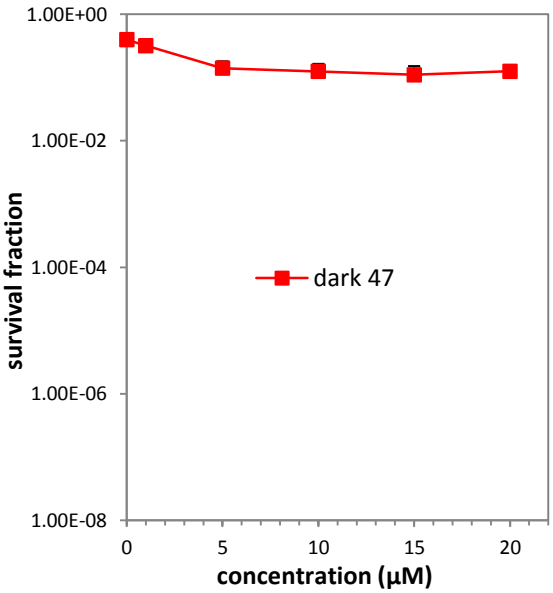

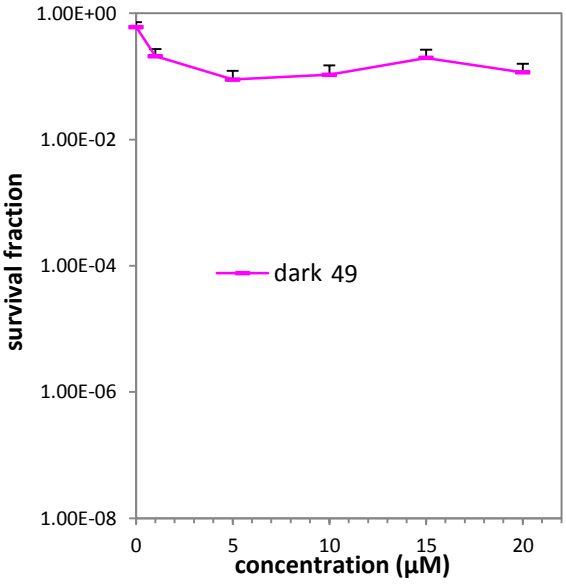

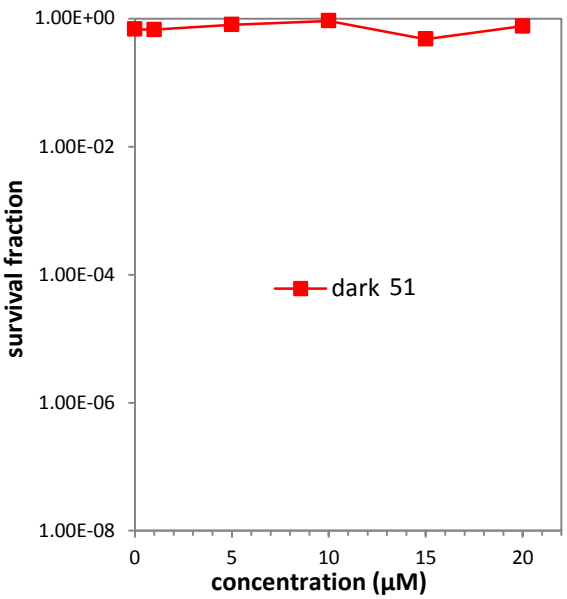
1.00E+00
1.00E-02
1.00E-04
1.00E-06
1.00E-08
survival fraction
dark 51
0
5
10
15
20
concentration (µM)

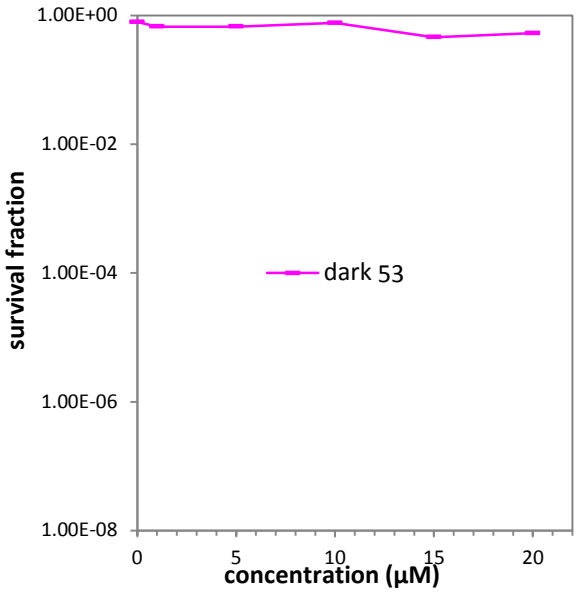
1.00E+00
1.00E-02
1.00E-04
1.00E-06
1.00E-08
survival fraction
dark 53
0
5
10
15
20
concentration (µM)

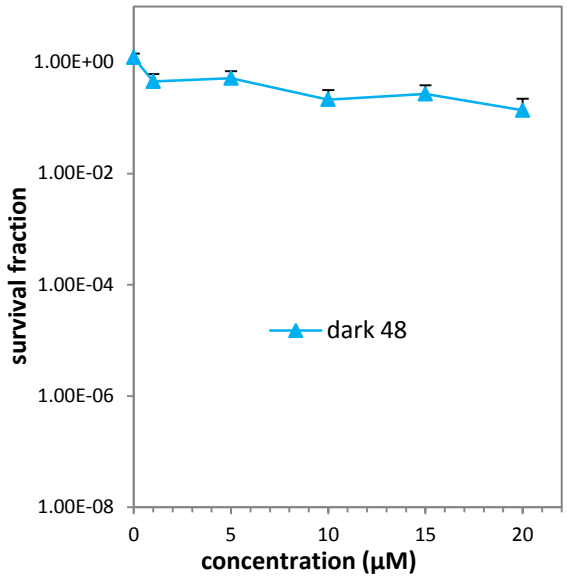
1.00E+00
1.00E-02
1.00E-04
1.00E-06
1.00E-08
survival fraction
dark 48
0
5
10
15
20
concentration (µM)

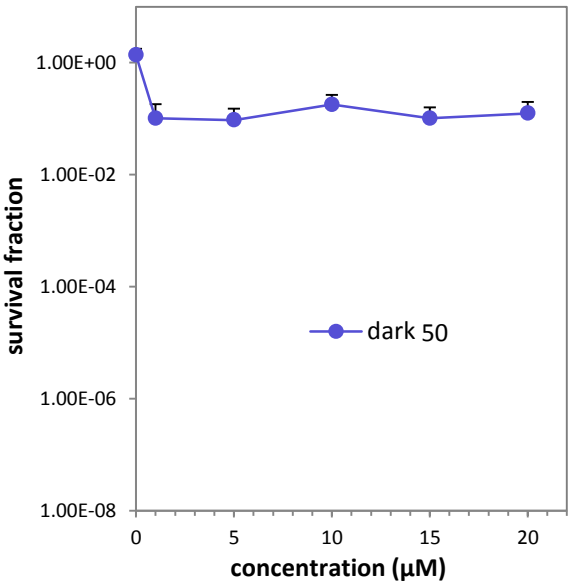
1.00E+00
1.00E-02
1.00E-04
1.00E-06
1.00E-08
survival fraction
dark 50
0
5
10
15
20
concentration (µM)

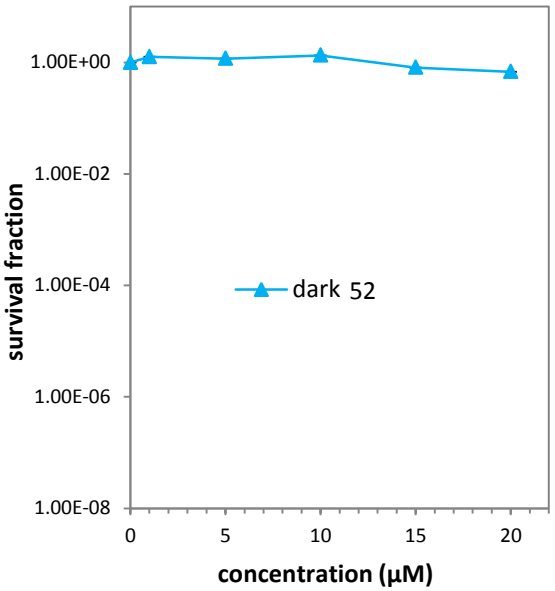
1.00E+00
1.00E-02
1.00E-04
1.00E-06
1.00E-08
survival fraction
dark 52
0
5
10
15
20
concentration (µM)

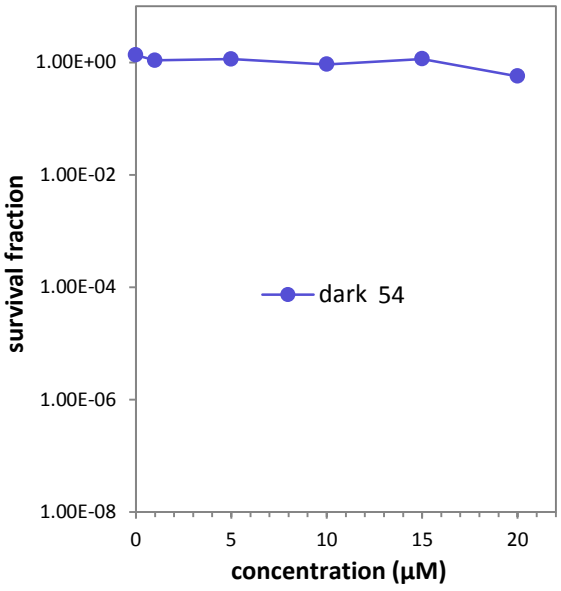
1.00E+00
1.00E-02
1.00E-04
1.00E-06
1.00E-08
survival fraction
dark 54
0
5
10
15
20
concentration (µM)

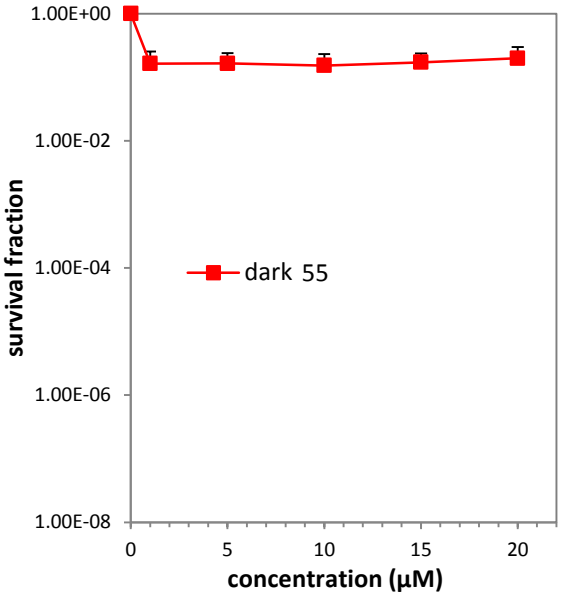
1.00E+00
1.00E-02
1.00E-04
1.00E-06
1.00E-08
survival fraction
dark 55
0
5
10
15
20
concentration (µM)

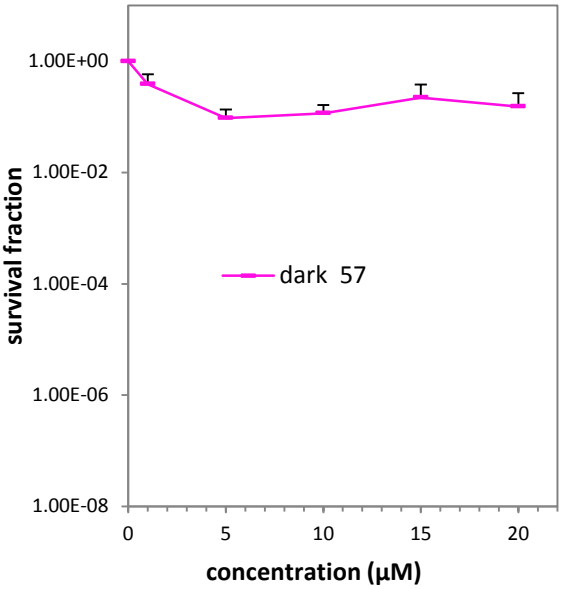
1.00E+00
1.00E-02
1.00E-04
1.00E-06
1.00E-08
survival fraction
dark 57
0
5
10
15
20
concentration (µM)

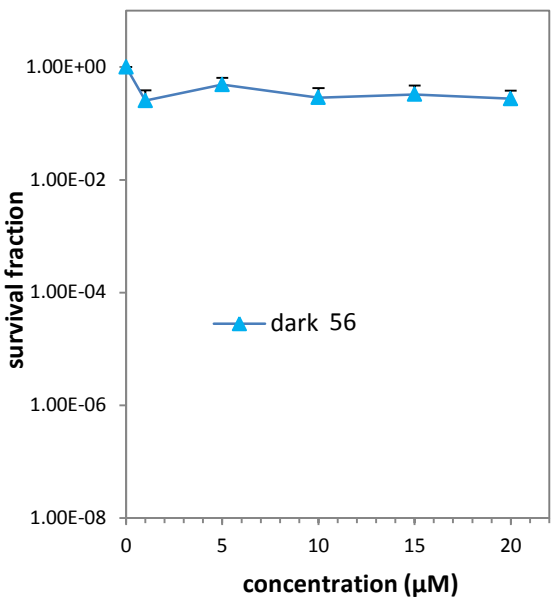
1.00E+00
1.00E-02
1.00E-04
1.00E-06
1.00E-08
survival fraction
dark 56
0
5
10
15
20
concentration (µM)

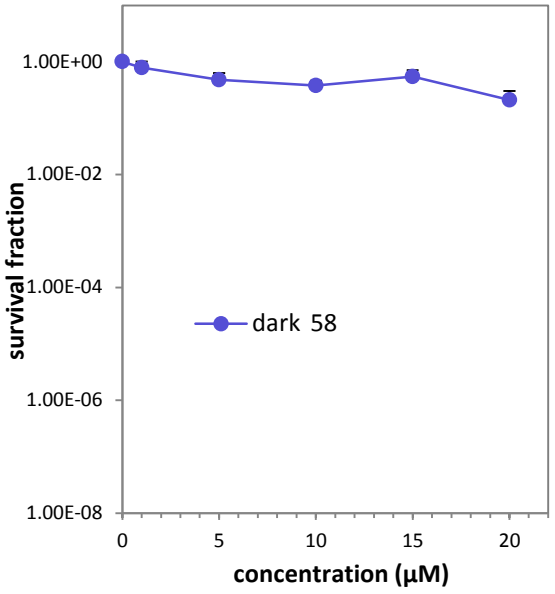
1.00E+00
1.00E-02
1.00E-04
1.00E-06
1.00E-08
survival fraction
dark 58
0
5
10
15
20
concentration (µM)

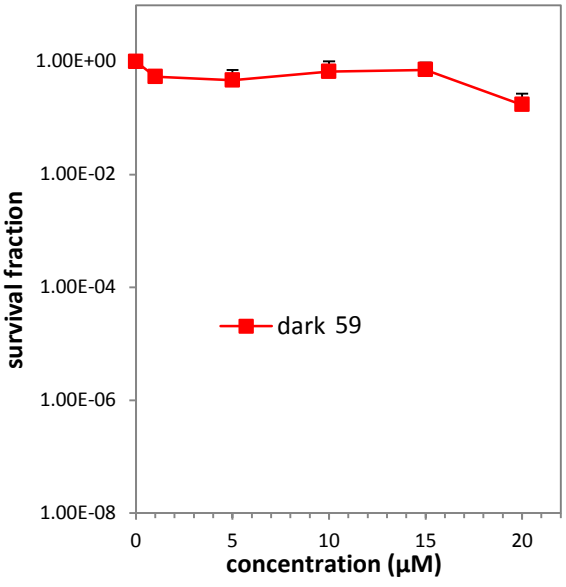
1.00E+00
1.00E-02
1.00E-04
1.00E-06
1.00E-08
survival fraction
dark 59
0
5
10
15
20
concentration (µM)

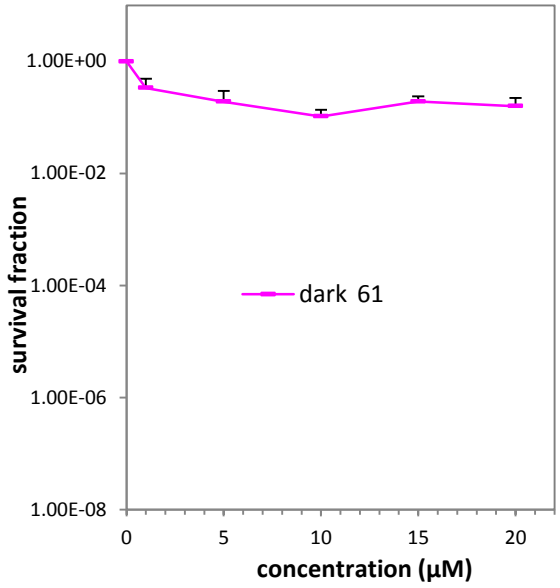
1.00E+00
1.00E-02
1.00E-04
1.00E-06
1.00E-08
survival fraction
dark 61
0
5
10
15
20
concentration (µM)

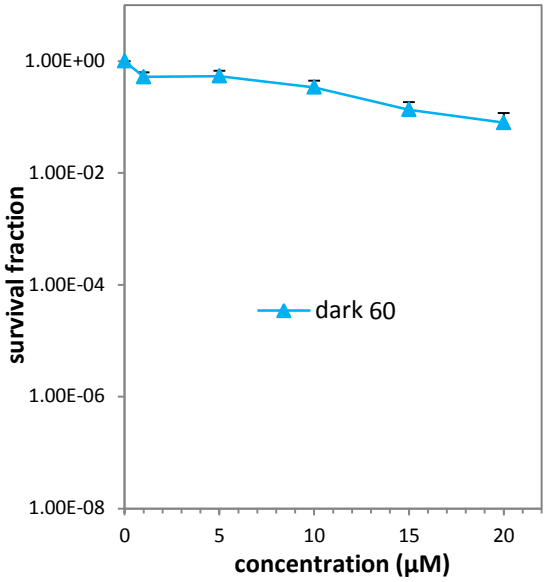
1.00E+00
1.00E-02
1.00E-04
1.00E-06
1.00E-08
survival fraction
dark 60
0
5
10
15
20
concentration (µM)

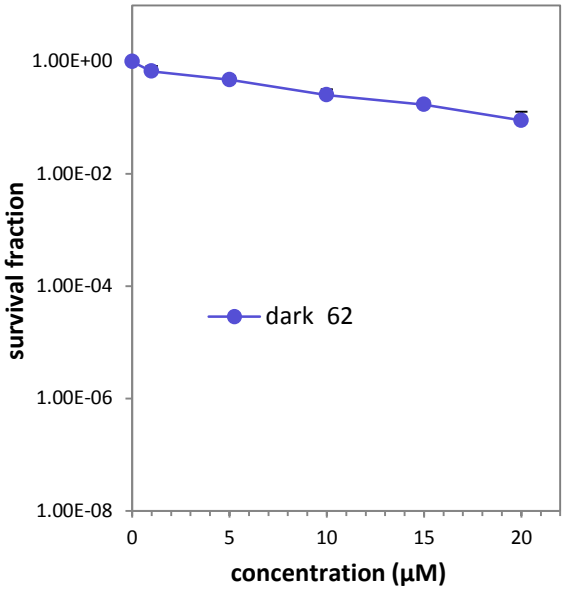
1.00E+00
1.00E-02
1.00E-04
1.00E-06
1.00E-08
survival fraction
dark 62
0
5
10
15
20
concentration (µM)

Appendix 3.3 Dark toxicity over the concentration range 0-16 µM of (A) MB, (B) **56**, (C) **58** and (D) **60** against NorA knockout (NorA-), wild-type (WT), and NorA-overexpressing (NorA++) *S. aureus* strains. Data represent the mean ± SEM from 3-4 independent experiments.

A

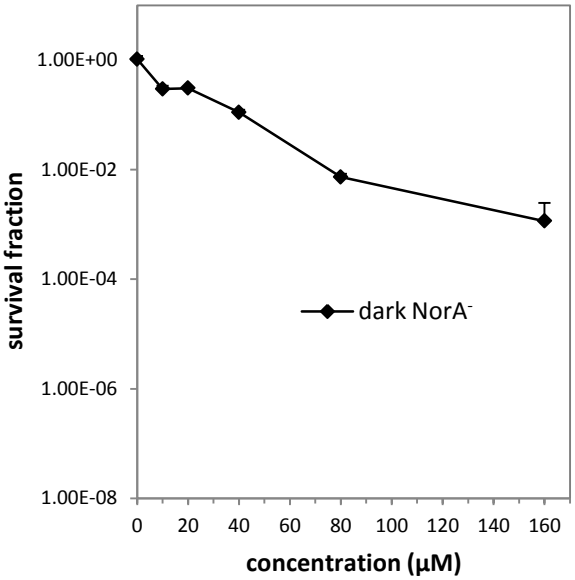

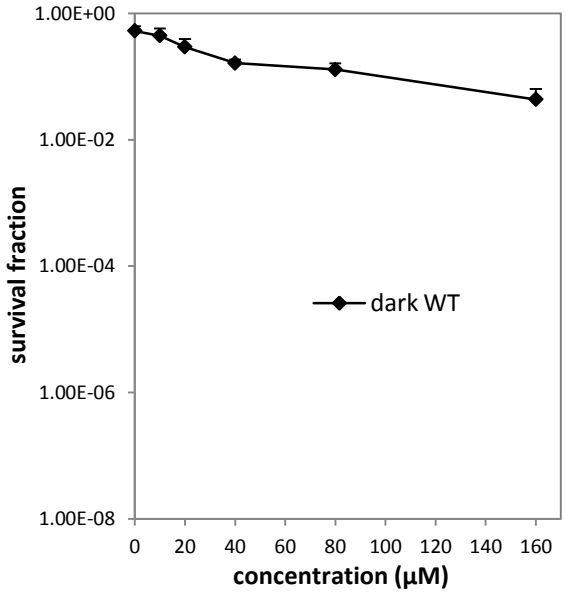

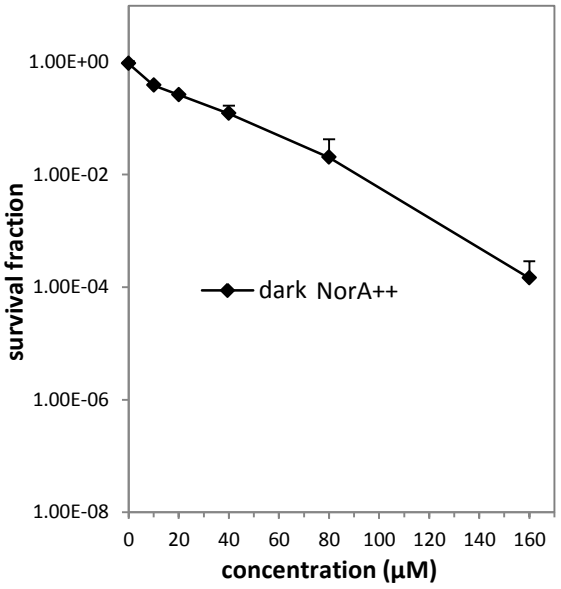

B

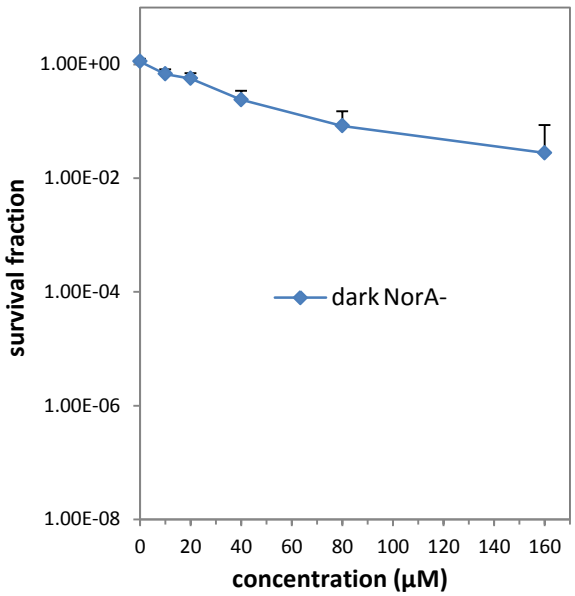
1.00E+00
1.00E-02
1.00E-04
1.00E-06
1.00E-08
survival fraction
dark NorA-
0 20 40 60 80 100 120 140 160
concentration (µM)

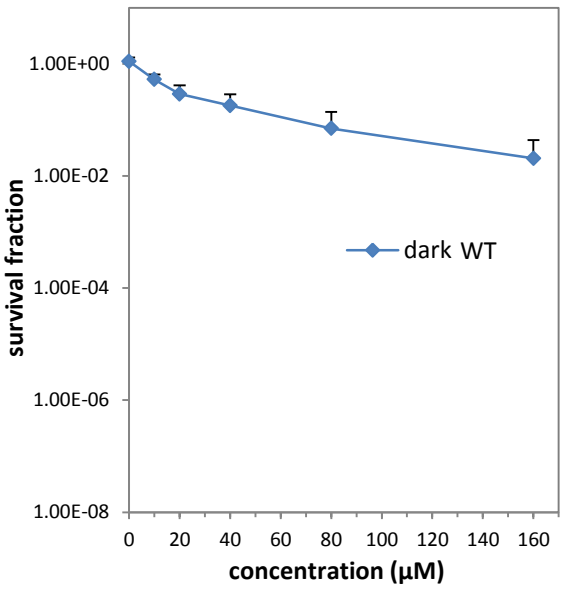
1.00E+00
1.00E-02
1.00E-04
1.00E-06
1.00E-08
survival fraction
dark WT
0 20 40 60 80 100 120 140 160
concentration (µM)

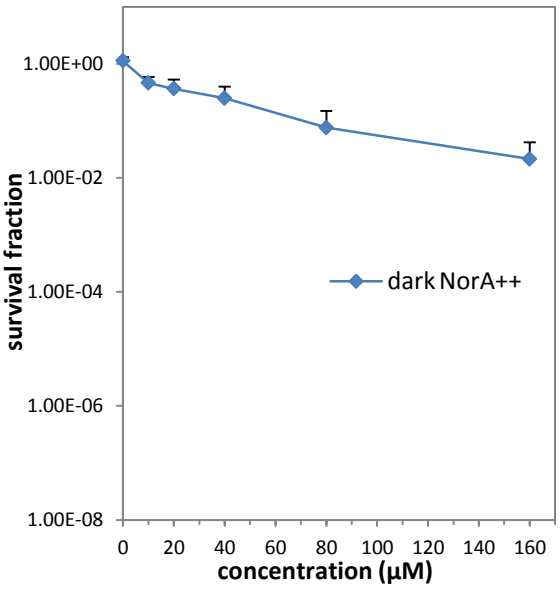
1.00E+00
1.00E-02
1.00E-04
1.00E-06
1.00E-08
survival fraction
dark NorA++
0 20 40 60 80 100 120 140 160
concentration (µM)

C

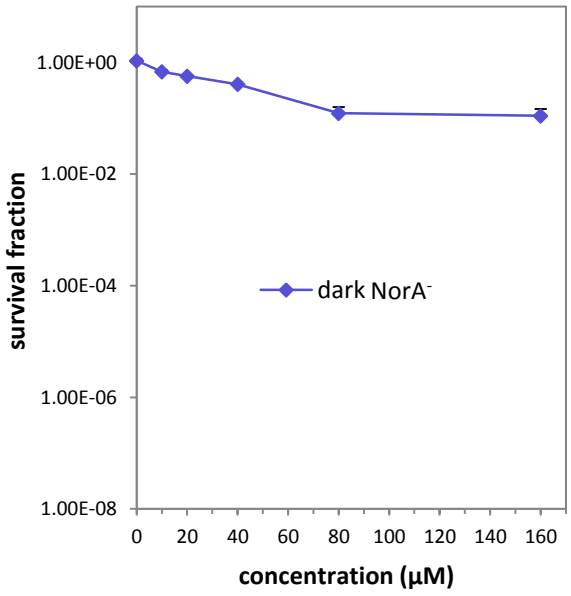
1.00E+00
1.00E-02
1.00E-04
1.00E-06
1.00E-08
survival fraction
dark NorA-
0 20 40 60 80 100 120 140 160
concentration (µM)

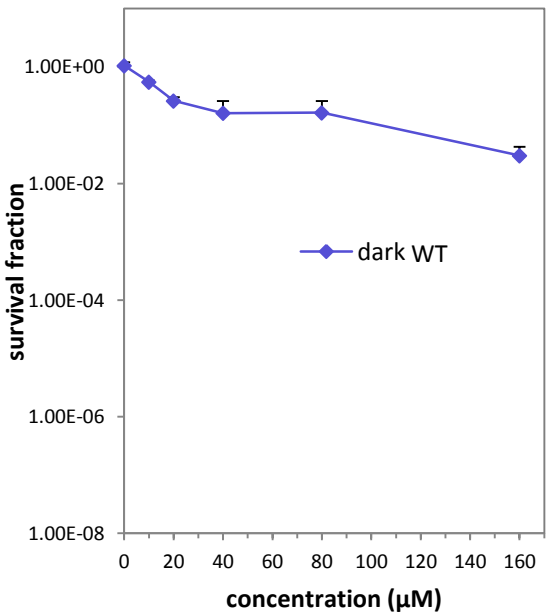
1.00E+00
1.00E-02
1.00E-04
1.00E-06
1.00E-08
survival fraction
dark WT
0 20 40 60 80 100 120 140 160
concentration (µM)

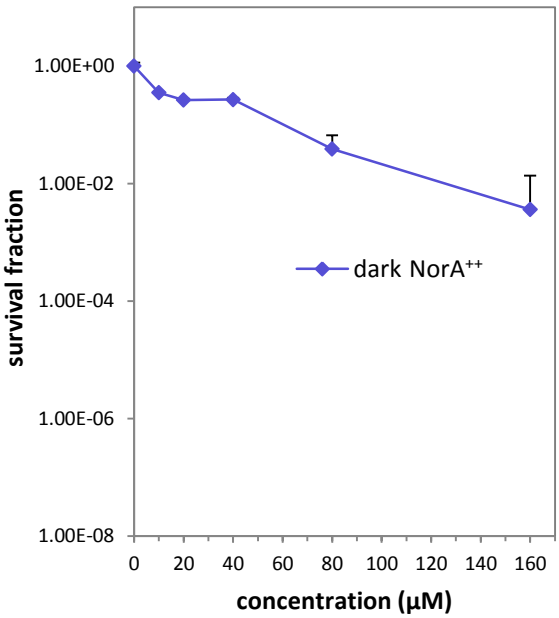
1.00E+00
1.00E-02
1.00E-04
1.00E-06
1.00E-08
survival fraction
dark NorA++
0 20 40 60 80 100 120 140 160
concentration (µM)

D

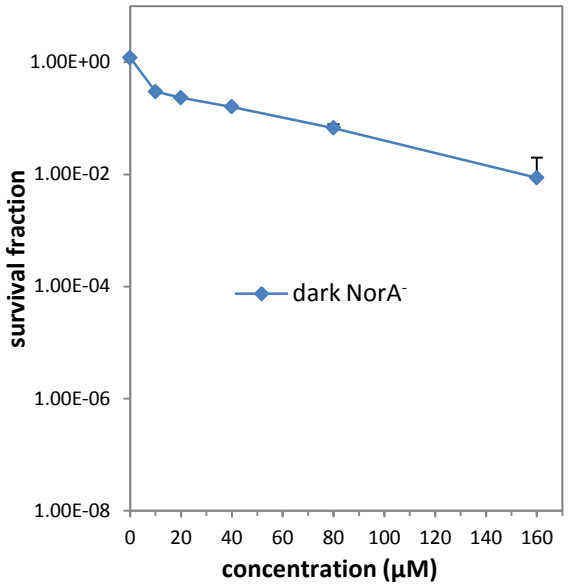
1.00E+00
1.00E-02
1.00E-04
1.00E-06
1.00E-08
survival fraction
dark NorA-
0 20 40 60 80 100 120 140 160
concentration (µM)

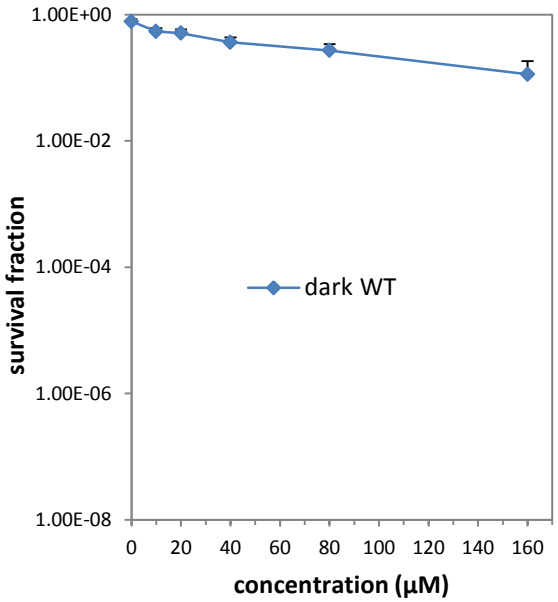
1.00E+00
1.00E-02
1.00E-04
1.00E-06
1.00E-08
survival fraction
dark WT
0 20 40 60 80 100 120 140 160
concentration (µM)

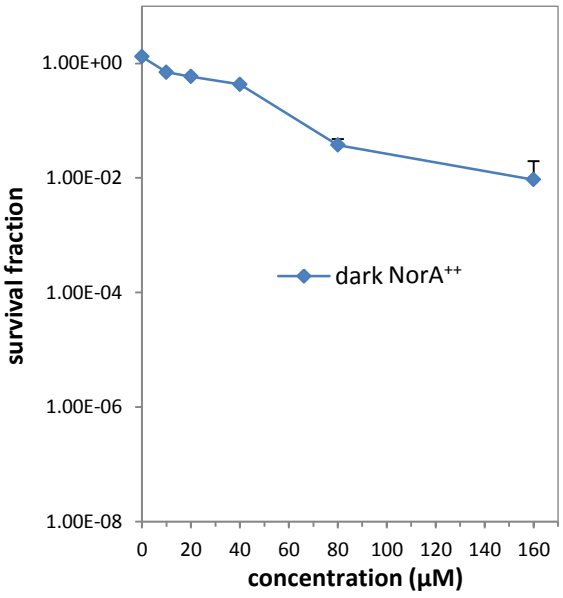
1.00E+00
1.00E-02
1.00E-04
1.00E-06
1.00E-08
survival fraction
dark NorA++
0 20 40 60 80 100 120 140 160
concentration (µM)

Appendix 4.1 Light-dose responses (mean ± SEM) for dark controls in (A) Groups B and (B) Group D in the bioluminescence MRSA wound infection model. Data are presented as normalized relative luminescence units (RLU). Data from Figure 4.3 for the equivalent aPDT Groups C (MB) and D (**58**) are included for comparison.

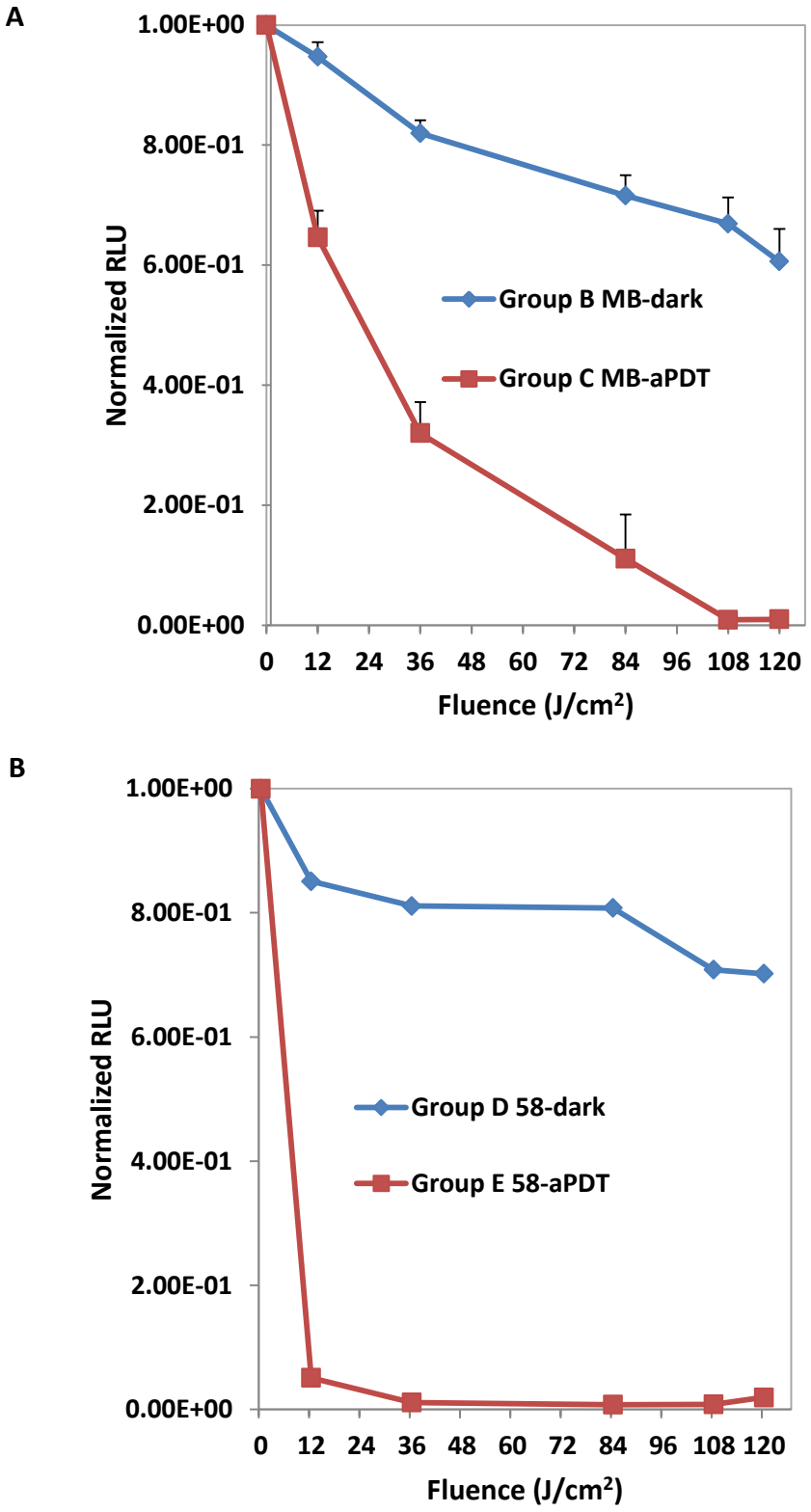

Appendix 4.2 Daily bioluminescence images obtained from representative animals in Groups A-E during 10 days of post-treatment monitoring.

	Group A Control	Group B MB dark	Group C MB PDT	Group D **58** dark	Group E **58** PDT
Day 1	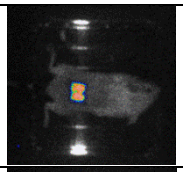	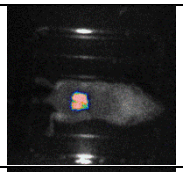	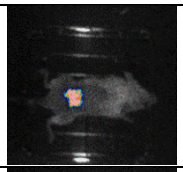	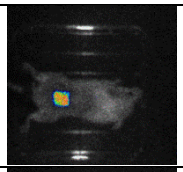	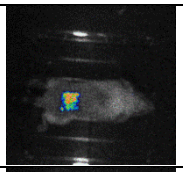
Day 2	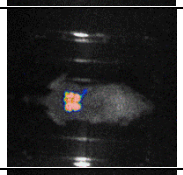	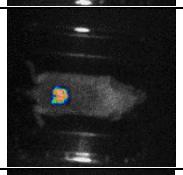	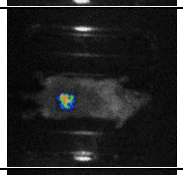	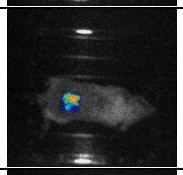	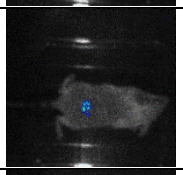
Day 3	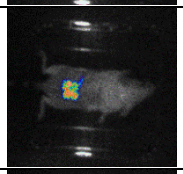	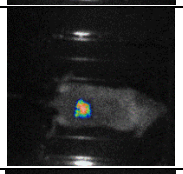	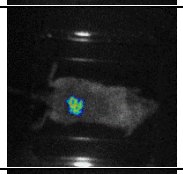	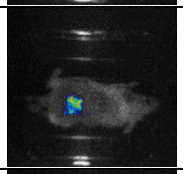	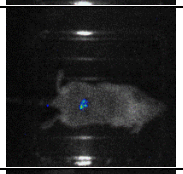
Day 4	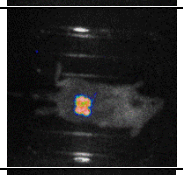	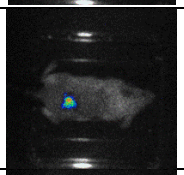	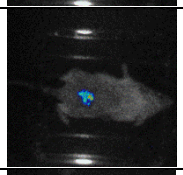	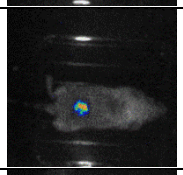	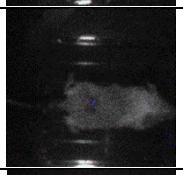
Day 5	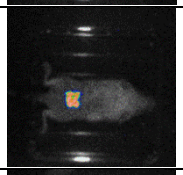	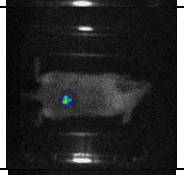	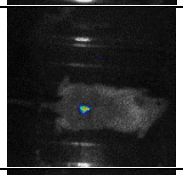	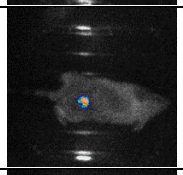	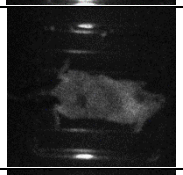
Day 6	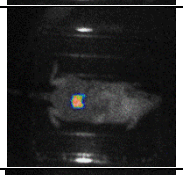	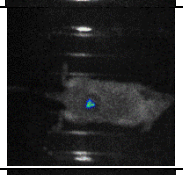	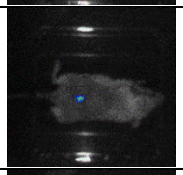	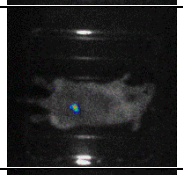	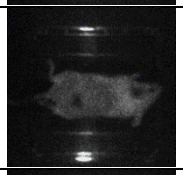
Day 7	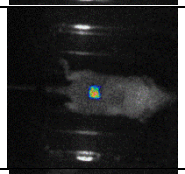	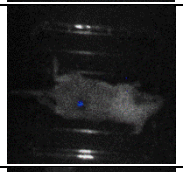	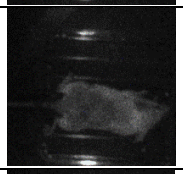	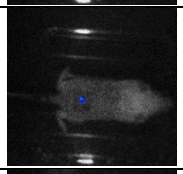	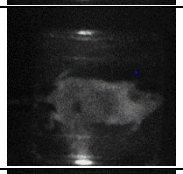
Day 8	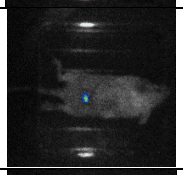	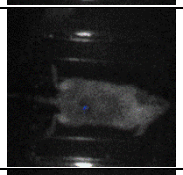	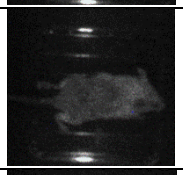	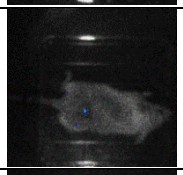	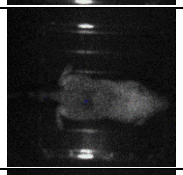
Day 9					
Day 10					